THE UNIVERSITY
of EDINBURGH

Uncovering signatures of geomorphic process through high resolution topography

Stuart Grieve

Thesis submitted in fulfillment of
the requirements for the degree of
Doctor of Philosophy
to the
University of Edinburgh — 2016

Declaration

I declare that this thesis has been composed solely by myself and that it has not been submitted, either in whole or in part, in any previous application for a degree. Except where otherwise acknowledged, the work presented is entirely my own.

Stuart Grieve

May 2016

Abstract

The measurement of topography is a key aspect of geomorphology research, and the prevalence of high resolution topographic data predominantly from Light Detection And Ranging (LiDAR) in the past decade has facilitated a revolution in the quantitative study of planetary surface processes. From this increased quality of data, many techniques have been developed to quantify processes occurring at diverse spatial and temporal scales; from the flow of material down a hillslope to the uplift and subsequent erosion of mountain ranges. Such insights have identified signatures of processes imprinted on landscapes. These include physical processes such as wildfires and landslides, biological processes such as animal burrowing and tree throw, in addition to tectonic uplift and large scale sediment transport. These signatures are observed in both the morphology of hillslopes and their connection to the channel network, thereby allowing measures of topography to provide quantitative measures of the rates of processes shaping the Earth's surface. This thesis is concerned with the development and application of reproducible topographic analysis techniques, to yield new insights into hillslope sediment transport and to provide accurate metrics for quantifying hillslope properties, including hillslope length (L_H) and relief (R).

The measurement of hillslope length can be performed through the inversion of drainage density, or the analysis of slope-area plots. However, in Chapter 3 I present a method which quantifies the length of hillslopes through the generation

of hillslope flow paths. The flow path method is shown to be the most reliable of these methods, and is able to provide measurements of the properties of individual hillslopes, rather than the basin or landscape averaged techniques commonly employed. The topographic predictions of the L_H-R relationship of the nonlinear sediment flux law, stating that the rate of sediment transport is nonlinearly dependent on hillslope gradient, are also tested and contrasted with the predictions of a linear sediment flux law. This provides the first purely topography based test of a sediment flux law. Through the fitting of a prediction of the nonlinear flux derived model to these measurements of hillslope length and relief, the critical gradient of each landscape, a key parameter in the nonlinear sediment flux law, is also constrained.

A nondimensional framework for erosion rate and relief, which allows the comparison of hillslopes with differing properties in order to identify landscape transience is presented in Chapter 4. This analysis technique builds upon the work performed in Chapter 3, utilizing similar measurements of hillslope properties, including hillslope length and relief. The software produced alongside this chapter is shown to reproduce the results of previous studies which have employed this technique. The method is employed on a new landscape in Coweeta, North Carolina where subtle evidence of topographic decay is presented, consistent with models of Miocene topographic rejuvenation in this location. A detailed sensitivity analysis of the technique is performed, highlighting the need for careful parameterization of any analysis, to ensure meaningful results. This method is also employed to estimate an average critical gradient for each landscape, presenting more evidence building upon the evidence presented in Chapter 3 that a broad range of critical gradients exist for any given landscape.

The work presented in Chapter 5 attempts to constrain the limits of the geomorphic analyses presented in the previous chapters, when they are applied to low resolution topographic data. A series of topographic datasets are generated

at resolutions ranging from 1 to 30 meters upon which topographic analyses are performed. I test two common channel extraction algorithms and find that a simple geometric method, which identifies tangential curvature thresholds in the landscape, provides a more accurate representation of the channel network in low resolution topographic data than a process based method which identifies the topographic signature of channel initiation. The measurement of curvature is also evaluated, and alongside the estimation of diffusivity, is shown to be sensitive to data resolution, however landscape properties also exhibit a strong control on these measurements, where the larger scale curvature signal of Gabilan Mesa, California is more robust than the sharp ridgelines of Santa Cruz Island, California. Finally, the techniques developed in Chapter 3 to measure hillslope length and relief are tested and are shown to be robust at grid sizes up to 30 meters, with the caveat that an accurate channel network can be constrained.

Acknowledgements

I would like to dedicate this thesis to my grandfather, William Tulloch, who has always encouraged my curiosity, regardless of what direction it would take me in.

In undertaking my Ph.D. I have benefited from the support, advice and kindness of too many people to list. However, I am still going to try. If I missed you, my sincerest apologies.

My eternal gratitude goes to Simon Mudd, who started supervising me in 2010 and three degrees later I'm still here. It is no understatement to say that I would not be the scientist I am today without your mentoring and advice. Simon's breadth of knowledge is almost as inspiring as his hatred of poorly indented code and I would like to thank him for always having patience with me and providing me with the freedom to pursue the ideas I found interesting. Finally I would like to credit Simon for the instigation of LSDTopoTools, as the development of software on this project has taught me that nothing is impossible, as long as you don't get a memory leak.

As part of this project I have also had the privilege to work with T.C. Hales and Rob Parker, both in North Carolina and in Cardiff, whose expertise has greatly shaped the direction of my research. In the field I was also joined by Fiona Clubb and David Milodowski who proved to be excellent companions in the field, even if they didn't share my passion for barbecue. Fiona and Dave have also co-authored

2 of the papers which have come out of this thesis, and their insights, dedication and creativity cannot be overstated. Martin Hurst has also been a co-author and his advice, particularly in the early stages of my research career, has been invaluable.

At Edinburgh we are lucky to have a vibrant group of people in Land Surface Dynamics, and I would like to thank all of the members of the group, past and present, for their support, encouragement, feedback and friendship. I had a desk in Lower Lewis throughout my Ph.D. and would like to thank everyone there for making it such a great place to work, and Lizzie in particular for putting up with my unique style of software development.

My friends have provided me with much support, and often a much needed distraction from the challenges I was facing. In particular, long lunches with Graeme at Reekie's Smokehouse provided an excellent venue to get perspective on problems, in addition to eating lots of pulled pork.

My parents, Dorothy and Leslie, and my brother, Duncan, have supported me since long before I undertook this degree, and I owe them a debt of gratitude for their support, particularly through periods of ill health. They, alongside my partner, have seen me through several difficult periods over the last 4 years and beyond, and I would not have completed my first degree, let alone this Ph.D., without their kindness and understanding.

Finally, and most importantly, I would like to thank my partner, Charlotte Pike, whose love and understanding has carried me though many periods of self doubt. Without you by my side I would have struggled to complete this thesis and that I am writing this in May rather than later in the year is testament to the sacrifices you have made to support me.

Stuart Grieve – May 2016

Contents

List of Tables

List of Figures

Chapter 1

Introduction

1.1 Overview

High resolution topography has facilitated a revolution in geomorphology, with the development of a diverse suite of techniques which can be used not only to study the processes acting upon landscapes, but to quantify those processes (Passalacqua *et al.*, 2015). It is therefore possible to use high resolution topography to falsify predictions made using models of sediment production, transport and deposition on hillslopes. This thesis is concerned with the development and application of such topographic analysis methods to provide new insights into sediment transport and to facilitate reproducible research which can be readily applied to a range of landscapes. The research presented herein develops and evaluates techniques for the measurement of hillslope length and uses such measurements to test common sediment flux laws (cf. Dietrich *et al.*, 2003). A sediment flux law is a mathematical statement of the relationship between sediment flux and landscape properties, such as topographic gradient. Quantifying such flux laws is essential if we are to make predictions of how tectonic

and climatic perturbations will affect sedimentation, erosion and landscape evolution in the future. Using my new algorithms to extract data about landscape properties, I then cast landscape properties in a dimensionless context to evaluate patterns of relief and hilltop curvature, with the aim of identifying landscape transience and further testing sediment flux laws. These methods are also used to evaluate the sensitivity of various topographic metrics to decreasing the resolution of topographic data used, with the aim of constraining the possibilities of applying methods developed for high resolution topography on lower resolution data, opening up geomorphic research and techniques to more areas of the Earth's surface.

1.2 Theoretical Background

The surface of the Earth is sculpted by the processes which act upon it, effecting changes ranging from the motion of individual grains of sediment to the collision of continents, across timescales encapsulating individual events to those occurring over geological epochs. Many of these processes yield characteristic topographic signatures which have been qualitatively observed for over a century (Davis, 1892; Gilbert, 1896, 1909). Consequently, the morphologies of landforms across this range of scales have been recognized as having the potential to be employed as recorders of these past events, and through a combination of theoretical and technical developments their analysis can now yield quantitative insights into how the processes acting on landscapes operate.

Through such detailed study, topographic signatures of biologic (Gabet, 2000; Yoo *et al.*, 2005; Gabet and Mudd, 2010; Roering *et al.*, 2010), tectonic (Hilley and Arrowsmith, 2008; DiBiase *et al.*, 2012; Hurst *et al.*, 2013b) and climatic (Gabet *et al.*, 2004; Riebe *et al.*, 2004; Hales and Roering, 2007; Dixon *et al.*,

2009) processes have been identified, alongside the controls such processes, in conjunction with lithology (Korup, 2008; Hurst *et al.*, 2013c), can exert on topographic development. The contributions of both chemical (Riebe *et al.*, 2003; Mudd and Furbish, 2004; Burke *et al.*, 2007; Yoo *et al.*, 2011) and mechanical (Anderson, 2002; Cohen *et al.*, 2009, 2010) weathering to surface lowering have also been quantified in part through the study of topographic forms. Such weathering converts bedrock into sediment, the transport of which can be quantified through its relationship to topographic gradient (cf. Dietrich *et al.*, 2003). Through the use of topographic observations and measurements, a diverse range of sediment flux laws has been proposed to describe such sediment transport (Culling, 1960; Andrews and Bucknam, 1987; Roering *et al.*, 1999; Braun *et al.*, 2001; Furbish and Fagherazzi, 2001; Heimsath *et al.*, 2005; Roering, 2008; Foufoula-Georgiou *et al.*, 2010; Tucker and Bradley, 2010; Furbish and Roering, 2013). In addition to applying such laws in numerical modeling of hillslope development (Braun *et al.*, 2001; Herman and Braun, 2006; Roering, 2008) and falsifying predictions made through their use (Roering *et al.*, 1999, 2007; Pelletier *et al.*, 2011).

As the resolution of topographic data has increased and the costs associated with high performance computing have decreased, our ability to collect and analyze topographic data at finer scales has emerged. From such advances it is now possible to identify and measure specific landscape features directly, such as the initiation point of channels (Lashermes *et al.*, 2007; Tarolli and Dalla Fontana, 2009; Vianello *et al.*, 2009; Passalacqua *et al.*, 2010; Pelletier, 2013; Clubb *et al.*, 2014), the morphology of rivers (Fisher *et al.*, 2013) and debris fans (Schürch *et al.*, 2011) and the properties of landslides and debris flows (Booth *et al.*, 2009). Taken as a whole, these techniques and theoretical advances comprise the discipline of topographic analysis, which has become a fundamental tool for modern quantitative geomorphology.

1.2.1 Initial observations of topographic form

In his seminal work on the geology of the Henry Mountains, Utah, Gilbert (1877) made observations of the relationship between the morphology of drainage divides and the processes which were eroding the landscape. Such observations inspired work to formalize ideas of soil creep as the dominant process transporting sediment in badlands, and consequently linked the convex profile of these drainage divides to a specific process (Davis, 1892). From this initial suggestion of a relationship between the morphology of convex hillslopes and the processes transporting sediment across them, a more detailed qualitative understanding of the processes sculpting such landscapes was achieved (Gilbert, 1909). Such a relationship between the morphology of convex hillslopes and soil creep formed the basis of much quantitative work in the latter half of the 20^{th} century (e.g., Culling, 1960).

Hicks (1892, 1893) took the observations made by Gilbert (1877) and Davis (1892) and suggested that the convexity of badland hillslope profiles was not driven purely by the creep of particles, but by depth dependent weathering facilitating differential rates of surface lowering along hillslope profiles. This hypothesis presented the idea that the nature of weathering of a surface can yield a distinct topographic form, and that more than one process can be invoked to account for the nature of a landform.

A different scale of process was considered by Gilbert (1896), whilst studying the formation of Meteor Crater (then known as Coon Butte) in Arizona, performing a range of analyses supported by topographic data, field evidence and analogue modeling. A comparative study of the topography of the crater and the surrounding areas, employing topographic maps and profiles, was used alongside a reconstruction of topography without the crater to demonstrate the impact origin of the landform (Figure 1.1). Constraints were also placed on the size of

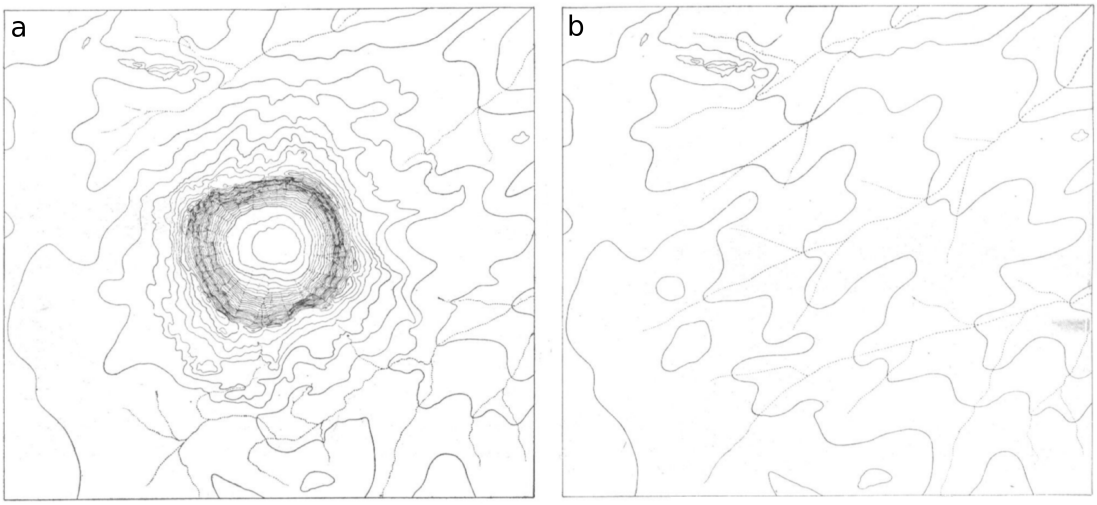

Figure 1.1: (a) Contour map of Meteor Crater with a contour spacing of 10 feet (solid lines) and channels denoted by dotted lines. **(b)** Topographic reconstruction of the landsurface prior to the formation of the crater. Figure reproduced from Gilbert (1896).

the meteorite which struck the Arizona desert through the throwing of clay balls at a clay surface, to create an analogue model of crater formation. Such initial discussions which linked the topographic form of a landscape to the processes acting upon it were generally observational and not directly quantitative, but in many cases such ideas remain the theoretical underpinning of many aspects of modern geomorphology.

1.2.2 Contour map analysis

A progression from the predominantly descriptive, theoretical work of Davis, Gilbert and their contemporaries to more quantitative analysis took place in the following decades. This progression occurred as a result of the increasing availability of topographic maps. Much of this initial work focused on the study

of rivers and their basins, with much less direct consideration of measurement of hillslopes.

The definition of a river network as a directed graph, defined by sources, junctions and outlets and with an index applied to each link was developed by Horton (1932, 1945). Horton's scheme of stream ordering was improved upon by Strahler (1952, 1957), resulting in the Horton-Strahler scheme. It defines first order channels as the outermost extent of the network, corresponding to channels with no tributaries. Where two streams of the same order meet, the order of the downstream channel is incremented by one and when two streams of different orders meet, the higher order is retained.

The ordering scheme developed by Shreve (1966) defines first order channels in the same manner as the Horton-Strahler scheme but then assigns all other orders following an additive method, whereby the order downstream of a junction is given as the sum of the orders of the channels meeting at a junction. This produces a measure of the number of channels upstream of a channel and gives a better measure of the topological relationship between channels than the Horton-Strahler scheme (Shreve, 1967).

Such a description of the topology of channel networks resulted in the development of a series of quantitative relationships between channel properties and drainage basins (Tarboton *et al.*, 1991). The initial quantitative work of Horton (1932, 1945) defined many key relationships and definitions beyond that of stream ordering. A negative exponential relationship was identified between topographic gradient and stream order, which conforms to qualitative observations of the reduction of river gradient with distance downstream. The drainage density (D_d) of a landscape given as,

$$D_d = \frac{L_T}{A}, \tag{1.1}$$

where L_T is the total length of channels in a basin and A is the basin area, can be considered a metric of the extent of dissection in a landscape. Such concepts were expanded upon to attempt to identify relationships between D_d and flood response (Chorley and Morgan, 1962; Gregory and Walling, 1968), and landscape properties (Kirkby, 1980).

Building upon the framework of Horton, several authors developed empirical power law relationships between topographic slope and contributing area (Leopold and Maddock Jr., 1953; Leopold and Miller, 1956; Flint, 1974). Broscoe (1959) demonstrated a similarity between the average change in elevation between nodes in a channel network across a range of stream orders. Such relationships became integral in the understanding of landscape morphology with the advent of digital topographic data, allowing such relationships to be tested across diverse locations and scales (e.g., Dietrich *et al.*, 1992).

The relationships between the logarithm of a range of hydraulic variables were shown to be quasi-linear functions of basin order by Leopold and Miller (1956), with detailed considerations of the relationships between channel length, density of channels, channel slope, channel width and discharge provided. As noted by Tarboton *et al.* (1991), all of these factors will scale with basin area, highlighting the control that basin area plays on many channel properties. Chorley (1957) computed an index of climate and vegetation using precipitation data and demonstrated a linear relationship between this index and channel properties, suggesting that climate and vegetation both control landscape morphology.

Schumm (1956) performed an extensive study of channels in New Jersey, USA within the Horton-Strahler channel analysis framework and found that many of the hydrologic properties of these channels were equivalent to the predictions

made by Horton's Laws (Horton, 1932, 1945). This work led to the observations of a relief ratio, given as the ratio of basin elevation to basin length which was used as a predictor for hydrologic variables, and facilitated the comparison of diverse drainage basins. The patterns of overland flow, and hillslope sediment transport were also considered within the context of their linkages to channel incision and the characteristic support area required to establish a channel. Such work demonstrates the utility of topographic analysis to elucidate processes acting both within channels and on the hillslopes coupled to those channels.

Such analyses necessarily incorporated errors due to the sampling resolution of the surveys, and the uncertainty of where the channels precisely initiated. Workers were aware of such limitations, *e.g.,*

> *Although the accuracy of these maps may be open to question, there is no reason to suppose that the individual degrees of accuracy are of such a different order of magnitude as to prohibit the comparison of results* (Chorley, 1957),

but were still able to make significant contributions to our understanding of how the morphology of rivers, their basins and the landscape as a whole can inform about the processes acting upon the Earth's surface.

1.2.3 Digital elevation models (DEMs)

The development of DEMs

The application of topographic analysis from contour maps is challenging because the resolution of the topographic information is typically low, as no data exist

between contours, and because the maps were never created to be a tool for scientific research in their own right. As a consequence of these limitations, other methods were employed to represent topographic data. As computers became more ubiquitous and their ability to process data efficiently increased, consideration was given to the representation and analysis of digital topographic information.

Vector representations of elevation data

Topographic analysis schemes which implemented digital contours and analysis of the data therein were implemented and retained favor amongst many workers due to their low memory requirements, allowing the analysis of large datasets. Applications were predominantly focused on hydrology with schemes to compute topographic and hydrologic properties from digital contours developed by a number of authors (e.g., O'Loughlin, 1986; Moore *et al.*, 1988). These schemes all employed digitized contour information taken from topographic maps and computed flow paths at tangents to contours spaced using either a fixed value or a landscape derived length scale computed as the ratio between the catchment area and the channel length (O'Loughlin, 1986). The intersections of these sets of contours and flow lines could then be computed and used to generate discrete polygons which represent patches of each drainage basin.

Digital contour-based elevation models were used to model catchment hydrology (Moore *et al.*, 1988; Moore and Grayson, 1991; Vertessy *et al.*, 1993), channel source areas (Montgomery and Foufoula-Georgiou, 1993), landslide hazard (Montgomery and Dietrich, 1994; Wu and Sidle, 1995) and erosion dynamics (Dietrich *et al.*, 1992). Such diversity of applications demonstrated the utility of representing a landscape as a series of discrete, hydrologically significant elements.

Initially, such systems had large advantages over gridded data due to the low memory requirements of storing contour data, and the better representation of catchment hydrology through flow lines and contours than regular grids (Wise, 2000). However, it is much more challenging to analyze contour data computationally due to the irregularity of the landscape units and many analyses had similar limitations to older analogue contour map based studies, but at a finer resolution. As the ability to generate and process gridded elevation data at finer resolutions increased, these limitations in the implementation of topographic analysis using digital contours became more pronounced and the use of gridded data became a de facto standard for researching the Earth's surface.

Another vector based method of representing elevation data within a computer to facilitate topographic analysis is the construction of Triangular Irregular Networks (TINs) (Peucker *et al.*, 1978). Although many authors considered these to be a more appropriate method of representing a surface than a gridded model (e.g., Moore *et al.*, 1991; O'Callaghan and Mark, 1984), the predominant vector-based topographic representation was digital contours, due to their perceived ability to break landscapes into hydrologically meaningful units, rather than abstract triangles (Wise, 2000).

Gridded data

An alternative method to store and study topographic information using computers was to store elevation values in gridded form, allowing elevation values to be stored as two dimensional arrays and calculations to be performed upon these regular data. This produces very large memory requirements for such data when contrasted with contour information, with no ability to readily scale the sampling frequency based on the complexity of the terrain, with some notable exceptions

which have failed to be adopted by the community at large due to the challenges inherent in implementing such schemes (e.g., Liu *et al.*, 2014).

The implementation of gridded elevation data is advantageous to geomorphic research due to the conceptual simplicity of the representation of elevation values as measurements regularly spaced in the x and y dimensions. Such a data structure is also readily incorporated into computer memory as a series of arrays, which allows the application of standard computing algorithms to manage data, in addition to the application of computer vision techniques such as edge detection (e.g., Marr and Hildreth, 1980; Canny, 1986; Perona and Malik, 1990), connected component labeling (e.g., Rosenfeld and Pfaltz, 1966; Samet, 1981; Dillencourt *et al.*, 1992) and the application of artificial light sources to generate shadows, commonly referred to as hillshading (e.g., Horn, 1981). Data stored in such a manner can provide a better representation of the true land surface as there is generally less interpolation performed on gridded data when contrasted with contour data of similar resolution (Casas *et al.*, 2006). However, the representation of networks such as channels in gridded data is inefficient when compared to vector based data models (Moore *et al.*, 1991). However this limitation can be overcome in part through the use of data structures such as quadtrees (Samet, 1984) or the construction of graphs (Braun and Willett, 2013).

Early digital topographic information was collected through the interpolation of elevation values manually derived from contour maps (Clarke *et al.*, 1982), which themselves were generated through manual photogrammetry or field surveying. These techniques produce an imperfect representation of an interpolated surface which itself is built upon discrete sampling of true elevation values. Such a method provides considerable abstraction were the digital data to be compared with the true landsurface. The implementation of such a method is also subjective and prone to operator errors, and challenging to perform on large areas due to time constraints (Hughes *et al.*, 1971; Horn, 1981).

As a consequence of such challenges, methods were developed and employed to automate the collection or interpolation of elevation values from stereo aerial photography and contour maps. Many stereocomparitors began to provide direct outputs of the elevation values being manually generated by their operator (Löscher, 1967; Hughes *et al.*, 1971), which allowed more accurate and rapid incorporation of elevation data into digital elevation models.

From as early as the 1960s work was being undertaken to automate the extraction of elevation data from stereo pairs of images, with the aim of rapid generation of digital topographic information and the reduction of subjectivity in data collection (Bertram, 1969; Horn, 1981; Chandler, 1999). Some of the earliest positive results from the automated stereo analysis of images came from the development of the United States National Elevation Dataset and the SPOT (Satellite Pour l'Observation de la Terre) global satellite (O'Callaghan and Mark, 1984; Moore *et al.*, 1991).

These data generation methods produced DEMs for the mainland United States (Moore *et al.*, 1991) and lower resolution global elevation coverage (Brockelbank and Tam, 1991), although the vertical accuracy of some derived products was limited (Giles and Franklin, 1996). Such automated and semi-automated stereo analysis of imagery to produce digital elevation models continues to this day, with increasing sensor resolution and computational power generating higher resolution, more accurate data products than were possible only a few decades prior. For a detailed review of the production and application of photogrammetry to DEM generation for geomorphic research see the review by Lane *et al.* (2000).

In locations where high resolution topographic surveys or aerial photography have been used to generate detailed contour maps, these maps are often used as a source for gridded topographic data (e.g., Moore *et al.*, 1991). Wise (2000) outlined four techniques which can be used to convert digitized contour lines into a regularly

spaced grid of elevation values: (1) Treat the contours as point samples and apply an interpolation to those points; (2) Calculate the line of steepest descent between each contour and interpolate along each profile; (3) Generate a TIN (Peucker *et al.*, 1978) from the contours and regularly sample the elevation values from the TIN surface; and (4) Fit a polynomial surface to the contours and sample elevation values from the fitted surface. There are a range of methods of interpolation which can be used to conform discrete elevation measurements, regardless of their source, to a regular grid and these are described by Clarke *et al.* (1982); Mitasova and Mitas (1993); Mitasova and Hofierka (1993) and Mitas and Mitasova (1999).

Such techniques formed the basis of the generation of many national elevation datasets, which are still used as key analysis datasets, particularly in areas where higher resolution elevation data have not been collected. Such data suffer from many of the same problems as manually interpolated elevation data from contour maps and the presence of contour artifacts in such datasets are common (Guth, 1999).

Through all these methods there has been a progression towards the ability to gather more accurate data at finer spatial scales, and with each innovation our ability to study the morphology of the Earth's surface is enhanced. The progression from digital contours to gridded elevation data has facilitated the development of efficient, quantitative topographic analyses. For the remainder of this thesis the term Digital Elevation Model (DEM) will be used solely to describe gridded data, and not the use of digital contours or other digital methods of representing elevation data.

Topographic analysis on gridded elevation data

Initial topographic analyses were predominantly focused on the development of tools to perform hydrologic operations on DEMs. An early problem which was identified in hydrologic research was the presence of pits or depressions within DEMs (Mark, 1984; Jenson and Domingue, 1988). Such features, which are considered to be processing artifacts in most cases (Martz and Garbrecht, 1998), are cells within a DEM which do not have a downslope neighbor, such that if hydrologic flow is routed into that pixel, the flow becomes trapped, and the generation of a complete drainage network from a DEM is not possible.

A simple approach to hydrologically correcting DEMs entails the smoothing or reinterpolation of topographic data prior to the operation of any hydrological processing (e.g., O'Callaghan and Mark, 1984; Hutchinson, 1989). However, such an operation will reduce the overall information content of the DEM (Tribe, 1992). Such processes are noted by Mark (1984) to improve the outcome of channel identification algorithms, by removing false positive channels, but at the expense of creating a disconnected channel network. Consequently, more direct algorithms for the identification and removal of pits have been developed, with the aim of only modifying topographic data where a pit is identified. The work of Poggio and Soille (2012) placed such pit correction algorithms into three broad categories, incremental algorithms which increase elevation values to remove pits, decremental algorithms which decrease elevation values and hybrid methods which aim to combine the two techniques to minimize alteration of the original topographic data (Figure 1.2).

Incremental algorithms operate by identifying depressions in the landscape and increasing the elevation value in each pit incrementally until flow can exit the depression (O'Callaghan and Mark, 1984; Jenson and Domingue, 1988; Soille

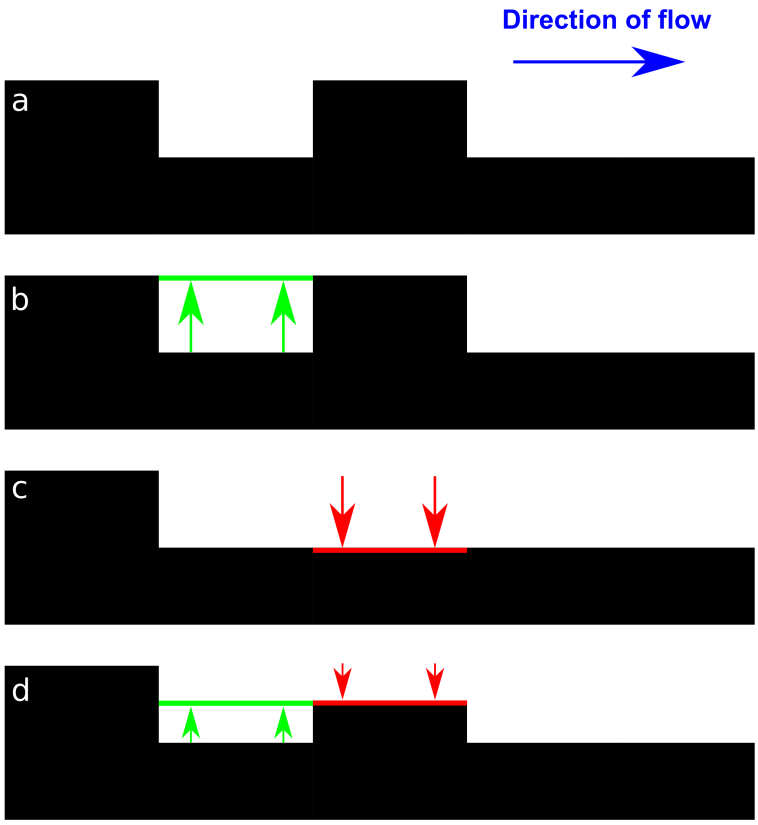

Figure 1.2: Schematic diagram of different categories of pit filling algorithms. **(a)** Simple representation of a pit to be filled, **(b)** Incremental, **(c)** Decremental and **(d)** Hybrid.

and Ansoult, 1990). Conceptually this is analogous to flooding the depression with water and mapping its outflow point (Martz and Garbrecht, 1998). This flooding technique is often preferred in landscapes where some pits may be natural features (Martz and Garbrecht, 1998) and due to its conceptual and computational simplicity a version of these algorithms has been implemented in many modern GIS and hydrology packages (Wang and Liu, 2006). Some of these algorithms do not directly modify elevation values, but rather create a flow pointer directing flow out of depressions in a downslope direction (Morris and Heerdegen, 1988).

Decremental algorithms operate in a similar manner to incremental algorithms,

but remove depressions by decreasing the elevation values of topographic obstructions in the downslope direction until the flow obstruction is removed (Martz and Garbrecht, 1998; Soille *et al.*, 2003). Such a technique is more complex to implement than the incremental method but produces hydrologically meaningful results with fewer flat areas generated (Soille, 2004a).

The hybrid method combines the two above techniques to attempt to minimize the alteration of the topographic surface in the generation of a hydrologically competent DEM. Such techniques have been proposed by Soille (2004b) and Lindsay and Creed (2005) and their effectiveness demonstrated (Poggio and Soille, 2012); however, their complexity means that the hybrid technique has yet to be adopted by many users.

With the generation of a hydrologically competent DEM, the calculation of overland flow properties can be undertaken. In most cases this involves the calculation of flow direction and the subsequent partitioning of flow across the topographic surface to calculate the upslope contributing area of each pixel in the grid.

A method for determining channelized portions of a landscape was developed by Peucker and Douglas (1975) which performed comparisons between each cell and its 4 cardinal neighbors, marking the highest elevation cell in each kernel. Once each cell in the DEM has been compared, the points which are not marked are considered to be the channelized points of the the landscape.

This method, denoted D4, is recognized by Mark (1984) to produce extensive pits and disconnected flow paths, and by Shelef and Hilley (2013), to produce angular flow paths following cardinal flow directions. The development of the D8 or steepest descent algorithm by O'Callaghan and Mark (1984) rectified many of these problems by directly considering the elevations of the 8 cell neighborhood

surrounding each pixel. Several variations of this algorithm exist, the most common being one which identifies the neighbor with the lowest elevation relative to the center cell and allocates flow into that cell (Mark, 1984; O'Callaghan and Mark, 1984; Tarboton *et al.*, 1991). Other schemes extend this process by implementing rules to account for neighborhoods which have 2 or more cells with equal minimal elevations (e.g., Jenson and Domingue, 1988), a problem which is particularly apparent when working with integer elevation data.

Of these two methods, the D4 algorithm is rarely employed, whereas the D8 algorithm is adopted by most modern GIS packages and is employed in many models of fluvial incision (e.g., Braun and Willett, 2013). The use of a D8 algorithm results in flow being partitioned at 45 degree angles, following the centers of each of the 8 neighborhood cells; this simplification allows for more efficient computation, at the expense of the accuracy of the modeling of true hydrology (Figure 1.3).

This problem was recognized by Lea (1992) who computed the flow direction for each pixel using pixel aspect, routing flow as a point source within each pixel. Such an algorithm has been extended by Hurst *et al.* (2012) to model flow across hillslopes in high resolution topography. Tarboton (1997) designed a new algorithm, based upon the work of Lea (1992), designated D∞, which fitted triangular planes to the centers of a 9 cell neighborhood and calculated the surface slope of each plane. The aspect of the plane with the steepest gradient designates the flow direction, reported as a real number between 0 and 2π. If the flow direction crosses more than one pixel as it is projected along the axis of the triangular plane, the flow is partitioned into both cells. Such an algorithm is more readily implemented on large gridded datasets and ensures that anomalous high elevation values do not unduly affect downslope flow directions, as can be the case with the Lea (1992) algorithm.

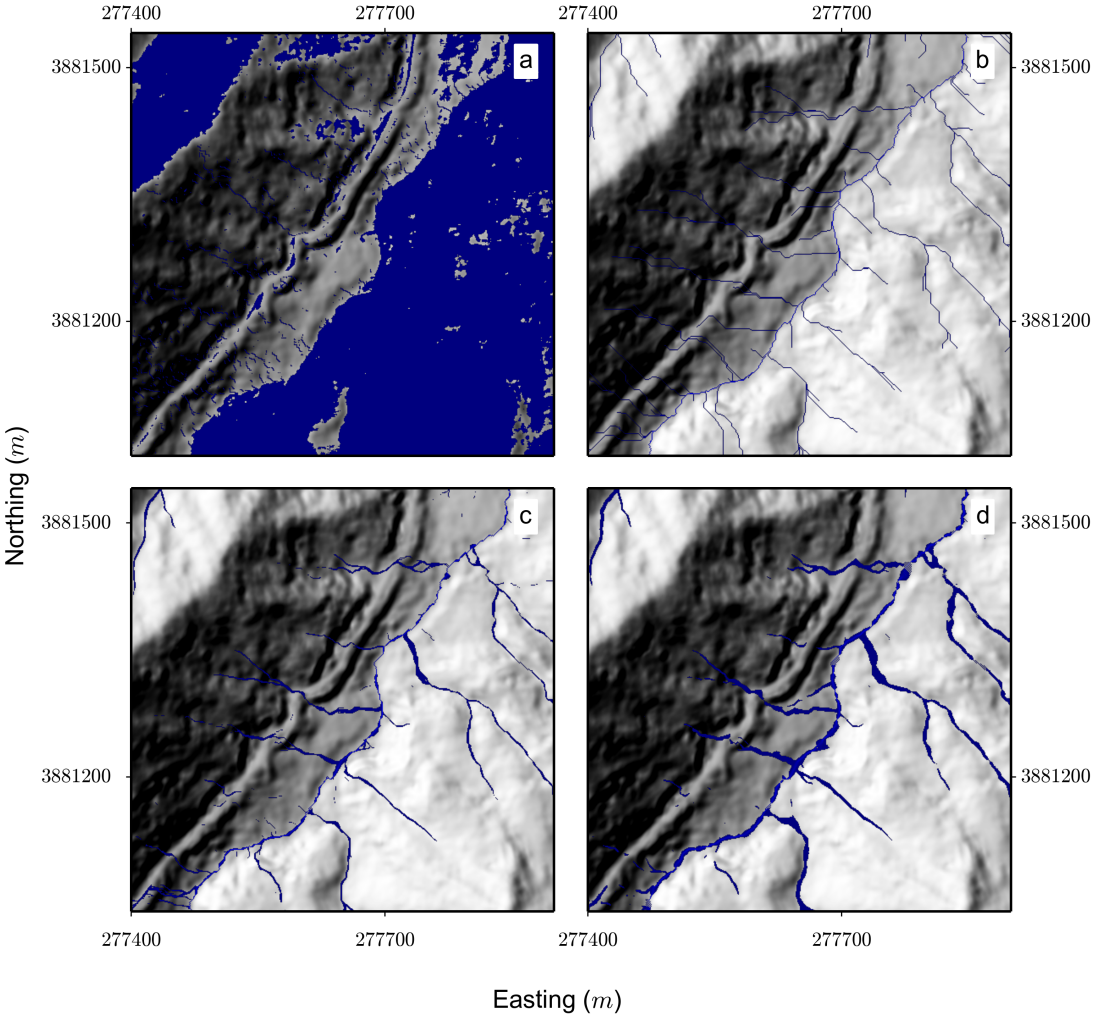

Figure 1.3: Examples of four flow routing methods, applied to a section of Coweeta, North Carolina. **(a)** D4, **(b)** D8, **(c)** D∞ and **(d)** MD. The large blue patches in **(a)** correspond to large areas of false positives, not to a prediction of large bodies of water.

Each of the methods discussed above generates broadly convergent flow paths and forces channelized flow, even on divergent hillslopes. Due to this limitation multiple direction flow routing algorithms, known as MD, were developed by a number of authors. In general, such algorithms work in a similar manner to the D8 method, whereby the elevations of the 8 neighbors of the cell of interest

are compared to the center cell. However instead of choosing the cell with the steepest gradient into which to apportion flow, every downslope cell receives a share of the upslope contributing area, proportional to its contribution to the sum of the elevation differences between the center cell and its eight neighbors. This approach was presented by Quinn *et al.* (1991) and Freeman (1991), where the only difference in their algorithms was the correction factor applied to the flow accumulation values to account for the inherent bias in allocating flow using a square grid. It is also possible to implement a variation of either of these algorithms which only disperses flow between the 2 lowest elevation neighbors, although such a scheme, designed to minimize computational complexity, does not markedly change the resulting channel networks.

Determining the upslope contributing area and the flow directions for each pixel can yield a channel network based on a threshold drainage area being used to identify areas of concentrated flow which correspond to channels (O'Callaghan and Mark, 1984; Band, 1986; Tarboton *et al.*, 1991). This channel identification scheme produces contiguous channels without further processing, unlike the methods of Peucker and Douglas (1975) and consequently has been adopted as the de facto standard channel extraction technique in GIS software packages. However, such a concept of a constant support area for a channel assumes that stream power and hydraulic scaling are the only factors which influence channel incision (Tarboton *et al.*, 1991). Yet it has long been recognized that such a scheme cannot truly represent the initiation points of channels in a landscape due to the complexity of the processes identified as influencing the location of a channel head. Montgomery and Dietrich (1989) noted that the channel head's location will be defined by the maximum upslope extent of fluvial incision, which is a function of climate, vegetation and lithology (Montgomery and Foufoula-Georgiou, 1993; Tucker and Bras, 1998), factors which can all vary at the hillslope scale.

Scaling relationships between the order of a channel and the change in elevation

from the source to the outlet of the channel were first presented by Horton (1932, 1945) and formalized by Broscoe (1959). This relationship, described as 'the law of constant drop' has the potential to allow the calibration of threshold drainage areas by varying the density of the channel network iteratively until the optimal scaling relationship can be identified. Tarboton *et al.* (1991) tested such concepts using digital topographic data against the channel extraction method presented by (Peucker and Douglas, 1975) and found that the constant drop method provided more reliable channel networks, although resolution limitations were identified and further research is required to understand if such relationships hold across the range of resolutions presently available for study. Such relationships have the potential to provide wide scale insights into the distribution of channel networks; however, their focus on stream hydraulics in the derivation of the scaling relationship does not consider the diverse processes operating on landscapes at a range of scales and the importance of hillslope processes in setting and maintaining a given drainage density (Montgomery and Foufoula-Georgiou, 1993; Tucker and Bras, 1998).

A refinement of the simple area-based scaling to identify channel initiation points comes from the inclusion of a measure of topographic gradient within the calculations. Plots of local slope against upslope contributing area were used by many workers to demonstrate the presence of a signature of fluvial incision whereby gradient decreases as contributing area increases (Montgomery and Dietrich, 1988, 1989; Dietrich *et al.*, 1992; Dietrich and Dunne, 1993). Thus it was possible to use an area-slope product in place of an area as the threshold for channel extraction. Such ideas make sense conceptually, with drainage area and gradient both appearing to be appropriate metrics of the first order controls on the extent of fluvial incision in a landscape (Tucker *et al.*, 2001), an observation also supported by field evidence (Montgomery and Dietrich, 1988, 1989). However, such a scaling law has been shown to be unable to distinguish between high

gradient threshold hillslopes and fluvial channels in landscapes with a large amount of exposed bedrock (Montgomery and Foufoula-Georgiou, 1993).

With the advent of gridded topographic data the calculation of topographic derivatives was streamlined, with grid based approaches allowing local variations in gradient, curvature and aspect to be computed efficiently for the first time. A large number of approaches to generating these derivatives has been developed, and such methods have been evaluated in detail by Skidmore (1989) and Schmidt *et al.* (2003).

The simplest method to calculate aspect and gradient was to compute the direction and magnitude of the maximum change in elevation within an 8 cell window around the cell of interest (Travis *et al.*, 1975). Second and third order finite difference methods were proposed using a 4 (Fleming and Hoffer, 1979) and 8 cell neighborhood (Horn, 1981). In addition to these techniques, the generation of topographic derivatives through the fitting of polynomial surfaces to a moving window of elevations using multiple linear regression has been proposed (Travis *et al.*, 1975; Evans, 1980; Zevenbergen and Thorne, 1987) and has become the most common method employed in modern geomorphic research (Schmidt *et al.*, 2003).

Applications of topographic analysis

Quantitative interrogations of the surface of the Earth have resulted in a range of techniques to constrain rates of erosion and other processes at a range of scales, from individual outcrops (Gosse and Phillips, 2001) or hillslopes (Hales *et al.*, 2012), to catchment or landscape average rates (Mudd *et al.*, 2016). Such measurements can come from the use of natural chronographies such as tree rings (e.g., Bollschweiler *et al.*, 2007; Stoffel and Bollschweiler, 2008), historical data for

more recent rates of erosion (Perroy *et al.*, 2012, 2010), through the measurement of the rate of decay of radioactive isotopes (e.g., Brown *et al.*, 1995; Granger *et al.*, 1996; Bierman and Steig, 1996) or through the use of stratigraphy to date uplift rates and associated rates of river incision (Lavé and Avouac, 2001).

Studies of topographic data in conjunction with such measurements have generated a number of techniques which can be used to estimate rates of forcing between hillslopes, catchments and landscapes, often with a particular focus on erosion rates and tectonics. Such techniques have the advantages of being rapidly applied with little or no a priori knowledge of a landscape required, allow direct comparisons between landscapes, can give a very high spatial resolution and have much lower costs associated than field and laboratory based estimates of erosion rates. Such techniques can also be used as a preliminary technique to focus more detailed research in future, facilitating more targeted use of resources to solve interesting geomorphic problems.

The tectonic and erosional history of landscapes can be estimated through the analysis of river long profiles. An index of channel steepness, calculated by normalizing channel slope for drainage area (Snyder *et al.*, 2000; Kirby *et al.*, 2003, 2007), will increase with erosion rate assuming bedrock incision can be described by the stream power law (Whipple and Tucker, 1999). This relationship has been demonstrated to be nonlinear when averaged across drainage basins (DiBiase *et al.*, 2010; Ouimet *et al.*, 2009) and has seen particular utility when considering variations in erosion rate across large spatial areas (e.g., Ouimet *et al.*, 2009; DiBiase *et al.*, 2010; Kirby and Ouimet, 2011). Such relationships have been shown to be able to discriminate changes in erosion rate between sections of landscapes where the hillslopes have become decoupled from the channel network (Cyr *et al.*, 2010) or the hillslopes are too steep to apply either hilltop curvature or mean basin slope (DiBiase *et al.*, 2010).

Ouimet *et al.* (2009) used 30 meter resolution topographic data to consider channel steepness, mean basin slope and mean basin channel slope for eastern Tibet, and contrasted hillslope and channel response to changing erosion rates. This demonstrated the utility of channel steepness over hillslope metrics to infer erosional histories in landslide dominated, tectonically active mountain ranges. Snyder *et al.* (2000) also employed 30 meter topographic data to an area of variable uplift, determined through marine terrace dating, along the California Coast. Channel steepness was demonstrated to correlate with uplift rate; however the erodibility coefficient of the stream power law was shown to be spatially variable whilst channel concavities remain uniform across the uplift field. Such work demonstrated a key limitation in the analysis of landscape evolution through the study of channel properties alone, suggesting that in many landscapes a combined analysis of hillslopes and channels may yield better results. Work to understand the deformational and tectonic history of a section of the San Andreas Fault utilized both analysis of hillslope morphology and channel steepness running along the Bolinas Ridge to outline spatial variations in uplift, correlated with a transition to mass wasting at a threshold hillslope gradient (Kirby *et al.*, 2007). However, the authors acknowledge the limitation of using 10 meter resolution data for such analysis, with much of the hilllsope variability occurring across very few pixels.

An alternative method, termed the χ method, has also been proposed (Royden *et al.*, 2000; Perron and Royden, 2013) which performs a coordinate transformation upon river long profiles, to normalize values for drainage area. In a steady state landscape, all river channels will collapse onto the same line in χ-elevation space, and in more complex landscapes channels eroding at different rates, for example above and below a knickpoint, will have different gradients. A technique to identify such segments statistically was developed by Mudd *et al.* (2014) which facilitates the identification of variations in erosion rate across landscapes

through the analysis of topographic information collected from channels. Such analysis has been applied to map the geomorphic impact of extreme flood events in the Himalaya, providing a general predictor of areas of erosion and deposition directly from topographic data (Devrani *et al.*, 2015).

Both of these methods can only operate in landscapes where the stream power law can be applied, and this is not a uniform assumption (e.g., Lague, 2014) and as such the use of hillslope based measures of erosion rate estimation from high resolution topography may be more suited to a wider range of landscapes than these channel steepness indexes.

Many studies have employed topographic data, typically in conjunction with other lines of evidence in attempts to disentangle controls on the development of mountain ranges, with climate, tectonic and lithological variations operating at varying spatial and temporal scales. Due to the limits of studying hillslope morphology using low resolution data, acknowledged by Kirby *et al.* (2007), much topographic analysis was performed at the orogen scale, considering wide scale patterns in topography, with the aim of identifying large scale geomorphic processes. Burbank *et al.* (1996) employed topographic data in conjunction with dating of strath terraces and apatite fission-track dating to correlate uplift and incision rates in the northwestern Himalayas. It was demonstrated that at the scale of the mountain front the geometry of hilllsopes is set by a threshold incision rate, which governs the transition from creep dominated to bedrock landslide dominated hillslope denudation.

Gabet *et al.* (2004) performed analysis of rainfall and topographic data, at a higher resolution than available to Burbank *et al.* (1996) to demonstrate that mean topographic gradients decrease as rates of rainfall increase across the Himalaya. This is suggested to be due to bedrock being weakened through increases in pore pressure and rates of chemical weathering. Consequently, the generation

of topographic relief in such mountain ranges can be driven by climate, assuming a homogeneous lithology.

A climatic gradient running along the western Andes was employed by Rehak *et al.* (2010) to explore the generation of relief across a large mountain front. Along this transect the tectonic conditions are generally consistent whilst rainfall and glaciation vary significantly. By measuring the properties of 120 basins running along the mountain front, a reduction in relief and elevation with increasing glacier extent and increasing rainfall was demonstrated, a similar result to that of Gabet *et al.* (2004) working in the Himalaya. Working on the same mountain range, Trauerstein *et al.* (2013) performed similar morphometric analysis of basins along the climate gradient to suggest a threshold level of precipitation of approximately 400 mm yr^{-1} above which hillslope weathering matches or exceeds channel incision and below which channel incision dominates over hillslope weathering: this leads to changes in the rate of landscape adjustment to constant tectonic forcing. However, in the San Bernadino Mountains of California no relationship between precipitation and erosion rate is observed, with changes in erosion rate attributed to differing rates of tectonic uplift across the San Andreas Fault (Binnie *et al.*, 2010).

A topographic signature of lithology was identified by Korup (2008), who analyzed slope distributions of the mountains of New Zealand in conjunction with measures of landslide density and uplift rate. Each of the studied sites exhibited a range of uplift rates, annual precipitation and landslide density, and yet, it was demonstrated that the modal hillslope gradient from each study location was consistent, suggesting a lithological control on the gradient of threshold hillslopes in landslide dominated terrain and that the material properties of the bedrock are the most important factor in setting hillslope properties in mountainous landscapes.

1.2.4 High resolution topography

LiDAR acquisition

In the latter part of the 20th century a revolution in the collection and analysis of topographic data was instigated with the early application of Light Detection and Ranging (LiDAR) technology to collect high resolution topographic measurements (Roering *et al.*, 2013). The technology behind LiDAR was initially very expensive to acquire and run, resulting in small study areas collected for private enterprise or government applications (Carter *et al.*, 2001). The University of Florida and Florida International University became the first academic institutions to employ a LiDAR instrument for the purpose of Earth science research (Carter *et al.*, 2001). The potential of such systems was rapidly understood by the geomorphology community at large and the National Center for Airborne Laser Mapping (NCALM) was established shortly thereafter in the USA to coordinate the collection of LiDAR data for research purposes and the development of new LiDAR technologies (Roering *et al.*, 2013).

LiDAR data are typically collected from airborne platforms, such as planes, helicopters or unmanned aerial vehicles (UAVs) where an active sensor is mounted, firing high frequency laser pulses at the landsurface. The pulse travel time between the sensor and the landsurface is computed and converted into a distance, which can be used to provide an elevation against a fixed datum (Carter *et al.*, 2001). Early sensors operated at rates of 1000s of pulses per second and increased by an order of magnitude over the next few years (Slatton *et al.*, 2007) with current sensors now achieving a sampling frequency in excess of 150 000 pulses per second, translating to point densities exceeding 10 points per square meter in ideal use cases (Roering *et al.*, 2013). In addition to the increases in sampling frequency achieved in the last decade, the accuracy of the collected data has been enhanced

with improved GPS technology used to better constrain flight paths and platform orientation relative to the ground, to ensure that collected data are not impacted by turbulence or other factors affecting the stability of the data collection platform (Slatton *et al.*, 2007).

The development of smaller scale ground based Terrestrial Laser Scanners (TLS) has allowed even higher shot density surveys to be carried out at the local scale. Due to the proximity of the TLS to the objects to be scanned, much higher resolution measurements are possible with 1000s of points per square meter over kilometer scale areas or millimeter scale point density over meter scale areas (Hodge *et al.*, 2009). Such data collection can be time consuming but many techniques are now automated, rapidly increasing the rate and volume of data which can be collected (Heritage and Hetherington, 2007). Such techniques allow lower cost repeat measurements to be performed to compute the volume and magnitude of rapid changes to the Earth's surface, than can traditionally be undertaken using airborne platforms (e.g., Rosser *et al.*, 2005).

Both terrestrial and airborne platforms yield similar data, differing only in the spatial extent, and spatial and temporal resolution at which they are collected. Throughout this thesis the data employed are all collected by airborne platforms, to allow large scale landforms to be studied, and as such most of the literature reviewed below regards airborne LiDAR; however the techniques and concepts discussed can be applied to any high resolution topographic data, regardless of the method of collection.

From either terrestrial or airborne platforms the collected point cloud data need to be processed to identify the landsurface prior to any topographic analysis being performed. Typical processing involves the removal of erroneous data points such as those generated by birds flying between the sensor and the ground and the filtering of the point cloud into ground and non-ground points (Meng *et al.*,

2010). Ground returns can be identified manually although this is a very time consuming process so in most cases automated processes are used. The simplest filter to be applied keeps only the first return, attempting to remove data from laser pulses scattered by vegetation or other obstructions (Meng *et al.*, 2010). More sophisticated algorithms apply spatial filters to point cloud data to identify rapid changes in elevation or gradient between points within a search radius, indicative of non-ground features such as vegetation or buildings (e.g., Zhang and Whitman, 2005; Meng *et al.*, 2009). Evans and Hudak (2007) demonstrated an algorithm which iteratively filters points based on surface curvatures until a bare earth point cloud remains: this method is particularly designed to produce bare earth data in heavily forested environments. Meng *et al.* (2010) reviews several methods of point cloud classification and shows that the classification scheme used is dependent on the morphology of the landscape, the vegetation properties and the resolution of the survey and output data.

Once a point cloud has been classified into ground and non-ground points the ground returns can be processed into a bare earth DEM. This is performed using similar interpolation methods as were used to grid point measurements extracted from photogrammetry discussed in Section 1.2.3. One difference between modern techniques and previous methods is the volumes of data now being processed, with point clouds containing millions of points commonly being generated and analysed. Consequently, highly efficient algorithms have been developed (e.g., Kim *et al.*, 2006) which employ a local binning approach to grid large point clouds rapidly via a spatially indexed data structure.

Since the first applications of LiDAR data in a research environment almost two decades ago, the quality and availability of high resolution topographic data have increased exponentially (Roering *et al.*, 2013). Many states in the USA have statewide LiDAR holdings (e.g., Haugerud *et al.*, 2003) and the OpenTopography portal (Krishnan *et al.*, 2011) provides free access to topographic data from across

the USA. In the UK, data availability is more limited, with the Environment Agency providing free access to data covering large areas of England and Wales, whilst in Scotland similar data collected by the Scottish Government remains behind a paywall.

High resolution topographic analysis techniques

Working with data which are in many cases an order of magnitude higher resolution than that which was typically available prior to the acquisition of LiDAR data yields new challenges. Many algorithms which were developed for 30 meter data become unsuitable for use on high resolution data, without modification.

Higher resolution data leads to finer scale features being resolved on the landsurface, which can impact flow routing due to the roughness of a surface increasing flow length (Dunne *et al.*, 1991; Thompson *et al.*, 2010), or the measurement of more pits or obstructions which need to be corrected (Poggio and Soille, 2012). The increase in the volume of data being processed creates a decrease in the signal to noise ratio, as it has now become apparent that low resolution data can often act as a smoothing filter, and techniques which yield clear trends on 30 meter data fail to be reproduced when using LiDAR datasets. Such issues have led to attempts to understand how best to filter topographic data (Milledge *et al.*, 2009).

Another challenge in using high resolution data is that their processing requires more memory and compute power, so that algorithms often cannot simply brute force a solution. This results in the requirement to produce computationally efficient algorithms such as the Fastscape algorithm to solve the stream power law across large DEMs (Braun and Willett, 2013), the parallelization of other

algorithms (e.g., Tesfa *et al.*, 2011; Qin and Zhan, 2012; Schwanghart and Scherler, 2014) and the implementation of efficient data structures (e.g., Han *et al.*, 2012) to allow topographic analysis to be implemented more rapidly on ever larger datasets.

One key aspect of topographic analysis which has changed markedly with the transition to LiDAR data is the identification of the source areas of channel networks. It is now possible to resolve the topographic signature of channel heads, which generally exist at the meter scale (Clubb *et al.*, 2014), rather than infer the density of the channel network through assumptions regarding a critical area or area-slope threshold which can be applied across a landscape.

Modern channel extraction techniques can be broadly grouped into two categories: process based methods which attempt to identify a signature of a process transition between hillslope and fluvial processes; and geometric methods which attempt to identify a morphometric signal of channel initiation, typically through the analysis of topographic curvature measurements.

The geometric method proposed by Passalacqua *et al.* (2010) first filters the DEM using the nonlinear diffusive Perona-Malik filter (Perona and Malik, 1990), which smooths small scale topographic roughness whilst preserving the signal of channel incision. The properties of quantile-quantile plots of curvature are used to identify a tangential curvature threshold which is then applied to the landscape to identify channelized portions of hillslopes. The uppermost extents of these portions are then defined as the channel heads, corresponding to points on a landscape where a fluvial erosion threshold has been crossed.

The method outlined by Pelletier (2013) is similar to that of Passalacqua *et al.* (2010) in that it employs a tangential curvature threshold to identify channelized portions of the landscape. Pelletier (2013) applies an optimal Wiener filter

(Wiener, 1949) to the topographic data in order to amplify the signal of large scale channels against the signal of high frequency noise. Once the data have been filtered and the tangential curvature calculated, areas with a positive curvature are flagged as channels and negative curvature as hillslopes. This initial step produces the outline of the valley network, including unchanneled colluvial valleys; this is subsequently filtered using a user defined tangential curvature threshold to identify the fluvial portion of the landscape, and this extracted network can be considered to be theoretically equivalent to the network generated by Passalacqua *et al.* (2010).

Sofia *et al.* (2011) demonstrated an additional method of channel extraction, which utilizes a measure of topographic openness to identify concave portions of the landscape. Topographic openness was defined by Yokoyama *et al.* (2002) and describes the proportion of the sky visible from a point on the landscape, in a similar manner to topographic shielding calculations performed during cosmogenic radionuclide analysis (Codilean, 2006). The algorithm designed by Sofia *et al.* (2011) identifies areas of a landscape which have high openness and curvature values and employs a modified implementation of the Quinn *et al.* (1991) flow accumulation algorithm to identify areas of the landscape with the highest likelihood of being true channels. These patches of probable channelization are then filtered using a majority filter, which systematically removes outlying values within the search window, and connected using a connected component algorithm to generate a contiguous channel network.

The analysis of slope-area relationships has continued to be used to identify the hillslope fluvial transition, with algorithms now refined to compute drainage area and local slope at the meter scale for individual catchments, exploiting the high resolution nature of topographic data (e.g., Tarolli and Dalla Fontana, 2009). As elegantly demonstrated by Montgomery and Foufoula-Georgiou (1993), in upland catchments the local slope will increase with drainage area whilst

hillslope processes dominate and when these processes are out competed by fluvial processes slope will decrease whilst drainage area increases (Figure 1.4). Such plots, described as having a 'boomerang' shape by Roering *et al.* (2007), can be used to identify the threshold slope-area scaling for a landscape (e.g., Istanbulluoglu *et al.*, 2002; Jefferson and McGee, 2013) through the identification of the kink in the boomerang, either through a visual inspection of the plots or an algorithmic analysis of the data (Montgomery and Foufoula-Georgiou, 1993; Hancock and Evans, 2006; Tarolli and Dalla Fontana, 2009). Many authors have specific workflows to identify this transition, many of which are challenging to reproduce due to limited documentation or the availability of data. Hence the method described here is the standardized technique employed using open source software by Clubb *et al.* (2014).

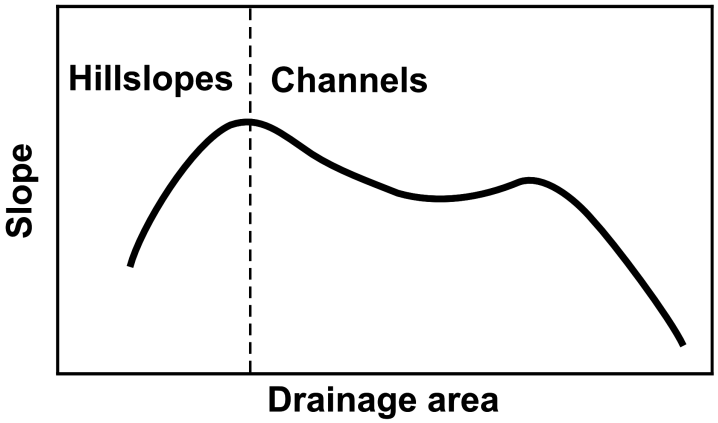

Figure 1.4: Schematic diagram of the theoretical relationship between local slope and drainage area. The dashed line denotes the transition from hillslopes to channels. Drainage area increases from left to right and slope increases from bottom to top.

Local slope and drainage area, computed using the D∞ algorithm of Tarboton (1997), are placed into logarithmically spaced bins, typically with a spacing of 0.1 in base 10 logarithmic space. A cubic spline is then fitted to the binned data points and the slope and area values of the point with the largest slope value are recorded. The product of the slope and area values at the identified inflection

point is then used to identify points on the landscape which exceed this threshold, which can be denoted as the channel network.

A new process based method for the identification of channel heads was proposed by Clubb *et al.* (2014), which operates by transforming river profiles into χ-elevation space employing the methods described by Royden *et al.* (2000) and Perron and Royden (2013). The algorithm first identifies concave portions of the landscape following the procedures of Pelletier (2013) to filter the DEM and the method of Passalacqua *et al.* (2010) to identify a curvature threshold. From the patches of curvature, a connected components analysis (He *et al.*, 2008) is performed to generate a contiguous network which is thinned using the skeletonization algorithm of Zhang and Suen (1984). For each of the first order channels identified the χ-elevation transformation (Royden *et al.*, 2000; Perron and Royden, 2013) is employed using the software released by Mudd *et al.* (2014). Theory states that in χ-elevation space rivers will plot as linear segments and hillslopes will have nonlinear profiles (Figure 1.5), and so the technique of Clubb *et al.* (2014) identifies this transition between hillslope and channel as the upstream limit of fluvial incision.

Alongside channel head identification, other landscape features which could previously not be resolved can now be studied directly though the use of LiDAR data and quantitative topographic analysis. A common aspect of such work is the application of feature detection to rivers with the aim of automating the measurement of channel geometries, allowing more accurate hydrological modeling to be applied.

LiDAR derived high resolution topography has been applied to river networks in the support of qualitative mapping of landforms, with the aim of improving the accuracy and rate of mapping of large rivers (Notebaert *et al.*, 2009). More quantitative efforts to measure landforms using LiDAR data have resulted in

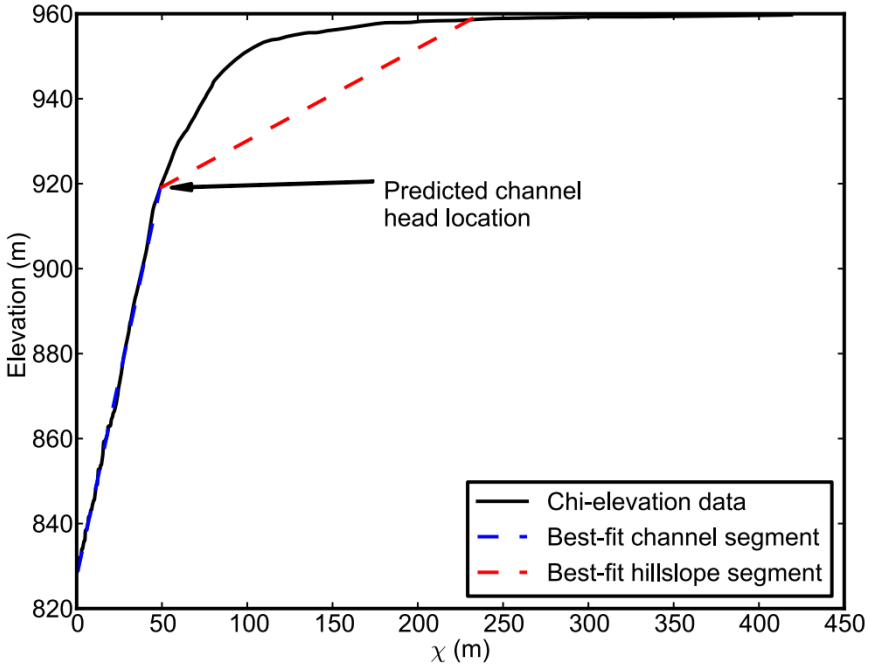

Figure 1.5: Diagram of the channel-hillslope transition in χ-elevation space. After Clubb *et al.* (2014).

measurements of floodplain geometries (Jones *et al.*, 2007). Trevisani *et al.* (2010) attempted to identify and categorize channel bed features, such as steps, pools and boulder cascades, finding that the ability to identify such features in channels was largely dependent on the scale of the feature and the resolution of the topographic data. More efforts to map channel bed features were described by Cavalli *et al.* (2008) who employed an index of surface roughness to differentiate between riffle and step pool reaches of rivers. Vianello *et al.* (2009) tested methods of deriving channel slope in headwater channels and found that LiDAR can be used to measure channel gradients accurately, as long as the overall channel morphology, such as the channel width, is considered within the slope analysis. Work to understand the relationship between channel width, and other hydraulic properties has also been aided through the use of LiDAR data (Sofia *et al.*, 2015). Such work presented a technique to extract the width of river channels from high

resolution topography, which was validated using field measurements, and shown to operate best under bankfull conditions.

James *et al.* (2007) employed LiDAR topographic data to map the extent of modern gullying under dense forest canopy in South Carolina, USA. It was demonstrated that high accuracy maps of gullying could be developed, which were tested using field surveys; however, no reliable morphometric information could be derived from the surface model due to the level of processing and filtering applied to the raw point cloud data in order to remove the forest canopy.

Rates of river bank erosion and the consequent alteration of channel morphology were studied by Thoma *et al.* (2005) and De Rose and Basher (2011) through the use of time series of topographic data. Thoma *et al.* (2005) employed two airborne LiDAR surveys one year apart to demonstrate the effectiveness of such surveys to quantify the rates of bank erosion and to estimate the volume of sediment input to the river. De Rose and Basher (2011) employed similar methods using a modern LiDAR survey and a historical DEM generated using aerial photography to quantify rates of bank erosion and other changes in river morphology over an approximately 50 year timescale. These studies highlighted the power of high resolution topography used in conjunction with repeat measurements to facilitate topographic analysis which can detect rapid changes in the Earth's surface.

Combinations of LiDAR and bathymetric data have been employed to better understand the full geometry of channels. Legleiter (2012) describes a complete framework for the integration of LiDAR and optically remotely sensed data to measure fine scale morphometric variations not only in overall channel morphology, but also the structure of channel beds. McKean *et al.* (2008, 2009) employed green LiDAR, the pulses of which can penetrate shallow water, to map river channels and their surrounding floodplains directly, and use the results to aid in the mapping of salmon habitats.

A key development in recent topographic analysis has been the application of LiDAR data to engineered landscapes, with the aim of understanding the scale and topographic signature of surface alterations caused by humans (Hooke, 2000). In an extensive review of the literature Tarolli and Sofia (2016) break such human alterations into three broad categories: mining, roads, and agriculture.

Francioni *et al.* (2015) and Salvini *et al.* (2015) used a combination of TLS derived DEMs and stereo images collected using UAVs to produce 3D stress field maps of engineered surfaces in an open pit mine. Slope stability was also considered in the area around open pit mines by Hancock *et al.* (2015) who created models of long term slope stability on engineered slopes using DEM data. The long term impact of sand mining on the California coast was quantified through the use of a time series of LiDAR surveys which showed the rate of coastal retreat in areas of former mining activity (Thornton *et al.*, 2006). In locations where coal mining has taken place, subsidence is a common hazard, and through the use of repeat LiDAR surveys with a 2 year return frequency areas of rapid subsidence can be identified (Palamara *et al.*, 2007).

The identification of roads from high resolution digital topography can be an important procedure in areas where maps do not exist. Sherba *et al.* (2014) demonstrated the identification of logging roads against field mapped roads using a slope comparison method. Tarolli *et al.* (2013) described an index of the impact of roads and trails on surface flow through the comparison between smoothed and unsmoothed sections of high resolution topography where roads were present. Another index used to identify areas of high anthropogenic influence such as roads and buildings has been developed through the analysis of the spatial autocorrelation of topographic gradient measurements (Sofia *et al.*, 2016).

The spatial autocorrelation of slope measurements was also applied to the study of agricultural terraces by Sofia *et al.* (2014). It was demonstrated that

using this measure two differing morphologies of terraced landscapes in southern and northern Italy could be discriminated from unterraced landscapes through the analysis of high resolution LiDAR data. The impact of such agricultural terraces on rates of soil erosion was considered through the use of high resolution topographic data in a review by Tarolli *et al.* (2014) who described the best practices for the use of LiDAR data in the management and monitoring of erosion on terraced hillslopes. Vineyard terraces are specifically considered for their role in erosion by Tarolli *et al.* (2015) whereby the index described in Tarolli *et al.* (2013) is applied to terraces and associated agricultural roads to quantify the rates of soil loss and land degradation associated with such terraces.

Passalacqua *et al.* (2012) present a method to identify channels in flat, typically engineered, landscapes such as agricultural areas where traditional channel extraction techniques do not perform well. Such information is vital in the calculation of soil loss and erosion in agricultural areas although the presence of anthropogenic features such as bridges and weirs presents challenges in the processing and interpretation of such datasets.

LiDAR data can also be used to understand natural surface deformations caused by volcanoes through the generation of high resolution surface models. Such LiDAR data can be used to identify areas of surface deformation and compute the volumetric change of the surface through time (Favalli *et al.*, 2009) or it can be used to map or predict the extents of lava flows (e.g., Bisson *et al.*, 2009). Of particular interest with regard to the study of volcanoes is the ability to use LiDAR to map crater and deposit morphologies in remote areas (Deardorff and Cashman, 2012). As the availability of LiDAR platforms and data increase, novel applications will continue to be found. For example, Shaw *et al.* (2005) outline a methodology employing LiDAR to track landmine detecting honey bees. Through renewed ability to identify and quantify features on the surface of the Earth, a

wide range of geomorphic questions can now be answered at a larger scale than ever before through the use of LiDAR data and topographic analysis.

Applications of high resolution topographic analysis

Through the use of topographic analysis techniques applied to high resolution LiDAR data, signatures of the processes acting upon the Earth's surface can be identified and the properties of such processes can be quantified at a range of spatial and temporal scales. Topographic analysis has been employed, in conjunction with field, experimental and laboratory evidence, to provide insight into the nature of hillslope sediment transport (e.g., Roering *et al.*, 1999, 2007), tectonics (e.g., Hilley and Arrowsmith, 2008; Hurst *et al.*, 2013b), weathering processes (e.g., Roering *et al.*, 2010; Booth *et al.*, 2013) and rates of erosion (e.g., Hurst *et al.*, 2012; Clubb *et al.*, 2016).

Sediment flux

The nature of hillslope sediment flux (cf. Dietrich *et al.*, 2003) has been explored through the topographic predictions made by flux laws in a range of settings. The rate of hillslope sediment flux controls how landscapes respond to forcing, sets the morphology of hillslopes in soil mantled landscapes, and is a key component of landscape evolution models. The simplest sediment flux law, proposed qualitatively by Gilbert (1877) and formalized mathematically by Culling (1960) states that the rate of sediment flux is linearly proportional to hillslope gradient (Figure 1.6). Several studies have tested this hypothesis, using measures of topographic gradient to demonstrate a linear relationship between these two parameters (McKean *et al.*, 1993; Small *et al.*, 1999). However, these tests were performed at predominantly low hillslope gradients, and on high

gradient landscapes the morphology of hillslopes was observed not to conform with predictions made by a linear sediment flux model (Roering *et al.*, 2001).

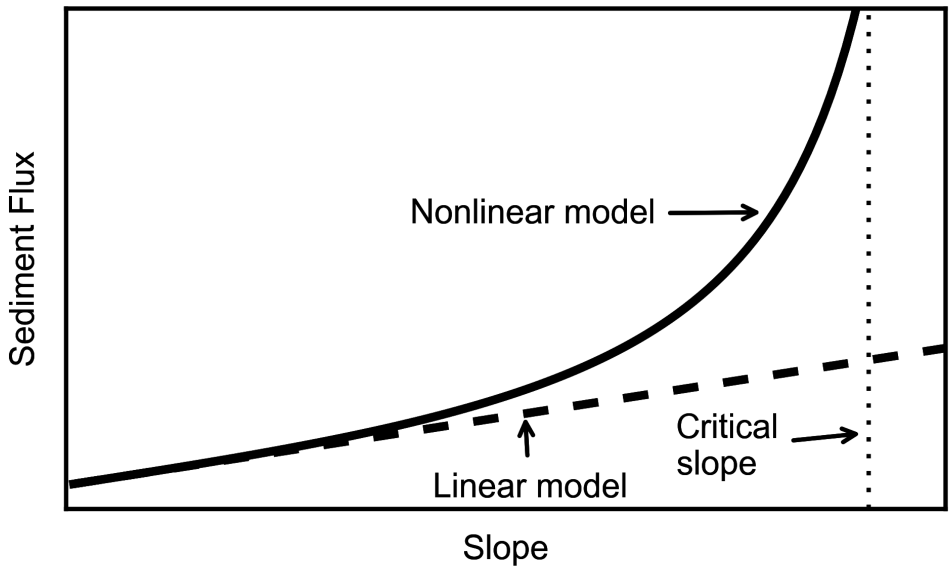

Figure 1.6: Relationship between sediment flux and topographic gradient for the linear and nonlinear models of sediment flux.

Consequently nonlinear models of sediment flux were developed, to account for the increasingly rapid transport of sediment downslope by diffusion-like processes as slopes approach a threshold gradient (Andrews and Bucknam, 1987; Howard, 1994; Densmore *et al.*, 1998; Roering *et al.*, 1999, 2001). These models are consistent with the observations of McKean *et al.* (1993) and Small *et al.* (1999) as they produce linear sediment flux at low hillslope gradients, and as the threshold gradient is approached the sediment flux increases nonlinearly with gradient (Figure 1.6), allowing the nonlinear flux law to capture better a full range of diffusive hillslope processes (Roering *et al.*, 2001). Topographic predictions made by nonlinear models have been tested through the analysis of hillslope profiles (Roering *et al.*, 1999, 2001) and the creation of dimensionless parameters of relief and erosion rate (Roering *et al.*, 2007; Hurst *et al.*, 2012, 2013b).

The linear and nonlinear models of sediment flux exist as two end-members across a continuum of models, which have good field and theoretical support and can be readily applied using only topographic measurements. Other models consider the depth dependence of hillslope sediment transport, often referred to as the depth-slope product, whereby the thickness of material at each point on a hillslope exerts a control alongside gradient on the rate of sediment flux (Roering, 2008). Such models have a good grounding in physical reality and in many cases appear to constrain sediment flux better than pure linear or nonlinear models (Braun *et al.*, 2001; Furbish and Fagherazzi, 2001; Heimsath *et al.*, 2005; Roering, 2008). However, the collection of high resolution soil thickness information is challenging and has never been achieved at a high resolution at more than a hillslope scale (Heimsath *et al.*, 2000, 2005; Roering, 2008; Gabet *et al.*, 2015). Consequently, a common method to test the topographic predictions of depth dependent sediment flux laws is to contrast the results of numerical models with topographic data over wide scales, whilst applying field data to more local scale tests of model and topographic analysis results (Heimsath *et al.*, 2005; Roering, 2008; Pelletier *et al.*, 2011).

Sediment flux has also been approximated through the use of probabilistic models of individual particle motion. Such models allow for a nonlocal component in hillslope sediment transport and have strong theoretical support (Foufoula-Georgiou *et al.*, 2010; Tucker and Bradley, 2010; Furbish and Roering, 2013). These theories suggest that sediment transport cannot be adequately explained by local measurements of hillslope properties and must incorporate information from a kernel around each point on a hillslope in order to account for particle motion. Such models are challenging to test using purely topographic analysis as the models do not have analytical solutions and consequently do not make falsifiable topographic predictions. High resolution topographic data have provided opportunities to test sediment flux laws (e.g., Roering *et al.*, 2007), even

in the absence of soil thickness information, by indicating that in many soil mantled landscapes sediment flux contains a nonlinear component, regardless of the influence of sediment thickness.

Tectonics

Some of the largest topographic features observed on the Earth are produced by tectonics, and tectonically active locations are amongst the most geomorphologically dynamic on Earth, with rapid denudation rates, extensive landsliding and abundant sediment production, transportation and deposition (e.g., Hovius *et al.*, 1997; Lavé and Avouac, 2001; Dadson *et al.*, 2004). Due to the challenges of measuring many tectonic processes directly, high resolution topography provides a unique opportunity to quantify rates of uplift across large spatial scales through the observation that hillslope morphology can act as a recorder of the processes acting upon it.

The work of Arrowsmith and Zielke (2009) applied sub-meter resolution topographic data collected along a section of the the San Andreas fault to map the surface expression of modern tectonic processes acting along the fault. This approach compared favorably to other methods of mapping fault related topographic features and has the benefit of rapid data collection over a large spatial area.

Hilley and Arrowsmith (2008) applied geologic and geomorphic mapping in conjunction with high resolution topographic analysis along a section of the San Andreas fault. This section, known as the Dragon's Back Pressure Ridge (DBPR) presents a rare opportunity to infer the influence of tectonic uplift on hillslope morphology through a space for time substitution, as, due to the motion of the San Andreas fault, the topography is effectively passing over a zone of fixed uplift such that distance along the ridge can be considered equivalent to time since uplift.

Due to the regularity of basins draining the DBPR, the uniformity of the climatic and biotic processes acting within them further allow the predominant signature of tectonics to be isolated from other factors (Hilley and Arrowsmith, 2008). This analysis demonstrated that hillslopes respond an order of magnitude more slowly than channels to tectonic forcing in the DBPR, with channels undercutting hillslopes to drive landsliding and generate increased relief following a phase of uplift.

Hurst *et al.* (2013b) extended this work by applying dimensionless measures of relief and hilltop curvature to identify a hysteresis in hillslope morphology, allowing the identification purely from high resolution topography of decaying and uplifting portions of a landscape. Such concepts were also explored by Mudd (2016) who demonstrated the limits of the detection of such topographic decay, via numerical modeling. Through these topographic analyses it was demonstrated that hillslope morphology could be used alongside channel morphology to infer detailed information about the tectonic forcing of landscapes.

DiBiase *et al.* (2012) combined high resolution topographic data with panoramic photographs to identify areas of bedrock exposure in the San Gabriel Mountains of southern California, an area of varying uplift rates connected to the San Andreas fault. This index of rock exposure was employed to explore threshold hillslope behavior alongside analyses of the fluvial and colluvial channel networks to demonstrate the presence of a topographic signature of changing rates of uplift, with more rapidly eroding sections of the landscape exhibiting more exposed bedrock and more extensive colluvial channels.

The recent topographic evolution of the southern Appalachians has also been explored through the application of topographic analysis in the study and correlation of knickpoints in rivers across the region (Gallen *et al.*, 2011, 2013). These

studies used high resolution topographic data and fluvial networks extracted using empirically derived drainage area thresholds to compare hillslope metrics, landslide inventories and basin hypsometry above and below knickpoints. The hillslopes below knickpoints are steeper and exhibit higher relief and more frequent landsliding than the unaltered relict surfaces above the knickpoints. This propagation of knickpoints is demonstrated to preserve topographic relief in the southern Appalachians, with the associated change in baselevel being dated to the Miocene.

Biological processes

The critical zone is the section of the Earth's surface which supports the majority of terrestrial life and is defined as the area of interaction between geology, atmosphere and hydrology (Anderson *et al.*, 2007). It is crucial to the Earth system, acting as a carbon sink and producing much of the sediment exported to oceans (Larsen *et al.*, 2014). This zone is the interface of biological, chemical, climatic and physical processes which convert bedrock into soil and in many cases the topographic signature of such processes can be identified from high resolution measurements of the topographic surface.

In soil mantled landscapes biological activity contributes significantly to sediment production and transport, particularly in low gradient landscapes where diffusion-like processes dominate. In such landscapes topographic analysis can be employed to identify characteristic landforms and topographic signatures of biological processes. Dietrich and Perron (2006) considered the general concept of a topographic signature of biological activity, attempting to inform research focused on other planetary surfaces. They considered a range of surface processes through published geomorphic transport laws (cf. Dietrich *et al.*, 2003) and explored the links between large scale landform development and biota. Planetary surfaces

with no apparent biological activity were used alongside terrestrial landscapes to demonstrate that there are no topographic features which are unique to surfaces with biological agents, yet rather the frequency distribution of landforms may be different depending on the presence or absence of biological agents (Dietrich and Perron, 2006). In the following decade more analyses have been developed which are beginning to better isolate biologically driven surface processes and are leading towards the creation of transport laws which can specifically account for different biological processes.

Roering *et al.* (2010) used high resolution topographic data to demonstrate a scaling break in the signature of two dimensional curvature, corresponding to the length scale of root wads exposed during tree throw events. Coupled with ground penetrating radar data this demonstrated that the soil surface and the subsurface soil-bedrock interface are both disturbed at similar length scales by the toppling of mature trees. This work demonstrates the potential for high resolution topographic and subsurface data to identify the signature of pit and mound topography.

The formation of mima mounds, broadly circular sediment mounds which are densely clustered on otherwise flat fields, has been the subject of many biotic and abiotic formation theories. The dominant formation theory is that the mounds are created by burrowing animals, and their distribution in space is controlled by the competition between individual animals. Compelling evidence for this theory was presented by Gabet *et al.* (2014) who used high resolution topographic data and numerical modeling to demonstrate a similarity between the topographic outcomes of a model of gopher burrowing and measurements of high resolution topography from a mima mound field in California.

Milodowski *et al.* (2015a) posited a relationship between erosion rates and measurements of above ground biomass of forest in the northern Sierra Nevada

of California, with rapidly eroding sections of the landscape supporting lower biomass, as measured directly from point clouds. Such relationships demonstrate the interconnectedness between ecology and geomorphic process and underline the complex feedbacks between surface process and biota.

Physical processes

In addition to the influence that biota have in shaping the surface of the Earth, physical processes also make a significant contribution to the sculpting of the Earth's and indeed other planetary surfaces (e.g., Mangold and Ansan, 2006; Lorenz *et al.*, 2008; Hobley *et al.*, 2014). High resolution topographic data collected on Santa Cruz Island, one of the California Channel Islands, has been employed by Perroy *et al.* (2010, 2012) to quantify rates of gullying and rilling on the island, predominantly driven by land use change following human habitation of the island in the 19$^{\text{th}}$ century. In addition to rates of erosion calculated for the pre- and post-disturbance landscape using cosmogenic radionuclides, the geometries of gullies were measured in three dimensions to provide estimates of the volume of sediment transported during storms on the island.

Wildfires act as significant geomorphic agents, destroying vegetation and weathering bedrock, leading to slope failures and debris flows which increase local erosion rates (Shakesby and Doerr, 2006). Roering and Gerber (2005) employed high resolution topographic data and measurements from post wildfire sediment traps to demonstrate firstly a nonlinearity in post-fire sediment flux, following the non-linear flux law proposed in Roering *et al.* (1999), before using measurements of topography to map the distribution of post fire erosion and deposition, showing an up to six-fold increase in background erosion rates in the years following wildfires.

Slope failures, including landslides and debris flows, present significant natural

hazards in many upland landscapes, and consequently many authors have employed high resolution topography in the mapping of such features. Tarolli *et al.* (2010) developed a methodology to extract the outlines of deep seated landslides and associated features using statistically derived curvature and slope thresholds to identify meter scale variations in surface morphology. This work was extended to be applied to forested catchments in Taiwan, demonstrating the method's applicability to a range of settings in the identification of landslide scars (Lin *et al.*, 2013). A more general topographic signature of landsliding associated with typhoons was demonstrated to be present in the slope-area relationships observed in a time series of LiDAR datasets collected before and after a large typhoon event (Tseng *et al.*, 2015).

McKean and Roering (2004) used measures of surface roughness over scales of 1.5 to 10 meters to distinguish between failed and unfailed terrain in New Zealand, demonstrating a statistical difference between both deep seated landslide scars and the surrounding topography, and between landslide scars of different ages. This suggests that the surface morphology of deep seated landslides has utility beyond solely mapping failed and unfailed areas. Spectral analysis was also applied to the topographic data, showing that rough, deep seated landslides have a distinct spectral character to the unfailed portions of the landscape. This spectral analysis was extended by Booth *et al.* (2009) to show an increase in spectral power at wavelengths on the order of tens of meters, an observation used successfully to map deep seated landslides in the Oregon Coast Range.

Volker *et al.* (2007) performed analysis of high resolution topographic data of a series of alluvial fans in Death Valley, California. By detrending the surface of each fan and considering local variations in relief across a range of length scales, it was demonstrated that it is possible to discriminate between alluvial fans formed by fluvial processes and those formed by dry debris flows.

Hurst *et al.* (2013c) studied the morphology of two sections of the Northern Sierra Nevada, California, composed of distinct lithologies. The curvature of ridges in each of these sites was used to calibrate the sediment transport coefficient, resulting in values differing by a factor of 2. Such differences are a function of the soil produced by each bedrock type and drive the variation in the morphology of soil mantled landscapes. The emergence of bedrock in a soil mantled landscape acts as an indicator that the rate of soil production cannot keep pace with rates of denudation on hillslopes. Milodowski *et al.* (2015b) developed a methodology to map meter scale topographic roughness from LiDAR data, validated through high resolution orthophotos, and demonstrated that such a metric can be used to identify patches of exposed bedrock on otherwise soil mantled hillslopes.

Determining erosion rates

In addition to the application of high resolution topography to the identification of topographic signatures of discrete processes, similar techniques have also been applied to constrain rates of erosion across landforms of varying scales. The concept that a drainage basin which contains hillslopes with a high mean gradient is eroding more rapidly, all other factors being equal, is intuitive and was employed prior to the widespread adoption of high resolution topography (e.g., Granger *et al.*, 1996; Montgomery and Brandon, 2002; Binnie *et al.*, 2007). DiBiase *et al.* (2010) employed this technique at a finer scale, coupled with cosmogenic radionuclides as part of a wider study into the relationship between erosion rate and hillslope morphology in the San Gabriel Mountains of southern California. It was demonstrated that mean hillslope angle within basins scales nonlinearly with erosion rate up to an erosion rate of 300 mm ka^{-1} beyond which hillslope gradient became insensitive to changes in erosion rate.

Hurst *et al.* (2012) employed similar catchment-averaging of topographic metrics

to test the sensitivity of hilltop curvature, C_{HT}, to erosion rate. In this case, Roering *et al.* (1999) demonstrated that within a nonlinear framework of sediment transport, ridgelines should increase in negative curvature as erosion rates increase, effectively stating that sharper ridgelines correlate with more rapidly eroding hillslopes. Hurst *et al.* (2012) demonstrated a similar reduction in sensitivity of mean basin slope to erosion rate beyond a threshold rate of erosion as DiBiase *et al.* (2010) but showed a linear relationship between C_{HT} and erosion rate, which operated at the most rapidly eroding sites in the northern Sierra Nevada of California.

A relationship between drainage density and erosion rate has long been proposed (e.g., Montgomery and Dietrich, 1989), and with the development of accurate channel extraction algorithms using high resolution topography these concepts could be tested. Clubb *et al.* (2016) used a combination of erosion rates derived from cosmogenic radionuclides and mean basin C_{HT} values to explore the relationship between drainage density and erosion rate and found that more rapidly eroding basins exhibit denser drainage networks, suggesting that the extent of fluvial networks could be used in the future as a proxy for erosion rate.

1.2.5 Future directions for topographic data

High resolution topographic data can now be collected without the need for either planes or helicopters through the use of UAV mounted LiDAR instruments, dramatically reducing the cost of data collection and allowing more frequent repeat surveying in areas where geomorphic change is occurring rapidly. However, much future topographic data can be collected without LiDAR instruments of any kind. Techniques such as structure from motion allow the generation of high resolution point clouds through the automated co-registration of multiple

overlapping photographs, which can be collected aerially from a UAV or on the ground using a consumer camera or even a smartphone (Westoby *et al.*, 2012; Javernick *et al.*, 2014; Micheletti *et al.*, 2015). This presents an opportunity to collect fine scale topographic information rapidly for site specific studies, and apply topographic analysis alongside more traditional change detection work to yield a better insight into the processes acting on the Earth's surface.

The reduction in cost of electronics in the last decade has placed into the hands of consumers incredibly powerful hardware, which can be modified to collect topographic data. One example is the Microsoft Kinect binocular camera which can collect millimeter scale topographic information, and can even acquire bathymetic data through shallow water (Mankoff and Russo, 2013). Such technologies have the potential to change how topographic analysis is performed in the coming years, with increased potential for time series data and the order of magnitude finer scale of these techniques when contrasted with airborne LiDAR, providing new insights into hitherto spatially and temporally unresolvable processes.

In addition to the collection of data using novel equipment at lower cost and at increasingly fine resolutions, the direct analysis of point clouds is also becoming more common (e.g., Brodu and Lague, 2012; Milodowski *et al.*, 2015a). The benefit of working directly with point clouds is that no data are lost during interpolation to a regular grid, which allows individual features to be more accurately identified and measured, rather than performing measurements on an interpolated surface. Direct analysis of point clouds was applied by Brodu and Lague (2012) who used data from terrestrial laser scanners to distinguish between riparian vegetation, bedrock, gravel and water in scans of riverbanks. The same software was extended by Lague *et al.* (2013) to perform differencing between point clouds of complex topography, to track surface changes in a rapidly eroding river canyon. Such techniques have also been applied to constrain aboveground

biomass in forests at the level of individual trees, rather than as a uniform canopy surface, to link levels of biomass to erosion rates (Milodowski *et al.*, 2015a).

Taking a historical viewpoint, direct pointcloud analysis has many of the same advantages as the vector based digital elevation models discussed in Section 1.2.3 (more accurate representation of the surface; variable spatial resolution), and can address many of the disadvantages inherent in gridded topographic data (surfaces are interpolations; inefficient storage in low gradient landscapes; not all features can be represented by grids). Its primary limitation appears to be computational, with the need to process and store billions of points and their associated attributes. However, computational complexity was long used as an argument against DEMs and so direct point cloud analysis could become the standard form of topographic analysis in the future.

1.3 Research Aims

From this review of the literature a number of opportunities have been identified surrounding the analysis of high resolution topography within the context of geomorphology. Firstly, it is clear that there is a need to develop frameworks from which reproducible topographic analysis can be performed. Many authors are employing different methods, often with little documentation, to perform standard analyses. A common example of this is the development of slope-area plots, which are described using differing methodologies by a wide range of authors (e.g., Montgomery and Foufoula-Georgiou, 1993; Roering *et al.*, 2007; Tarolli and Dalla Fontana, 2009). However, this is a more general challenge, exhibited in many if not all topographic analyses. Progress has been made on this front with the development of packages which link to MATLAB or GIS software (e.g., Schwanghart and Scherler, 2014), but these solutions are often not open source

or require proprietary software, and so are not available to the whole research community. Consequently, further work to develop open source tools to foster reproducible research is required.

Several methods have been applied in the past to measure hillslope length (e.g., Hovius, 1996; Tucker and Bras, 1998; Roering *et al.*, 2007; Hurst *et al.*, 2012), yet there has never been a critical assessment of these methods to understand how the differing techniques may influence the interpretation of landform development. The work of Roering *et al.* (1999, 2007) demonstrated that it was possible to use comparisons between the predictions of theoretical sediment flux laws and measured topography to test the validity of models of sediment flux. Yet these types of test have never been applied within the framework of the relief structure of landscapes, which will allow the analysis of sediment flux laws purely from topographic data. The critical gradient of landscapes, a parameter in the nonlinear sediment flux law, is often estimated manually, either from field exploration or the analysis of individual hillslope profiles (e.g., Roering *et al.*, 1999, 2007). This introduces considerable uncertainty in many analyses based on the nonlinear sediment flux law. Therefore, there is an opportunity to use high resolution topographic data and topographic analysis to estimate the critical gradient of soil mantled landscapes and place existing estimates into better context.

Throughout the development of digital elevation data, the resolution of the data being collected and analyzed has always been of paramount importance, with workers often being limited in their analyses by the data available at the time. Considerable work has been undertaken to constrain the limits of grid resolution in a wide range of contexts (e.g., Zhang and Montgomery, 1994; Vaze *et al.*, 2010) but little work has been undertaken with the specific objective of identifying the limitations of a range of topographic analyses as data resolution is reduced.

In summary, this thesis aims to:

1. Evaluate measures of hillslope length.
2. Test sediment flux laws through analysis of the relief structure of landscapes.
3. Place constraints on the critical gradient of landscapes.
4. Test the limits of topographic analysis as data resolution is degraded.
5. Develop open source software to facilitate reproducible research.

1.4 Thesis Structure

This work fits into a broader effort to produce reproducible open source tools for the surface processes community and links with the attempts of other researchers to quantify surface processes from topography.

In this thesis Chapters 3 to 5 are standalone research chapters, which can be read individually or as part of the wider discussion contained here. Chapter 3, concerning the extraction and application of measures of hillslope length has been published in Earth Surface Processes and Landforms. Chapter 4, concerning the development and application of software to nondimensionalize hilltop curvatures and reliefs has been published in Earth Surface Dynamics. Chapter 5, describing efforts to apply such techniques to low resolution data has been published as a discussion paper in Earth Surface Dynamics Discussions.

Chapter 3 evaluates the measurement of hillslope length through the inversion of drainage density, the analysis of slope-area plots and the measurement of flow paths across hillslopes. The flow path method is shown to be the most reliable, and is able to provide measurements of the properties of individual hillslopes, rather

than the basin or landscape averaged techniques commonly employed. Using these measurements of individual hillslopes the end-member sediment flux law operating on the landscape is identified, providing the first purely topography based test of a sediment flux law. Through the fitting of a prediction of the nonlinear flux derived model to these data, the critical gradient of each landscape, a key parameter in the nonlinear sediment flux law, is also constrained.

This technique was extended in Chapter 4, through the development of a software package for the application of the nondimensional framework for erosion rate and relief proposed by Roering *et al.* (2007). This framework facilitates the reproduction of previous studies employing this technique in a transparent manner. The method is employed on a new landscape in Coweeta, North Carolina where subtle evidence of topographic decay is presented, consistent with the observations of Gallen *et al.* (2013). This method is also employed to estimate an average critical gradient for each landscape, presenting more evidence following on from Chapter 3 that a broad range of critical gradients exists for any given landscape.

Chapter 5 evaluates our ability to make geomorphic observations on low resolution topographic data. Two common channel extraction algorithms are tested and it is found that a simple geometric method provides a more accurate representation of the channel network in low resolution data than a process based method. The measurement of curvature is also evaluated, and alongside the estimation of a sediment transport coefficient, is shown to be sensitive to data resolution. However landscape properties also exhibit a strong control on these measurements, where the larger scale curvature signal of Gabilan Mesa is more robust than the sharp ridgelines of Santa Cruz Island. Finally, the techniques developed in Chapter 3 are tested and are shown to be robust at grid sizes up to 30 meters, with the caveat that an accurate channel network can be constrained.

Chapter 2 presents an extended review of the five study areas used within the three research chapters in this thesis. This thesis is concluded with Chapter 6 which provides a synthesis of the results taken from Chapters 3 to 5 as a whole, considers potential directions for future research and ties together the overall conclusions of this body of work. The remainder of this Chapter provides a theoretical background to the application of topographic analysis to geomorphic research, placing this thesis within a broader context of geomorphic research.

Chapter 2

Study Areas

2.1 LiDAR Data Overview

This thesis focuses on using high resolution topographic data to extract information about sediment transport processes from eroding landscapes. My study areas are distributed across five locations in the United States. These areas were selected because they provide a range of tectonic, climatic and lithologic settings and are all covered by high resolution LiDAR data, collected by the National Center for Airborne Laser Mapping (NCALM). The datasets have all been successfully gridded at 1 meter resolution, using the algorithm of Kim *et al.* (2006), which is outlined in Chapter 5. Accuracy information for these datasets is recorded in their metadata, providing the horizontal and vertical accuracy of the LiDAR returns alongside the density of LiDAR returns per square meter and these values are placed in Table 2.1. Three locations in California, the northern Sierra Nevada, Santa Cruz Island and Gabilan Mesa, are used in addition to the Oregon Coast Range, Oregon and Coweeta Hydrologic Laboratory, North Carolina. These locations have been the subject of many previous studies (Reneau and Dietrich, 1991;

Roering *et al.*, 1999, 2001; Montgomery, 2001; Pinter and Vestal, 2005; Roering *et al.*, 2007; Perron *et al.*, 2009; Perroy *et al.*, 2010, 2012; Marshall and Roering, 2014), providing a basis for the evaluation of the results of this thesis in a wider geomorphic context.

Table 2.1: LiDAR point cloud metadata.

Location	Point density (points per m^2)	Vertical accuracy (m)	Horizontal accuracy (m)	Area (km^2)
Coweeta	8.91	0.17 ± 0.13	0.11	54.28
Oregon Coast Range	6.55	0.07 ± 0.03	0.06	43.45
Cascade Ridge	9.84	0.17 ± 0.13	0.11	49.33
Gabilan Mesa	5.56	0.20 ± 0.15	0.11	24.29
Santa Cruz Island	8.27	0.067^a	1.07^a	97.56

[a] Accuracy is the 95% confidence level of the root mean squared error of measurements compared to static GPS control points. Other accuracy data is provided by LiDAR equipment manufacturers and reported in metadata.

The topographic data collected at these 5 sites were collected over a period of 7 years, with the Oregon Coast Range data collected first in 2007 and the most recently collected data is Gabilan Mesa, flown in 2013. As the quality, accuracy and portability of LiDAR sensors have increased dramatically since the

first sensors were applied to earth observation (Carter *et al.*, 2001; Roering *et al.*, 2013), the newer datasets could be gridded to resolutions beyond 1 meter, but in order to ensure consistency between each of the study sites, all of the data were gridded to the same resolution, which is the limit of the data collected for the Oregon Coast Range.

2.2 Coweeta, North Carolina

The Coweeta Hydrologic Laboratory is located in the southern Appalachian Mountains in North Carolina, USA (Figure 2.1). The catchment is perched on the Natahala Escarpment of the Blue Ridge Mountains (Wooten *et al.*, 2007) and exhibits high relief and high gradient hillslopes (relative to the gentle landscape of the Gabilan Mesa), giving way to large broad floodplains where the majority of human activity is focused (Hales *et al.*, 2012). The majority of the hillslopes exhibit ridge hollow topography, which is typical of much of the Appalachian Mountains (Hack and Goodlett, 1960).

The landscape is underlain by Coweeta and Otto Group metasediments (Price *et al.*, 2005) which weather into soils approaching 2 m thickness in hollows (Hales *et al.*, 2012). Northern Hardwood forests dominate at high elevations alongside fire intolerant species such as mountain laurel (*Kalmia latifolia*) and *Rhododendron maxima*, spread due to anthropogenic fire suppression techniques in the last 80 years (Elliott and Swank, 2008; Hales *et al.*, 2009). This results in dense vegetation cover over much of the catchment, which plays a vital role in slope stability (Hales *et al.*, 2009).

Glaciation did not reach as far south as Coweeta during the last glacial maximum and consequently this location has preserved a soil mantle through the Holocene,

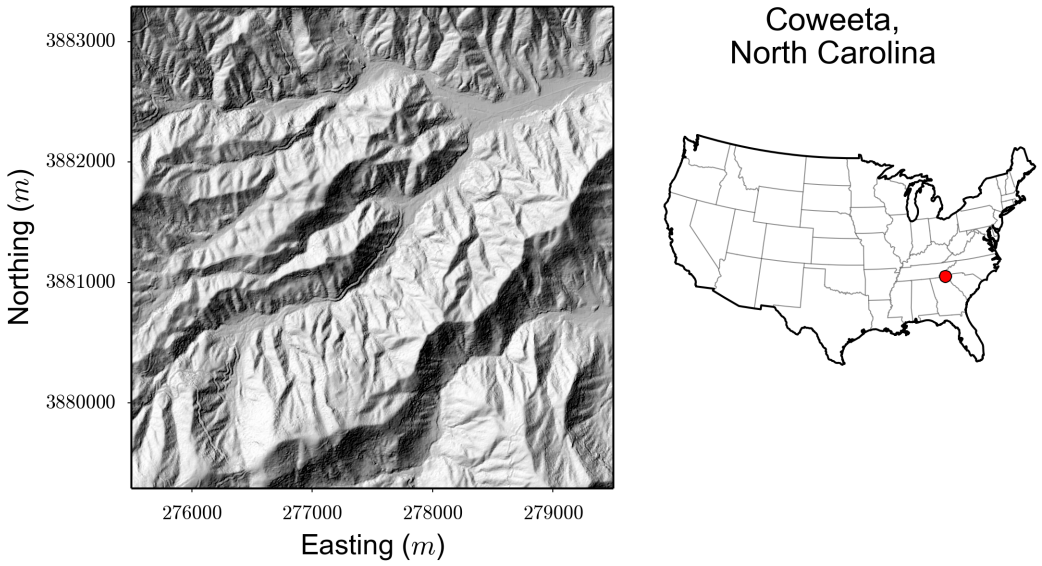

Figure 2.1: Hillshade of a section of Coweeta, North Carolina. Coordinates are in UTM Zone 17N.

which is particularly prone to sediment transport through soil creep and shallow landsliding (Witt, 2005; Wieczorek *et al.*, 2004; Hales *et al.*, 2012). Precipitation in Coweeta is dominated by small convective storms with occasional high intensity storms driven by hurricanes (Swift Jr. *et al.*, 1988; Hales *et al.*, 2009, 2012). Such storms drive slope failures and debris flows within the catchment (Hursh, 1941; Clark, 1987; Wieczorek *et al.*, 2000; Witt, 2005; Hales *et al.*, 2009).

The southern Appalachians are tectonically quiescent (Oyarzun *et al.*, 1997; Faill, 1998); however, the preservation of relief and the presence of large knickpoints in many rivers has led to debate regarding whether the landscape is in steady state (Baldwin *et al.*, 2003; Matmon *et al.*, 2003; Gallen *et al.*, 2011, 2013). Catchment average erosion rates for the southern Appalachians have been measured from cosmogenic radionuclides at between 0.023 and 0.031 mm yr^{-1} (Matmon *et al.*, 2003) and a pilot study exploring hillslope erosion rates inside the Coweeta watershed calculated the hillslope erosion rate to be between 0.051 and 0.111

mm yr^{-1} (Hales *et al.*, 2012). These data indicate that in steeply incised terrain, such as the Coweeta Hydrologic Laboratory, the rates of hillslope erosion are governed by the rate of soil production (Hales *et al.*, 2012).

2.3 Oregon Coast Range, Oregon

The Oregon Coast Range in Oregon, USA (Figure 2.2) is a steeply incised upland landscape with steep (topographic gradients can exceed 1), often planar hillslopes exhibiting pronounced small scale roughness, driven by tree throw (Roering *et al.*, 1999, 2010). The landscape is considered to be very regular with uniform 1st order drainage areas (Roering *et al.*, 1999, 2007); however more recent work has demonstrated the spatial variability of many topographic measurements in this landscape (Marshall and Roering, 2014).

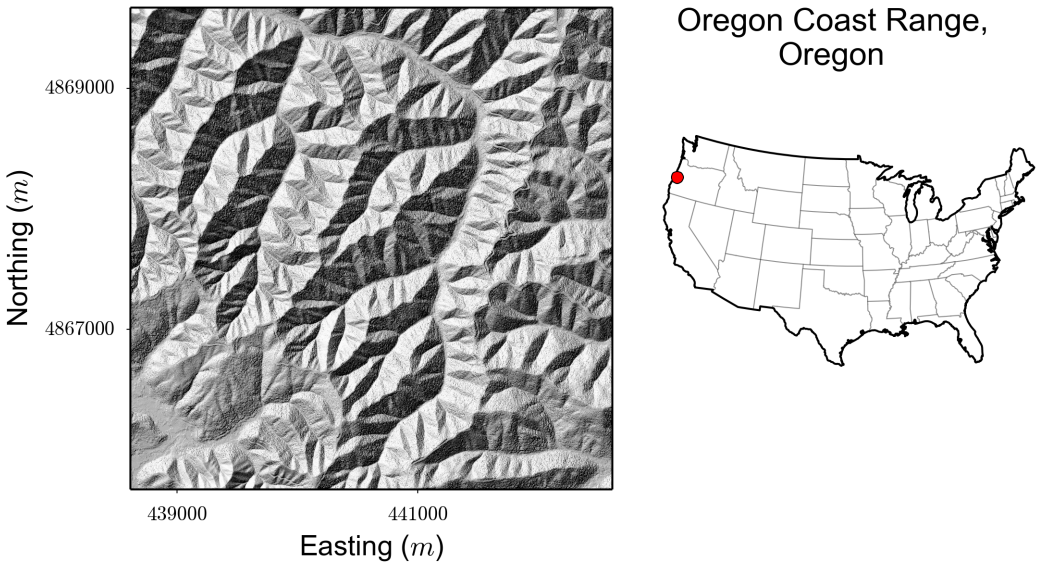

Figure 2.2: Hillshade of a section of the Oregon Coast Range, Oregon. Coordinates are in UTM Zone 10N.

The study area is predominantly underlain by Eocene sedimentary rocks of the Tyee Formation which are bedded and often graded, fining upwards from sands to silts (Baldwin, 1956; Snavely Jr *et al.*, 1964). Such lithology is weathered into well mixed, sandy soils with a low plasticity, ranging in thickness from 0.4 m on hilltops to 2 m in unchanneled valleys (Roering *et al.*, 2007; Schmidt *et al.*, 2001) and such unchanneled valleys have been identified as common debris flow source areas, similar to those observed in Coweeta (Dietrich and Dunne, 1978; Montgomery *et al.*, 2000; Heimsath *et al.*, 2001; Stock and Dietrich, 2003). The climate of the Oregon Coast Range is humid, with the majority of the precipitation falling in the winter months. Intense precipitation triggers the majority of shallow landslides and debris flows in the region (Schmidt *et al.*, 2001). These soils support dense vegetation, dominated by hardwood and coniferous forest in addition to abundant understory vegetation which is particularly evident in areas of past forest disturbance (Roering *et al.*, 2010). On steep slopes Douglas Fir (*Pseudotsuga menziesii*) and Western Hemlock (*Tsuga heterophylla*) are abundant, whereas on floodplains Oregon Maple (*Acer macrophyllum*) is more common (Schmidt *et al.*, 2001). Due to human activity little old-growth forest remains, but old stumps are still observed on the forest floor, providing additional root cohesion to the soils on these hillslopes (Roering *et al.*, 2010).

Uplift rates in the Oregon Coast Range have been measured at between 0.1 and 0.3 mm yr^{-1} from marine terrace data (Kelsey *et al.*, 1996) which corresponds with erosion rates measured using cosmogenic radionuclides of 0.07 to 0.15 mm yr^{-1} (Beschta, 1978; Reneau and Dietrich, 1991; Bierman *et al.*, 2001; Heimsath *et al.*, 2001). These data have been taken to suggest that the Oregon Coast Range is approximately in steady state (Reneau and Dietrich, 1991; Roering *et al.*, 1999, 2007, 2010; Roering, 2008; Montgomery, 2001).

2.4 Cascade Ridge, California

Cascade Ridge is a section of the northern Sierra Nevada in California, USA (Figure 2.3), which experiences a semiarid climate, with precipitation increasing from south to north along the range. This study area is referred to as the northern Sierra Nevada in Chapter 3. The characteristic topographic form of this landscape is a smooth, low relief relict surface which is heavily incised, creating steep canyons with an irregular spacing. The plateau surface is vegetated with oak forest including California black oak (*Quercus kelloggii*) and canyon live oak (*Quercus chrysolepis*) and pine forest containing ponderosa pine (*Pinus ponderosa*), Douglas fir (*Pseudotsuga menziesii*) and sugar pine (*Pinus lambertiana*), whereas the canyon is dominated by chaparral vegetation such as manzanita (*Arctostaphylos spp*) (Gabet *et al.*, 2015; Milodowski *et al.*, 2015a). These contrasting landscape morphologies have been shown to be eroding at different rates, with the plateau surfaces eroding an order of magnitude more slowly than the canyons (Riebe *et al.*, 2000; Hurst *et al.*, 2012). This range of vegetation is supported by soils of varying thicknesses: along the ridge soils vary in thickness from 0.1 to 1.4 meters (Gabet *et al.*, 2015) whilst further soil excavation pits in the region have yielded soil thicknesses approaching 1 meter on hillslopes (Yoo *et al.*, 2011).

The local geology is primarily ophiolitic, volcanic and sedimentary units of the Fiddle Creek Complex, in addition to intrusive granitoid bodies (Day and Bickford, 2004). A wide range of erosion rates has been measured in the northern Sierra Nevada, with low erosion rates found on the relict surfaces of 0.02 mm yr^{-1} and higher erosion rates of 0.25 mm yr^{-1} in canyons (Riebe *et al.*, 2000; Hurst *et al.*, 2012). However, these rates have been shown to vary through time due to accelerating tectonic uplift rates (Stock *et al.*, 2004). This results in a complex soil mantled landscape with spatially varying erosion rates driven by climatic and tectonic variations (Riebe *et al.*, 2000; Stock *et al.*, 2004; Hurst *et al.*, 2012).

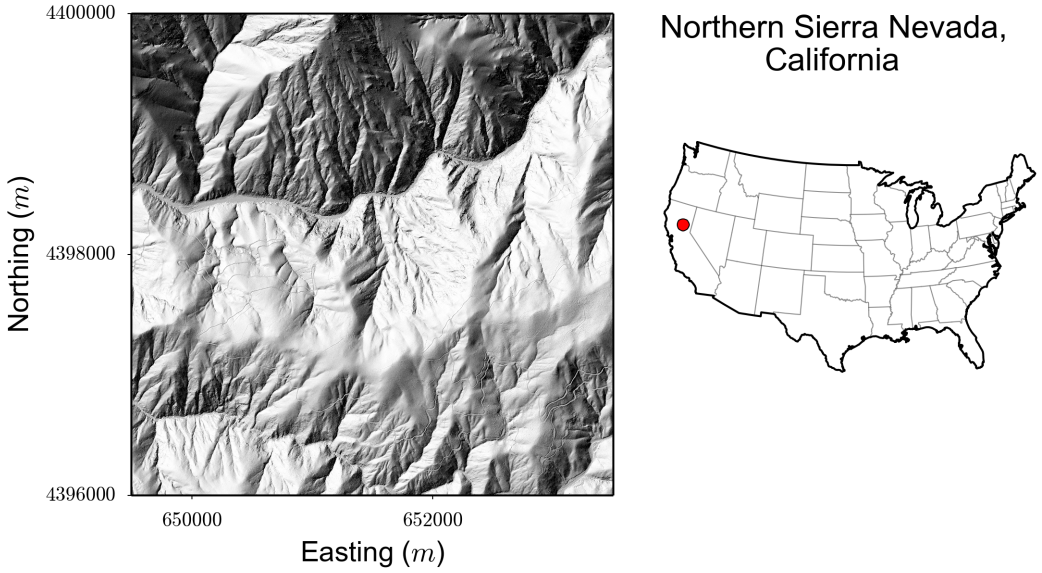

Figure 2.3: Hillshade of a section of Cascade Ridge, northern Sierra Nevada, California. Coordinates are in UTM Zone 10N.

Hurst *et al.* (2012) and Milodowski *et al.* (2015a) demonstrated that although the northern Sierra Nevada exhibits a wide range of erosion rates, due to the long response times of the channels in this landscape, the hillslopes have adjusted to local channel lowering and retain a steady topographic form. This was further demonstrated by Hurst *et al.* (2012) as this landscape plots on the steady state curve in E^* vs R^* space, whereas Hurst *et al.* (2013b) showed that transient landscapes should plot above or below the curve.

2.5 Gabilan Mesa, California

Gabilan Mesa is an unglaciated region, located within the Central Coast Ranges in California, USA (Figure 2.4) and is characterized by large linear canyons running northeast to southwest fed by smaller, parallel tributaries typically

orientated perpendicular to the canyons (Dohrenwend, 1978, 1979; Perron *et al.*, 2008a). These regularly spaced valleys present two distinct length scales in the landscape which have been observed qualitatively (Dohrenwend, 1978, 1979) and quantitatively through measurements of hillslope length distributions (Chapter 3). In contrast to the other fieldsites, the overall landscape morphology exhibits smooth hillslopes with broad ridgelines and gradual transitions into broad, flat floodplains within the largest valleys. The gradual nature of hillslope to valley transitions suggests that diffusion-like processes dominate the transport of sediment on hillslopes (Roering *et al.*, 2007).

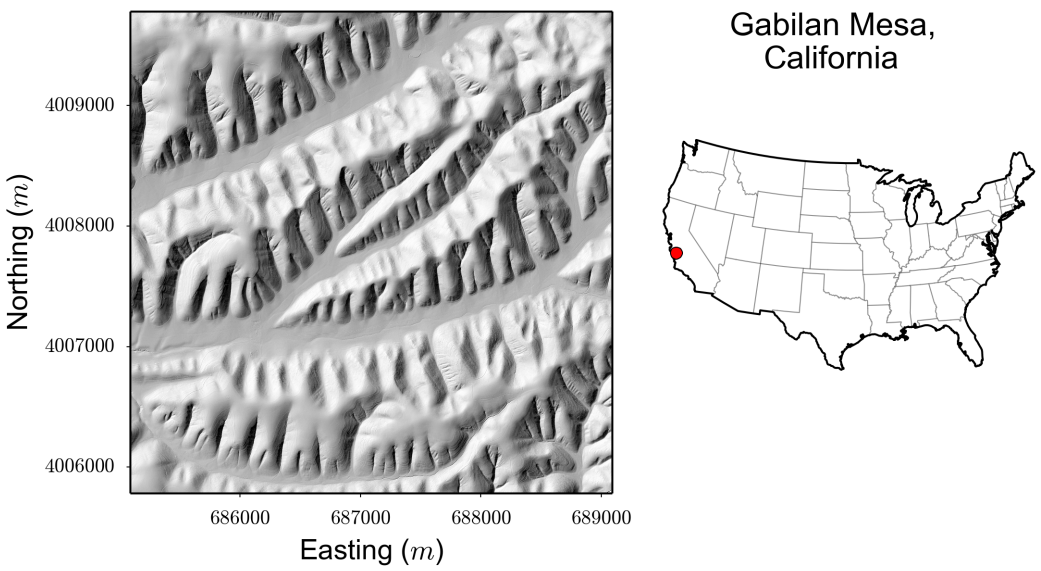

Figure 2.4: Hillshade of a section of Gabilan Mesa, California. Coordinates are in UTM Zone 10N.

The area has a semi-arid Mediterranean climate where most rainfall occurs between October and March (Dohrenwend, 1978), and vegetation densities are higher on northern slopes due to microclimatic variations (Dohrenwend, 1978). The vegetation of Gabilan Mesa is characterized by combinations of oak savannah containing Blue Oak (*Quercus douglasii*) and chaparral shrubland containing

Chamise (*Adenostoma fasciculatum*) (Shreve, 1927; Roering *et al.*, 2007). The nature of this lower density vegetation in comparison to other fieldsites allows a larger proportion of LiDAR pulses to reach the ground, requiring less processing and interpolation to generate a final bare earth DEM for analysis (Liu, 2008; Meng *et al.*, 2010). Soil thicknesses are reported by Roering *et al.* (2007) to be less than 1 meter thick on hilltops and thicker in unchanneled valleys and these soils overlie tectonically undeformed marine and continental sedimentary rocks of the Pancho Rico and Paso Robles Formations (Galehouse, 1967; Durham, 1974; Dohrenwend, 1978).

Long-term erosion rates in Gabilan Mesa have been estimated using surface exposure dating and the scale of valley incision into the Mesa at between 0.14 and 0.74 mm yr^{-1} (Roering *et al.*, 2007). Relationships between dimensionless erosion rate and relief, the uniformity of hilltop curvatures and the regularity of valley spacing have all been been used to assert that this landscape is in approximate topographic steady state (Roering *et al.*, 2007; Perron *et al.*, 2009).

2.6 Santa Cruz Island, California

The California Channel Islands lie off the west coast of California, with the 4 northernmost islands representing the peaks of a larger island, Santa Rosa, which was exposed during a sea level low stand at the last glacial maximum. Santa Cruz Island (Figure 2.5), is the largest of the group of islands and is divided by a large east-west trending valley, which follows the Santa Cruz fault (Pinter *et al.*, 2003; Muhs *et al.*, 2014). Parallel to this valley are two large ridges, one to the north and one to the south, which exhibit regularly spaced parallel channels draining north to south (Pinter *et al.*, 1998; Pinter and Vestal, 2005); this regular pattern is particularly evident in the northwest section of the study area. The Santa

Cruz fault has been demonstrated to have left-lateral strike slip motion, which deflects channels away from perpendicular to the main valley in the center of the island (Pinter *et al.*, 1998). Studies of marine terraces in the region suggest that the Channel Islands have been steadily uplifted through the late Quaternary at an average rate of between 0.1 and 0.2 mm yr^{-1} (Muhs *et al.*, 2014). Soils and alluvium in ungullied areas on the island approach 3 meters thick, particularly in topographic lows (Perroy *et al.*, 2010). This material overlies mixed lithologies ranging from breccias of the Santa Cruz Island Volcanics group and thinly bedded shales of the Monterey Formation (Pinter and Vestal, 2005).

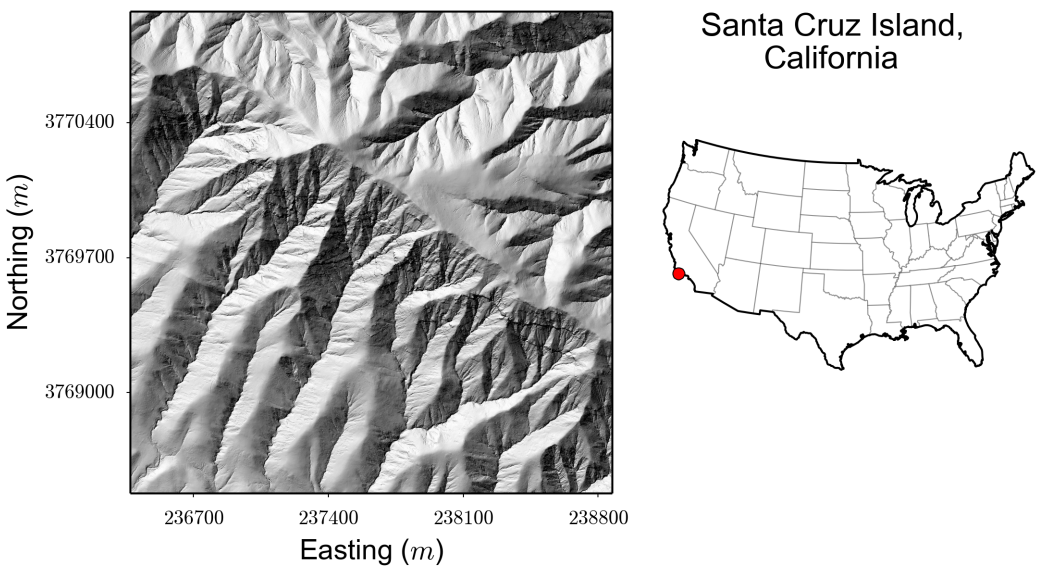

Figure 2.5: Hillshade of a section of Santa Cruz Island, California. Coordinates are in UTM Zone 11N.

The island has a Mediterranean climate similar to that of Gabilan Mesa (Pinter and Vestal, 2005), with such a climate supporting extensive grassland with occasional patches of pine forest (*Pinus muricata*) and chaparral vegetation (Pinter and Vestal, 2005; Perroy *et al.*, 2010, 2012). Human activities led to overgrazing across the island at the end of the 19^{th} century, causing a period

of gullying and rapid erosion, which was particularly evident in the southwest of the island (Pinter and Vestal, 2005; Perroy *et al.*, 2012). Erosion rates have been measured at between 0.08 mm yr^{-1} and 2.2 mm yr^{-1} depending on the rate of gullying in the region (Perroy *et al.*, 2012, 2010), and when these rates are compared to the rates of uplift measured by (Muhs *et al.*, 2014) it is clear that this landscape is not in topographic steady state. The LiDAR data collected for this location have been extensively tested and ground truthed, ensuring that they are suitable for use in a geomorphic context (Perroy *et al.*, 2010) and will be suited to performing topographic analysis at high spatial resolutions.

Chapter 3

How long is a hillslope?

A version of this chapter has been published in Earth Surface Processes and Landforms as:

Grieve, S.W.D, Mudd, S.M. and Hurst, M.D. (2016). How long is a hillslope? *Earth Surface Processes and Landforms.* 10.1002/esp.3884

The work presented here was performed in collaboration with my co-authors who contributed to the final writing of the manuscript and the development of some of the topographic analysis software. I performed the analysis, wrote topographic and data analysis routines, generated the figures and wrote the manuscript.

3.1 Abstract

Hillslope length is a fundamental attribute of landscapes, intrinsically linked to drainage density, landslide hazard, biogeochemical cycling and hillslope sediment transport. Existing methods to estimate catchment average hillslope lengths

include inversion of drainage density or identification of a break in slope-area scaling, where the hillslope domain transitions into the fluvial domain. Here I implement a technique which models flow from point sources on hilltops across pixels in a digital elevation model (DEM), based on flow directions calculated using pixel aspect, until reaching the channel network, defined using recently developed channel extraction algorithms. Through comparisons between these measurement techniques, I show that estimating hillslope length from plots of topographic slope versus drainage area, or by inverting measures of drainage density, systematically underestimates hillslope length. In addition, hillslope lengths estimated by slope-area scaling breaks show large variations between catchments of similar morphology and area. I then use the hillslope length-relief structure of landscapes to explore the nature of sediment flux operating on a landscape. Distinct topographic forms are predicted for end-member sediment flux laws which constrain sediment transport on hillslopes as being linearly or nonlinearly dependent on hillslope gradient. Because this method extracts hillslope profiles originating from every ridgetop pixel in a DEM, I show that the resulting population of hillslope length-relief measurements can be used to differentiate between linear and nonlinear sediment transport laws in soil mantled landscapes. I find that across a broad range of sites across the continental United States, topography is consistent with a sediment flux law in which transport is nonlinearly proportional to topographic gradient.

3.2 Introduction

Hillslopes cover a vast majority of the Earth's terrestrial surface and provide most of the sediment supplied to fluvial systems. Geomorphologists have long observed links between the geometric form of hillslopes and processes that transport hillslope material into channels, which are driven by a combination of climate,

tectonics and biological activity. Relationships between topographic gradient and sediment transport processes have been demonstrated at scales ranging from individual hillslopes to the scale of continental orogens (Ahnert, 1970; Pinet and Souriau, 1988; Burbank *et al.*, 1996; Montgomery and Brandon, 2002; Gabet *et al.*, 2004; Roering *et al.*, 2007). Biological processes such as animal burrowing and tree throw have been shown to leave a quantifiable topographic signature on hillslopes (Yoo *et al.*, 2005; Gabet and Mudd, 2010; Roering *et al.*, 2010). Hillslopes have also been demonstrated to contain information about a landscape's tectonic history within their morphology (Mudd and Furbish, 2005; Hilley and Arrowsmith, 2008; DiBiase *et al.*, 2012; Hurst *et al.*, 2013b). Thus topographic analysis has the potential to discriminate between different modes of sediment transport (Ahnert, 1970; Braun *et al.*, 2001; Furbish, 2003; Heimsath *et al.*, 2005; Herman and Braun, 2006; Roering, 2008). The high resolution of light detection and ranging (LiDAR) data means one can now resolve meter scale features such as headwater channels (Tarolli and Dalla Fontana, 2009; Vianello *et al.*, 2009; Tarolli *et al.*, 2014) and tree-throw mounds (Roering *et al.*, 2010) in addition to resolving channel beds (Smart *et al.*, 2004) and debris fan morphology (Schürch *et al.*, 2011). Therefore, by performing reproducible measurements of the geometry of hillslopes using high resolution topographic data, it is possible to understand and quantify the mechanical (Anderson, 2002; Cohen *et al.*, 2009), biotic (Yoo *et al.*, 2005; Gabet and Mudd, 2010; Roering *et al.*, 2010; Gabet *et al.*, 2014), chemical (Riebe *et al.*, 2003; Mudd and Furbish, 2004; Burke *et al.*, 2007; Yoo *et al.*, 2007), climatic (Gabet *et al.*, 2004; Riebe *et al.*, 2004; Hales and Roering, 2007; Dixon *et al.*, 2009; Dunne *et al.*, 2010) and tectonic (Hilley and Arrowsmith, 2008; DiBiase *et al.*, 2012; Hurst *et al.*, 2013b) processes which are shaping hillslopes, in addition to constraining the control underlying lithology exerts on the landscape (Korup, 2008; Hurst *et al.*, 2013c).

A fundamental measure of hillslopes is their down-slope length. Hillslope

length exerts a primary control on the rate of sediment transport through a catchment, which modulates flows of pollutants, nutrients and water, and in addition influences rates of soil erosion at both the hillslope and catchment scale (Mathier *et al.*, 1989; Dunne *et al.*, 1991; Gabriels, 1999; Liu *et al.*, 2000; Kinnell, 2009; Thompson *et al.*, 2010). Consequently, in a catchment which has short hillslope lengths, the signal of a storm event in the catchment's headwaters will be transmitted more rapidly to the outlet of the catchment than would be the case in an otherwise similar catchment with longer hillslopes (Dunne *et al.*, 1991).

Work to quantify the rate of sediment accumulation on hillslopes by estimating colluvial hollow filling rates requires accurate constraint on the length of the hillslope upslope of the accumulation zone (Reneau *et al.*, 1989; Reneau and Dietrich, 1991). Hillslope length also acts to constrain debris flow hazard in soil mantled landscapes: a scaling relationship between the area of a landslide scar and the volume of its deposit has been demonstrated (Guzzetti *et al.*, 2009; Klar *et al.*, 2011) and the length of a hillslope exerts a fundamental constraint on the maximum source area of landslides (Hurst *et al.*, 2013a).

Hillslope length is governed by the amount of dissection of a landscape by a channel network, a process governed by a range of factors including climate, erosion rate and hillslope morphology (Chorley, 1957; Abrahams and Ponczynski, 1984; Montgomery and Dietrich, 1989; Rinaldo *et al.*, 1995; Oguchi, 1997; Moglen *et al.*, 1998; Tucker and Bras, 1998; DiBiase *et al.*, 2012) and additionally by the roughness of the topographic surface (Dunne *et al.*, 1991; Thompson *et al.*, 2010). On highly diffuse hillslopes, with little vegetation cover to increase surface roughness, the length of overland flow will be reduced, when contrasted with a hillslope characterized by a large amount of microtopography or vegetation (Dunne *et al.*, 1991; Thompson *et al.*, 2010).

The importance of quantifying hillslope length has been recognized for many

decades, but doing so has been a challenge: Horton (1932) commented, 'The exact determination of the average distance which rain must travel overground to reach the stream-channels is impracticable.' Owing to advances in both topographic data resolution and computational power Horton's assertion is no longer true.

A number of methods have been proposed to measure hillslope length. It can be estimated through interpretation of slope-area plots (Roering *et al.*, 2007), analysis of drainage density data (Tucker *et al.*, 2001; DiBiase *et al.*, 2012) and by modelling flow paths along hillslopes (Tucker *et al.*, 2001; DiBiase *et al.*, 2012; Hurst *et al.*, 2012). An estimate of hillslope length averaged over a landscape can also be approximated through spectral analysis of characteristic length scales found in high resolution topography (Perron *et al.*, 2008a); however I do not consider this method, as it yields a single length scale for a landscape, which cannot be readily evaluated against the hillslope and basin scale measurements of other techniques.

Since sediment flux and overland flow are in part governed by hillslope length (Dunne *et al.*, 1991), I reason that characterizing hillslope length as a flow path at the hillslope, rather than catchment scale, should be the most reliable description. I therefore set out to compare the length of flow paths against other previously reported measures of hillslope length and consider the distribution of hillslope length measurements across four field sites in the continental United States.

The rate of hillslope sediment flux is a crucial component in understanding landscape evolution, as it is integral in determining both the geometry of hillslopes (Carson and Kirkby, 1972; Dietrich *et al.*, 2003) and their response to climatic and tectonic forcing (Armstrong, 1980; Rosenbloom and Anderson, 1994; Arrowsmith *et al.*, 1996; Fernandes and Dietrich, 1997; Roering *et al.*, 2001; Mudd and Furbish, 2005). Here I demonstrate that this method of measuring hillslope length via flow paths can be used to test two common sediment flux laws, by comparing the

hillslope length-relief structure of landscapes with theoretical predictions made by each flux law.

3.3 Sediment Flux Laws and Their Topographic Predictions

A large number of sediment flux laws (Dietrich *et al.*, 2003) have been proposed to describe sediment flux on hillslopes; within this continuum of laws sediment flux can be described as being linearly dependent on hillslope gradient (Culling, 1960; McKean *et al.*, 1993; Tucker and Slingerland, 1997; Small *et al.*, 1999; Booth *et al.*, 2013); nonlinearly dependent on hillslope gradient (Andrews and Bucknam, 1987; Koons, 1989; Anderson, 1994; Howard, 1997; Roering *et al.*, 1999; Pelletier and Cline, 2007); dependent on the product of soil thickness and hillslope gradient (Braun *et al.*, 2001; Furbish and Fagherazzi, 2001; Heimsath *et al.*, 2005; Roering, 2008) or described via the motion of individual sediment particles (Foufoula-Georgiou *et al.*, 2010; Tucker and Bradley, 2010; Furbish and Roering, 2013).

Spatially continuous soil thickness data is not available for my field sites and particle motion based models make a wide range of topographic predictions (Foufoula-Georgiou *et al.*, 2010; Tucker and Bradley, 2010; Furbish and Roering, 2013), as they have no analytical solution, meaning that neither of these groups of flux laws can be falsified using topographic data. However, it is possible to falsify the nonlinear or linear models of sediment flux as these two laws predict distinct relief structures which can be measured using high resolution topographic information. Previous tests of the appropriate sediment flux law for a given landscape typically combine topographic analysis and numerical modelling (Roering *et al.*, 2001; Roering, 2008), topographic analysis and field measurements

(Roering *et al.*, 1999; Heimsath *et al.*, 2005), field measurements and numerical modelling (Braun *et al.*, 2001; Herman and Braun, 2006; Pelletier *et al.*, 2011), or a combination of all three of these techniques (Pelletier *et al.*, 2011). Here I demonstrate a test of flux laws using topography alone.

One approach to examining the topographic outcome of different sediment flux laws is to calculate the predicted relief structure of a landscape. Roering *et al.* (2007) solved a statement of mass conservation along a one dimensional hillslope for hillslopes obeying a nonlinear flux law of the form (Andrews and Bucknam, 1987; Roering *et al.*, 1999):

$$q_s = \frac{KS}{1 - (|S|/S_c)^2}, \tag{3.1}$$

where q_s (in dimensions Length^2 Time^{-1}, dimensions henceforth denoted in square brackets as [L]ength, [M]ass and [T]ime) is a volumetric sediment flux per unit contour length, K [L^2 T^{-1}] is a sediment transport coefficient, S [dimensionless in L/L] is hillslope gradient and S_c [dimensionless] is a critical hillslope gradient; as S approaches S_c, q_s asymptotically progresses towards infinity (Figure 3.1a). Relief, R [L], defined as the elevation difference between the hilltop and the channel can be determined from Equation 3.1 in the case of steady-state hillslopes, where erosion balances uplift and soil thickness does not change over time (Roering *et al.*, 2007). Here, I employ the steady state definition of Mudd and Furbish (2004), whereby a hillslope which retains a steady form with regard to baselevel (the channel at the toe of the hillslope) is deemed to be in steady state (also known as steady topographic form).

Roering *et al.* (2007) demonstrated that on hillslopes with steady topographic form, R is a function of the erosion rate E [L T^{-1}], the sediment transport coefficient K and the hillslope length L_H [L] where sediment transport can

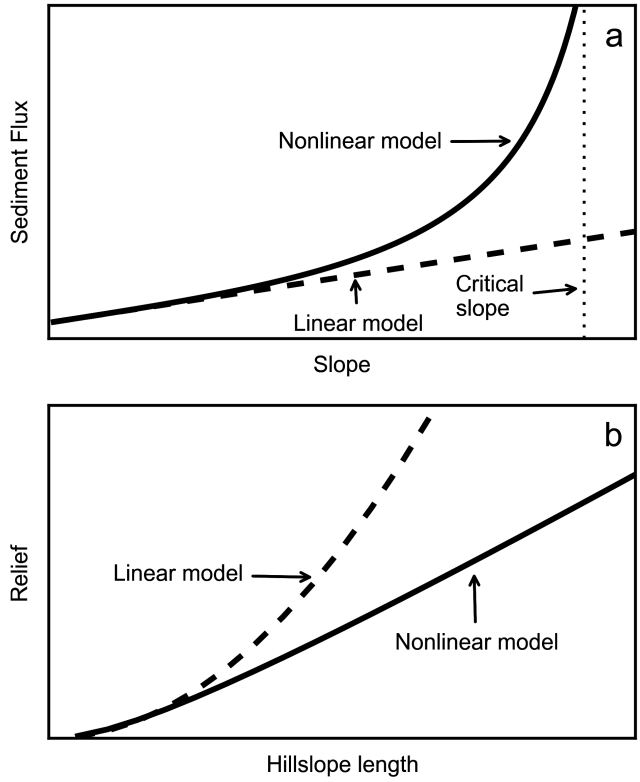

Figure 3.1: (a) Schematic plot of the relationship between slope and sediment flux for the linear (Equation 3.1) and nonlinear (Equation 3.3) flux laws. **(b)** Schematic plot of the predicted relationship between hillslope length and relief for linear and nonlinear flux laws described by Equations 3.7 and 3.8.

be described by Equation 3.1. Furthermore, Roering *et al.* (2007) found by normalizing the equation describing hillslope form for these hillslope properties, all steady state hillslopes obeying Equation 3.1 should fall on a single curve when nondimensional relief $R^* = R/(S_c L_H)$ is plotted against nondimensional erosion, $E^* = (-2C_{HT}L_H)/S_c$, where C_{HT} [L^{-1}] is the curvature of the hilltop. Hurst *et al.* (2012) was able to show that in a landscape with a wide range of erosion rates, along the Cascade Ridge in northern California, ridgeline-averaged E^* vs R^* data

of hilltops fell on the curve predicted by Roering *et al.* (2007), thus providing a test of the nonlinear sediment flux law.

One drawback of this approach is that it requires a distribution of erosion rates in a landscape; Roering *et al.* (2007) tested their theory in landscapes with more spatially homogeneous erosion rates (the Oregon Coast Range and Gabilan Mesa, California) and these two landscapes fell upon single points in E^* vs R^* space. Other efforts at constraining flux laws have examined manually selected hillslope profiles (Rosenbloom and Anderson, 1994; Arrowsmith *et al.*, 1996; Furbish and Roering, 2013) or a combination of manually selected hillslope profiles and high resolution topography (Roering *et al.*, 1999). Such profiles are both time consuming to identify and difficult to reproduce without transect coordinates.

Here I use the dimensional relationship between hillslope length, L_H, and relief, R, combined with algorithmic extraction of ridge to valley profiles to examine if topography is more consistent with a particular sediment flux law. One advantage of using dimensional instead of nondimensional length vs relief data is that hillslopes should have a wide range of hillslope lengths so relief and hillslope length may be tested on a large dataset in steadily eroding landscapes. Unlike previous tests of sediment flux laws, this procedure can be performed without field measurements or numerical modelling.

A simple statement of mass conservation on a one-dimensional hillslope, assuming negligible chemical weathering processes, is:

$$\rho_s \frac{\partial z}{\partial t} = -\rho_s \frac{\partial q_s}{\partial x} + \rho_r U, \tag{3.2}$$

where z [L] is the elevation of the surface, x [L] is the horizontal distance from the hilltop, U [L T^{-1}] is tectonic uplift and ρ_s and ρ_r [M L^{-3}] are soil and rock

densities, respectively. At steady state, $U = E$, $\partial z/\partial t = 0$, Equation 3.2 reduces to $(\rho_r \ / \ \rho_s)\mathrm{E} = \partial q_s/\partial x$. To close this equation, a sediment flux law, $\mathrm{q_s}$, must be defined.

One end member sediment flux law is a linear sediment flux law (Gilbert, 1909; Culling, 1960; Ahnert, 1987):

$$q_s = KS \tag{3.3}$$

which was first used primarily for its simplicity but has been supported by field studies (McKean *et al.*, 1993; Small *et al.*, 1999) and has been demonstrated to describe sediment transport by rainsplash (Furbish *et al.*, 2007; Dunne *et al.*, 2010). I also consider the nonlinear flux law of Equation 3.1. I do not consider depth dependent sediment flux because I do not have soil thickness data for all of my study sites; thus I cannot truly evaluate all possible flux laws. Rather my goal is to assess whether one of two popular flux laws is consistent with the data and show that, at a minimum, flux laws are falsifiable.

At steady state, the solution of Equation 3.2 for linear sediment flux is:

$$z(x) = \frac{\rho_r E}{2\rho_s K}(x^2 - {L_H}^2) \tag{3.4}$$

where the hilltop is located at $x = 0$ and the base of the hillslope is at $x = L_H$. The steady state solution of Equation 3.2 for nonlinear sediment flux is (Roering *et al.*, 2007):

$$z(x) = \frac{S_c}{\kappa}\Big[\ln\Big(0.5\Big[\sqrt{1 + x^2\kappa^2} + 1\Big]\Big) - \sqrt{1 + x^2\kappa^2} + 1\Big] \tag{3.5}$$

where

$$\kappa = \frac{\rho_r E}{2\rho_s K}. \tag{3.6}$$

The relief is found by subtracting the elevation at the hilltop from the elevation at the hillslope base. In the linear case, relief is:

$$R = \frac{\rho_r E}{2\rho_s \kappa} {L_H}^2 \tag{3.7}$$

and in the nonlinear case steady state relief is:

$$R = \frac{S_c\left[\sqrt{1+\kappa^2 {L_H}^2} + \ln(3) - 1 - \ln\left(2+\sqrt{1+\kappa^2 {L_H}^2}\right)\right]}{\kappa}. \tag{3.8}$$

Equations 3.7 and 3.8 describe contrasting relationships between hillslope length and relief. If sediment transport can be described by a linear flux law, hillslope relief should go as the square of the hillslope length given constant densities, transport coefficients and erosion rates. On the other hand, relief will be approximately linear as a function of hillslope length if sediment flux can be described by a nonlinear sediment flux law of the form in Equation 3.1 (Figure 3.1b).

In order to test if theoretical predictions of relief as a function of hillslope length are consistent with real topography, one must first ensure that topographic measurements are consistent with the assumptions contained within the equations of sediment flux and mass conservation. Equations 3.7 and 3.8 are formulated for one-dimensional, soil mantled hillslopes, therefore one must restrict analysis to

hillslope profiles that can be approximated as one-dimensional, and where one can be confident of a persistent soil mantle.

Quasi-one-dimensional hillslope traces are identified by comparing the measured hillslope length to the Euclidean distance between the start and end point of the flow path. If these two values are approximately equal, within a tolerance of 0.02%, I conclude that a trace is planar, and can be described using Equations 3.7 and 3.8. In addition, any traces which were initiated on hilltops with a positive hilltop curvature or a slope value of greater than 1.2 are excluded from this analysis, ensuring that hillslopes studied are soil mantled. This filtering can introduce a bias towards shorter hillslopes, as the longer traces have more opportunity to diverge from planarity, and this limitation should be considered when evaluating hillslope length-relief relationships.

Identifying sections of a landscape which approximate one-dimensional hillslope profiles is a key challenge of attempting to test one-dimensional models with topographic data, because significant proportions of upland, soil mantled landscapes are characterized by planform curvature, forcing topographic profiles to deviate from a one-dimensional profile (Roering *et al.*, 1999). My method generates a large amount of traces for a landscape, and can filter them automatically to find all of the quasi-one-dimensional traces in an area. However, such traces can be rare, limiting the validity of tests of flux laws using this method, particularly where only a small area of a landscape is covered by the filtered topographic data.

3.4 Methods

3.4.1 Topographic processing

In order to implement and test techniques for extracting hillslope length from high resolution topography one must ensure consistency in how topographic processing is performed. The topographic derivatives of slope, aspect and curvature are required for all three of the hillslope length extraction techniques. I calculate these derivatives following techniques outlined by Lashermes *et al.* (2007); Roering *et al.* (2010) and Hurst *et al.* (2012) to fit a polynomial surface to elevation values within a circular window, passed across every cell in the DEM. The radius of the circular window is determined by identifying breaks in values of the interquartile range and standard deviation of curvature as a function of window size. This ensures that the slope values are representative of slope at the hillslope scale rather than a function of the combination of microtopographic variations, such as the roughening of hillslopes from tree throw, and measurement noise produced during LiDAR data acquisition (Roering *et al.*, 2010; Hurst *et al.*, 2012).

The foundation of the hilltop flow routing and drainage density inversion methods is being able to define the location of channels. Without an accurate constraint of the location of the channel network neither method will be accurate. Each of these techniques therefore requires precise mapping of the location of the channel head, either through field exploration (Julian *et al.*, 2012; Jefferson and McGee, 2013), a process based method (Clubb *et al.*, 2014), or geomorphometric analysis of a DEM (Passalacqua *et al.*, 2010; Orlandini *et al.*, 2011; Pelletier, 2013) or contour map (Oguchi, 1997). Here, I extract channels from the DEM following the DrEICH method outlined by Clubb *et al.* (2014), using the parameters outlined in Table 3.1.

Table 3.1: Parameters used when extracting a drainage network.

Location	Contributing pixels[a]	A_0[b]	$\frac{m}{n}$ ratio[c]	Linked pixels[d]	Window Radius (m)[e]
Coweeta	100	1000	0.365	10	7
Oregon Coast Range	100	1000	0.45	10	4
Gabilan Mesa	100	1000	0.45	10	5
Sierra Nevada	100	1000	0.3	10	6

For more details about these parameters and their applications see Clubb *et al.* (2014).

[a]Threshold number of pixels used to generate the initial channel network.

[b]A constant drainage area value used in the analysis.

[c]The ratio between the m and n exponents of the stream power law.

[d]The minimum number of contiguous pixels required to identify a valid channel segment.

[e]The window radius used in the surface fitting routine.

Due to the single pixel width of the extracted channel network, it is also necessary to identify floodplains from the topographic data, as these portions of the landscape will not conform to hillslope sediment transport laws and will consequently contaminate the topographic signal of hillslopes if not excluded from the analysis. To identify large floodplains, two filters are applied to the

unprocessed topographic data, one to identify patches of low positive local relief and another to identify patches of low gradient. Local relief was calculated as the range in elevations within a circular moving window, of the same radius as the window used to fit the polynomial surface, and calculate the gradient. Where a low relief and low gradient patch are spatially coincident, that area is flagged as floodplain. These flagged areas were then then manually combined to create contiguous patches of floodplain (Figure 3.2). This floodplain mask was then combined with the channel network, ensuring that only the hillslope portion of each landscape is sampled.

Basins are extracted by identifying junctions in the channel network where the Strahler stream order increases and then identifying all of the upslope pixels for that junction. Drainage area is calculated using the D∞ algorithm (Tarboton, 1997).

3.4.2 Extracting hillslope length using slope-area analysis

Relationships between local slope and drainage area have been used to identify process transitions in landscapes (Montgomery, 2001; Stock and Dietrich, 2003; Roering *et al.*, 2007; Tarolli and Dalla Fontana, 2009; Booth *et al.*, 2013; Tarolli *et al.*, 2014; Tseng *et al.*, 2015). In areas where hillslope processes dominate, slope increases with drainage area and in areas where fluvial processes dominate slope decreases with increasing drainage area (Montgomery and Foufoula-Georgiou, 1993). Therefore, the transition between the hillslope and fluvial domain can be identified as the first inflection point in slope-area space (Montgomery and Foufoula-Georgiou, 1993; Hancock and Evans, 2006; Tarolli and Dalla Fontana, 2009). As drainage area increases beyond this transition point, further scaling

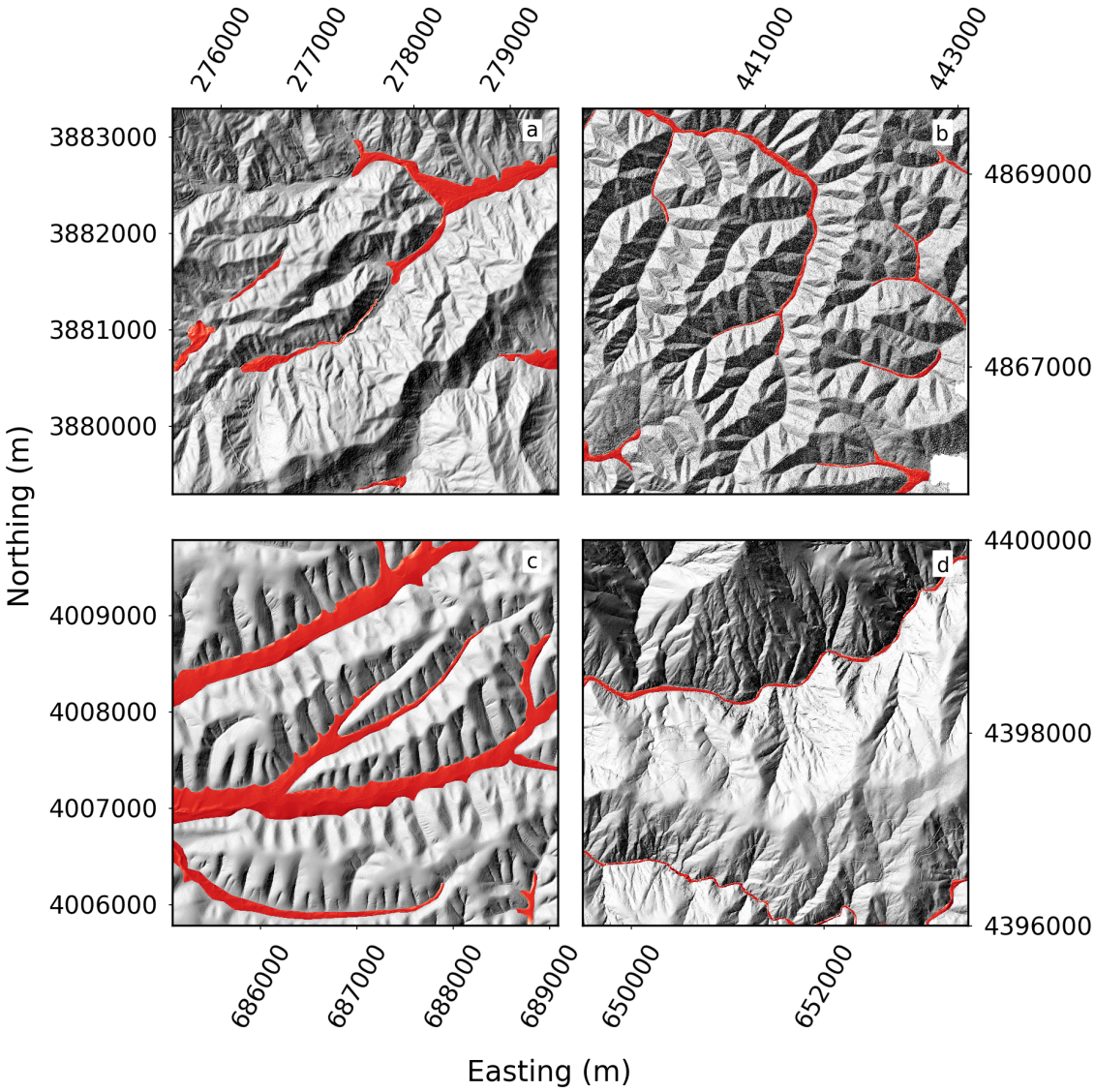

Figure 3.2: Shaded relief map of a representative section of each field site, with the floodplain mask colored red. All coordinates are in UTM. (a) Coweeta, North Carolina, UTM Zone 17N. (b) Oregon Coast Range, Oregon, UTM Zone 10N. (c) Gabilan Mesa, California, UTM Zone 10N. (d) Northern Sierra Nevada, California, UTM Zone 10N.

breaks have been demonstrated to correspond with large-scale landsliding (Tarolli and Dalla Fontana, 2009; Booth *et al.*, 2013; Tarolli *et al.*, 2014; Tseng *et al.*, 2015).

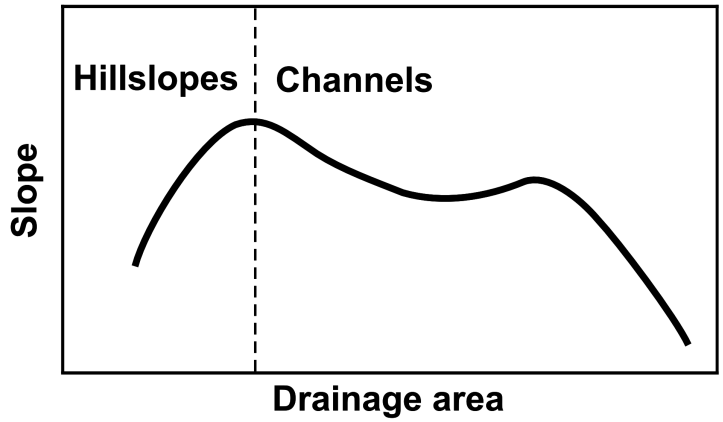

Figure 3.3: Schematic diagram of a slope-area plot showing the predicted relationship between slope and drainage area in a catchment in a soil mantled landscape. Slope increases with increasing drainage area on hillslopes, while in channels, slope decreases as drainage area increases. The inflection point between these two domains, denoted by the dashed line, is identified as the characteristic drainage area, which is transformed into a representative hillslope length for the particular catchment. The second inflection point corresponds to the signature of large-scale landsliding (Tseng *et al.*, 2015).

Slope and drainage area [L^2] are sampled on a per pixel basis for each catchment in the landscape and the resulting values are placed in logarithmically spaced bins with a width of 0.1 in base 10 logarithmic space, with area measured in units of m^2. Binned values are then plotted in log-log space and the algorithm searches for the binned point with the maximum slope value. This maximum slope bin is identified as the inflection point and the corresponding drainage area is recorded. I also record the drainage area of the maximum slope of a cubic spline fitted to the binned data following Roering *et al.* (2007). I have found these two methods produce indistinguishable results and thus results presented in figures use maximum binned slope values as this is less computationally expensive. The resulting characteristic drainage area, often used to identify the threshold area for channel initiation (Montgomery and Dietrich, 1992; Montgomery and

Foufoula-Georgiou, 1993) is then converted into a characteristic hillslope length by dividing the area by the unit contour width (Roering *et al.*, 2007), which can be approximated as the DEM resolution (Montgomery and Dietrich, 1989; Moore *et al.*, 1991; Costa-Cabral and Burges, 1994; Mitasova *et al.*, 1996; Tarboton, 1997).

3.4.3 Inversion of drainage density to extract hillslope length

Drainage density (D_D [L]) is a fundamental landscape parameter which has been shown to vary with climate (Chorley, 1957; Abrahams and Ponczynski, 1984; Rinaldo *et al.*, 1995; Moglen *et al.*, 1998), relief (Schumm, 1956; Oguchi, 1997) and dominant sediment transport process (Montgomery and Dietrich, 1989; Willgoose *et al.*, 1991; Tucker and Bras, 1998). It is defined as the total length of the channel network divided by catchment area (Horton, 1932):

$$D_D = \frac{L_T}{A}. \tag{3.9}$$

The drainage density of a catchment provides a measure of the level of dissection of a landscape, the inverse of which will reflect the catchment average hillslope length. This parameter is described by Horton (1932, 1945) and Tucker *et al.* (2001) as the mean distance water must travel from a random point in a catchment to reach a channel and is considered by Schumm (1956) to be equivalent to the catchment average length of overland flow.

This measurement can be quantified as (Horton, 1932; Schumm, 1956; Tucker *et al.*, 2001):

$$L_H \approx (2D_D)^{-1} \tag{3.10}$$

where L_H [L] is hillslope length; thus drainage density can be transformed into a measurement of the average flow path length of hillslopes in the catchment.

3.4.4 Using hilltop flow routing to measure hillslope length

Building on the work of Hurst *et al.* (2012), I have, in addition, developed a measure of hillslope length in which hillslope length is defined as the typical travel distance from divide to channel (Roering *et al.*, 2007). The simplest method employed to model flow paths is the D8 algorithm, which distributes flow at 45° azimuth angles into the eight neighboring grid cells (Mark, 1984; O'Callaghan and Mark, 1984; Tarboton *et al.*, 1991). This technique operates well when constraining channelized flow (Shelef and Hilley, 2013) and is a commonly used method for extracting a channel network from a DEM (Braun and Willett, 2013). However, when using this algorithm in the hillslope domain, the direct flow paths do not reflect the dispersive nature of overland flow (Tarboton, 1997; Pelletier, 2010; Shelef and Hilley, 2013) and as such the resulting measured hillslope lengths are biased towards short hillslopes. Hurst *et al.* (2012) modified this approach and modelled flow from hilltop to channel as a point source crossing each DEM cell.

Hilltops are extracted by identifying the edges of basins which share a stream order following techniques outlined by Hurst *et al.* (2012). From each of these selected hilltop pixels a trace can be run to measure its flow path to the channel.

I then modify the algorithm of Lea (1992) to model the flow of a point source of water from the ridge line down to the channel. Flow is modelled within each DEM cell, flowing from an inlet point on each cell edge to an outlet point on another cell edge, with the flow path within each cell following that cell's aspect angle. Flow is then routed across each cell from the inlet point (or cell center for hilltop pixels where tracing begins) across to its outlet point. This in-pixel routing is repeated recursively, with the flow outlet becoming the subsequent new inlet as the routing proceeds, until the trace has reached a channel or floodplain pixel. If two cells flow into each other the algorithm calculates the secondary aspect of these two pixels and flow is pushed along the cell edge which corresponds to this secondary aspect until it enters another cell whereby flow can continue.

When using aspect angle calculated from a polynomial fit, areas of high topographic noise can generate large sinks in the topography, where flow cannot be routed to the channel. These large areas commonly correspond to low gradient areas of a landscape, such as terraces, valley fills or areas filled by DEM pre-processing to remove pits. It is not possible to allow flow to pass across these zones without extensive smoothing of the landscape or the trace paths themselves, which will destroy any topographic signal which could otherwise be measured. Therefore these traces, which account for $<5\%$ of the total number of traces in the noisiest landscapes and $<0.5\%$ in smoother landscapes are excluded from all final analysis.

The initial starting point of the trace is given by Lea (1992) as the cell center for computational simplicity. In high resolution topographic data this placement has little influence on the final results as hillslope length is effectively sampled at intervals along each ridgeline equal to the data resolution. See Figure 3.4 for an example of the distribution of hillslope flow paths for a ridgeline in Gabilan Mesa.

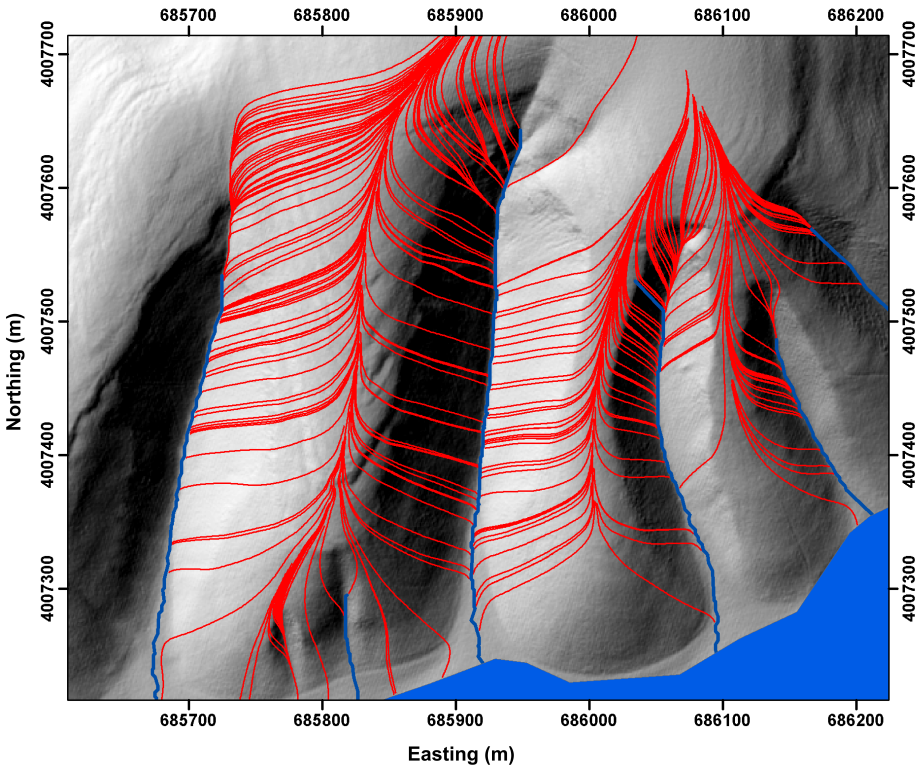

Figure 3.4: Example flow paths (red) plotted over a shaded relief of a section of Gabilan Mesa. Channels and floodplain are marked in blue. All coordinates are in UTM Zone 10N.

When the routing algorithm is used to measure hillslope length I am implicitly choosing to quantify sediment transport over millenial timescales, because the calculation of aspect averages the land surface over several cycles of geomorphic roughening (Mudd and Furbish, 2007) rather than event-based routing of water, so flow is routed over topography which is effectively smoothed using an aspect driven routing technique.

The hilltop flow routing algorithm records a small number of basins with short average hillslope lengths, which is consistent with the typical implementation of the algorithm which will measure hillslope lengths near the basin outlet, where the hillslope length approaches the effective channel width. In some basins the

only hilltops that are sampled are these interfluves, due to the filtering of hilltops outlined in this section, to ensure that hillslopes sampled are soil mantled. These values are valid measurements; however their bias in smaller basins requires careful analysis of basin average results and motivates the use of median and median absolute deviation values to minimize the influence of these exceptional measurements on the dataset.

My flow tracing method not only can be used to measure hillslope length, but it can also be used to measure local relief at the hillslope scale, by calculating the difference in elevation between the start and end point of each trace. I use data collected for hillslope length measurements to explore the relationships between hillslope length and relief at the hillslope scale.

3.5 Results

3.5.1 Basin average measurements of hillslope length

To ensure techniques are compared against equivalent datasets, the hilltop flow routing method results are averaged over the same second-order basins used for results from slope-area and drainage density analyses. Both drainage density inversion and slope-area plots provide information about the landscape and sediment transport over millennial timescales, as both methods generalize topography through surface fitting and spatial averaging. Aspect angle is utilized in the hilltop flow routing algorithm and the surface fitting algorithm from which aspect is computed provides an effective smoothing of the topography without altering the elevation values needed for subsequent analysis. Therefore one can

gain a sensible comparison between the three measures, without the influence of small-scale topographic noise on the results.

In Coweeta the basin median hillslope length from hilltop flow routing is 123 m with a median absolute deviation (MAD) of 50 m (Figure 3.5a). The median absolute deviation is a measure of statistical dispersion that is robust, i.e. performs well for probability distributions that are non-normal (Hampel *et al.*, 2011) such as the measured distributions of hillslope lengths. The large outliers seen in this dataset correspond to the large basins present in Coweeta. The slope-area data exhibit underestimation of hillslope length with a median of 28 m with a MAD of 14 m (Figure 3.5b). Few of the longer hillslopes seen in the hilltop flow routing data are reflected in the slope-area data with a strong clustering around the median value. Hillslope length values from drainage density measurements in the southern Appalachians (Figure 3.5c) reflect the smaller area covered by the Coweeta study site with a sparser distribution than seen in the other landscapes. The median lies at 58 m with a MAD of 33 m.

In the Oregon Coast Range the hilltop flow routing algorithm produces basin average hillslope lengths with a median of 89 m and a MAD of 17 m (Figure 3.6a). Results derived from slope-area measurements for this location show a skewed distribution where the majority of measurements are below 10 m, with a median value of 6 m and a MAD of 1 m (Figure 3.6b). The Oregon Coast Range drainage density derived hillslope length data is normally distributed about a median of 39 m with a MAD of 10 m (Figure 3.6c).

For Gabilan Mesa the median hillslope length from hilltop flow routing is 103 m with a MAD of 26 m (Figure 3.7a). The slope-area data for Gabilan Mesa show fewer measurements overestimating hillslope length than in the other landscapes with a median value of 112 m with a MAD of 56 m (Figure 3.7b). Similar to the slope-area data, the drainage density derived measurements do not form a

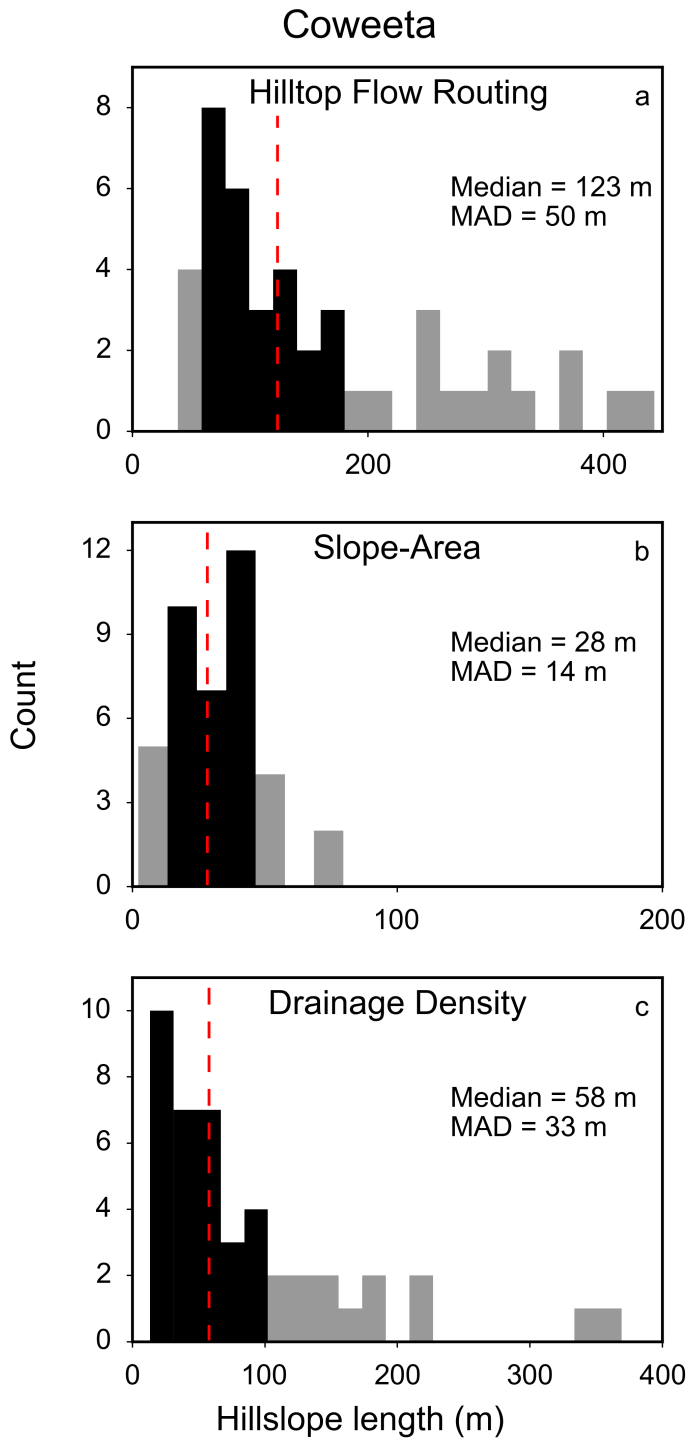

Figure 3.5: Histograms of basin median hillslope length for Coweeta, North Carolina calculated using: **(a)** hilltop flow routing; **(b)** slope-area analysis; and **(c)** inversion of drainage density. The red dashed line denotes the median and black bars indicate ± 1 median absolute deviation (MAD), with the grey bars showing the remaining data. The median and MAD values for each technique are also reported.

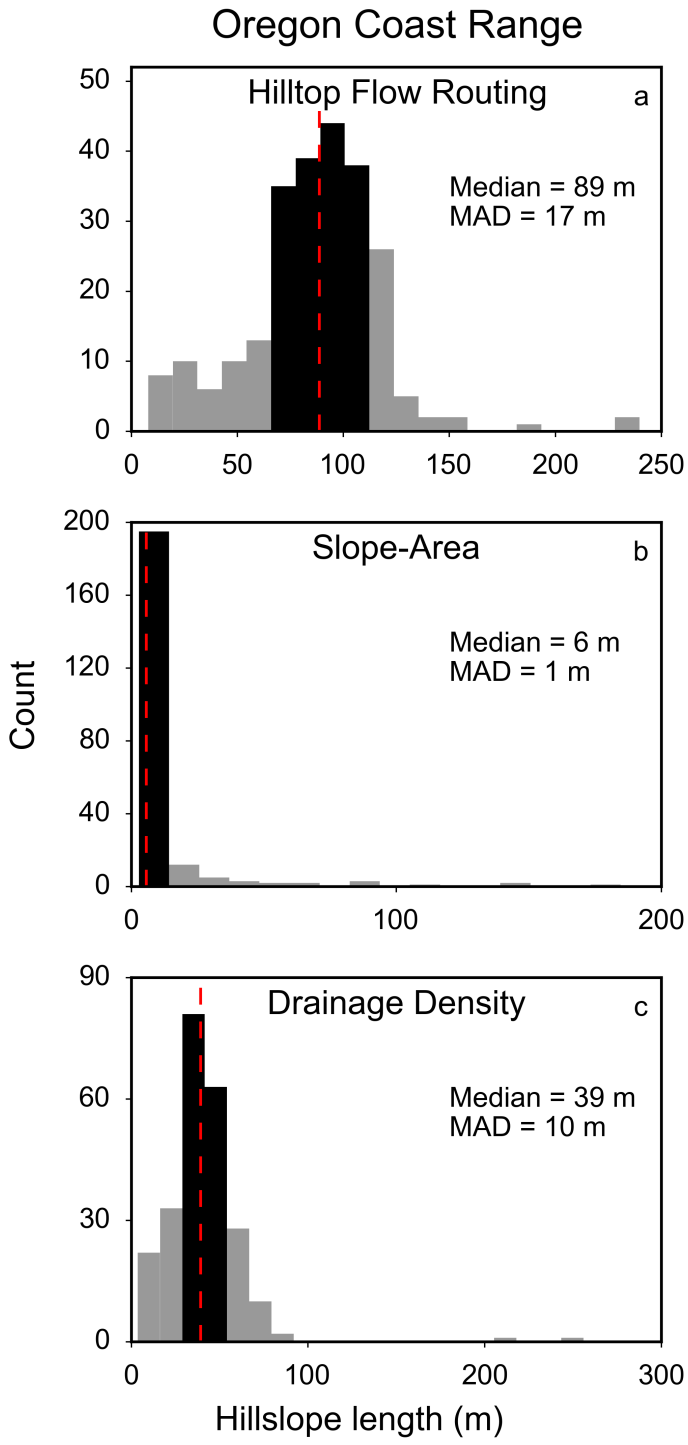

Figure 3.6: Histograms of basin median hillslope length for Oregon Coast Range, Oregon calculated using: **(a)** hilltop flow routing; **(b)** slope-area analysis; and **(c)** inversion of drainage density. The red dashed line denotes the median and black bars indicate ± 1 median absolute deviation (MAD), with the grey bars showing the remaining data. The median and MAD values for each technique are also reported.

continuous distribution, with a lower median hillslope length of 42 m and a MAD of 14 m (Figure 3.7c).

In the northern Sierra Nevada the hilltop flow routing data show a long tail extending to 400 m with a median of 104 m, and a MAD of 35 m (Figure 3.8a). Slope-area measurements for this location exhibit a skewed distribution of hillslope lengths, extending towards 2.75×10^5 m with a median value of 177 m and a MAD of 173 m (Figure 3.8b). The northern Sierra Nevada drainage density data has a similar median to the Oregon Coast Range at 33 m, but with a larger MAD of 13 m (Figure 3.8c), driven by the presence of a number of outlying basins exceeding a median hillslope length of 200 m.

3.5.2 Individual hillslope measurements

The Oregon Coast Range data have a median value of 98 m (Figure 3.9b) and the least variance of the four datasets, with a (MAD) of 35 m. The Coweeta and Sierra Nevada data have similar right skewed distributions but their medians differ by 100 m from 228 to 127 m, respectively (Figure 3.9a, d). The Coweeta data show a much larger MAD of 140 m compared with the Sierra Nevada data at 71 m. The Gabilan Mesa data are less right skewed than the Coweeta and Sierra Nevada data with a median of 140 m and a MAD of 60 m (Figure 3.9c). The dataset shows several smaller peaks which correspond to the different length scales that can be identified in the Gabilan Mesa data.

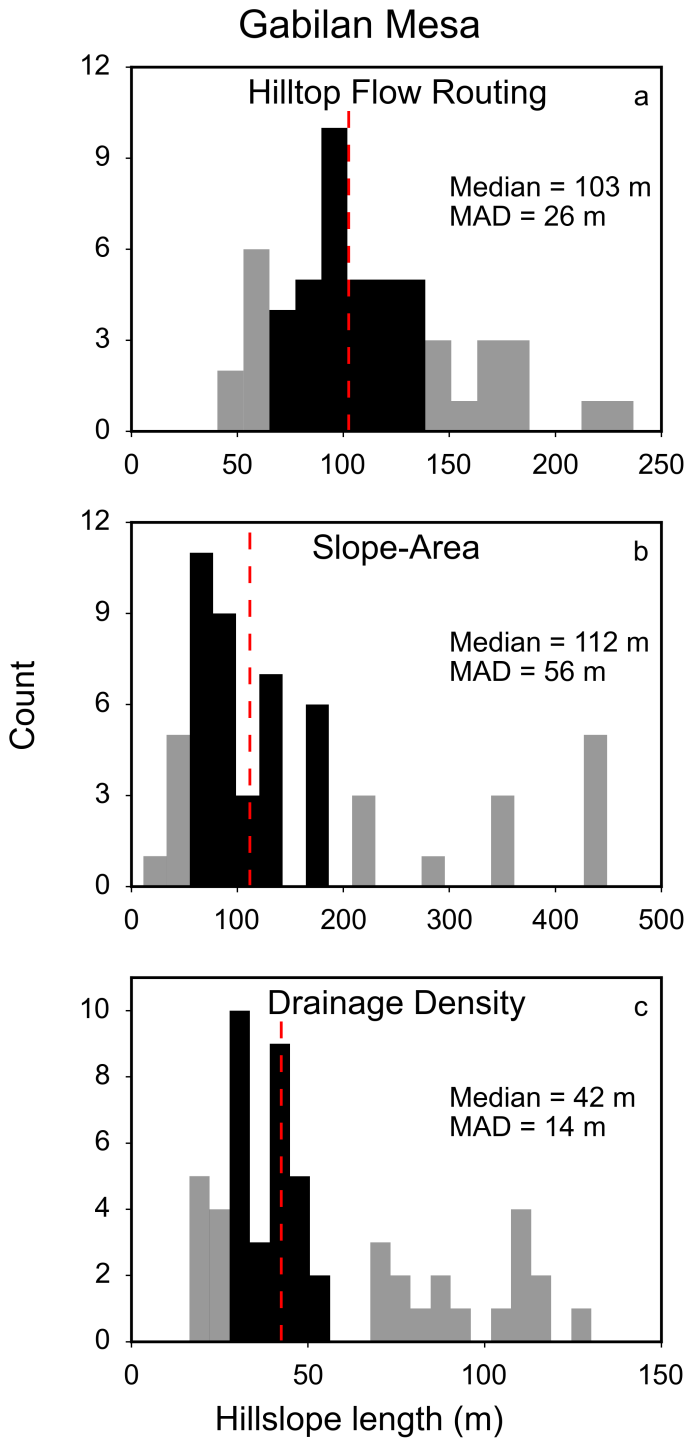

Figure 3.7: Histograms of basin median hillslope length for Gabilan Mesa, California calculated using: **(a)** hilltop flow routing; **(b)** slope-area analysis; and **(c)** inversion of drainage density. The red dashed line denotes the median and black bars indicate ± 1 median absolute deviation (MAD), with the grey bars showing the remaining data. The median and MAD values for each technique are also reported.

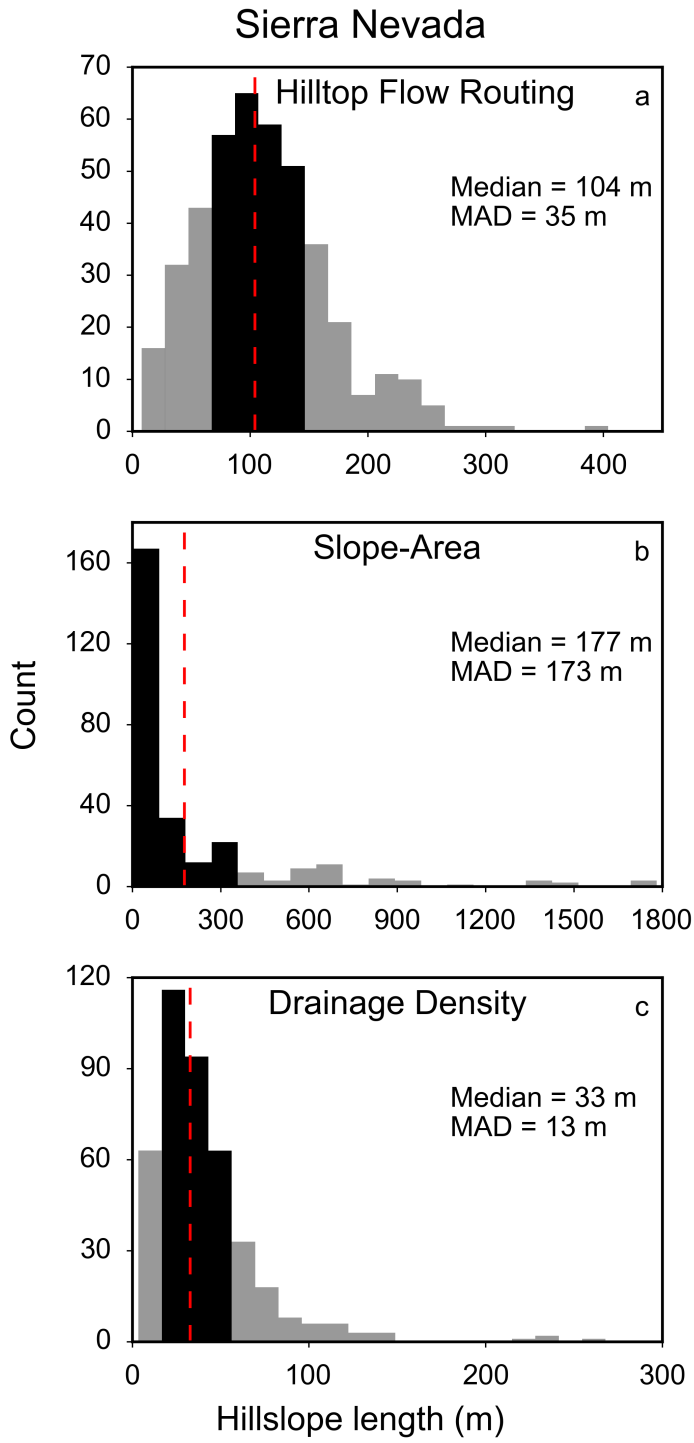

Figure 3.8: Histograms of basin median hillslope length for northern Sierra Nevada, California calculated using: **(a)** hilltop flow routing; **(b)** slope-area analysis; and **(c)** inversion of drainage density. The red dashed line denotes the median and black bars indicate ± 1 median absolute deviation (MAD), with the grey bars showing the remaining data. The median and MAD values for each technique are also reported.

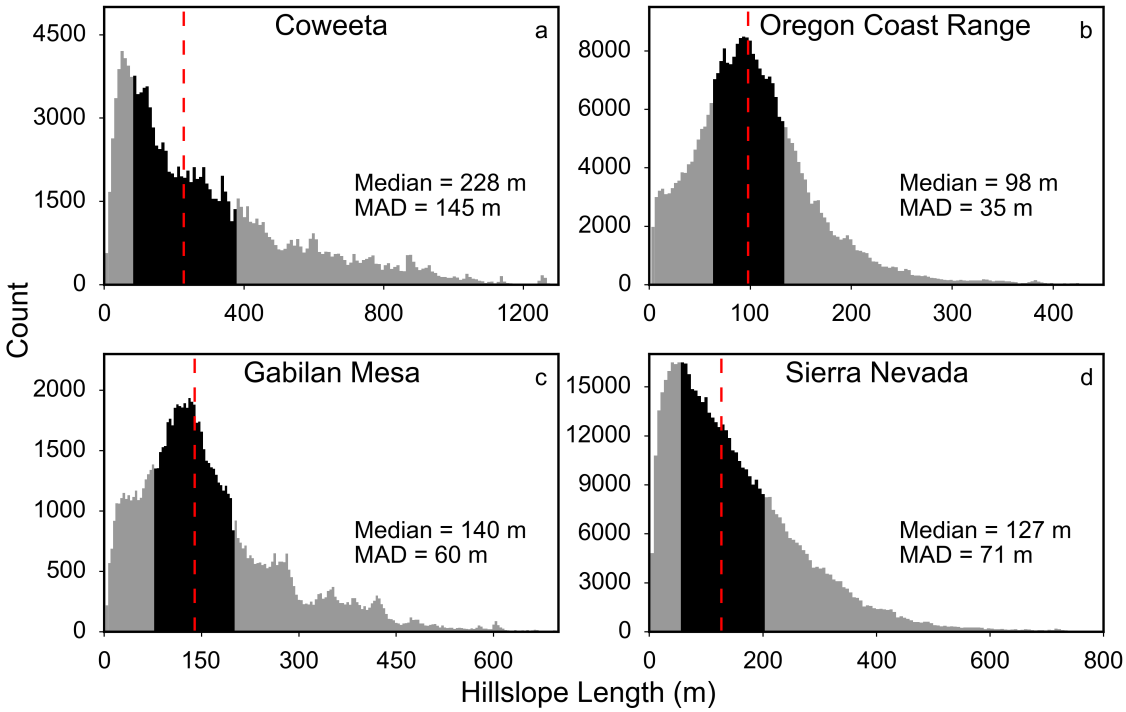

Figure 3.9: Histograms of hillslope length from every measured trace in each landscape. The red dashed line denotes the median and black bars indicate ± median absolute deviation (MAD), with the grey bars showing the remaining data. The median and MAD values for each site are also reported. **(a)** Coweeta, North Carolina. **(b)** Oregon Coast Range, Oregon. **(c)** Gabilan Mesa, California. **(d)** Northern Sierra Nevada, California.

3.6 Discussion

3.6.1 Comparison of hillslope length measurement techniques

Figure 3.10 presents the median and MAD hillslope length value for each technique across the four test landscapes. The slope-area derived hillslope length

values for the Oregon Coast Range are distinctly different to the expected range of measurements for this locality, with most basins being underestimated by at least an order of magnitude. However the underestimation does not appear to be systematic as some of the basins have values outside the range of the expected hillslope lengths, with one basin showing a predicted median hillslope length exceeding 2×10^4 m. In both the northern Sierra Nevada and Coweeta slope-area derived datasets the large range within the data is driven by the large variation in basin areas found in the landscape with the largest measurements skewing the median data. As with the Oregon Coast Range the modal values are at the lowest end of the distribution, showing a similar underestimation in hillslope lengths to the Oregon Coast Range data. In Gabilan Mesa the slope-area measurements appear to correlate more strongly with the hillslope length values measured from the landscape using hilltop flow routing, suggesting that the regularity of valley spacing and smoothness of the landscape in this location may facilitate more accurate slope-area measurements.

These data show the difficulty in measuring hillslope length using slope-area plots, and although in Gabilan Mesa the estimated values show good agreement with measured hillslope lengths, this pattern is not repeated in the other three landscapes. This failure of slope-area plots to predict hillslope length is not systematic, with both over- and under-estimates observed. This suggests that in steep, complex terrain with a range of processes acting upon it the slope-area technique fails to capture the hillslope to valley transition point accurately.

A fundamental problem in using slope-area plots to infer hillslope length is that the value identified by the kink in the curve is an area, not a length. This value is converted into a length by dividing the area by the unit contour width, which assumes a uniform shape of the upstream contributing area. As can be observed in nature, zero order basins are rarely this uniform, resulting in the derived length value possibly having little bearing on the actual geometry of the landscape.

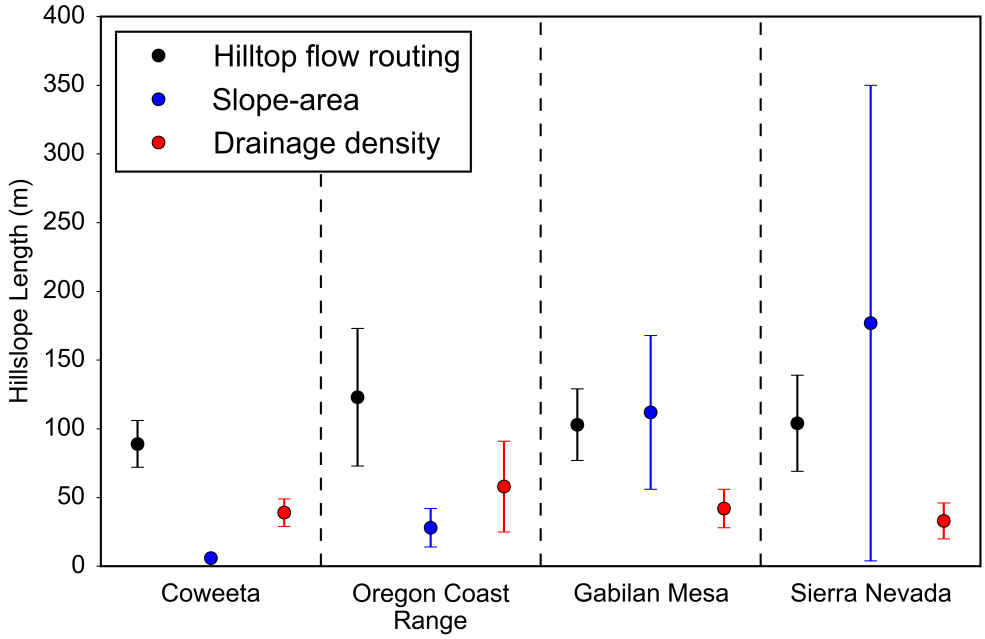

Figure 3.10: Comparison between the three hillslope length measurement techniques, hilltop flow routing (black), slope-area analysis (blue) and drainage density inversion (red). Error bars indicate ±1 MAD around the median value for each landscape. Black dashed lines separate measurements from different landscapes.

In order to generate a slope-area plot following techniques described by Hancock and Evans (2006), Roering *et al.* (2007) and Tarolli and Dalla Fontana (2009), the raw slope and area data must be binned and smoothed in order to highlight the trend. This introduces free parameters and reduces the repeatability of the technique across different landscapes where different parameters may be needed to extract the inflection point (Figure 3.3). Although the technique can be shown to work in selected cases, it needs user supervision and modification for each individual basin to which it is applied and therefore caution is required if it is to be used at the landscape scale. In this analysis the identification of an inflection point is performed automatically and in each location there are several basins where the inflection point identified far exceeds the possible range of hillslope lengths which can be observed in the landscape (Figure 3.11).

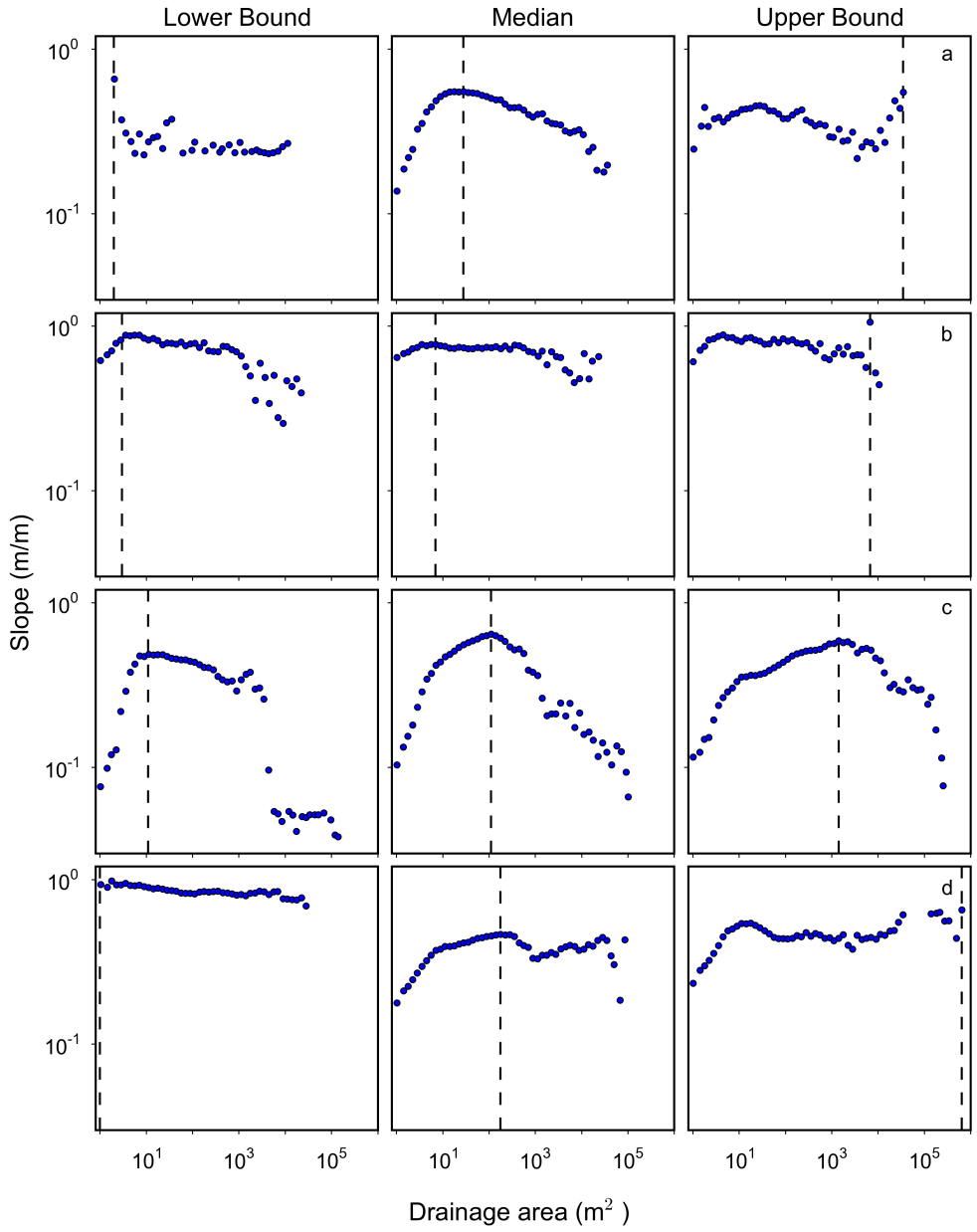

Figure 3.11: Three slope-area plots for each landscape, demonstrating the range of hillslope length values generated using this method, from the lowest estimate, to the median value to the highest estimate. Each data point is logarithmically binned from the raw data, following the methods outlined in Section 3.4.2. The dashed line indicates the location of the inflection point, as identified by the algorithm. **(a)** Coweeta, North Carolina. **(b)** Oregon Coast Range, Oregon. **(c)** Gabilan Mesa, California. **(d)** Northern Sierra Nevada, California.

The technique is also limited by a minimum basin size, as a sufficient number of data points are required in order to extract a signal from the data; such a limitation does not exist in the hilltop flow routing technique, which can extract hillslope lengths for individual hillslopes.

Measurements of hillslope length from drainage density systematically underestimate the value measured through hilltop flow routing in all four landscapes. Each location also has a very low variance when compared with the hilltop flow routing measurements. This highlights the inability of this method to capture the true variability in hillslope lengths which can be observed in a landscape, with the majority of basin measurements falling within a very small range of values, even in locations such as Coweeta which has a range of basin areas that scale over an order of magnitude.

The drainage density technique only requires generation of a channel network, which is routinely generated for most forms of topographic analysis, although the value will be sensitive to the choice of method for identifying channel heads. However, the drainage density approach can only provide a single basin average value whereas measurement techniques using flow paths demonstrate that hillslope length can vary substantially within a basin and can therefore provide a range of values for a single basin, allowing more complex patterns of hillslope length variations to be studied across smaller spatial areas. Another benefit of using drainage density to quantify hillslope length is that it is computationally efficient and unambiguous in its implementation compared with other techniques that have many free parameters.

I observe, however, that using drainage density systematically underestimates hillslope length values when compared with flow path derived measurement techniques. Such systematic underestimation is driven by the technique's inability to capture small-scale local variations in hillslope length. This is a necessary

outcome of using a basin average method and one which cannot be overcome; the urge to use smaller and smaller basins to increase the measurement resolution consequently will decrease the accuracy of the measurements as fewer streams will be included in each basin's drainage density value, making the resulting value less robust.

3.6.2 Spatial patterns of hillslope length from hilltop flow routing

The large ranges observed in both the individual hillslope and basin average hilltop flow routing data for Coweeta and the northern Sierra Nevada are driven by variations in hillslope and basin morphology. These landscapes appear transient, with incision into plateaus creating populations of steep, short hillslopes and long hillslopes running across lower gradient plateaus. The large range of basin areas, varying over an order of magnitude, produces the potential for longer hillslopes, particularly in Coweeta. When contrasting Coweeta and northern Sierra Nevada it is clear that the Coweeta dataset is not as well constrained, due to the smaller size of the area covered by the dataset, limiting the number of basins that can be studied.

The more uniform valley spacing of the Gabilan Mesa and Oregon Coast Range (Roering *et al.*, 2007; Perron *et al.*, 2009) results in a less skewed distribution of hillslope length measurements when contrasted with the other two landscapes. This is particularly apparent in Gabilan Mesa where the more rounded nature of the landscape, with fewer sharp transitions between hillslope and channel regimes, minimize variation in hillslope length. In the Oregon Coast Range the majority of basin average hillslope length data are within 1 MAD of the median, emphasizing the uniformity in valley spacing and basin area in this

landscape. However, with these uniform landscapes a wide range of individual values is observed, highlighting the utility of the hilltop flow routing algorithm for capturing topographic information at the hillslope scale.

3.6.3 Comparing relief with predictions from linear and nonlinear flux laws

The data from Coweeta are sparse (Figure 3.12a) with only 82 traces identified as planar across the landscape, and all of these traces occurring in lower relief sections of the landscape, yet they still follow a broadly linear trend. The reduction in planar traces in this landscape may be connected to the general morphology of the Coweeta catchment, which has fewer regularly spaced valleys than other similar sites such as the Oregon Coast Range, presenting more opportunity for longer traces to diverge from planarity. This is exacerbated by the high incidence of landsliding reported in the study area (Hales *et al.*, 2009) which leads to increased topographic roughening.

The Oregon Coast Range data are tightly grouped along a linear trend (Figure 3.12b), showing a broad range of L_H and R values which correspond to observations of the range of valley spacing and relief made in this location (Roering *et al.*, 1999). These data highlight that the planar trace filtering method is not biasing the sampling towards certain spatial locations or topographic patterns and that the trends of L_H and relief reflect the study area as a whole.

The Gabilan Mesa is a smaller geographic area than the other three sites and correspondingly has fewer data points than the Oregon and Sierra Nevada data. However, as with the Oregon Coast Range data, a broad range of values has been sampled, highlighting the ability of this technique to operate across a range of

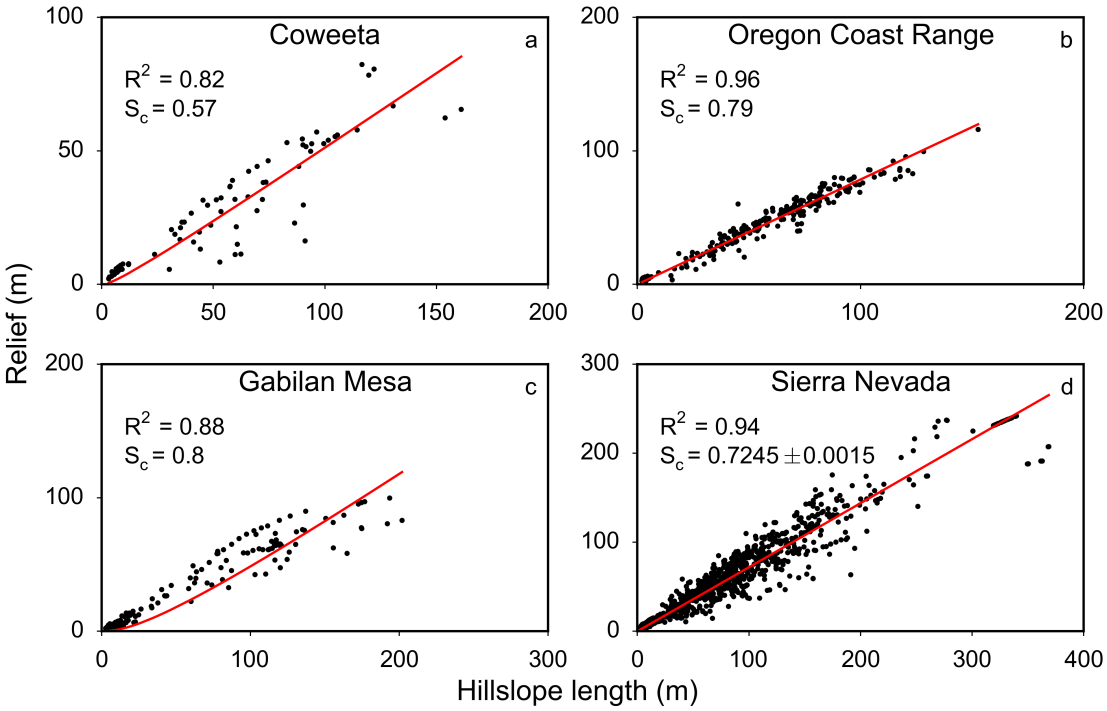

Figure 3.12: Scatter plots of the relationship between hillslope length and relief for each landscape. Each data point corresponds to a single hillslope trace. Red lines reflect Equation 3.8 fitted to the data using parameters in Table 3.2. The best fit critical slope value and corresponding R^2 value are also reported. **(a)** Coweeta, North Carolina. **(b)** Oregon Coast Range, Oregon. **(c)** Gabilan Mesa, California. **(d)** Northern Sierra Nevada, California. The critical slope for this location is computed using a range of erosion rates, producing a maximum and minimum critical gradient for this landscape which differ by 0.003. As these two best fit lines are visually indistinguishable, only the line generated using the upper erosion rate bound is displayed.

landscape morphologies, and again the data show a linear trend. However, at longer L_H, R values stop increasing, reaching an apparent limit at approximately 100 m (Figure 3.12c) suggesting that in the highly diffusive landscape relief greater than this threshold cannot be sustained.

In the northern Sierra Nevada (Figure 3.12d) the data follow a similar pattern to the Oregon Coast Range, although there is more scatter and a larger range of values. This increased scatter is indicative of the wider range of topography in the northern Sierra Nevada, as these data capture hillslope traces from the rapidly incising canyons and from the more slowly eroding plateaus. Being able to identify a linear trend in such variable data, with no need for special processing, highlights the robustness and fundamental character of the $L_H - R$ relationship and its ability to predict nonlinear sediment flux.

In both the Oregon Coast Range and the northern Sierra Nevada the data at low R and low L_H values show much less variance than the remainder of the data for each site. These data points correspond to hilltops located close to the outlet of catchments, which produce very short, planar traces with little variation in the measurements. Such a lack of variation has no impact on the overall patterns in the data and as such there is no requirement to exclude these points from further analysis. This independent evidence for nonlinear flux is not dependent on collecting erosion rate data or an erosion gradient in a landscape, as is required when analyzing E^*R^* data to constrain sediment flux laws (Roering *et al.*, 2007; Hurst *et al.*, 2012). This technique provides clear evidence for the nonlinear sediment flux law operating on a range of landscapes and highlights that hillslopes are able to record information about the sediment transport process which can be quantified through topographic analysis.

Through the use of published parameters K, ρ_r, ρ_s and E (see Table 3.2 for parameter values), Equation 3.8 can be fitted to each dataset to test how well this model explains real topography. The best fit of Equation 3.8 to the Coweeta dataset uses $S_c = 0.57$ ($\mathrm{R}^2 = 0.82$). This predicted critical gradient is low and suggests that processes other than the creep-like sediment transport described by Equation 3.1 may be operating in Coweeta that limit relief of hillslope traces. I can say with confidence, however, due to this strong relief limit, that a linear

sediment flux law such as that described by Equation 3.3 is not appropriate in this landscape.

Table 3.2: Parameters used to fit Equation 3.10 to $L_H - R$ data.

Location	K (m^2 yr^{-1})	E (m yr^{-1})	ρ_s[a] (kg m^{-3})	ρ_r[a] (kg m^{-3})	Reference
Coweeta	0.005	0.00027	1.4	2.4	Matmon *et al.* (2003)
Oregon Coast Range	0.003	0.0001	1.4	2.4	Roering *et al.* (1999, 2007)
Gabilan Mesa	0.038	0.00036	1.4	2.4	Roering *et al.* (1999, 2007)
Sierra Nevada	0.0086	0.00025[b] 0.00002[c]	1.4	2.4	Hurst *et al.* (2012)

[a]Soil and rock densities are average values of representative lithologies taken from Hillel (1980).

[b]Measurement from the canyon.

[c]Measurement from the plateau surface.

In the Oregon Coast Range the predicted S_c is 0.79 with $R^2 = 0.96$; this gradient falls below the value reported by Roering *et al.* (2007) of 1.2 ± 0.1, but it is within published ranges of critical slope values for similar landscapes (Hurst *et al.*, 2012).

This predicted critical gradient is lower than a large proportion of the hillslopes in the Oregon Coast Range, and this discrepancy may indicate that Equation 3.8 does not fully capture the range of sediment transport processes occurring in the Oregon Coast Range.

A similar critical gradient of 0.7245 ± 0.0015 ($R^2 = 0.94$) is predicted for the northern Sierra Nevada, with the small error bounds generated by performing the fit using the erosion rate from the rapidly eroding canyon and from the more slowly eroding plateau, which is similar to the predicted value of 0.8 from Hurst *et al.* (2012), which was estimated using E^*R^* data. The estimate of Hurst *et al.* (2012) requires averaging relief and ridgetop curvature along ridgetop segments, which are then themselves binned and averaged. In addition, the E^*R^* technique requires a range of erosion rates to constrain the value.

The predicted critical gradient for the Gabilan Mesa is equal to the lower bounds of the previously published value of 1.2 ± 0.4 (Roering *et al.*, 1999) at 0.8 with $R^2 = 0.88$. However, due to the highly diffusive nature of Gabilan Mesa the model does not explain the $L_H - R$ relationship as well as in other landscapes. However, the published values of erosion rate and the sediment transport coefficient are less well constrained for Gabilan Mesa than in the other landscapes (Roering *et al.*, 2007). If the sediment transport coefficient is reduced toward the lower bound of the published range, or the erosion rate is increased toward the upper bound, this fit considerably improves, suggesting that these values may have been over- or under- estimated, respectively.

A limitation of estimating the critical gradient for a landscape using a best fit relationship is that approximately 50% of hillslopes in the landscape will have a gradient in excess of this best fit value. This can explain the discrepancy between critical gradients predicted in this study and those of Roering *et al.* (1999) which were generated by estimating the erosion rate for planar hillslopes

from their morphology, and identifying the values of K and S_c which minimized the deviation from the landscape average erosion rate.

A landscape can be expected to exhibit a probability density of critical gradients, controlled by local scale variations in soil, vegetation and topographic properties (Hales *et al.*, 2009). The best fit S_c value generated using $L_H - R$ data is an averaged S_c value, representative of an average hillslope in the landscape, whereas the technique of Roering *et al.* (1999) may better constrain an upper bound for a landscape critical gradient.

3.7 Conclusions

I implement a technique to measure the length of individual hillslopes from digital topography, modelling flow as a point source travelling through DEM cells from hilltop to channel. Through the implementation of this technique two previous methods used to generate basin average hillslope lengths are evaluated. Inverting drainage density produces normally distributed hillslope lengths which systematically underestimate the true lengths of hillslopes found in a landscape. Analyzing slope-area plots for their inflection point in order to extract a characteristic hillslope length is found to be very sensitive to catchment morphology and user defined parameters, producing large amounts of uncertainty in their accuracy.

Hilltop flow routing produces robust results across a range of landscape morphologies, coping with erosional gradients, vegetation changes and differing tectonic regimes. The technique allows for exploration of the variability of hillslope length within a landscape for the first time. By using this flow path method the relationship between relief and hillslope length is explored, providing evidence of nonlinear

sediment transport processes in four test landscapes. It is also shown that the critical gradient used in the nonlinear flux model can be constrained. In three of the four test landscapes the predicted critical gradient is shown to be lower than previously published, suggesting that this value may represent the average of a population of critical gradients across a landscape, highlighting the heterogeneity of landscape properties which can be found in steady state landscapes.

Chapter 4

A nondimensional framework for exploring the relief structure of landscapes

A version of this chapter has been published in Earth Surface Dynamics as:

Grieve, S.W.D., Mudd, S.M., Hurst, M.D. and Milodowski, D.T. (2016).
A nondimensional framework for exploring the relief structure of landscapes.
Earth Surface Dynamics, 309-325. 10.5194/esurf-4-309-2016

The work presented here was performed in collaboration with my co-authors who contributed to the final writing of the manuscript and the development of some of the topographic analysis software. I performed the analysis, wrote topographic and data analysis routines, generated the figures and wrote the manuscript.

4.1 Abstract

Considering the relationship between erosion rate and the relief structure of a landscape within a nondimensional framework facilitates the comparison of landscapes undergoing forcing at a range of scales, and allows broad-scale patterns of landscape evolution to be observed. I present software which automates the extraction and processing of relevant topographic parameters to generate nondimensional erosion rate and relief data rapidly for any landscape where high-resolution topographic data are available. Individual hillslopes are identified using a connected-components technique which allows spatial averaging to be performed over geomorphologically meaningful spatial units, without the need for manual identification of hillslopes.

The software is evaluated on four landscapes across the continental United States, three of which have been studied previously using this technique. I show that it is possible to identify whether landscapes are in topographic steady state. In locations such as Cascade Ridge, CA, a clear signal of an erosional gradient can be observed. In the southern Appalachians, nondimensional erosion rate and relief data are interpreted as evidence for a landscape decaying following uplift during the Miocene. An analysis of the sensitivity of this method to free parameters used in the data smoothing routines is presented which allows users to make an informed choice of parameters when interrogating new topographic data using this method. A method to constrain the critical gradient of the nonlinear sediment flux law is also presented which provides an independent constraint on this parameter for three of the four study landscapes.

4.2 Introduction

The Earth's surface evolves dynamically in response to the interplay of climatic, tectonic and other factors operating at timescales ranging from minutes to millennia. High-resolution topographic data generated from terrestrial and airborne laser scanning, in combination with increased computational power, have facilitated a revolution in geomorphology, allowing the quantitative interrogation of landscape form to provide insight into the forces shaping a landscape. Relationships have been found between topography and the tectonic (e.g., Wobus *et al.*, 2006; Hilley and Arrowsmith, 2008; DiBiase *et al.*, 2012; Hurst *et al.*, 2013b), climatic (e.g., Gabet *et al.*, 2004; Anders *et al.*, 2008; Champagnac *et al.*, 2012), and biotic (e.g., Roering *et al.*, 2010; Milodowski *et al.*, 2015a) forcing of a landscape in addition to links between topography and bedrock properties (e.g., Korup, 2008; Clarke and Burbank, 2010, 2011; Hurst *et al.*, 2013c).

Such fundamental relationships provide important insight into landscape evolution; however, many of these techniques are challenging to implement, due to variable or poorly defined methods, or require proprietary software to obtain data. This highlights the need for standardized techniques and tools to allow the analysis of topographic data to be reproduced and falsified, strengthening our understanding of the processes that shape planetary surfaces. In this contribution I focus on methods exploiting high-resolution topographic data in soil-mantled landscapes that aim to elucidate both sediment flux laws (e.g. Dietrich *et al.*, 2003) and the transient evolution of landscapes (e.g., Hurst *et al.*, 2013b).

My approach is rooted in a nondimensional framework that describes relationships between erosion rates and hillslope topography in soil-mantled landscapes (Roering *et al.*, 2007). This framework facilitates the direct comparison of landscapes of widely varying morphology and process. It has been shown to provide compelling

insight into the identification of landscape transience (Hurst *et al.*, 2012), complex tectonic signals from topography (Hurst *et al.*, 2013b), and process controls on the density of channels (Sweeney *et al.*, 2015). Extracting the nondimensional parameters from high-resolution topography can be difficult, subject to choices about how the metrics are calculated, and there has been no investigation into how different methods might influence results, and therefore the interpretation of landscapes.

Here I present a framework and methodology for extracting the required topographic parameters and processing the resulting data. This software uses a clear methodology to allow researchers to generate these data for new landscapes and can replicate published relationships between nondimensional erosion rate and relief. Such relationships can be used to discriminate between landscapes in topographic steady state, where erosion rate is balanced by uplift rate, and those undergoing transience or topographic decay.

Additionally I present a method for generating spatially contiguous hilltop patches, required as a spatial averaging tool in many studies (e.g., Perron *et al.*, 2009; Hurst *et al.*, 2012, 2013b) to identify individual hillslopes for analysis. An analysis on the influence of spatial averaging and data smoothing on the interpretation of topographic data is undertaken and hillslope and basin average data are also used to estimate the critical gradient, a key parameter in the nonlinear sediment flux model.

4.3 Theoretical Background

Numerous sediment flux laws (cf. Dietrich *et al.*, 2003) have been developed and tested, particularly since the advent of cosmogenic radionuclide dating and high-resolution topographic measurements. In addition to the conceptually simple linear flux law (Culling, 1960; McKean *et al.*, 1993; Tucker and Slingerland, 1997; Small *et al.*, 1999; Booth *et al.*, 2013), models of depth-dependent (Braun *et al.*, 2001; Furbish and Fagherazzi, 2001; Heimsath *et al.*, 2005; Roering, 2008) and nonlinear sediment flux (Andrews and Bucknam, 1987; Roering *et al.*, 1999, 2001, 2007) have been employed, alongside models which directly consider sediment particle motion (Foufoula-Georgiou *et al.*, 2010; Tucker and Bradley, 2010; Furbish and Roering, 2013).

Models which consider particle motion are challenging to apply to real topography as they do not have an analytical solution and without high-resolution soil depth information it is challenging to apply a soil-thickness-based sediment flux law to landscape-scale analysis (Chapter 3). However, topographic predictions of the nonlinear flux law have been successfully tested (Roering *et al.*, 2007) suggesting that, at a minimum, it can constrain broad-scale sediment transport processes across landscapes. The nonlinear flux law is (Andrews and Bucknam, 1987; Roering *et al.*, 1999, 2001, 2007)

$$q_\mathrm{s} = \frac{KS}{1 - (|S|/S_\mathrm{c})^2}, \tag{4.1}$$

where S is the topographic gradient in dimensions of length/length (dimensions henceforth denoted in square brackets as $[L]$ength, $[M]$ass and $[T]$ime), S_c [dimensionless] is the hillslope critical gradient, K $[L^2T^{-1}]$ is a sediment transport coefficient, and q_s $[L^2T^{-1}]$ is a volumetric sediment flux per unit contour length.

As S tends towards S_c, the sediment flux asymptotically increases towards infinity, corresponding to an increase in landsliding on an increasingly planar hillslope.

Roering *et al.* (2007) modeled the relief structure of theoretical one-dimensional hillslopes which evolve under Equation 4.1 and found that relief, the difference in elevation between a hilltop and the point on the channel to which it is coupled, is controlled by the erosion rate, hillslope length, and the sediment transport coefficient. Equation 4.1 has been found to be consistent with observations of topography and erosion rates across several landscapes (e.g., Roering *et al.*, 1999, 2007; Roering, 2008; Hurst *et al.*, 2012)

Roering *et al.* (2007) normalized relationships describing these one-dimensional hillslopes using topographic parameters to produce a dimensionless erosion rate,

$$E^* = \frac{E}{E_R} = \frac{\rho_r}{\rho_s} \cdot \frac{2EL_H}{KS_c} = \frac{-2C_{HT}L_H}{S_c}, \tag{4.2}$$

where E $[LT^{-1}]$ is the erosion rate, ρ_r and ρ_s $[ML^{-3}]$ are the rock and soil bulk densities, respectively, C_{HT} $[L^{-1}]$ is the hilltop curvature, L_H $[L]$ is the hillslope length, E_R $[LT^{-1}]$ is a reference erosion rate denoted as

$$E_R = \frac{KS_c}{2L_H(\rho_r/\rho_s)}, \tag{4.3}$$

and the dimensionless relief is given as

$$R^* = \frac{R}{S_c L_H}, \tag{4.4}$$

where R $[L]$ is the topographic relief. Parabolic hillslope profiles are generated when E^* values are less than or equal to 1, such that R^* increases approximately linearly with erosion rate. Planar hillslopes near the critical gradient, S_c, indicate that R^* is insensitive to erosion rate when E^* approaches or exceeds 1. This prediction is consistent with observations that, when erosion rates are high, relief

becomes limited by a critical slope angle, set by the material properties of the underlying bedrock (e.g., Binnie *et al.*, 2007; DiBiase *et al.*, 2012). A combination of high E^* and R^* values indicates a landscape with steep, planar hillslopes and frequent landsliding, whereas low values suggest more convex hillslopes with lower overall relief (Roering *et al.*, 2007).

For landscapes in topographic steady state with uniform erosion rates, values of E^* and R^* will plot on the steady-state curve described by

$$R^* = \frac{1}{E^*}\left(\sqrt{1+(E^*)^2} - \ln\left(\frac{1}{2}\left(1+\sqrt{1+(E^*)^2}\right)\right) - 1\right). \tag{4.5}$$

Here, I define steady state using the formulation of Mudd and Furbish (2004), which considers a hillslope to be in steady state if it retains a constant topographic form with regard to its local base level, the channel at its base. Steady-state hillslopes which experience spatially uniform erosion rates will plot on a single point on the curve (Roering *et al.*, 2007), whereas landscapes experiencing an erosion gradient will plot at many points along this curve, as demonstrated by Hurst *et al.* (2012). These nondimensional landscape properties have utility beyond steady-state landscapes. Hurst *et al.* (2013b) used this formulation to distinguish between growing and decaying parts of a landscape by identifying hysteresis in E^*R^* space. Sweeney *et al.* (2015) applied similar techniques to analogue landscape evolution models to demonstrate that the efficiency of hillslope sediment transport controls drainage density. These cases of differing landscape properties and histories highlight the power of using topography and E^*R^* analysis to interpret landscape evolution.

The application of such a framework to real data is limited by the challenge of applying a one-dimensional model of hillslope evolution to two-dimensional topographic data. Attempts to apply such models typically identify non-convergent

portions of the landscape upon which to perform tests through either field surveying planar hillslopes (Rosenbloom and Anderson, 1994), the algorithmic identification of convergent topography (Chapter 3), manual identification of planar topography from digital elevation models, or the exclusion of areas of high convergence from hillslope profiles through a valley extraction algorithm as is employed by Hurst *et al.* (2012) and in this study. All such methods are compromises between computational efficiency, reproducibility, and the accuracy with which a one-dimensional hillslope profile can be extracted. Consequently, the conclusions drawn using this, or any other, application of one-dimensional theory to two-dimensional data must be considered within the context of their potential errors.

4.4 Hilltop Patches

The extraction of signals from high-resolution topographic data can often require smoothing of raw data to filter out both topographic and artificial noise (Lashermes *et al.*, 2007; Roering *et al.*, 2010; Sofia *et al.*, 2013). This smoothing can be performed either by processing the raw digital elevation model (DEM) before any analysis is performed (e.g., Roering *et al.*, 2010) or by smoothing the output data (e.g., Tucker *et al.*, 2001; Tarolli and Dalla Fontana, 2009). In order to understand landscape properties at a hillslope scale it is often desirable to perform local smoothing to group individual DEM pixels into collections of pixels that correspond to individual hilltops and their connected hillslopes.

This was performed by Hurst *et al.* (2012) through a process of vectorizing hilltops, then splitting the vectors by a threshold length and discarding all split segments shorter than an arbitrary length of 50 m. The final split vectors are then converted back into rasters in order to create a network of hilltop patches of a defined

minimum length. These patches are typically 2 pixels wide, spanning both sides of a drainage divide. This technique is challenging to reproduce, as it relies upon several user-defined parameters and a subjective assessment of which vector segments to discard.

4.4.1 Automated generation of hilltop patches

Connected-components analysis is a technique typically used in computer vision to label contiguous pixels in raster images (e.g. Rosenfeld and Pfaltz, 1966; Samet, 1981; Lumia *et al.*, 1983; Dillencourt *et al.*, 1992; Suzuki *et al.*, 2003; He *et al.*, 2013). Here, I implement a computationally efficient connected-components algorithm developed by He *et al.* (2008) to generate contiguous hilltop patches, resulting in a network of hilltop patches, each coded with a unique ID number (Figure 4.1). Finally, in order to allow better replication of the original concepts used in Hurst *et al.* (2012), a minimum patch area can be supplied, which is used to remove any hilltop patches which are smaller than this user-defined threshold.

This hilltop patch identification method is very efficient and has been demonstrated to operate effectively on large, complex images (He *et al.*, 2008) without an impact on performance. This technique has utility beyond E^*R^* calculations, as it can be used in any work where discrete patches of hilltop need to be identified (e.g., Perron *et al.*, 2009) or where individual hillslopes must be analyzed using topographic data.

4.5 Generating Topographic Data

4.5.1 Extraction of a channel network

A key component of most topographic analysis is the delineation of a channel network, without which many topographic parameters cannot be estimated. Channel networks can be extracted by using either a process-based method which uses the stream power model to identify the point in a landscape where fluvial processes begin to dominate over hillslope processes (Clubb *et al.*, 2014) or by using a geomorphometric method which identifies channels using curvature thresholds (Passalacqua *et al.*, 2010; Orlandini *et al.*, 2011; Pelletier, 2013).

In order for the E^*R^* data to capture the true range of erosion rates and reliefs inherent in a landscape, it is important to define a channel network which correctly identifies the hillslope–fluvial transition, including the delineation of colluvial channels, which are often challenging to identify using non-geomorphometric methods (Pelletier, 2013). Here I follow Pelletier (2013) and apply a Wiener filter (Wiener, 1949) to remove noise from the raw topographic data. Subsequently, channelized portions of the drainage network are identified based on a tangential curvature threshold (e.g., Pelletier, 2013). The appropriate curvature threshold is identified from the properties of its quantile–quantile plot (e.g., Lashermes *et al.*, 2007; Passalacqua *et al.*, 2010). These channelized patches of the landscape are combined by performing a connected-components analysis (He *et al.*, 2008) which merges discrete patches of channel into a contiguous channel network. Following methods outlined in Chapter 3, floodplain masks are also created and combined with this channel network, which separates the landscape into two domains: hillslopes and channels. This has the effect of terminating hillslope traces when they reach a hollow or enter the floodplain, ensuring that the trace properties only

reflect the hillslope domain and the E^*R^* measurements are not contaminated by sampling parts of the landscape to which the nondimensional framework does not apply.

If the channel network is incorrectly defined, some fluvial erosion could impact the correct measurement of E^*R^* values. However, due to the number of individual measurements per landscape ($> 160\,000$ in each case) and the small number of points on a landscape where such erroneous measurements could occur, such measurements will have little impact on landscape-scale trends, particularly when spatial averaging is applied.

4.5.2 Extraction of topographic parameters

All of the key measurements required to generate E^*R^* data can be extracted from high-resolution topography (Roering *et al.*, 2007). Calculation of E^* using Equation 4.2 requires hillslope length and hilltop curvature, and calculation of R^* using Equation 4.4 requires the relief and hillslope length to be measured from high-resolution topography.

In Chapter 3 I measured hillslope length by generating overland flow paths running from hilltop to channel pixels for every hilltop in a DEM, thereby generating a diverse range of measurements shown to characterize the range of hillslope properties inherent within a landscape. From these traces, each hilltop's local relief is also measured by taking the difference between the elevation at the start (hilltop) and end (channel) of each trace. Finally, the hilltop curvature for each hilltop pixel is extracted following Hurst *et al.* (2012), whose techniques demonstrated that hilltop curvature scales linearly with erosion rate below hilltop gradients of 0.4. Correspondingly, I also sample the hilltop gradient (S_{HT}) at the start of each trace to allow data to be filtered later by this value. By using the

methods outlined in Chapter 3 a 4-tuple of information for each hilltop pixel in the landscape containing $(L_{\mathrm{H}}, R, C_{\mathrm{HT}}, S_{\mathrm{HT}})$ can be generated.

4.5.3 Smoothing topographic parameters

In previous studies that have generated E^*R^* data, some form of smoothing has been employed to extract meaningful trends from the inherently noisy topographic data. Roering *et al.* (2007) hand-selected basins with uniform morphologies and minimal anthropogenic disturbance to measure topographic parameters from, effectively removing the majority of noise in the landscape and producing a small number of data points considered to be characteristic of their two steady-state landscapes.

Hurst *et al.* (2012) used semi-automated methods to extract the required topographic parameters, and averaged the resulting data spatially over hilltop segments of a defined minimum length. Hurst *et al.* (2013b) utilized the same methodology, but further averaged the data by grouping segments into bins defined by their distance along the Dragon's Back pressure ridge so as to explore the topographic expression of a transient uplift signal along the ridge. As these techniques do not self-select idealized hillslopes or basins as in Roering *et al.* (2007), some filtering of the raw data was required (see Section 4.6.1). These latter methods allow E^*R^* data to be used to interrogate transient landscapes, increasing the power of the method and providing a vital tool in the topographic analysis of landscapes.

Here, I extract topographic parameters from raw topographic data and smooth the resulting measurements, in accordance with previous authors' methods, firstly performing spatial averaging at a basin scale. The basins that are used to average the topographic parameters can be defined in an automated manner to produce

an average value over all basins of a given stream order, or a more user-defined approach can be undertaken to select basins manually in order to more closely replicate the work of Roering *et al.* (2007). Secondly the parameters can be averaged at a hillslope scale by using the discrete hilltop patches generated using the technique outlined in Section 4.4.1. The data are filtered using the same constraints outlined in Hurst *et al.* (2012), removing hilltops with a $S_{\mathrm{HT}} > 0.4$ or a patch size < 50 m, with the additional filtering of hillslope length and relief values below a user-defined threshold, typically 2–5 m for each parameter; this ensures that hilltops sampled are true hilltops and are not interfluves sitting adjacent to a basin outlet, which will not conform to models of hillslope sediment transport. The data are also returned to the user filtered, but not averaged, allowing users to explore the raw data to ensure that the smoothed data are a good reflection of the overall trends inherent in a landscape. Example basins and hilltop patches, used in the smoothing routines and the hillslope traces which produce the topographic measurements, are displayed in Figure 4.1.

4.6 Processing the Topographic Data

Once the topographic data have been extracted, they are filtered to ensure that only data which conform to the nondimensional framework described by Roering *et al.* (2007) are used in any further analysis.

4.6.1 Filtering

The key filtering process which must be performed is the removal of any data points which have an S_{HT} above 0.4. This is the threshold gradient beyond which sediment flux no longer scales linearly with slope and thus hilltop curvature

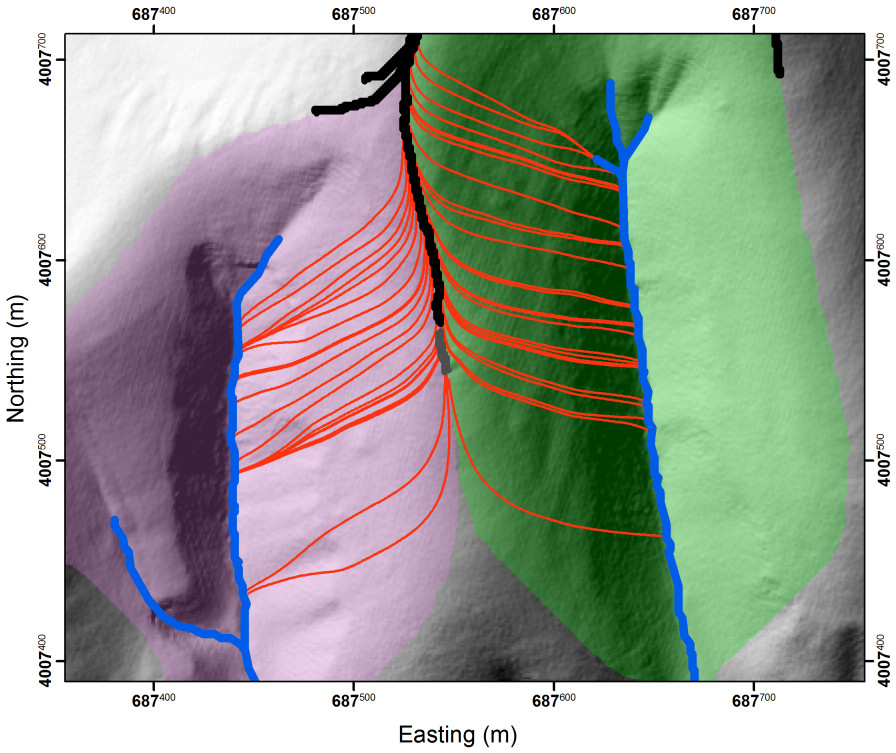

Figure 4.1: Map of a section of Gabilan Mesa, California (UTM Zone 10N), showing the examples of the spatial units used in the analysis of E^*R^* data. Two second-order basins, colored green and purple, are bisected by a ridge with two hilltop patches, a large black patch and a smaller grey patch. From these patches, representative hillslope traces, outlined in red, travel down the hillslope and terminate at the channel network. Only 10 % of the total traces generated for this ridge have been plotted and other surrounding hilltop patches and their associated traces are not displayed, to aid clarity. Coordinates are in meters.

does not reflect erosion rate, for K values representative of published values for my field sites (Roering *et al.*, 1999, 2007; Matmon *et al.*, 2003; Hurst *et al.*, 2012). Therefore data points with gradients above this value cannot be used in Equation 4.2 as a proxy for erosion rate. Across all of the data sets, gradients which exceed 0.4 are removed from further analysis. In the case of the two spatially averaged data sets, individual hilltop pixels which exceed this threshold gradient within a patch or basin are removed from the averaging process for each

measurement, ensuring that no invalid data contribute to the final calculations. To ensure the validity of each basin average measurement, a count of the valid pixels contained within each basin following gradient filtering is performed and any basins with fewer valid measurements than a user-defined threshold can be removed from the analysis. This threshold is typically equal to the minimum patch size used in Section 4.4.1 as this provides consistency between measurements.

4.6.2 Log binning

One method of non-spatial averaging of geomorphic data used effectively to generate slope–area plots (e.g., Tarolli and Dalla Fontana, 2009) is log binning. Such a method provides an opportunity to interrogate the data at a landscape scale while still removing the noise inherent in topographic measurements. Each E^*R^* pair is placed into evenly spaced bins in base 10 logarithmic space. The bin spacing is a function of the number of bins specified by the user, and the range of E^* values within the data set and its impact on interpretation of the data are considered in Section 4.7.2. To ensure that a valid number of data points make up each bin, a minimum bin size can also be specified by the user; this value will depend on the size and nature of the data set.

This type of averaging will work best in landscapes where an erosion gradient is expected, as it will produce a range of E^*R^* values across the domain, as can be seen in Hurst *et al.* (2012). In presumed steady-state locations such as Gabilan Mesa most of the data are expected to cluster around a single point (Roering *et al.*, 2007), and so imposing evenly spaced bins in log space onto such data may construct an artificial trend. It is therefore recommended to consider the raw data in conjunction with the binned data to ensure that the trends in the data are valid.

4.6.3 Visualizing data

The software allows the user to plot any combination of the E^*R^* data sets, facilitating the rapid generation of basin and landscape average data following Roering *et al.* (2007), hilltop-averaged and log-binned data following Hurst *et al.* (2012, 2013b), and raw data which have previously not been available. It is also possible to interrogate the raw measurements as a density plot, which more accurately conveys the trends in the raw data as in large landscapes many measurements share the same location in E^*R^* space. By allowing simple inter-comparisons between plotting methods it becomes trivial to assess the most suitable data visualization techniques for a specific landscape.

4.7 Results and Discussion

By using data from previous studies which utilize E^*R^* analysis, it is possible to assess the ability of this software to reproduce existing results in addition to understanding how the varying techniques for smoothing the data, discussed in Section 4.5.3, can impact on the interpretation of the processes operating on a landscape. Four landscapes in the continental USA have been selected to evaluate the software: the Oregon Coast Range and Gabilan Mesa, used by Roering *et al.* (2007); Cascade Ridge, used by Hurst *et al.* (2012); and the Coweeta Hydrologic Laboratory. High-resolution LiDAR data are available from the National Center for Airborne Laser Mapping (NCALM) for each site and each site's point cloud data have been gridded to 1 m resolution DEMs following Kim *et al.* (2006). Accuracy information for each point cloud can be found in Table 2.1.

4.7.1 Reproducing previous work

Oregon Coast Range and Gabilan Mesa

Roering *et al.* (2007) estimated the topographic parameters L_{H}, R, and C_{HT} for the Oregon Coast Range and Gabilan Mesa field sites. The characteristic hillslope length for each landscape was estimated by identifying the inflection point in a spline curve fitted though a plot of local slope against drainage area. This inflection point is considered to correspond to the transition between the hillslope and channel domain in a landscape (Montgomery and Foufoula-Georgiou, 1993; Hancock and Evans, 2006; Tarolli and Dalla Fontana, 2009; Tarolli, 2014; Tseng *et al.*, 2015).

Roering *et al.* (2007) estimated mean relief by calculating the mean of the differences between the maximum and minimum elevation within a kernel of radius equal to the characteristic hillslope length for each point on the landscape. Hilltop curvature was sampled from manually defined hilltops with a gradient below $0.05S_{\mathrm{c}}$ and averaged across each landscape. The critical gradient was calculated for the Oregon Coast Range to be 1.2 by Roering *et al.* (1999), and Roering *et al.* (2007) assumed that this value is also correct for Gabilan Mesa.

The data from Gabilan Mesa (Figure 4.2a) reveal many hilltop patches which correspond closely to the predicted E^*R^* values from Roering *et al.* (2007). The data are predominantly clustered around a single point, showing strong agreement with observations that the landscape is in approximate steady state. However, the majority of the basin average data points and a considerable number of the hilltop patch data plot below the steady-state curve, which could be interpreted as evidence for topographic decay. However, the uniform hilltop curvatures and valley spacing, coupled with measurements of long-term erosion rates, suggest that

this landscape is not undergoing topographic decay (Roering *et al.*, 2007; Perron *et al.*, 2009). An alternative explanation for the data falling below the steady-state curve is that an S_c value of 1.2 is too large for this landscape. Chapter 3 used similar topographic parameters to estimate the critical gradient for this landscape as 0.8. By replotting these data using this revised S_c, the data plot more closely to the steady-state curve (Figure 4.2b).

The Oregon Coast Range data are more tightly constrained than the Gabilan Mesa data (Figure 4.3a), and have a similar range of R^* values. However, as is the case for Gabilan Mesa, the majority of the data plot below the steady-state curve. This can be interpreted as evidence for topographic decay; however, due to the preponderance of evidence supporting a steady-state hypothesis for this landscape (e.g., Reneau and Dietrich, 1991; Roering *et al.*, 2007), it is also possible that a critical gradient of 1.2 is too large in this location. By using the S_c value of 0.79 constrained in Chapter 3, the data move closer to the steady-state curve (Figure 4.3b). Using this average S_c value several R^* measurements exceed 1. This indicates that these hillslopes are too steep to sustain soil mantle in this landscape, which corresponds to field observations of the Oregon Coast Range, where frequent shallow landsliding is reported (e.g., Benda and Dunne, 1997; Montgomery *et al.*, 1998) and where periodic wildfires expose large (tens of square meters) patches of bedrock (Jackson and Roering, 2009).

As acknowledged by Roering *et al.* (2007), extracting the relief from a moving window fails to capture the complete range of relief values in a landscape, resulting in an average value which dampens the true signal, reducing R in high relief landscapes such as the Oregon Coast Range. My method of measuring relief of individual hillslope traces circumvents this problem.

The majority of the data points in Figures 4.2 and 4.3 have larger E^* values than those from Roering *et al.* (2007). Chapter 3 showed that estimating L_H

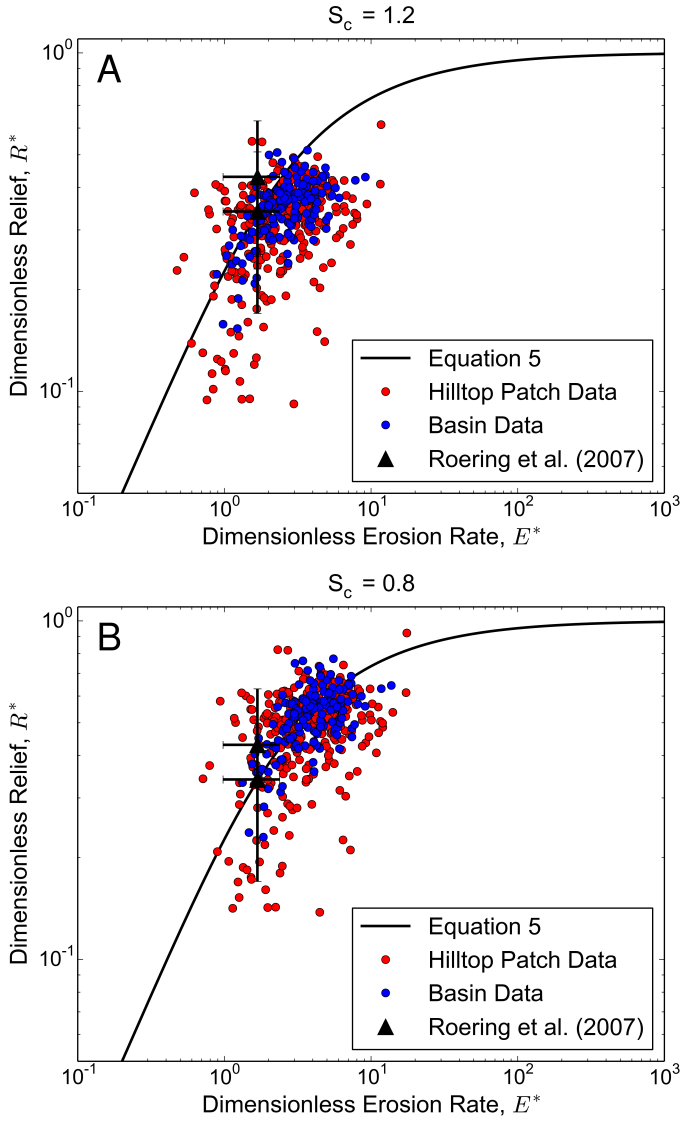

Figure 4.2: Hilltop patch and basin average data for Gabilan Mesa plotted using a critical gradient of 1.2 **(a)** and 0.8 **(b)** alongside data from Roering *et al.* (2007) for the same location. Error bars are the standard error.

using slope–area plots systematically underestimates L_{H} by as much as an order of magnitude in some landscapes. Such an underestimate would reduce the E^* value for a landscape and explains the systematic differences between this study and the results of Roering *et al.* (2007). The larger range of hilltop patch data

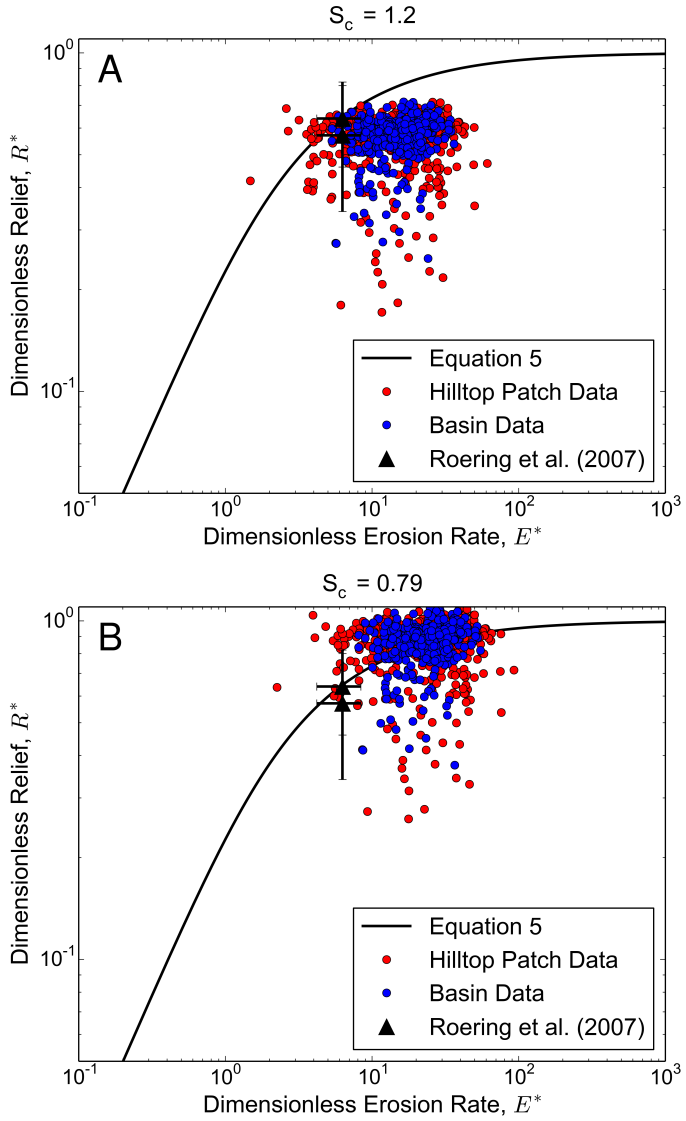

Figure 4.3: Hilltop patch and basin average data for the Oregon Coast Range plotted using a critical gradient of 1.2 **(a)** and 0.8 **(b)** alongside data from Roering *et al.* (2007) for the same location. Error bars are the standard error.

highlights the range of E^*R^* values inherent even in a uniform landscape which is in approximate topographic steady state.

Cascade Ridge

Cascade Ridge is a more morphologically complex landscape than the Oregon Coast Range or Gabilan Mesa; correspondingly, the E^*R^* data for this landscape are predicted to plot along the steady-state curve at a broad range of E^* values, as was demonstrated by Hurst *et al.* (2012). Using an S_c value of 0.8, as proposed by Hurst *et al.* (2012), produces data spanning a much wider portion of E^*R^* space than the data for the steady-state landscapes of Gabilan Mesa and the Oregon Coast Range (Figure 4.4a). The binned hilltop patch data show good agreement with the data from Hurst *et al.* (2012), spanning a similar range of E^* values with the steady-state curve falling within the standard error of each bin. This supports observations of a range of erosion rates and landscape morphologies and highlights the utility of this method in gaining a first-order approximation of the tectonic and erosional setting of a landscape where no field data are available.

At the Cascade Ridge site, in Chapter 3, I estimated S_c to be 0.72, calculated from topographic parameters. Using this value there is little change in the trends in the data (Figure 4.4b): most of the points now fall above the line and at high values of E^*, and more data points have R^* values in excess of 1. These high R^* values are consistent with field observations of this transient landscape wherein rapid valley downcutting may decouple hillslopes from the channel network (Milodowski *et al.*, 2015b) and drive shallow landsliding. In a complex landscape such as Cascade Ridge, which is known to have a broad range of erosion rates and hillslope morphologies, a landscape average S_c value will regress towards the mean. Consequently, as more of the landscape is covered by the low-gradient plateau than the steeper canyons, the S_c value of 0.72 does not reflect the parts of the landscape with larger E^*R^* values, which may fall closer to the value of 0.8 used by Hurst *et al.* (2012).

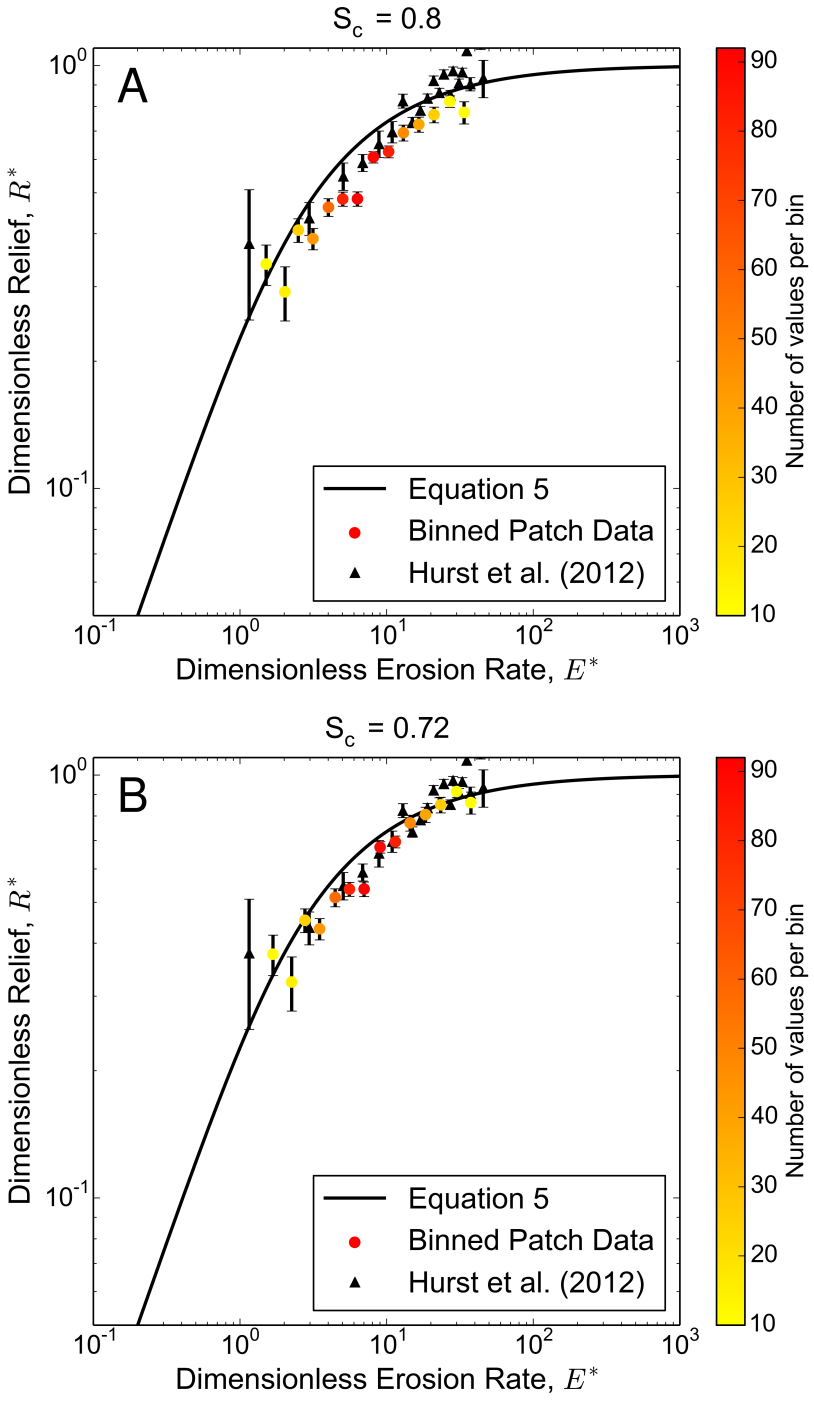

Figure 4.4: Binned hilltop patch data spanning a wide range of E^* values in Cascade Ridge, generated using a critical gradient of 0.8 **(a)** and 0.72 **(b)** alongside data from Hurst *et al.* (2012) for the same location. Error bars are the standard error of the data. Error bars from Hurst *et al.* (2012) are generated from the original data.

Coweeta

The southern Appalachian Mountains have never previously been investigated using E^*R^* methods and so can be used to evaluate the technique's ability to interrogate a complex landscape and assist in the interpretation of topographic signals. Figure 4.5 outlines the range of methods which can be used to interpret E^*R^* data. As in Section 4.7.1 the critical gradient used is taken from Chapter 3. The raw data in Figure 4.5a show the range of reliefs observed in the southern Appalachians. The landscape median E^*R^* value falls within the zone of maximum probability density; this highlights the level of noise inherent in high-resolution topographic data when interrogating them in E^*R^* space, outlining the requirement to smooth or bin the data in order to extract meaningful information from them.

Comparing the data in Figure 4.5b and 4.5c to data for steady-state landscapes such as Gabilan Mesa or the Oregon Coast Range, they show similar levels of clustering, with the location of the cluster of hilltop patch and basin average values corresponding with the Oregon Coast Range data (Figure 4.3). This corresponds well to field observations of hillslope morphology in these two locations, with planar hillslopes and frequent shallow landsliding reported (Benda and Dunne, 1997; Montgomery *et al.*, 1998; Roering *et al.*, 1999), and this clustering suggests that there is less spatial variation in erosion rate in Coweeta than in Cascade Ridge, an assertion supported by measured erosion rates from both locations (e.g., Riebe *et al.*, 2000; Matmon *et al.*, 2003; Hales *et al.*, 2012; Hurst *et al.*, 2012). Figure 4.5d shows the binned data for Coweeta and highlights the smaller range of E^* values for this landscape when compared to Cascade Ridge. It also draws attention to the need to analyze E^*R^* data using numerous methods to avoid an incorrect interpretation, as discussed in Section 4.6.2.

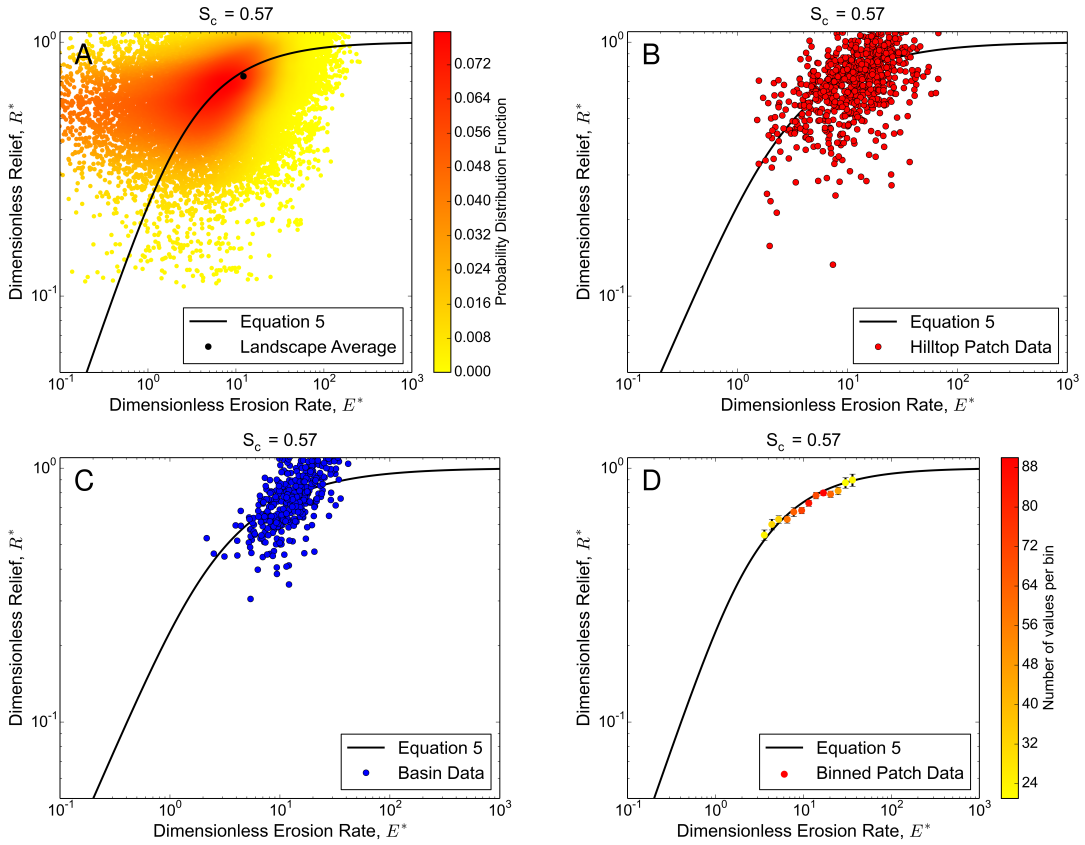

Figure 4.5: Comparison of the different methods which can be used to visualize E^*R^* from Coweeta, using a critical gradient of 0.57. **(a)** Raw data colored by the density of points in E^*R^* space alongside the landscape average value. Error bars plot inside the data point. **(b)** Data averaged over hilltop patches. **(c)** Data averaged over second-order drainage basins. **(d)** Hilltop patch data placed into logarithmically spaced bins. Error bars are the standard error.

The Coweeta E^*R^* data cluster around a point on the steady-state curve, and it could be concluded that this landscape is in approximate steady state. However, the value of S_c used in Figure 4.5 is significantly smaller than any previously published S_c value. Field observations of Coweeta reveal that many channels are alluviated and such deposition at the base of hillslopes will alter the mean properties of a hillslope and move its idealized profile away from the model hillslopes defined by Roering *et al.* (2007). As a valley fills with sediment, the

hillslope relief will be reduced more rapidly than other hillslope properties, due to the difference between rates of hillslope and channel response to forcing (Hurst *et al.*, 2012). Such a reduction in relief will reduce R^*, resulting in a reduced best-fit S_c value. Such an alteration of mean hillslope properties could explain the considerable underestimation of the critical gradient when it is constrained through hillslope length–relief relationships.

The Oregon Coast Range, a broadly similar landscape to Coweeta, based on the range of E^* values, general landscape morphology and observations of sediment transport processes, has a critical gradient of 0.79 (Chapter 3). This value is similar to the S_c of many other landscapes (DiBiase *et al.*, 2010; Hurst *et al.*, 2012) and as such I use this value to explore the patterns of E^*R^* in Coweeta when a larger critical gradient which more closely resembles predicted values for other landscapes is employed. In such a case the majority of the data plot below the steady-state curve (Figure 4.6). Hurst *et al.* (2013b) observed E^*R^* data plotting below the steady-state curve, along the Dragon's Back pressure ridge, where these sections of the landscape are understood to be topographically decaying following a pulse of uplift. If this S_c is correct it could lend support to the idea of a Miocene rejuvenation of topography in the southern Appalachians (Gallen *et al.*, 2013) followed by a period of gradual topographic decay into the present. However, the nature of sediment transport in Coweeta may not be best constrained using Equation 4.1, as modeling work performed by Mudd (2016) suggests that a deviation of this magnitude from the steady-state curve indicates that a landscape is not undergoing pure nonlinear sediment flux.

4.7.2 Sensitivity analysis of averaging methods

Several of the techniques utilized to average the raw E^*R^* data have free parameters, the selection of which can influence the final results. In the following

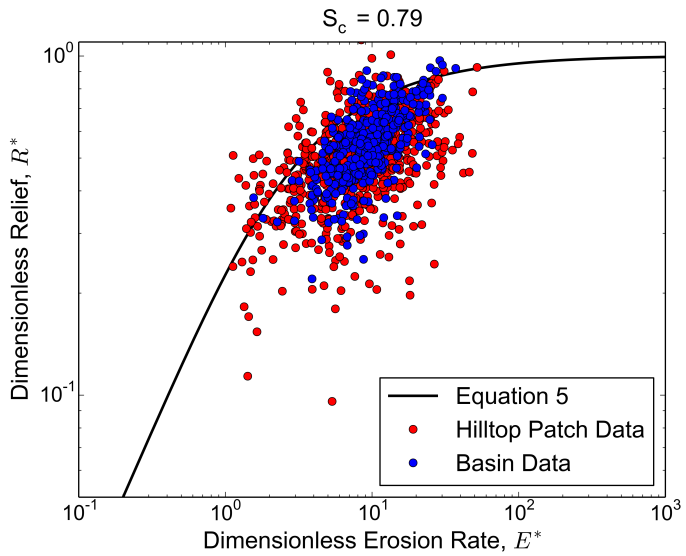

Figure 4.6: Hilltop patch data from Coweeta plotted using the higher S_c value of 0.79, demonstrating that the majority of the hillslopes in this landscape plot below the steady-state curve when using a larger critical gradient.

section I explore the influence that averaging technique, minimum hilltop patch and basin area, basin stream order, and binning parameters can have on the interpretation of E^*R^* data.

Averaging methods

As outlined in Section 4.5.3, the topographic parameters, $L_{\mathrm{H}}, R, C_{\mathrm{HT}}$, and S_{HT}, must be smoothed in order to extract meaningful trends from the inherently noisy signal. The main technique for performing this smoothing is to average the data spatially over either hilltop patches or drainage basins. These averages can be computed as either the mean or the median of each spatial area. Figure 4.7 presents a comparison between hilltop patch data computed using means and medians for the Oregon Coast Range, showing little change between the measurements using the two techniques. Because there is little difference

between the two methods, I use median values throughout this paper, as this ensures that any extreme values will have a lesser impact on landscape-scale metrics.

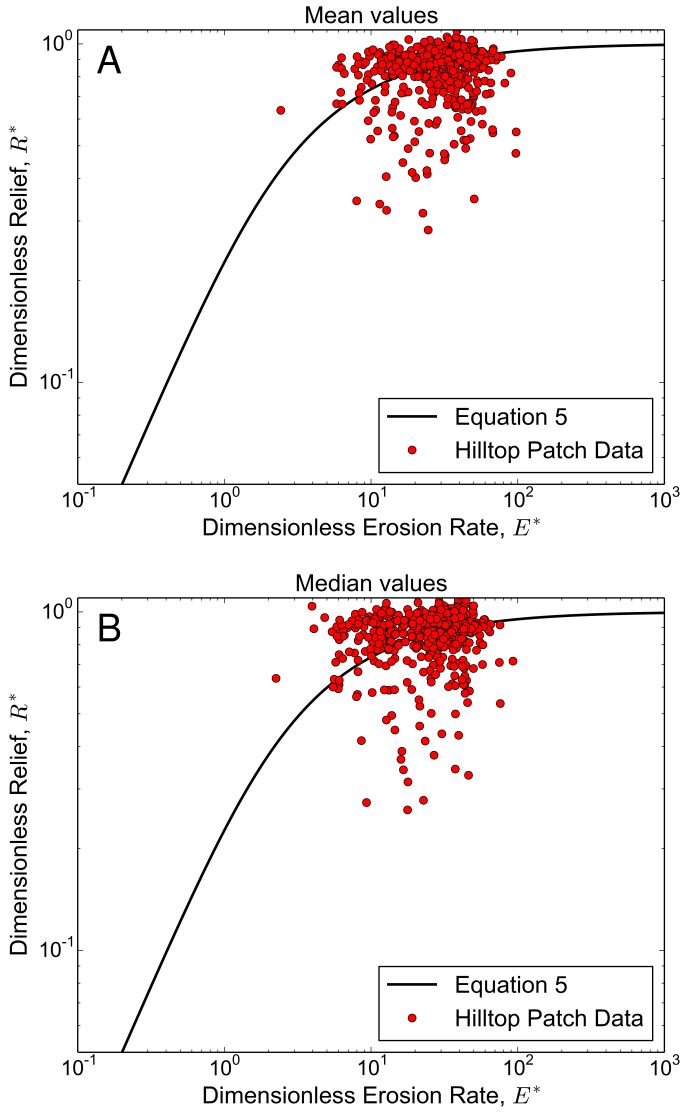

Figure 4.7: Comparison between hilltop patch values generated using a spatial mean **(a)** and a spatial median **(b)** for the Oregon Coast Range.

Spatial averaging parameters

The hilltop patch identification process described in Section 4.4.1 requires one user-defined parameter, the minimum patch area. This value is used to remove any small patches from the analysis and is included to ensure that patches conform to geomorphologically significant hillslopes, and not small patches of hilltop that are not representative of the hillslope as a whole. By varying the size of the minimum patch area from 0 through to 500 pixels it is possible to observe how this parameter can impact the interpretation of E^*R^* data (Figure 4.8a). As the threshold is increased, fewer patches are considered valid and the density of the data is reduced, having the effect of removing many of the outlying data points. This reinforces the need to set a minimum size for a hilltop patch to ensure that a small number of measurements do not have too large an impact on the interpretation of the data.

The technique in Section 4.4.1 has no method to limit the maximum size of the hilltop patches, as the aim is to find spatially contiguous zones of hilltop and artificially breaking these patches may result in oversampling some sections of a landscape. Large patches make up a very small proportion of the total population of patches and correspondingly do not have a large impact on the overall trends in an individual data set.

The stream order of the basin used to generate basin average values will also have an influence on the interpretation of the results. In Chapter 3 I used second-order basins to generate basin average topographic parameters as this order generated a large number of basins which all had a large enough area to generate numerous data points per basin, effectively sampling as much of the landscape as possible. Figure 4.8b shows the effect of increasing the stream order of the basins used in Coweeta from first to fourth order. As each increasing order

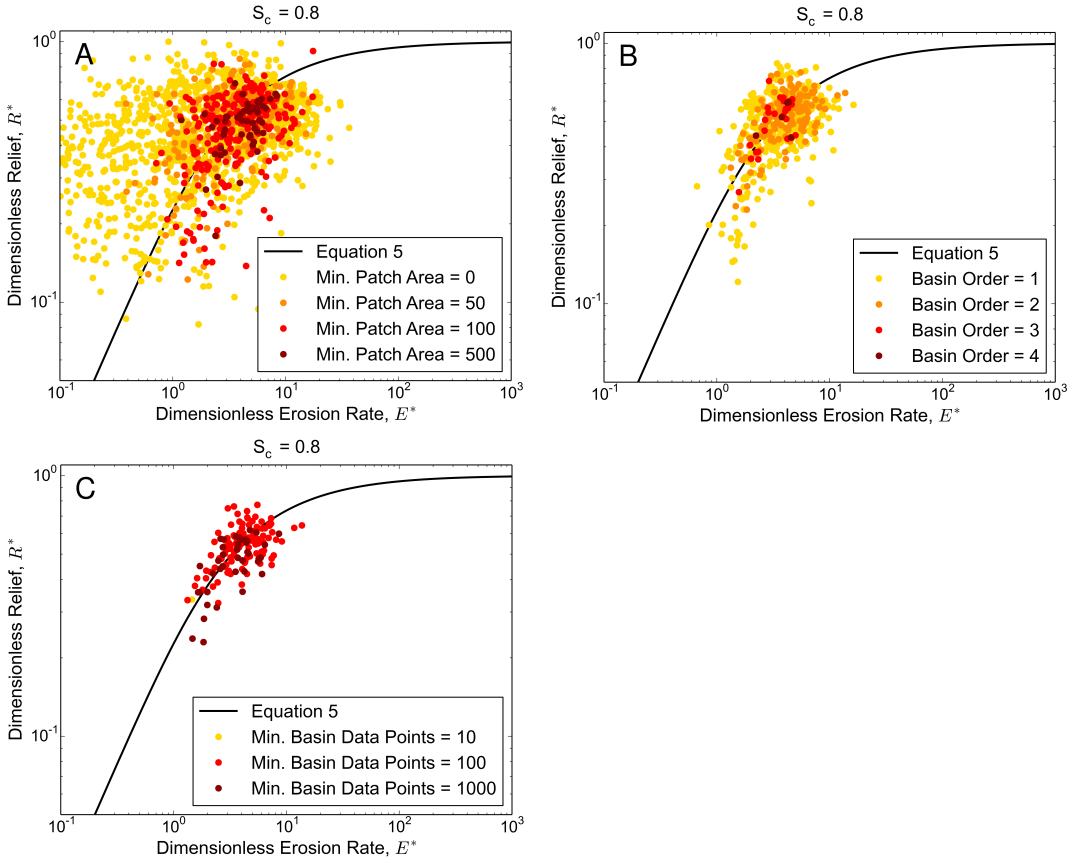

Figure 4.8: Comparison of the influence of changing spatial averaging method on the interpretation of E^*R^* data for Gabilan Mesa. **(a)** Variations in the minimum patch area threshold from 0 (no threshold) to 500 pixels highlighting the reduction in noise when a minimum patch area is applied. **(b)** Increasing the basin steam order, which reduces variance in the data, as bigger basins are sets containing basins of smaller orders, dampening any extreme values. **(c)** Variations in the minimum basin pixels threshold. Outlying basins have very few data points, so they are influenced more strongly by single atypical values.

basin can be considered a set containing the previous order basins, the basin average points all plot in very similar locations in E^*R^* space, suggesting that increasing basin order may be a useful method of smoothing basin average data in noisy landscapes. However, this comes with the limitation that, as the basin

order increases, the number of basins in a landscape decreases, resulting in fewer data points representing larger spatial areas and the possible homogenization of topographic signals occurring at spatial scales smaller than the average basin area.

The number of valid data points contained within a basin used to generate an average value is another free parameter that the user must set. As with the hilltop patch area, selecting a sensible value is important to ensure that each basin average data point corresponds to the basin as a whole and not just a spatial subset. As the threshold is increased, outlying basins are removed (Figure 4.8c), indicating that many outlying data points are generated by a small number of irregular hillslopes in otherwise typical basins. However, if the threshold is too large, too many basins will be excluded. In order to ensure consistency between spatial averaging techniques it is recommended that the minimum number of pixels in a basin be kept equal with the minimum patch area.

Log bin parameters

When computing logarithmically spaced bins there are two free parameters, the number of bins (equivalent to the bin width) and the minimum number of data points which must fall within a bin for the binned point to be valid. Figure 4.9a highlights the influence of changing the number of bins on the interpretation of the Cascade Ridge data. If the number of bins is too low, it becomes difficult to identify a trend in the data as the nature of a landscape can vary considerably across large ranges of E^*, and by homogenizing these measurements a transient signal can be lost.

However, as the number of bins is increased, fewer values are placed into each bin, meaning that if there is a single value which is significantly different to the rest of the values in the bin, it can vastly alter the result. It is also the case that,

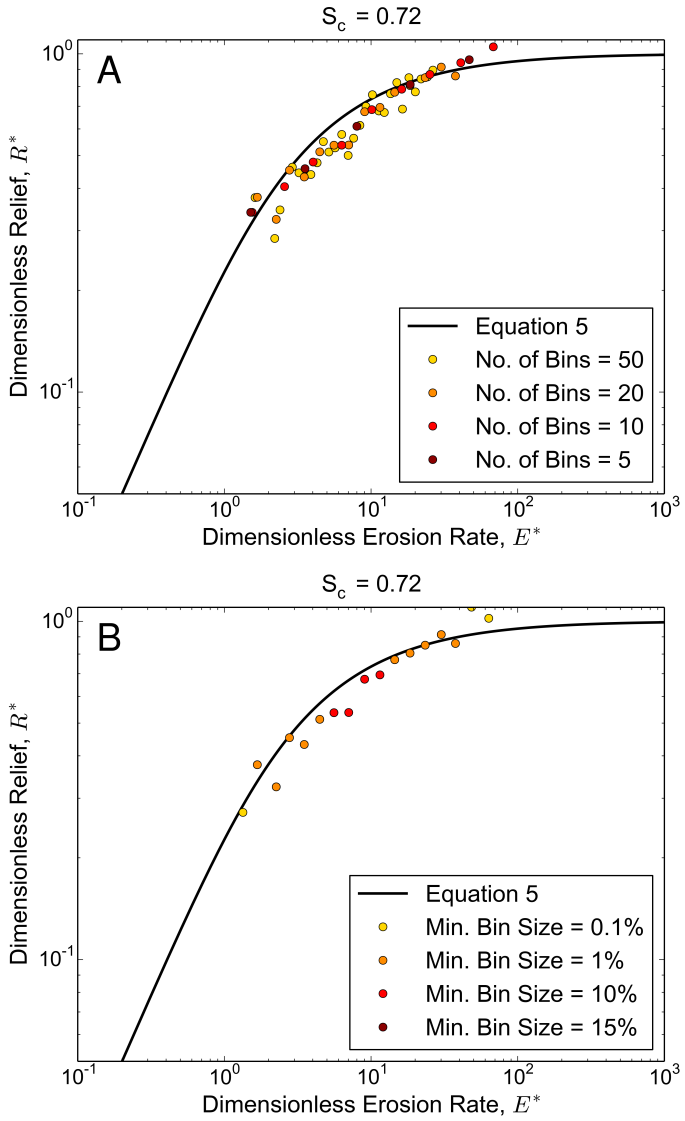

Figure 4.9: Comparison of the influence of binning parameters on the interpretation of E^*R^* data for Cascade Ridge. **(a)** Varying the number of bins used, equivalent to the bin width in E^* space. As the number of bins reduces it becomes harder to identify patterns in the data, and as the number of bins increases, the number of data points in each bin reduces, thereby reducing the power of the binning technique. **(b)** Varying the minimum number of data points required in a basin. As this value increases, fewer points are preserved, which compresses the range of the data and can obscure the observation of an erosional gradient. Too small a threshold can result in bins containing very few values which do not represent the landscape as a whole.

as the number of bins increases, the chance of a bin being removed for having too few data points increases, which will be particularly apparent at low and high E^* values, where the data are sparser. I have found that using 20 bins reaches a good compromise between data density and data smoothing, and corresponds well with the 21 bins used by Hurst *et al.* (2012), where no filtering was performed based on bin size.

The minimum size of each bin can also have an impact on the final interpretation of the data. If no threshold is applied, some bins can contain a single value, while others can contain hundreds of values, which makes interpreting the data difficult as one cannot be sure of the robustness of each binned value. If the threshold is placed too high, then valid data will not be included in the final analysis and the interpretation of a landscape's evolution could be incorrect. Figure 4.9b highlights this issue using data from Cascade Ridge at a range of bin size thresholds, identified as percentages of the total data set size. I have found that using a minimum bin size of 1–5 % of the total data set ensures a good binning result.

4.7.3 Constraining S_c

Landscapes which are in topographic steady state should plot at a single location on the curve described by Equation 4.5. In principle this would mean that an erosion gradient would be required in order to constrain S_c, by fitting the data to the steady-state curve. However, as observed in Figures 4.2 and 4.3, even in idealized steady-state landscapes, there is still considerable variability in the E^*R^* data. This variability is consistent with patterns of dynamic reorganization of low-order drainage basins within models of steady-state landscapes performed by Reinhardt and Ellis (2015). Therefore, it becomes possible to estimate the

critical gradient of the nonlinear sediment flux law (Equation 4.1) for a landscape without a strong erosion gradient, using E^*R^* data.

As with previous analyses, the raw data must be spatially averaged in order to reduce the level of noise present in E^*R^* space before an estimate of S_c can be made. The optimal value of S_c is estimated using a nonlinear least-squares method (Jones *et al.*, 2001) which computes the sum of the square of the deviation between each measured E^*R^* value and the value predicted by Equation 4.5. This calculation is performed for a range of critical gradients until the S_c with the lowest corresponding deviation from the steady-state curve is found.

The accuracy of this optimized S_c value is constrained through bootstrapping the optimization procedure. The data are sampled with replacement to generate 100 000 data sets, consisting of values randomly drawn from the population of patch or basin average data. For each of these sampled data sets the optimal value of S_c which minimizes the error between the data and the steady-state curve is calculated. The final S_c value for each landscape is the mean value of these 100 000 iterations, with a 95 % confidence interval.

Table 4.1: Previously published S_c values alongside the values generated from the best fit to the steady-state curve for the patch and basin average data.

	Roering *et al.* (2007)	Hurst *et al.* (2012)	Chapter 3	Patch average[a]	Basin average[b]
Oregon Coast Range	1.2 ± 0.2	—	0.79	0.83 ± 0.01	0.83 ± 0.01
Gabilan Mesa	1.2 ± 0.4	—	0.8	$0.8^{+0.06}_{-0.05}$	$0.8^{+0.05}_{-0.04}$
Cascade Ridge	—	0.8	0.72	0.78 ± 0.02	0.82 ± 0.02

[a] Calculated as the value which minimizes the sum of the squared residuals to the steady-state line for the patch average data. Error is the 95 % confidence interval generated by bootstrapping the calculation 100 000 times.

[b] As above but using basin average data.

Table 4.1 contains estimates of the critical gradient generated using both basin and patch average values alongside previously published values for Cascade Ridge, the Oregon Coast Range, and Gabilan Mesa. The predicted patch and basin average values for Gabilan Mesa and the Oregon Coast Range are similar to those presented in Chapter 3. This method of estimating the best-fit S_c will produce an average value representative of the maximum probability density of S_c values for a landscape, whereas the method of S_c estimation employed by Roering *et al.* (1999) can better be considered as the maximum S_c value for a landscape.

The data for Cascade Ridge show better agreement with the value used by Hurst *et al.* (2012), which was also derived using E^*R^* data, than the lower estimate from Chapter 3. The pairs of S_c values calculated for each landscape are very similar, suggesting that, in large enough data sets, the constraint of S_c is insensitive to the spatial scale of data averaging. However, the scale of spatial averaging has been demonstrated to have an impact on the interpretation of E^*R^* data and thus care must be taken to select appropriate methods of spatial averaging and data processing in order to ensure that results generated are not simply a function of user-defined parameters.

The similarity of the average S_c values obtained using the bootstrapping procedure across three diverse landscapes highlights the presence of a distribution of E^*R^* values existing for each landscape, and the nature of an average S_c measurement. Such a distribution occurs due to local variations in topography, process, and material properties, and similarities can be drawn between the results presented in Table 4.1 and other similar studies (DiBiase *et al.*, 2010; Hurst *et al.*, 2012).

The values of S_c constrained using this bootstrapping procedure are similar to those derived from the relationship between hillslope length and relief demonstrated in Chapter 3; however, there is no need to estimate material properties such as the soil and rock density and thus this method provides an independent constraint on S_c. However, the computational expense of bootstrapping the S_c fitting calculations from the E^*R^* data is very high, when contrasted with the estimation of S_c using L_H-R relationships presented in Chapter 3. Additionally, using this bootstrapping method in landscapes which do not plot on the steady-state curve in E^*R^* space can yield an incorrect S_c value with a low error estimate. Consequently, I recommend estimating the critical gradient of a landscape using this method and the method outlined in Chapter 3, when field data are available, in order to best constrain the critical gradient of a landscape. However, careful

consideration of the differences between a maximum S_c and a best-fit-derived average S_c should be undertaken to ensure that a valid geomorphic interpretation of a landscape is employed.

4.8 Conclusions

I present a software package which automates the extraction and processing of high-resolution topographic data to generate nondimensional erosion rate and relief measurements. Topographic data can be averaged at a hilltop scale by generating unique hilltop patches or can be averaged over drainage basins automatically extracted from the channel network. Alongside the raw data, these spatially averaged data sets are shown to reproduce the findings of previous studies. In steady-state landscapes such as the Oregon Coast Range and Gabilan Mesa, E^*R^* data plot in a cluster around a single point on the steady-state curve, supporting the conclusions drawn in previous studies (Roering *et al.*, 2007), and in Cascade Ridge, a transient erosion signal similar to that identified by Hurst *et al.* (2012) is observed. This technique is also tested on a landscape in the southern Appalachian Mountains, with the results suggesting that topography is decaying, supporting models of Miocene topographic rejuvenation proposed by Gallen *et al.* (2013). These results, alongside the ability to reproduce previous work, emphasize the value of this software to the geomorphology community as, until now, there has been no clear framework within which to produce nondimensional erosion rate and relief measurements.

The average critical gradient used in Equation 4.1 is also constrained for three of the studied landscapes, with the values falling within expected ranges. However, due to the noise inherent in this form of analysis and the challenges of evaluating the goodness of fit between such noisy data and a model, it is recommended

that other methods to constrain S_c using the same raw data be utilized instead. Finally, the influence of free parameters on the final interpretation of the data is explored, providing the user with clear guidance on how to select parameters which control the level of smoothing or binning performed on the topographic data. The most significant of these are the minimum hilltop patch and basin size thresholds which must be carefully selected to balance smoothing the data with preserving landscape-scale trends.

Chapter 5

How does grid-resolution modulate the topographic expression of geomorphic processes?

A version of this chapter has been published in Earth Surface Dynamics Discussions as:

Grieve, S.W.D., Mudd, S.M., Milodowski, D.T., Clubb, F.J., and Furbish, D.J (2016). How does grid-resolution modulate the topographic expression of geomorphic processes? *Earth Surface Dynamics Discussions*, doi:10.5194/esurf-2016-28

The work presented here was performed in collaboration with my co-authors who contributed to the final writing of the manuscript and the development of some of the topographic analysis software. I performed the analysis, wrote topographic and data analysis routines, generated the figures and wrote the manuscript.

5.1 Abstract

In many locations, one's ability to study the processes which shape the Earth is greatly enhanced through the use of high resolution digital topographic data. However, although the availability of such datasets has increased markedly in recent years, many locations of significant geomorphic interest still do not have high resolution topographic data available. Here, I aim to constrain how well one can understand surface processes through topographic analysis performed on lower resolution data. I generate digital elevation models from point clouds at a range of grid sizes from 1 to 30 meters, which covers the range of widely used data resolutions available globally, at three locations in the United States. Using this data, the relationship between curvature and grid resolution is explored, alongside the estimation of the hillslope sediment transport coefficient (K, in $m^2\ yr^{-1}$) for each landscape. Curvature, and consequently K, values are shown to be generally insensitive to grid resolution, particularly in landscapes with broad hilltops and valleys. Curvature distributions, however, become increasingly condensed around the mean, and theoretical considerations suggest caution should be used when extracting curvature from landscapes with sharp ridges. Two methods of extracting channels from topographic data are tested. A geometric method of channel extraction that finds channels by detecting threshold values of planform curvature is shown to perform well at resolutions up to 30 meters in all three landscapes. The landscape parameters of hillslope length and relief are both successfully extracted at the same range of resolutions. These parameters can be used to detect landscape transience and these results suggest that such work need not be confined to high resolution topographic data. A synthesis of the results presented in this work indicates that although high resolution (e.g., 1 m) topographic data do yield exciting possibilities for geomorphic research,

many key parameters can be understood in lower resolution data, given careful consideration of how analyses are performed.

5.2 Introduction

Geomorphologists have always made use of topographic data, from initial qualitative observations of surface morphology and its link to process (e.g., Gilbert, 1909) to directly measuring landscape geometries from contour maps, constraining river dynamics and deriving morphometric relationships (e.g., Horton, 1932; Schumm, 1956; Chorley, 1957). Further quantitative analyses of the Earth's surface were facilitated through the advent of gridded topographic data. Work to generate Digital Elevation Models (DEMs) from photogrammetry, contour maps and active remote sensing platforms (Yamaguchi *et al.*, 1998; Wolock and McCabe, 2000; Rabus *et al.*, 2003; Walker and Willgoose, 2006) produced datasets at tens to thousands of meters grid resolution, along with geomorphic analyses designed for such datasets (O'Callaghan and Mark, 1984; Tarboton *et al.*, 1991; Montgomery and Dietrich, 1994; Burbank *et al.*, 1996; Tarboton, 1997). Algorithms have subsequently been developed which exploit the higher resolution topographic data now available, predominantly from Light Detection And Ranging (LiDAR), which not only refined existing techniques (Passalacqua *et al.*, 2010; Pelletier, 2013; Clubb *et al.*, 2014) but also allowed the study of hitherto unresolvable features on landscapes (Tarolli and Dalla Fontana, 2009; Vianello *et al.*, 2009; Roering *et al.*, 2010; DiBiase *et al.*, 2012; Tarolli, 2014; Milodowski *et al.*, 2015b).

Presently, LiDAR data coverage is predominantly focused around locations of particular scientific interest or infrastructural importance, as can be seen on many LiDAR data portals (e.g., Krishnan *et al.*, 2011). It is unlikely that global LiDAR

coverage can be achieved in the near future, leaving the provision of commercially available 12 meter TanDEM-X data (Krieger *et al.*, 2007) and freely available 30 meter Shuttle Radar Topography Mission (SRTM) data (Rabus *et al.*, 2003) as the best available data options for many study sites.

As a consequence of this data availability it is crucial to understand the limitations of lower resolution data when performing topographic analysis for geomorphic research. Extracting channels from topography is a common requirement of many analyses and it is expected that the accuracy of extracted channel networks will be affected by increasing grid resolution (Orlandini *et al.*, 2011). Roering *et al.* (2007), Hurst *et al.* (2013b) used measurements of hillslope length and relief to identify signals of landscape transience. However, all such work was performed on high resolution topography and the impact of grid resolution on these metrics is unknown. Roering *et al.* (2007) and Hurst *et al.* (2012) demonstrated that the curvature of ridgelines measured from high resolution topography can be used as a proxy for erosion rates in soil mantled landscapes. This observation has been used in many studies where cosmogenic radionuclide derived erosion rates are unavailable (Pelletier *et al.*, 2011; Hurst *et al.*, 2013c,b). However, it can also be used in locations with an independent constraint on erosion rates in order to quantify a sediment transport coefficient that relates hillslope sediment flux to topographic gradient, which is set by the material properties of soils (Furbish *et al.*, 2009). Therefore, understanding the effect of grid resolution on the extraction of curvature is crucial in order to evaluate the applicability of calculating the sediment transport coefficient from coarse resolution data.

Here, I grid topographic data at a range of resolutions in order to test the sensitivity of these techniques to increasing grid size, with the aim of placing constraints on the estimation of common geomorphic parameters when LiDAR topographic data are unavailable.

5.2.1 Previous work

It has long been recognized that the scale of topographic data used in an analysis or model will have an impact on the scale of the processes which can be measured (Vaze *et al.*, 2010). It is intuitive that in order to measure the properties of hillslope processes the resolution of the data must be high enough that variations in hillslope form can be captured adequately. The resolution of topographic data defines the Nyquist frequency, given as $(2Res)^{-1}$ where Res is the grid resolution of the dataset (Warren *et al.*, 2004). The inverse of this frequency yields the minimum wavelength resolvable from a given dataset. In the example of a 1 meter grid size, the smallest features that could be resolved would have a length scale of 2 meters. Recognizing this, many authors (e.g., Quinn *et al.*, 1991) have attempted to quantify this uncertainty, aiming to answer the question: at what point does a dataset become unsuitable for a given analysis?

Many attempts to constrain the error content of topographic measurements have focused on comparisons between elevation values taken from differing resolution data products, often in conjunction with field survey data, with the aim of discriminating between DEM generation methods. Walker and Willgoose (2006) performed a comparison of DEMs generated using cartometric and photogrammetric methods against field surveyed elevation data. They demonstrated that at grid resolutions of 6.25, 12.5 and 25 meters the cartometric DEM produced less error than the photogrammetric DEM when compared to the field surveyed data, collected at 3.25 meter intervals.

The advent of LiDAR-derived topographic data provided a new technique, and increased the range of possible grid resolutions to evaluate. Hodgson *et al.* (2003) assessed the quality of high resolution topographic data sourced from interferometry and LiDAR for a heavily vegetated catchment in North Carolina.

This analysis demonstrated that, under such conditions, the LiDAR-derived DEM outperformed the interferometric data in addition to both classes of USGS DEM product. However, concerns were raised about the overall accuracy of the LiDAR data with a requirement for improved methodologies to be developed to process multi-storey vegetation. Further work was carried out in North Carolina to constrain the minimum number of LiDAR returns required to generate a DEM at a given grid size (Anderson *et al.*, 2006). This work indicated that a 5 meter grid (the finest resolution used) required approximately 115 points per hectare, whereas at 30 meter grid resolution the requirement reduced to approximately 35 points per hectare.

Vaze *et al.* (2010) resampled a 1 meter LiDAR-derived DEM to a range of grid sizes up to 25 meters, and assessed the accuracy of elevation values for each of these resampled grids when compared to a 1 meter resolution field survey. It was found that there was little variation in the distribution of elevation values between the resampled data sets. However, when the data were compared with 25 meter DEMs generated from topographic maps and contour generalization, there were considerable errors, supporting earlier authors' conclusions that LiDAR-derived topographic data contain more useful geomorphic information than other methods of topographic data collection.

Topographic gradient (or slope) is one of the most fundamental topographic derivatives across the disparate disciplines which utilize topographic data. This measurement has been used in geomorphology (e.g., Burbank *et al.*, 1996), ecology (e.g., Milodowski *et al.*, 2015a), soil science (e.g., Nearing, 1997) and hydrology (e.g., Zhang and Montgomery, 1994). Wolock and McCabe (2000) endeavored to constrain the accuracy with which this parameter can be calculated as grid resolution is increased from 100 to 1000 meters and showed that as the grid size is increased, there is a clear reduction in the slope values produced for a landscape. Similar wide scale analysis has also been performed within the context

of global hydrological analysis (e.g., Hutchinson and Dowling, 1991; Jenson, 1991), indicating that from meter to kilometer scale the reduction in quality of slope measurements is an issue which must be considered when working with topographic data.

Gao (1997) considered the accuracy of slope measurements at locations manually classified as valleys, peaks and ridges. They found an initially small increase in the error of slope measurements at intermediate resolutions (10 to 20 meters) and a much more rapid increase in error between 20 to 30 meters resolution, suggesting a threshold minimum resolution for analysis of these landforms. More recent work has considered how high resolution LiDAR data impact upon the quality of slope measurements. Vaze *et al.* (2010) demonstrated a similar trend to previous authors working with lower resolution data: as grid resolution is decreased from 1 to 25 meters, there is a considerable reduction in the slope values generated for a landscape. Warren *et al.* (2004) evaluated the reliability of slope measurements by contrasting 10 methods of gradient calculation against field measurements of topographic gradient. The error between DEM and field-derived slope measurements was shown to increase with grid resolution (from 1 to 12 meters), resulting in the recommendation to increase data resolution wherever possible to decrease errors in topographic analysis.

Numerous authors have considered the impact of grid resolution on hydrological applications, which often require slope calculation as a fundamental processing step. It has been demonstrated across many landscapes and scales that as grid resolution is decreased the upslope contributing area will increase and the local slope will decrease, which will have a significant impact on any hydrological analysis (Wolock and Price, 1994; Zhang and Montgomery, 1994; Wu *et al.*, 2008). Similarly, from the perspective of modeling global scale sediment fluxes to the oceans, Larsen *et al.* (2014) noted that measurements of slope dropped

logarithmically with increasing grid spacing, and failing to account for this may lead to a substantial underestimate of the contribution of steep, montane regions.

Kenward *et al.* (2000) performed analyses on the accuracy of hydrological networks generated through photogrammetry and radar interferometry at 5 and 30 meters grid resolution respectively. Their error analysis was extended to consider the vertical errors generated both through the downsampling of the topographic data, as well as from the techniques used to capture the topographic information. Predicted catchment runoff was up to 7% larger in the lower resolution datasets, which was considered to be driven by both the vertical errors and the reduction in spatial resolution increasing variables such as upslope drainage area.

Topographic Wetness Index (TWI), calculated as $ln(A/S)$ where A is the specific upslope area and S is the slope, is used as a single variable to compare the hydrological setting of differing parts of the landscape, providing insight into factors including groundwater properties and overland flow rates. Sørensen and Seibert (2007) used LiDAR data to test the robustness of TWI calculations at spatial scales ranging from 5 to 50 meters, concluding that the most sensitive part of the TWI calculation was the specific upslope area measurements. This sensitivity resulted in significant variation in the TWI values across the range of resolutions tested.

The accuracy of channel network extraction from topographic data was tested by Murphy *et al.* (2008), who tested a 1 meter LiDAR DEM and a 10 meter photogrammatically generated DEM against a field mapped channel network in a catchment in Alberta, Canada. The 1 meter LiDAR derived channel network was found to be the best representation of the field mapped channel network, exceeding the quality of an additional channel network mapped by hand from aerial photographs. However, as no intermediate datasets were tested it is not

possible to understand at what resolution the degradation in channel network extraction quality occurs for this location.

As models of agricultural soil loss depend heavily on topographic variables such as slope, work has been carried out to understand the influence of grid resolution on calculated rates of soil loss. Schoorl *et al.* (2000) tested data resolutions from 1 to 81 meters and demonstrated that in all cases, rates of predicted soil loss increased with grid resolution. However, the rates of soil loss were also influenced by the type of flow routing utilized, with the multiple flow direction algorithm (e.g., Freeman, 1991; Quinn *et al.*, 1991) proving most sensitive to resolution decreases. Work by Erskine *et al.* (2007) considering models of crop yields in Colorado, USA, demonstrated that on relatively flat surfaces, such as agricultural fields, the spatial resolution is less important than the vertical accuracy when predicting crop yields, with significant errors being produced due to centimeter scale vertical displacements. Increasing the grid size from 5 to 30 meters had a limited effect on the yield calculations.

Although considerable work has been carried out on the sensitivity of various factors to grid resolution, much of it has been focused on a specific application (e.g., Wolock and Price, 1994; Schoorl *et al.*, 2000; Erskine *et al.*, 2007; Sørensen and Seibert, 2007) with few studies considering the impact of DEM grid resolution within a geomorphic context. Here I aim to extend existing methodologies to constrain the utility of low resolution data products across a suite of geomorphic analyses to understand: (1) How hillslope length, topographic curvature and relief vary with grid resolution, (2) How best to extract channel networks in lower resolution datasets in order to minimize errors, and (3) If it is possible to estimate sediment transport coefficients from low resolution topographic data, where an independent constraint on erosion rate is available.

5.3 Theory and Methods

5.3.1 Generating topographic data

Previous studies that have explored the impact of changing grid resolution on topographic or geomorphic parameters have typically produced coarser resolution topographic data by downsampling the highest resolution data product available for their study sites (e.g., Thompson *et al.*, 2001; Anderson *et al.*, 2006; Claessens *et al.*, 2005; Sørensen and Seibert, 2007). Work has been undertaken to understand the influence of various re-gridding schemes on topographic measurements (Wu *et al.*, 2008), with focus placed upon understanding the use of downsampling high resolution data in order to facilitate computationally expensive analysis on larger spatial areas with minimal loss in data fidelity. However, as computational power increases, cost decreases and more efficient algorithms are developed (Tesfa *et al.*, 2011; Qin and Zhan, 2012; Braun and Willett, 2013; Schwanghart and Scherler, 2014) the need to downsample data for computational convenience becomes reduced. Instead, it becomes more important to understand the limitations of available data products, to facilitate geomorphic analysis in locations where high resolution topographic data are not available. This is of particular importance in many studies of natural hazards (e.g., Saha *et al.*, 2002; Carranza and Castro, 2006) where data quality is limited. It will also open geomorphic research up to communities which do not have the resources to acquire high resolution topographic data.

As a consequence of these constraints I have generated topographic data for three study sites without downsampling or re-gridding high resolution data products, as is commonly performed (Thompson *et al.*, 2001; Anderson *et al.*, 2006; Claessens *et al.*, 2005; Sørensen and Seibert, 2007). Instead I have

followed established techniques to grid the processed LiDAR point cloud data provided by OpenTopography (http://www.OpenTopography.org) at a range of data resolutions which span from 1 meter, considered to be the limit of the Oregon Coast Range dataset in Chapter 2 to 30 meters, which is equal to the grid resolution of the global SRTM dataset (Rabus *et al.*, 2003), the Advanced Spaceborne Thermal Emission and Reflection Radiometer (ASTER) dataset (Yamaguchi *et al.*, 1998) and in excess of the TanDEM-X dataset (Krieger *et al.*, 2007) and as such should span the vast majority of grid resolutions used in modern geomorphic research. The error estimates of the raw point clouds used in this re-gridding process are provided by OpenTopography and can be found in Table 2.1.

The point clouds are gridded using Points2Grid, which employs a local binning algorithm, searching for points within a circular window of radius defined by Kim *et al.* (2006) as,

$$Radius = \lceil \sqrt{2} Res \rceil. \tag{5.1}$$

An inverse distance weighted averaging approach is then performed to assign an elevation value to each grid cell. This approach, which has been employed in Chapters 3 and 4, yields a reliable representation of the topographic surface, with few data gaps and a minimal amount of interpolation.

The topographic data used in this study have been gridded at 20 resolutions, and Figure 5.1 provides representative hillshades of a section of Santa Cruz Island, California, highlighting the degradation of topographic information as grid resolution is decreased.

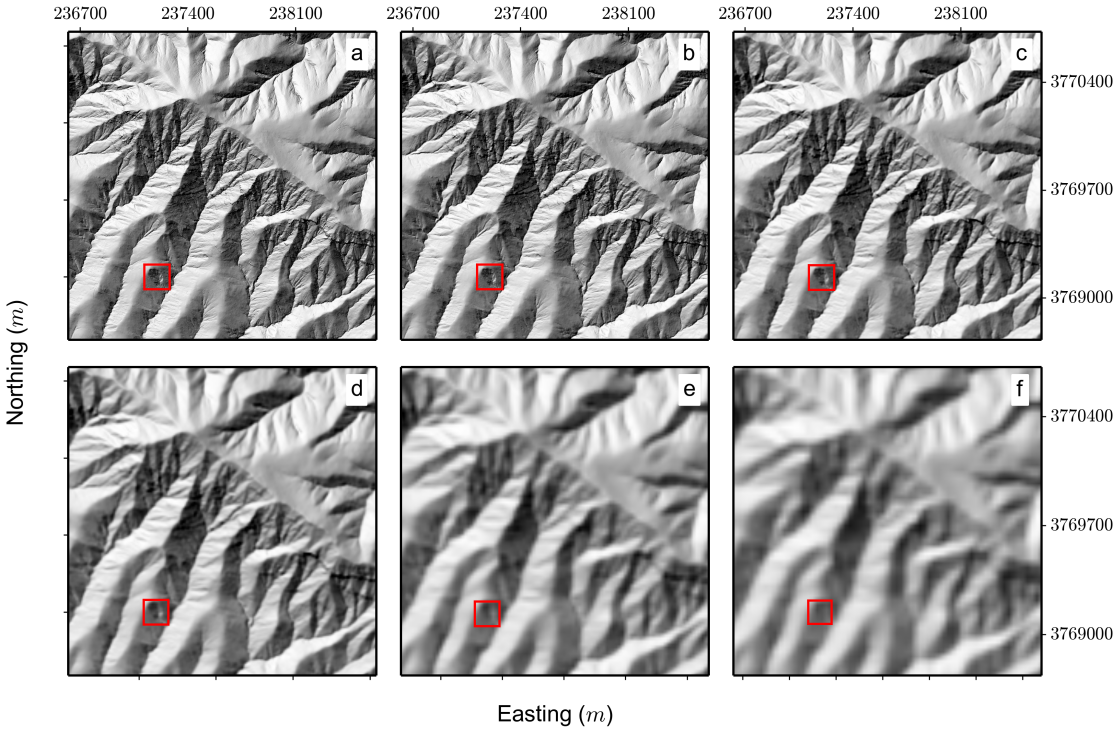

Figure 5.1: Example shaded reliefs of the same section of Santa Cruz Island at decreasing grid resolutions. All coordinates are in UTM Zone 11N. Panels **(a)** to **(f)** represent resolutions of 1, 2, 5, 10, 20 and 30 meters. The red box outlines an extensively gullied first order drainage, clearly visible in the highest resolution data, but as the grid size is increased, this feature, and its internal structure becomes indistinguishable from the surrounding hillslopes.

5.3.2 Measuring curvature from topography

Landscape curvature has long been recognized as a key geomorphic characteristic of landscapes, from Gilbert's (1909) qualitative observations of hilltop convexity to more recent approaches to quantify landform curvature using digital topography (e.g., Schmidt *et al.*, 2003; Hurst *et al.*, 2012). However, unlike other key landscape properties such as gradient (Gao, 1997; Wolock and McCabe, 2000; Warren *et al.*, 2004; Vaze *et al.*, 2010), hydrology (Wolock and Price, 1994; Zhang

and Montgomery, 1994; Murphy *et al.*, 2008; Wu *et al.*, 2008) or soil characteristics (Schoorl *et al.*, 2000; Erskine *et al.*, 2007), the influence of grid resolution on curvature has not been fully explored, particularly within a geomorphic context.

This is particularly important with the proliferation of high resolution topographic data from LiDAR, allowing the analysis of curvature at increasingly fine scales. Recent developments in channel extraction techniques (Lashermes *et al.*, 2007; Passalacqua *et al.*, 2010; Pelletier, 2013; Clubb *et al.*, 2014) typically require the identification of topographic convergence in high resolution topography using a curvature threshold. Roering (2008) and Hurst *et al.* (2012) demonstrated that hilltop curvature scales with erosion rate and as such demonstrated the importance of accurately constraining the impact of grid resolution on this landscape parameter. Its importance is highlighted by an increasing number of studies using this relationship as a proxy for erosion rate (Pelletier *et al.*, 2011; Hurst *et al.*, 2013c,b). Hilltop curvature can also be used to constrain the sediment transport coefficient of a landscape where an independent constraint on erosion rate is available (Hurst *et al.*, 2013c).

The measured curvature of a topographic surface depends on the orientation of the measurement. Here, I consider two common types of curvature, with the following definitions: (1) Total curvature (C_{Total}), the curvature of a surface calculated in 2 dimensions (Evans, 1980; Zevenbergen and Thorne, 1987; Moore *et al.*, 1991); and (2) Tangential curvature (C_{Tan}), the curvature calculated normal to the slope gradient (Mitasova and Mitas, 1993). These two measures are employed to extract hilltop curvature and channel networks, respectively. However, these definitions vary between studies and software packages: see Schmidt *et al.* (2003) for a full review of the varying nomenclature and definitions of curvature measurements used in the literature.

Work by Schmidt *et al.* (2003) utilized 10 meter resolution DEMs to evaluate the

most accurate method for calculating curvature from digital topographic data. It was concluded that curvature could be calculated most accurately when a 9 term polynomial was fitted to the elevation surface, with the caveat that this will only be effective where the data quality is high enough. In cases where the data are of lower accuracy, Schmidt *et al.* (2003) recommended using quadratics to fit the elevation data. This work was extended by Hurst *et al.* (2012) to consider whether these patterns held for high resolution topographic data, and it was found that fitting a 6 term quadratic or 9 term polynomial yielded similar results. Therefore, Hurst *et al.* (2012) chose to use the 6 term quadratic to compute curvature. For this study I also chose to use the 6 term quadratic in order to reduce computation time and, more importantly, to provide more robust curvature values as the data quality is degraded to resolutions below 10 meters (Schmidt *et al.*, 2003).

I calculate curvature using a circular window passed across the landscape, with a radius defined by identifying scaling breaks in the standard deviation and inter-quartile range of curvature calculated at increasing window sizes, consistent with the length scales of individual hillslopes (Lashermes *et al.*, 2007; Roering *et al.*, 2010; Hurst *et al.*, 2012). Consequently, curvature measurements at the hillslope scale can only be considered at data resolutions high enough to resolve individual hillslope features, considered here to be no more than 10 meters, based on the window sizes identified for each landscape. A quadratic function of the form,

$$\zeta = ax^2 + by^2 + cxy + dx + ey + f, \tag{5.2}$$

is then fitted to the elevation values within the window by least squares regression (Evans, 1980), where ζ is the elevation, x and y are horizontal coordinates and a through f are fitting coefficients. The fitted coefficients of this polynomial can be used to calculate differing types of curvature:

$$C_{Total} = 2a + 2b, \tag{5.3}$$

and

$$C_{Tan} = \frac{2ae^2 - 2cde + 2bd^2}{(d^2 + e^2)\sqrt{(1 + d^2 + e^2)}}. \tag{5.4}$$

From the measure of C_{Total} for every cell in a DEM, I can also extract a subset of curvature values from the hilltops. The value of curvature at a hilltop (C_{HT}) can be readily evaluated if the positions of the hilltops are known. To extract hilltops I follow Hurst *et al.* (2012) in defining a hilltop as the boundary between two drainage basins of the same stream order. These points in the landscape can be extracted algorithmically once a channel network is defined through the identification of points in the landscape where two channels of the same Strahler order meet, and the identification of that point's upslope contributing area. Each of these areas defines a basin of a given order and by repeating this process across the range of Strahler orders found in the landscape, a network of hilltops can be defined. This network is then used to sample the curvature values at these locations to provide the C_{HT} values across the landscape. To ensure consistency between C_{HT} measurements at changing grid resolutions, the same channel network, generated using the geometric method described in Section 5.3.3 from 1 meter resolution data, is used as the basis of the hilltop extraction algorithm.

For the data on hilltop curvature, C_{HT}, hilltops with a gradient exceeding 0.4 are excluded as Hurst *et al.* (2012) demonstrated that this gradient is the point at which $> 15\%$ of sediment transport is nonlinear. Under nonlinear sediment flux hilltop curvature scales nonlinearly with erosion rate (Roering, 2008), and consequently cannot be used as a proxy for erosion rates. As hilltops have a

convex form, their curvature should be negative, so as a final step any points identified as hilltops which have a positive curvature are excluded from further analysis.

5.3.3 Channel extraction

Extracting channel networks from digital topographic data remains a fundamental challenge for many areas of topographic analysis. Without the ability to discriminate between fluvial and hillslope domains, it is not possible to extract many topographic metrics such as hillslope length (Chapter 3), mean basin slope (DiBiase *et al.*, 2010) or hilltop curvature (Hurst *et al.*, 2012), and the accuracy of each of these metrics will be influenced by the accuracy of the channel network extracted. At a more fundamental level, the ability to identify where channels initiate will facilitate better understanding of the processes acting at the transition between diffusive (hillslope) and advective (fluvial) sediment transport (Perron *et al.*, 2008a).

Many authors have made use of field mapped channel heads both as a basis for geomorphic analysis and as a method for evaluating channel extraction methods (Montgomery and Dietrich, 1989; Orlandini *et al.*, 2011; Julian *et al.*, 2012; Jefferson and McGee, 2013; Clubb *et al.*, 2014). Prior to the availability of high resolution topographic data, contributing area and slope-area scaling thresholds were commonly used to define the location of channel heads directly from DEMs (Mark, 1984; O'Callaghan and Mark, 1984; Montgomery and Dietrich, 1989; Tarboton *et al.*, 1991; Dietrich *et al.*, 1992, 1993). The influence of increasing grid size on such channel extraction methods was evaluated by Orlandini *et al.* (2011), who demonstrated a strong sensitivity in predicted channel head location to grid resolution, suggesting that coarser resolution data may not be suitable for channel extraction through an area threshold. I apply the method described by

Orlandini *et al.* (2011) to quantify the accuracy of an extracted channel network, detailed in Section 5.3.4.

Several methods have been proposed to identify channel heads from high resolution topography. Typically these methods exploit the high resolution nature of topographic data to resolve morphometric or process based signatures of channel initiation, or the transition between the hillslope and fluvial domain (Lashermes *et al.*, 2007; Passalacqua *et al.*, 2010; Pelletier, 2013; Clubb *et al.*, 2014). Here I evaluate how two techniques, one geometric method built upon work by Pelletier (2013) and Passalacqua *et al.* (2010), and one process based method, the DrEICH algorithm, developed by Clubb *et al.* (2014), are influenced by increasing grid cell size.

The DrEICH method was selected for evaluation as the technique on which it is based has been shown to operate successfully in lower resolution data (Mudd *et al.*, 2014). The DrEICH method makes use of χ analysis, performed by integrating drainage area along a river profile to facilitate comparisons between river profiles of differing drainage area, with fewer uncertainties than traditional slope-area analysis (Royden *et al.*, 2000; Perron and Royden, 2013). When plotting the χ value against elevation for a river profile, river channels will plot as linear segments, whereas hillslopes will display nonlinear segments. The DrEICH algorithm identifies the transition between these linear and nonlinear segments as the best fit location of the channel head.

The geometric method, used Chapter 4, removes noise from the raw topographic data using a Wiener filter (Wiener, 1949), as recommended by Pelletier (2013). This smoothed topography is then processed to identify channelized portions of the landscape using a tangential curvature threshold (e.g., Pelletier, 2013), selected using the deviation of the probability density function of curvature from a normal distribution on a quantile-quantile plot (e.g., Lashermes *et al.*,

2007; Passalacqua *et al.*, 2010). The identified areas of channelization are then combined into a contiguous channel network by employing a connected components algorithm (He *et al.*, 2008) and thinned into a final channel network skeleton using the algorithm of Zhang and Suen (1984).

Channels were extracted from the 5, 10, 20 and 30 meter DEMs generated in Section 5.3.1 using both of the channel extraction methodologies. Parameters required in the operation of each algorithm were selected based on values used in Chapters 3 and 4 and these values can be found in Table 5.1.

Table 5.1: Parameters used by the geometric and process based techniques in the extraction of channel networks.

Location	Window radius (m)	Drainage area (m^2)[a]	Connected components (Pixels)[b]	$\frac{m}{n}$ ratio[c]	Reference
Santa Cruz Island	4	4	5	0.50	This study
Gabilan Mesa	5	4	5	0.45	Chapters 3 and 4
Oregon Coast Range	4	4	5	0.45	Chapters 3 and 4

[a] Used to thin the initial extracted network by removing channels which have a drainage area below the threshold value.

[b] Defines the point at which a group of contiguous channel pixels is considered to be connected.

[c] The $\frac{m}{n}$ ratio is determined using software provided by Mudd *et al.* (2014) and its use within this context is discussed in detail in Clubb *et al.* (2014).

5.3.4 Comparing channel networks

To assess the accuracy of the channel networks extracted using both methods, I employ two measures of quality described by Orlandini *et al.* (2011). These measures operate on classifications of the predicted location of channel heads placing each channel head into one of three categories: true positives (TP); false

positives (FP) and false negatives (FN). A TP is where a predicted channel head from low resolution data occupies the same spatial location as the channel head derived from 1 meter resolution topography. A FP is where a predicted channel head is placed in a location where there is no channel head in the high resolution data. A FN is when a channel head from high resolution topography does not have a predicted channel head from low resolution topography in the same spatial location.

I follow Orlandini *et al.* (2011) in employing a 30 meter search radius around the 1 meter-derived channel heads, and consider a low resolution channel head falling within this radius to be spatially coincident. This has the effect of normalizing the size of each channel head point, to ensure that one can perform comparisons between predictions made at different spatial resolutions.

The reliability, r, of a channel extraction method is the ability of a method not to predict channel heads in areas where none are located and is calculated as

$$r = \frac{\sum TP}{\sum TP + \sum FP}, \tag{5.5}$$

where $\sum TP$ is the total number of true positives and $\sum FP$ is the total number of false positives. The sensitivity, s, of a channel extraction methodology is given by

$$s = \frac{\sum TP}{\sum TP + \sum FN}, \tag{5.6}$$

where $\sum FN$ is the total number of false negatives. The sensitivity is the ability of a method to predict all of the channel heads expected. Using these two indexes it is possible to quantify the quality of channel heads predicted using low resolution data, as well as understand why a particular method fails, by distinguishing between methods which fail due to either over or under predicting the number of

channel heads in a landscape, or by simply placing channel heads in the wrong spatial location.

5.3.5 Estimating the hillslope sediment transport coefficient from hilltop curvature

The sediment transport coefficient, K $[L^2T^{-1}]$ (dimensions of [M]ass, [L]ength and [T]ime denoted in square brackets), of a landscape is a measure of its sediment transport efficiency and was demonstrated by Furbish *et al.* (2009) to be controlled by the material properties of soil such as grainsize, cohesion and thickness. The value of K within a landscape will exert a control on the morphology of hillslopes (e.g., Roering *et al.*, 1999). Diffusion-like hillslope evolution can be modeled using a 1D mass conservation equation, assuming that the contribution to surface lowering from chemical processes is negligible when contrasted with the signal of surface lowering from physical processes (e.g., Roering *et al.*, 1999; Mudd and Furbish, 2004):

$$\rho_s \frac{\partial \zeta}{\partial t} = -\rho_s \frac{\partial q_s}{\partial x} + \rho_r U, \tag{5.7}$$

where ζ [L] is the elevation of the land surface, ρ_s and ρ_r $[ML^{-3}]$ are densities of dry soil and rock, respectively and U $[LT^{-1}]$ is the uplift rate. In steady state landscapes, where $U = E$ and $\partial\zeta/\partial t = 0$, Equation 5.7 simplifies to

$$\frac{\rho_r}{\rho_s} E = \frac{\partial q_s}{\partial x}, \tag{5.8}$$

with E $[LT^{-1}]$ denoting the erosion rate. To solve this equation, a statement of the volumetric sediment flux per unit contour length, q_s $[L^2T^{-1}]$, must be derived.

A nonlinear relationship between sediment flux and topographic gradient has been proposed by a number of authors (Andrews and Bucknam, 1987; Koons, 1989; Anderson, 1994; Howard, 1997; Roering *et al.*, 1999, 2001; Pelletier and Cline, 2007). Support for such models has been found from both tests of the resulting topographic predictions (Roering *et al.*, 2007; Hurst *et al.*, 2012), as well as through independent measurements of sediment flux across hillslopes (Roering *et al.*, 2001; Roering, 2008).

The nonlinear model proposed by Andrews and Bucknam (1987) and Roering *et al.* (1999) is of the form,

$$q_s = KS\left[1 - \left(\frac{|S|}{S_c}\right)^2\right]^{-1}, \tag{5.9}$$

where S_c is a critical gradient, and as the hillslope gradient approaches this threshold, q_s asymptotes towards infinity.

At low hillslope gradients (e.g. on hilltops), the term within brackets in Equation 5.9 approximates to unity (Hurst *et al.*, 2012). Equation 5.9 can therefore be substituted into Equation 5.8 and can be solved for K on low gradient hilltops, assuming that an independent constraint on E is available:

$$K = -\frac{E\rho_r}{C_{HT}\rho_s}. \tag{5.10}$$

5.3.6 Hillslope length and relief

Hillslope length (L_H) is a crucial landscape parameter to constrain as it controls the rate of mass flux by overland flow within catchments (Dunne *et al.*, 1991; Thompson *et al.*, 2010; Dunne *et al.*, 2016), influences rates of soil erosion (Liu

et al., 2000), and presents a first order control on the maximum source area of landslides (Hurst *et al.*, 2013a). Furthermore, it may be used to demonstrate nonlinearity in hillslope sediment flux (Roering *et al.*, 1999, 2007).

Many studies have attempted to calculate hillslope length through the inversion of drainage density (Tucker *et al.*, 2001), analysis of plots of local slope against drainage area (Roering *et al.*, 2007), direct measurements from topographic maps (Hovius, 1996; Talling *et al.*, 1997), and by measuring the length of overland flow from ridgeline to channel (See Chapter 3). Chapter 3 demonstrated that the most geomorphologically suitable technique to use, particularly in the context of hillslope sediment transport, was that of measuring the length of overland flow. An additional measure which can be derived from this technique is the topographic relief, which is the difference in elevation between a hilltop and channel connected by a hillslope flow path. Topographic relief has been estimated in a number of ways and is frequently used in studies of tectonic geomorphology (e.g., Gabet *et al.*, 2004; Hilley and Arrowsmith, 2008; Gallen *et al.*, 2011, 2013). Furthermore, topographic relief may be used to generate dimensionless erosion and relief plots (Roering *et al.*, 2007; Hurst *et al.*, 2012; Sweeney *et al.*, 2015), which can be used to identify landscape transience (Hurst *et al.*, 2013b; Mudd, 2016). Consequently, I intend to test the robustness of measuring hillslope length and relief as grid resolution decreases, with the aim of facilitating increased confidence in geomorphic analyses performed in locations where high resolution topography is unavailable.

Using the 20 topographic datasets generated in Section 5.3.1 for each of the three landscapes, hillslope length measurements were generated following the methods outlined in Chapter 3. I measured hillslope length on each dataset using two different channel networks. Firstly, channel heads were extracted from the highest resolution data set, in each case 1 meter, using the geometric method outlined in Section 5.3.3. These high resolution channel heads were mapped onto the

coarser resolution topographic data, to ensure that changing channel extraction results will not have an influence on the measures of hillslope length. This allows improved isolation of the factors driving variations in hillslope length as grid resolution is decreased. Secondly, the analysis was performed using coarser resolution channel networks extracted using the geometric method of channel extraction. I use the geometric method as opposed to the DrEICH method because, as I will show below, the geometric method is less sensitive to grid resolution. These two channel networks effectively provide upper and lower bounds on the accuracy of hillslope length and relief measurements.

5.4 Results

5.4.1 Curvature

Figure 5.2 illustrates the variations in total curvature with grid resolution for a section of Santa Cruz Island. As the cell size is increased the range of C_{Total} measurements is reduced, with much of the landscape becoming apparently planar. Within the black box, which covers the same spatial area as the boxes in Figure 5.1, the impact of degrading resolution on small topographic features is observed, with the curvature signal of this first order feature being lost as the grid size approaches 30 meters.

Figure 5.3 displays the variations in the distribution of total and tangential curvature measurements with grid resolution for each of the study landscapes. Santa Cruz Island shows little variation in mean and median curvature with resolution, with the majority of the changes in each distribution with resolution occurring at the extremes of the curvature distribution for each dataset, as the

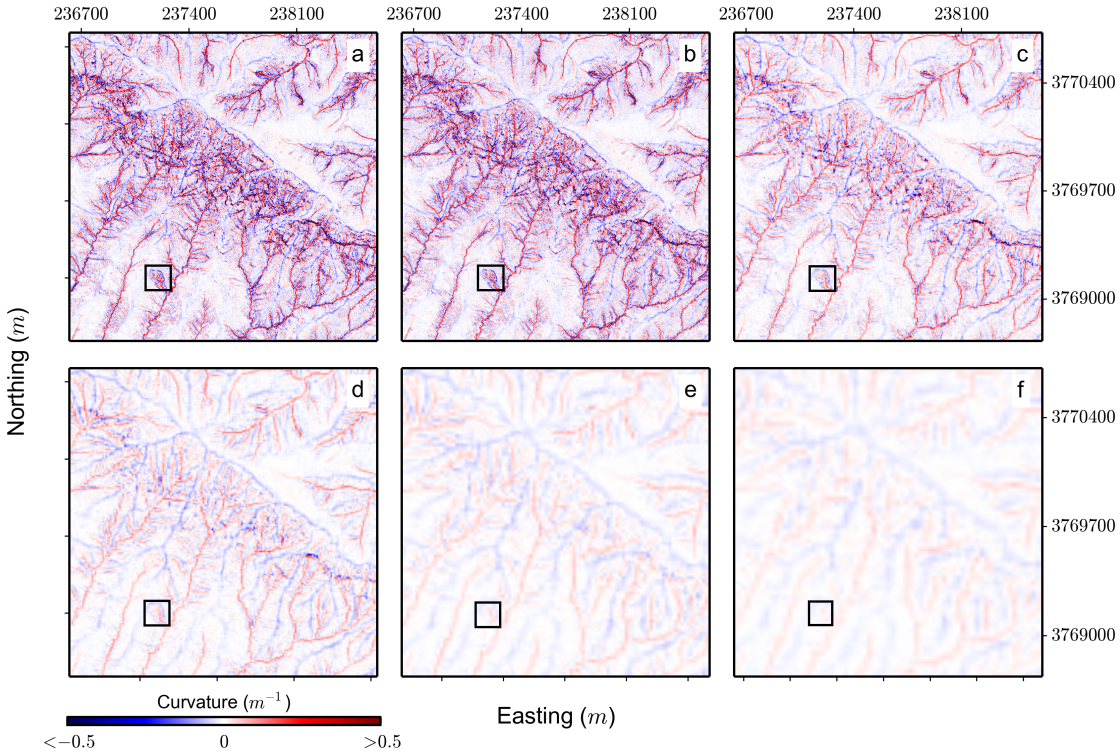

Figure 5.2: Maps showing the spatial variation in total curvature measurements as grid resolution is decreased for the same section of Santa Cruz Island as displayed in Figure 5.1. All coordinates are in UTM Zone 11N. Panels **(a)** to **(f)** represent resolutions of 1, 2, 5, 10, 20 and 30 meters. The black boxes outline the same features as highlighted in Figure 5.1, showing the reduction in the curvature signal with grid resolution for such a feature.

representation of ridgelines and channel bottoms becomes increasingly diffuse. As resolution is decreased, the range between 2^{nd} and 98^{th} percentiles and the 1^{st} and 3^{rd} quartiles decreases, with a more rapid reduction in the more extreme values than in the quartiles. While this effect is most marked at the extremes, the distributions are condensed across all percentile intervals as grid resolution is increased beyond 3-4 meters. This behavior is observed for both C_{Total} and C_{Tan} as grid size is increased.

In the Oregon Coast Range for both measurements of curvature there is little

variation between the 1, 2 and 3 meter datasets, with a broad range of measurements shown in the probability distributions. Beyond this point the mean and median do not significantly change but, as in Santa Cruz Island, the overall distribution of measurements compresses towards the average value for the landscape. The Gabilan Mesa data show similar trends to those of Santa Cruz Island, but exhibit less variability at lower resolutions. The probability distributions of each measurement also exhibit less change with resolution than the other two datasets, indicating a reduced sensitivity to grid resolution at this location.

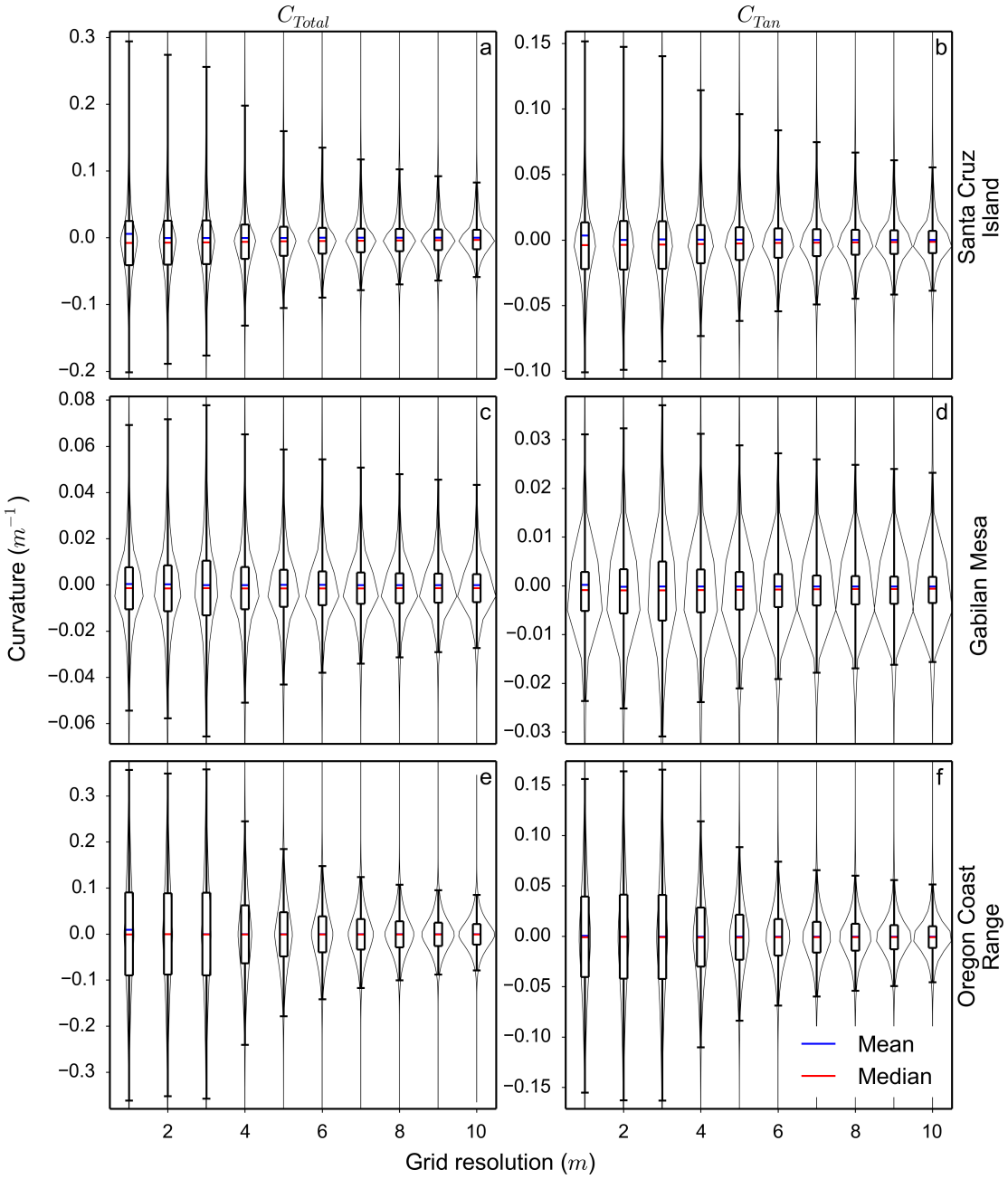

Figure 5.3: Plots of the reduced of C_{Total} (**(a)**, **(c)** and **(e)**) and C_{Tan} (**(b)**, **(d)** and **(f)**) measurements as resolution is decreased for each of the study landscapes. Whiskers are the 2nd and 98th percentiles; the box covers the 25th and 75th percentiles; the blue bar is the mean and the red bar is the median. The gray outline is the probability density function of each dataset.

5.4.2 Channel networks

Figure 5.4 provides a qualitative overview of the changes of channel network extent with decreasing grid resolution for both methods, across the three test landscapes. In each case the general patterns are that as the grid resolution is decreased, the lowest order channels are lost, as they exist at a spatial scale below that of the data resolution. In contrast, many of the predicted networks appear to occupy similar

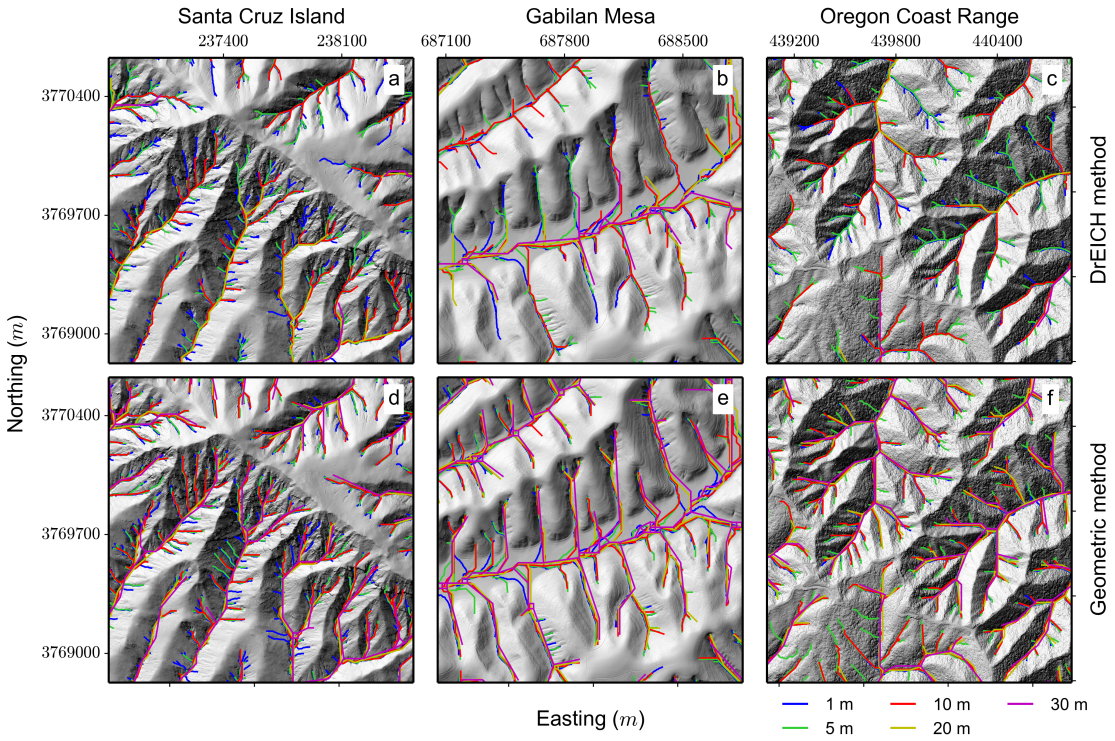

Figure 5.4: Representative sections of each landscape's channel network displaying the extent of each network as grid resolution is decreased. Plots **(a)**, **(b)** and **(c)** are generated using the DrEICH method of channel extraction. Plots **(d)**, **(e)** and **(f)** are generated using the geometric method. All coordinates are in UTM. The left column is from Santa Cruz Island, UTM Zone 11N, the central column is from Gabilan Mesa, UTM Zone 10N and the right column is from the Oregon Coast Range, UTM Zone 10N.

spatial locations in larger, higher order channels where the topographic signal of a channel is more pronounced. The geometric method shows less reduction in drainage density than the DrEICH method, as data resolution is decreased.

Figure 5.5 provides a quantitative assessment of channel extraction quality by presenting the indexes of reliability and sensitivity for both the geometric channel extraction and extraction based on DrEICH, as the grid size is increased. In Gabilan Mesa the channels extracted by the geometric method exhibit a high reliability which does not decrease considerably with increasing grid size, suggesting that for each resolution step a large proportion of the predicted channel heads are spatially coincident with the channel heads generated from the 1 meter data. The sensitivity values for this method and location are lower, and decline more steadily with decreasing grid resolution, suggesting an increasing number of channel heads being missed by the algorithm as grid size is increased. The DrEICH method does not perform as well in Gabilan Mesa, with lower index values for the 5 meter data than the geometric method, and a rapid decline towards index values of 0, suggesting that the predicted channel heads bear little relation to the channel heads from the 1 meter data.

In Santa Cruz Island the geometric method's reliability index is similar to Gabilan Mesa, but the sensitivity index is not as high, which indicates a large number of channel heads are being missed. However, where a prediction is made it is typically accurate. The DrEICH method exhibits a similarly large reliability initially, but again shows more rapid degradation in the index value as grid size is increased. The sensitivity values again decline more rapidly and reach a 0 value at 20 meter grid resolution.

The data for the Oregon Coast Range show similar patterns for both methods, although the geometric method exhibits systematically larger index values. In each case the reliability increases slightly from 5 to 10 meter resolution and then

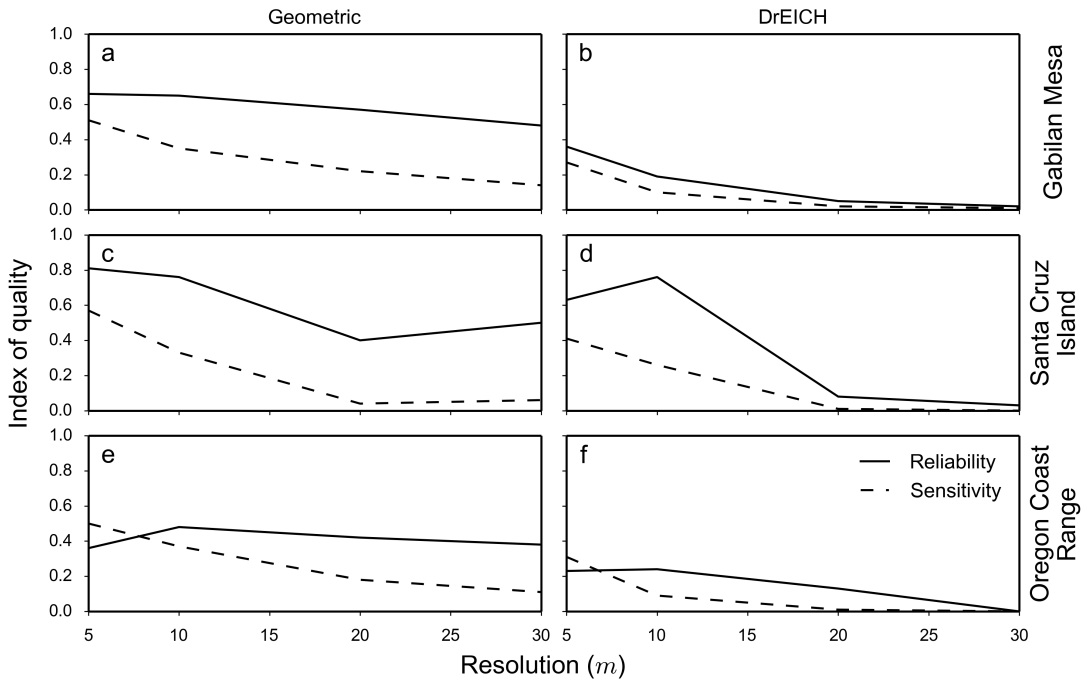

Figure 5.5: The variations in reliability (Equation 5.5) and sensitivity (Equation 5.6) of each channel network with decreasing grid resolution. Plots **(a)**, **(c)** and **(e)** are generated using the geometric method of channel extraction. Plots **(b)**, **(d)** and **(f)** are generated using the DrEICH method. The top row is from Gabilan Mesa, the middle row is from Santa Cruz Island and the bottom row is from the Oregon Coast Range. The full results from this analysis can be found in Tables 5.2 and 5.3.

Table 5.2: Reliability and sensitivity metrics for the DrEICH method of channel extraction.

Location	Resolution (m)	$\sum TP$	$\sum FP$	$\sum FN$	r	s
Gabilan Mesa	5	555	982	1489	0.36	0.27
	10	210	879	1875	0.19	0.1
	20	42	734	2088	0.05	0.02
	30	13	609	2122	0.02	0.01
Santa Cruz Island	5	3295	1971	4799	0.63	0.41
	10	2454	793	6865	0.76	0.26
	20	69	838	8235	0.08	0.01
	30	27	915	8284	0.03	0.0
Oregon Coast Range	5	507	1718	1131	0.23	0.31
	10	144	445	1462	0.24	0.09
	20	16	105	1623	0.13	0.01
	30	2	442	1639	0.0	0.0

Table 5.3: Reliability and sensitivity metrics for the geometric method of channel extraction.

Location	Resolution (m)	$\sum TP$	$\sum FP$	$\sum FN$	r	s
Gabilan Mesa	5	1019	519	987	0.66	0.51
	10	712	380	1301	0.65	0.35
	20	448	332	1592	0.57	0.22
	30	292	333	1775	0.48	0.14
Santa Cruz Island	5	4280	991	3109	0.81	0.57
	10	2473	777	4998	0.76	0.33
	20	334	505	7861	0.4	0.04
	30	475	470	7659	0.5	0.06
Oregon Coast Range	5	792	1438	788	0.36	0.5
	10	562	602	938	0.48	0.37
	20	276	374	1275	0.42	0.18
	30	475	277	1418	0.38	0.11

declines gradually towards 30 meter grid size. The sensitivity indexes for both methods begin at a larger value than the reliability indexes, and steadily decline towards 0. A sensitivity value exceeding the reliability value suggests that in this landscape there are fewer missed channel heads in the 5 meter data, but at the expense of too many predicted channel heads in locations where there are none predicted in the 1 meter data.

5.4.3 Sediment transport coefficient

Using the values for hilltop curvature generated in Section 5.4.1, published parameters for erosion rate and material properties outlined in Table 5.4 and Equation 5.10, the average sediment transport coefficient (K) of each landscape can be calculated as a function of grid resolution. Figure 5.6 displays the relationship between the sediment transport coefficient and grid resolution for each of the three study sites. The data for Santa Cruz Island and Oregon Coast Range both show a gradual increase in the sediment transport coefficient with grid size, the rate of which reduces with increasing grid size. The Gabilan Mesa data does not exhibit the same trend, with little variability in calculated K values as resolution is decreased. Although the Oregon Coast Range and Santa Cruz Island datasets exhibit an increase in estimated K, all of the values for each location fall within the range of values for K compiled by Hurst *et al.* (2013c).

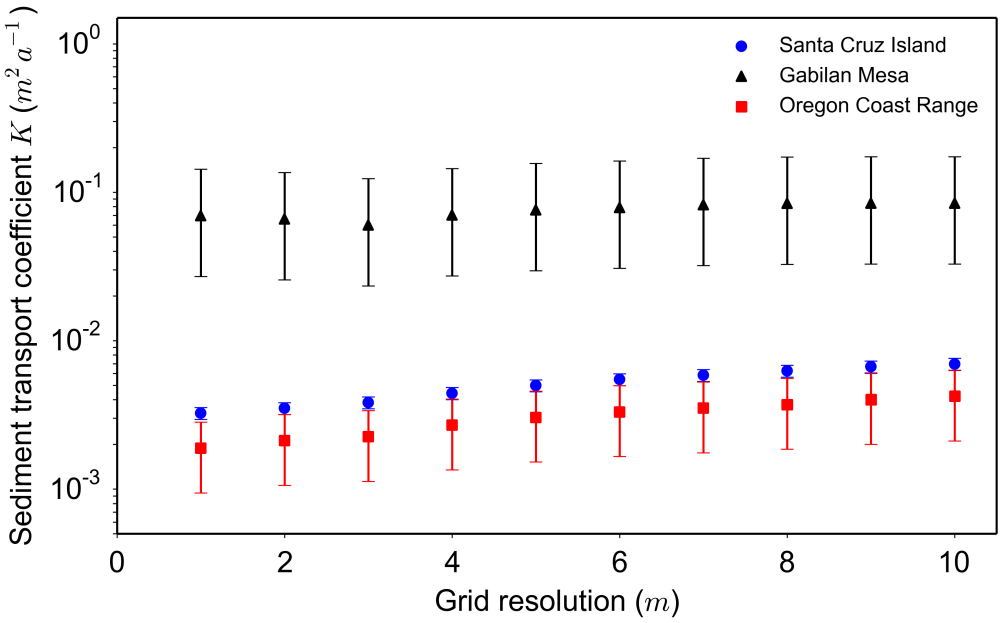

Figure 5.6: Changes in the estimated sediment transport coefficient, K, calculated using Equation 5.10 and parameters in Table 5.4 for each of the three study landscapes, for a range of grid resolutions. The errorbars on each datapoint represent the uncertainties reported for each landscape's erosion rate data.

Table 5.4: Parameters used to calculate the sediment transport coefficient.

Location	Soil density $(kgm^{-3})^a$	Rock density $(kgm^{-3})^a$	Erosion rate $(mmyr^{-1})$	Reference
Santa Cruz Island	1.4	2.4	0.069 ± 0.007	Perroy *et al.* (2012)
Gabilan Mesa	1.4	2.4	$0.36^{+0.38}_{-0.22}$	Roering *et al.* (2007)
Oregon Coast Range	1.4	2.4	0.1 ± 0.05	Roering *et al.* (1999)

[a] Soil and rock densities representative of typical measurements of the fieldsites and are taken from Hillel (1980).

5.4.4 Hillslope length and relief

The hillslope length measurements for Santa Cruz Island calculated using 1 meter channel heads (Figure 5.7a) show little variation in the distribution of the data up to 10 meter resolution, with the main difference being the increase with grid size in the 2nd percentile measurements, which is a trend observed within each of the datasets. The mean and median values also gradually decrease towards the 10 meter resolution dataset, before gradually increasing towards the 30 meter resolution step. However, these variations are very small, with the overall distributions of hillslope length and relief not varying considerably between resolution steps. When the same hillslope length algorithm is applied using channel networks extracted using the geometric method for each resolution step (Figure 5.7c), there is little change in the distribution or average values of L_H until beyond the 10 meter resolution step. Beyond this point the measurements of hillslope length are clearly affected by the reduction in accuracy of the channel network. The relief measurements for both channel head methods (Figure 5.7b, d) in Santa Cruz Island exhibit little resolution dependence up to 10 meter cell sizes, beyond which point the values increase steadily. In the case of the 1 meter channel heads the distribution becomes compressed around the average values at lower resolutions, whereas with the variable channel head dataset the distribution of values increases with decreasing resolution.

In Gabilan Mesa the hillslope length measurements calculated using 1 meter channel heads (Figure 5.8a) show a gradual reduction in mean and median values between the highest resolution data and the 8 meter resolution data before a small plateau and then a small increase until the 30 meter dataset. The average relief values calculated for the same dataset increase steadily by approximately 20 meters between the highest and lowest resolution datasets (Figure 5.8b). The distribution of relief measurements is broadly consistent between 1 and 5 meter

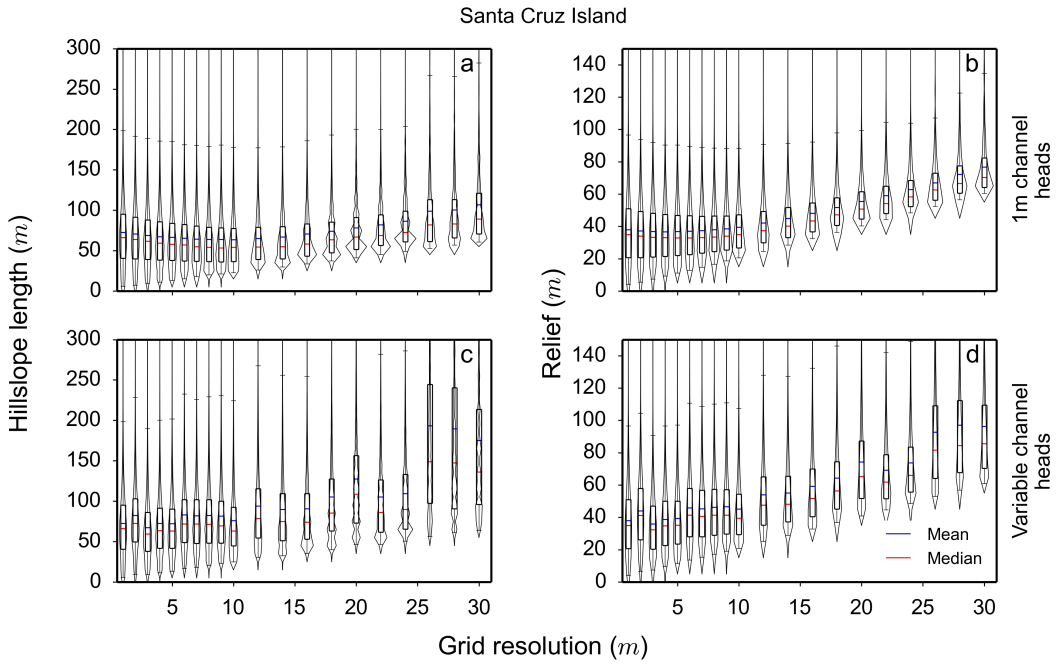

Figure 5.7: Plots of the distribution of hillslope length (**(a)** and **(c)**) and relief (**(b)** and **(d)**) measurements as resolution is decreased for Santa Cruz Island. Whiskers are the 2nd and 98th percentiles; the box covers the 25th and 75th percentiles; the blue bar is the mean and the red bar is the median. The gray outline is the probability density function of each dataset. The top row presents the best case scenario, where an independent constraint on the channel network is available for the lower resolution data and the bottom row uses the channel networks extracted using the geometric method outlined in Section 5.3.3 for each resolution step.

resolutions before reducing about the median as grid size is increased. The same trends are apparent in the hillslope length and relief data calculated using the variable channel heads (Figure 5.8c, d) with little change between the two pairs of datasets.

The hillslope length measurements for the Oregon Coast Range with channel heads from the 1 meter data (Figure 5.9a) again show a gradual reduction in the median values with a gradual increase in the mean values until 20 meter grid

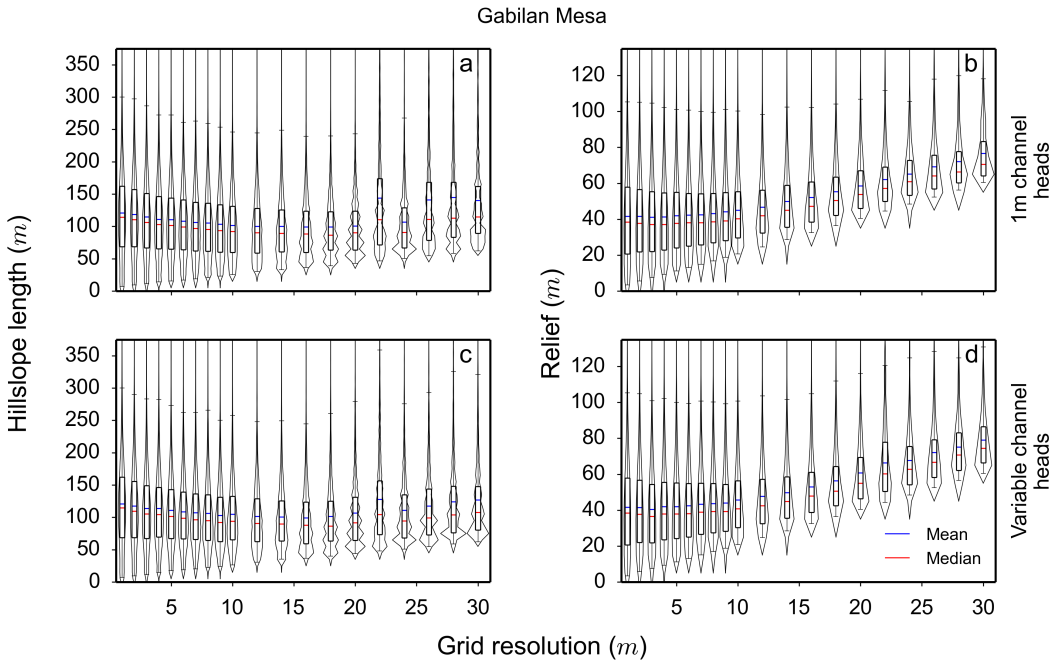

Figure 5.8: Plots of the distribution of hillslope length (**(a)** and **(c)**) and relief (**(b)** and **(d)**) measurements as resolution is decreased for Gabilan Mesa. Whiskers are the 2nd and 98th percentiles; the box covers the 25th and 75th percentiles; the blue bar is the mean and the red bar is the median. The gray outline is the probability density function of each dataset. The top row presents the best case scenario, where an independent constraint on the channel network is available for the lower resolution data and the bottom row uses the channel networks extracted using the geometric method outlined in Section 5.3.3 for each resolution step.

resolution. Beyond this point the data become considerably more variable, with a large increase in both the mean and median results. The relief data shown in Figure 5.9b are the most consistent of the three landscapes with very little variation in the values until they begin increasing with cell size at approximately 20 meter resolution. The data presented in Figure 5.9c and d show the most sensitivity to grid resolution of the three landscapes. Average hillslope length values reduce towards 10 meters before stabilizing and then rapidly increasing in the same manner as the fixed channel head data. The relief measurements show a

gradual decline in mean relief across the range of resolutions from 1 to 10 meters, where the fixed data show much less variation.

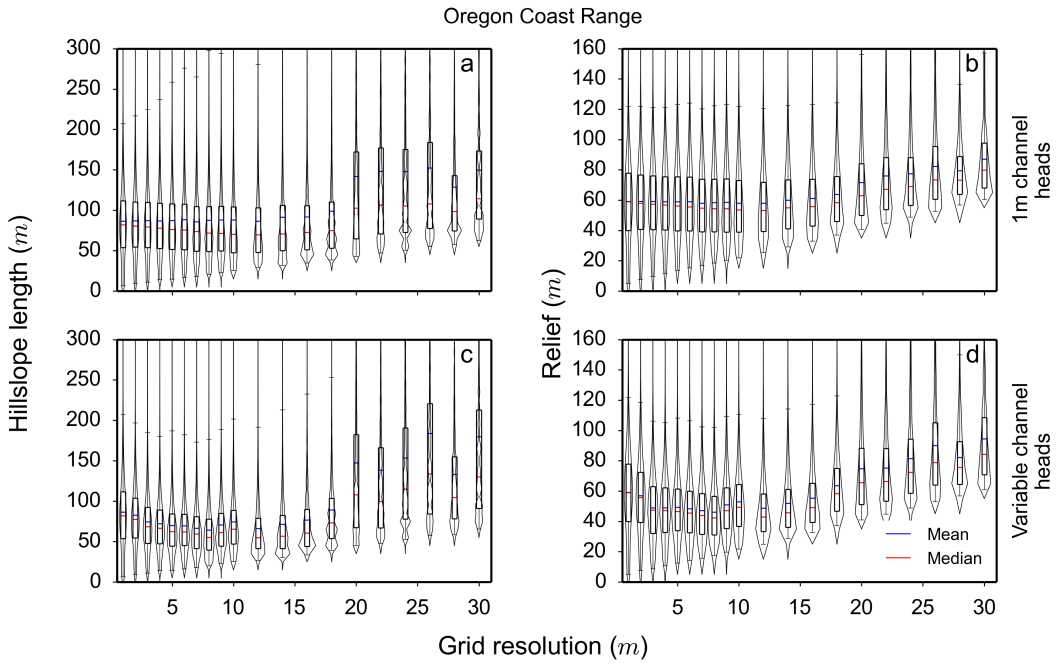

Figure 5.9: Plots of the distribution of hillslope length (**(a)** and **(c)**) and relief (**(b)** and **(d)**) measurements as resolution is decreased for the Oregon Coast Range. Whiskers are the 2nd and 98th percentiles; the box covers the 25th and 75th percentiles; the blue bar is the mean and the red bar is the median. The gray outline is the probability density function of each dataset. The top row presents the best case scenario, where an independent constraint on the channel network is available for the lower resolution data and the bottom row uses the channel networks extracted using the geometric method outlined in Section 5.3.3 for each resolution step. At higher resolution steps the 98th percentile data are not shown in the plot, to better highlight the distribution of measurements between the 25th and 75th percentiles, which make up the majority of the data points.

5.5 Discussion

5.5.1 Curvature and the problem of resolution-dependent filtering

Across the three landscapes the variance of the distributions of both total and tangential curvature values is systematically reduced as resolution is decreased, an effect that is particularly notable after the grid resolution exceeds 3-4 meters (Figure 5.3). In each of the three datasets, the inter-quartile ranges remain relatively constant, whereas beyond 4 meters resolution in each case the range between the 2^{nd} and 98^{th} percentiles reduces rapidly (Figure 5.10), demonstrating that the majority of the loss of curvature information occurs at the extremes of the distribution.

In producing a DEM, I am sampling a complex two-dimensional elevation signal, in which spatial variations in geomorphic process drive variations in topographic amplitude at different wavelengths (Perron *et al.*, 2008b). Decreasing the grid resolution of DEMs acts as a low-pass filter on this topographic signal, which preferentially degrades features in the topography that have significant amplitude at small wavelengths, such as sharp ridgelines, narrow valley bottoms, and local topographic roughness generated by, for example, landslides, tree throw and rock exposure (Figures 5.1 and 5.2). While the position of ridges and valleys is preserved in coarser resolution data, the magnitude of their associated curvature values is reduced as cell sizes increase; this effect is particularly marked for hillslopes in which curvature is focused at the ridge crest and valley bottoms, a common characteristic of more rapidly eroding landscapes (Roering *et al.*, 1999, 2007). For first order landscape features, such as gullies, landslide scars and

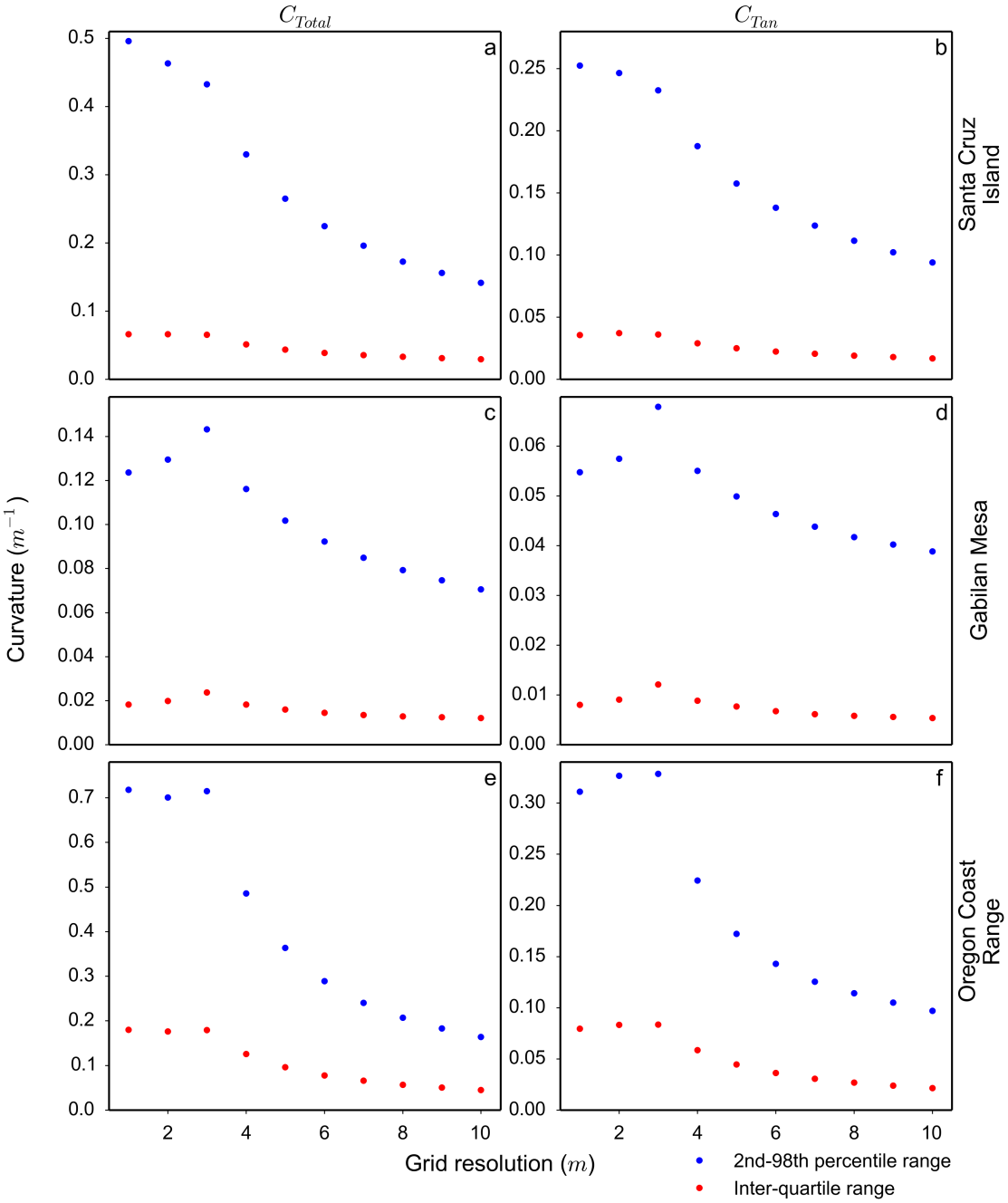

Figure 5.10: Plots of the reduction in range between the 2nd and 98th percentiles (blue) and the inter-quartile range (red) of C_{Total} (**(a)**, **(c)** and **(e)**) and C_{Tan} (**(b)**, **(d)** and **(f)**) measurements as resolution is decreased for each of the study landscapes.

first order channels, increasing grid size eventually results in the complete loss of topographic information, as highlighted in Figure 5.1 and Figure 5.2.

Topographic filtering and its implications for curvature and slope measurements

To interpret the observed loss of fidelity that accompanies coarser grids evident in Figures 5.3 and 5.10, it is illustrative to examine the spectral behavior of a simplified 1 dimensional system. I acknowledge that a 1 dimensional approach cannot fully describe the complex two dimensional topography of real landscapes, but a one dimensional system is amenable to mathematical treatment that can at least give us qualitative insight into trends observed in these data. In addition, some of the features of interest, for example ridgelines and channels, can be roughly approximated as one dimensional structures within a two dimensional landscape.

Curvature in one dimension, C_x [L^{-1}], is often approximated with the differencing equation:

$$C_x = \frac{\zeta_{(x-\Delta x)} - 2\zeta_x + \zeta_{(x+\Delta x)}}{(\Delta x)^2}, \tag{5.11}$$

where ζ [L] is the elevation of the land surface, x [L] is a location in space, C_x is the curvature at location x, and Δx [L] is the grid interval. The subscripts denote the discrete locations where elevation is evaluated. One can calculate the wavenumber response function ($H(\omega; \Delta x)$) from this filter (Jenkins and Watts, 1968):

$$H(\omega;\Delta x) = \frac{2}{(\Delta x)^2}[cos(\omega\Delta x) - 1)], \tag{5.12}$$

where $\omega = 2\ \pi/L$ [L^{-1}] is the wavenumber with wavelength L [L] (that is, higher wavenumbers correspond to higher frequencies and thus shorter wavelengths). Using this function, one can calculate the gain, $G(\omega;\Delta x)$, which is the amplitude of the filtered signal (in this case curvature) to the amplitude of the original signal (in this case elevation) at the wavenumber ω. The theoretical gain for continuous waveforms (i.e., not discrete filters like Equation 5.11) is ω^2. The gain of a discrete filter is the modulus of the wavenumber response function (Jenkins and Watts, 1968), so in the case of Equation 5.12 the resultant gain, $G(\omega;\Delta x)$ is:

$$G(\omega;\Delta x) = \frac{2}{(\Delta x)^2}[1 - 2cos(\omega\Delta x) + cos^2(\omega\Delta x)]^{1/2}. \tag{5.13}$$

In the case of this curvature filter (Equation 5.11), the gain function reveals how high frequency waveforms (e.g., ridgecrests, treethrow mounds, local roughness) in the elevation data involve relatively large values of curvature, whereas low frequency elevation waveforms (e.g., ridge-valley features or geologic folds) with the same amplitude involve relatively small curvatures. Crucially, however, the discrete filter does not retain all of the high frequency information. One can calculate what information is lost by calculating the fidelity, which is the ratio between discrete gain (Equation 5.13) and the theoretical gain (ω^2):

$$F(\omega;\Delta x) = \frac{2}{(\Delta x)^2\omega^2}[1 - 2cos(\omega\Delta x) + cos^2(\omega\Delta x)]^{1/2}. \tag{5.14}$$

Fidelity is a function of the ratio between the grid interval and the wavelength (Figure 5.11); when the fidelity is unity, the discrete filter exactly reproduces

the underlying continuous function. As the frequency approaches the Nyquist wavenumber ($\Delta x/L = 1/2$), fidelity decreases; a fidelity of only approximately 0.4 is achieved at the Nyquist wavenumber itself. To achieve a fidelity, F, of 0.9 requires that $L/\Delta x$ is equal to approximately 6 grid points per wavelength. A fidelity $F = 0.95$ requires 8 points per wavelength, and $F = 0.99$ requires 18. Therefore, while the grid resolution imposes a minimum wavelength that can be resolved (defining the Nyquist wavenumber), the behavior of the fidelity function (Figure 5.11) clearly illustrates that curvature information will be lost when calculated for features with wavelengths greater than, but still close to, the minimum resolvable at the Nyquist wavenumber. In this simple example, using 1 meter resolution data, one could only capture the curvature of a one dimensional ridgeline that had a wavelength of 3-4 meters (one does not need the entire wave to capture the peak of the waveform), but with loss of fidelity on the magnitude of the curvature (i.e., underestimating its value).

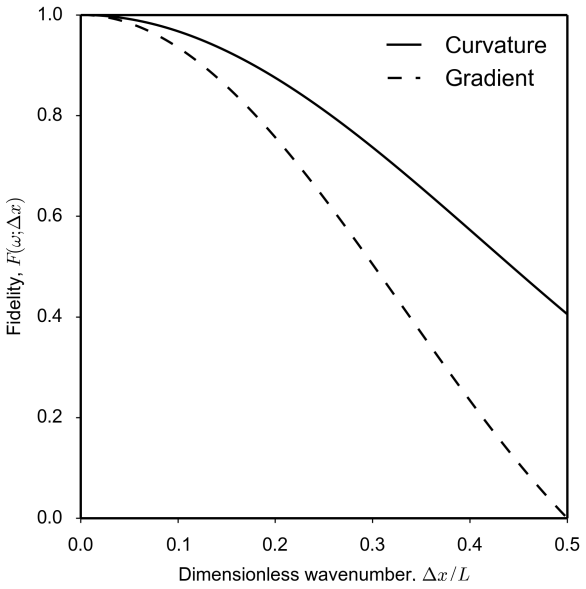

Figure 5.11: Plot of fidelity (F) of two one dimensional differencing operations: curvature (Equation 5.11) and topographic gradient (Equation 5.15) as a function dimensionless wavenumber $\Delta x/L$ to the Nyquist wavenumber, $\Delta x/L = 0.5$.

In this study I have not computed how topographic gradient varies as a function of grid resolution because this has been examined by many previous authors (e.g., Gao, 1997; Warren *et al.*, 2004; Vaze *et al.*, 2010). However this treatment of the properties of a one dimensional filter can give some insight into previous results. Consider a simple central-difference approximation of the topographic gradient (S_x, dimensionless):

$$S_x = \frac{\zeta_{(x+\Delta x)} - \zeta_{(x-\Delta x)}}{2\Delta x}. \tag{5.15}$$

One can follow the same series of operations performed on Equation (5.11) to arrive at the fidelity of Equation (5.15), denoted as F_S, taking into account that the theoretical gain is ω:

$$F_S(\omega; \Delta x) = \frac{1}{\Delta x \omega}[sin(\omega \Delta x)]. \tag{5.16}$$

The form of Equation 5.16 (Figure 5.11) formally illustrates why estimates of slope tend to decrease systematically with increasing grid interval Δx. Namely, an increasing Δx is able to resolve less local (high wavenumber) elevation structure while picking out the slope of more regional structure. The fidelity increases as the ratio of the grid interval to the wavelength, $\Delta x/L$, decreases (Figure 5.11). To achieve a fidelity $F_S = 0.9$, for example, requires $L/\Delta x$ or approximately 8 grid points per wavelength. A fidelity $F_S = 0.95$ requires 11 points per wavelength, and $F_S = 0.99$ requires 18. The fidelity of the one dimensional gradient operator goes to zero when approaching the Nyquist wavenumber ($\Delta x/L = 0.5$). These results explain the pronounced loss of gradient information in coarse resolution data observed by many authors (e.g., Gao, 1997; Warren *et al.*, 2004; Vaze *et al.*, 2010).

Total and tangential curvature

Having explored simplified one dimensional filters, I now return to the two dimensional results. Although real landscapes are two dimensional and I use polynomial fitting rather than simple differencing as in Equation 5.11, it is still possible to use Equation 5.14 as a qualitative indicator of the grid spacing required for appropriate curvature estimates. In Gabilan Mesa, where ridgelines are broad, lower resolution data can still capture the curvature with relatively high fidelity. However, in locations with sharper ridgelines, such as Santa Cruz Island, the narrowest ridgelines are no longer adequately resolved as the grid size is increased, as can be seen in Figure 5.2.

The loss of fidelity predicted by the simple one dimensional system (Equation 5.14) qualitatively predicts the pattern observed in Figures 5.3 and 5.10, namely that at lower resolution the curvature values are smeared over a greater length-scale leading to apparently broader ridges, and peak elevations are systematically underestimated. This highlights that in conjunction with data quality, landscape morphology also exerts a control on the optimal resolution to use for a given study, where landscapes with more gradual hillslope to valley transition morphologies can be analyzed using coarser resolution topographic data with more confidence.

Santa Cruz Island and the Oregon Coast Range have the highest tangential curvature at 1 meter resolution. High tangential curvature at Santa Cruz Island corresponds to observations of extensive gullying and hillslope erosion (Pinter and Vestal, 2005; Perroy *et al.*, 2012). In the Oregon Coast Range, features such as pit and mound topography produced by tree throw and other biotic activity are resolved in the LiDAR dataset (Roering *et al.*, 2010; Marshall and Roering, 2014), which manifest as an increase in values of curvature. However this could also

be indicative of non-topographic noise in the DEM surface produced during the processing of the point clouds, which is particularly required in heavily forested locations (Liu, 2008; Meng *et al.*, 2010) such as the Oregon Coast Range. This suggests an unfortunate collinearity between the two causes of small wavelength topographic noise and warrants further testing in future to disentangle synthetic and natural noise from high resolution topographic measurements. However, high curvature is not solely a manifestation of stochastic disturbance on local topographic roughness, but is also generated at narrow valley bottoms, and at ridgelines where erosion rates are rapid relative to the hillslope sediment transport coefficient (Roering *et al.*, 2007; Hurst *et al.*, 2012). Gabilan Mesa exhibits much lower curvature values than the other two locations, which is a consequence of a landscape with a large sediment transport coefficient, indicating that sediment transport at Gabilan Mesa is dominated by diffusion-like processes (Roering *et al.*, 2007), smoothing the landscape and reducing the tangential curvature of the hillslope surface.

5.5.2 Channel extraction

It is intuitive to consider that when extracting channel networks at any data resolution, regardless of method, the higher order, larger channels will be more accurately constrained than lower order channels. This pattern is observed in each of the study landscapes, with the majority of the variations in channel locations occurring in first and second order channels. Such loss of low order channels from datasets has implications for studies focusing on upland areas, in particular where detailed measurements which depend on channel network position are performed.

The contrast between the extent of channel networks and their indexes of quality for the two methods shows that a geometric method of channel extraction outperforms the process-based DrEICH algorithm. Due to the relative simplicity

of the geometric method of channel extraction, errors inherent in the DEM are not compounded at the same scale as with the DrEICH algorithm, which performs more operations on topographic data. As the geometric method identifies channels based on their tangential curvature, although channel head features may be smoothed out of the DEM as cell size is increased, the channel will still express some positive curvature in lower resolution data. The initiation point may be located downslope of the true channel head, but even in this worst case most of the channel network will be extracted correctly. This is observed in Figure 5.4 which shows a gradual reduction in drainage density as the grid resolution is decreased.

The indexes of quality defined by Orlandini *et al.* (2011) provide a clear framework to understand the quality of channel head predictions using these two methods as data resolution is decreased. In each case, the geometric method outperforms the DrEICH method, both in the accuracy of the channel heads which are predicted, and in the ability of the method not to predict channel heads in locations where no channel exists. These indexes are influenced by the size of the search radius around each channel head, and reducing this radius would decrease the index values. However, the use of a 30 meter search radius allows comparisons to be drawn between predictions made at different data resolutions, and also between this study and that of Orlandini *et al.* (2011).

This assessment of high resolution methods on degraded quality data demonstrates the ongoing challenges that channel extraction poses to the geomorphology community. Orlandini *et al.* (2011) performed extensive testing on channel extraction using threshold channel extraction methods, and demonstrated similar limitations when channels were extracted using lower resolution data. These results suggest that a geometric method of channel extraction will provide an optimal channel network as data quality is reduced, particularly in uniform landscapes such as Gabilan Mesa. However, the only way to ensure the highest quality results

is to employ high resolution data in conjunction with field mapping of channel network extents.

5.5.3 Sediment transport coefficient

The predicted values of the sediment transport coefficient (K) for the 1 meter data fall within the range of values compiled by Hurst *et al.* (2013c), and estimated for the Oregon Coast Range and Gabilan Mesa by Roering *et al.* (1999) and Roering *et al.* (2007). This suggests that this method can produce useful estimates of K when employing high resolution topography.

The sediment transport coefficients calculated at the Oregon Coast Range and Santa Cruz Island locations both increase with grid resolution, reflecting the sensitivity of C_{HT} to grid resolution in each of these locations. Despite the Oregon Coast Range eroding 45% more rapidly (Table 5.4) than Santa Cruz Island, the rate of increase in K measurements remains similar between the two landscapes. Gabilan Mesa data are generally insensitive to an increase in grid cell size, as the scale of hilltop widths measured in Gabilan Mesa is on the order of tens of meters. This allows datasets with cell sizes approaching half the width of a hilltop to provide an accurate estimate of hilltop curvature and thus, the sediment transport coefficient.

These data suggest that estimating K from low resolution topographic data is possible in many landscapes, particularly those which have average ridgelines broader than the grid resolution of the topographic data. In the case of landscapes with sharper ridgelines such as Santa Cruz Island and the Oregon Coast Range, it is more challenging to constrain K effectively as the grid resolution is increased. The magnitude of overestimation of K between the highest and lowest resolution sediment transport coefficient estimates, 0.0023 m^2a^{-1} in the case of the Oregon

Coast range, will be a product of the uncertainty within the calculation of the erosion rate and material densities in addition to the local variations of K within each landscape.

5.5.4 Hillslope length and relief

Measurements of hillslope length and relief have been used to test sediment flux laws (Roering *et al.*, 2007) and to identify landscape transience (Hurst *et al.*, 2013b; Mudd, 2016). Such analyses have previously been restricted to high resolution topographic data. When considering hillslope length, one must select a grid resolution that is at least half the median hillslope length in order to resolve any useful information. However, in reality more than 2 pixels are required if any meaningful information is to be extracted from topographic data. As the median hillslope length for many landscapes has been shown to be in excess of 100 meters (Chapter 3), this requirement for several pixels per hillslope falls well within the range of many lower resolution data products. Therefore, the results show that meaningful hillslope length measurements can be made from lower resolution topographic data, with data products approaching 30 meter resolution proving suitable in some cases.

The relief measurements for each landscape, however, show more sensitivity to grid resolution, with a systematic increase in the median values in each location beyond 10 meters grid resolution. As increasing grid size acts as a low-pass filter on the landscape, reducing the elevation of ridges, whilst raising the elevation of channel beds, producing a net reduction in topographic relief. However, the increased relief observed with increasing grid size is produced by the decrease in drainage density with increasing grid size observed in Figure 5.4, producing fewer channels reaching up towards ridgelines leading to hillslope flow paths traveling further downslope before reaching a channel.

By contrasting the L_H and R results computed using fixed and variable channel heads, it is clear that the optimal method for measuring hillslope length and relief is to employ as accurate a channel network as possible. However, the variable channel head data show that the signal of average hillslope length and relief is broadly insensitive to data resolution up to grid sizes of at least 10 meters. This would facilitate the analysis of landscape transience using these measurements at a global scale, using high resolution satellite derived DEMs, such as TanDEM-X (Krieger *et al.*, 2007). This relationship is again strongest in Gabilan Mesa, the landscape with the least topographic complexity which demonstrates the least sensitivity to curvature measurements and the estimation of the sediment transport coefficient. However, even in the more noisy landscape of the Oregon Coast Range, meaningful hillslope length and relief measurements can still be made through the use of a geometric channel extraction algorithm and lower resolution topographic data.

5.6 Conclusions

Through generation of topographic data spanning the range of grid resolutions currently used in much of geomorphic research, a number of key metrics have been evaluated for their sensitivity to grid resolution. I have demonstrated the reduction in the range of total and tangential curvature values as grid resolution is decreased, across three test landscapes. These curvature measurements are important in the estimation of the hillslope sediment transport coefficient (K), in their use as a proxy for erosion rate, and in the extraction of channel networks from topographic data. I demonstrate that the estimation of K from low resolution topographic data is possible, particularly in landscapes such as Gabilan Mesa where hilltops are broad. Higher resolutions are required to extract meaningful curvature information in steep landscapes with sharp ridges and narrow gullies.

The extraction of channel networks from digital topographic data is a significant challenge at all spatial scales, as the definition of a channel network is integral in the execution of many analyses (e.g., DiBiase *et al.*, 2012; Hurst *et al.*, 2012). I demonstrate that the use of a geometric channel extraction algorithm produces channel networks for all three of the studied landscapes which correspond well to networks extracted from high resolution topography. This correspondence is tested through the computation of quality indexes for each predicted network, which outline the suitability of this algorithm over a process based method at coarse DEM resolutions.

Average values of hillslope length and relief for each landscape are shown to be broadly insensitive to grid resolution up to grid sizes which correspond to the highest resolution topographic data globally available. This indicates that these measurements can be used to identify landscape transience in locations where LiDAR data are unavailable. The accuracy of these measurements is dependent on the accuracy of the channel network used, however, as using a geometric method of channel extraction from the 1 meter DEM still provides robust measurements of hillslope length and relief.

The relationships between decreasing grid resolution and the geomorphic parameters explored here demonstrate the influence of the spatial scale of the topographic expression of process on the quality of results which can be extracted from lower resolution topography. From these analyses it is challenging to identify a clear threshold below which data become unsuitable for use in geomorphic analysis. Rather, it is important to highlight the influence of landscape morphology and the dominant processes acting upon it in the selection of an appropriate data resolution for a study. Using this work as a framework, it is now possible to place constraints on the accuracy of results derived from coarse resolution topographic data, particularly in locations where no high resolution data are available.

Chapter 6

Conclusions

My overarching goal for this thesis was to quantify both sediment flux laws (cf. Dietrich *et al.*, 2003) and landscape dynamics using topographic indicators. In doing so, I developed several novel algorithms for exploring high resolution topographic data that have been specifically designed to test geomorphic hypotheses. These algorithms were deployed across field sites in the United States which spanned a broad range of climate, lithology and tectonic history (Chapter 2). The sites had the advantage of being covered by freely available, high-resolution (>5 points per square metre) LiDAR. In meeting this goal I was able to achieve my aims, set out in Chapter 1, to test measures of hillslope length, quantify sediment flux laws and their associated critical gradients and explore the impacts of grid resolution on topographic analysis, all through the development and application of open source software.

Chapter 3 presented a method of measuring hillslope length by modeling flow over hillslopes that was compared to existing techniques of hillslope length estimation. I demonstrated that the method which models hillslope flow was the most reliable, in addition to its ability to yield measurements at a finer spatial scale than by

using either drainage density measurements or by extracting a length scale from plots of topographic gradient plotted against drainage area. The latter method is widely used in geomorphic research (theory predicts a break in scaling in slope-area space where hillslopes give way to channels) but my work has demonstrated that this method is unreliable at best, and potentially misleading. By calculating the topographic relief of each hillslope alongside its length using my flow routing technique, I was able to falsify an end-member prediction of hilsllope sediment flux (wherein flux is linearly proportional to topographic gradient), and demonstrated that in the four upland soil mantled landscapes tested, the topographic signature was consistent with predictions made by the nonlinear sediment flux model. The critical gradient of the nonlinear sediment flux model, the gradient at which sediment flux asymptotes towards infinity, was also estimated for each landscape, with the resulting figures falling below previously published values.

Following on from this analysis of the calculation of hillslope length, Chapter 4 extended these techniques to use hillslope length, relief and hilltop curvature values for the same landscapes to generate dimensionless relief and erosion rate measurements. Both Roering *et al.* (2007) and Hurst *et al.* (2012) found these metrics to be a robust means with which to test the nonlinear sediment flux law, and Hurst *et al.* (2013b) demonstrated that this technique could be used to distinguish growing landscapes, possibly forced by tectonic activity, from those that are inactive. However, the computation of such measurements has not been widely adopted, possibly due to the computational complexity in applying such calculations across large spatial areas. I have designed and tested software that automates calculation of these metrics, and explored their use across several landscapes. Alongside the publication of the paper associated with Chapter 4, an open source software package has been released to perform these calculations efficiently and in a reproducible manner. This software framework allowed the reproduction of previous studies applying this technique in addition to the

application of this dimensionless analysis to Coweeta, where the results are used to infer topographic decay in the southern Appalachian mountains. The analysis of dimensionless relief and erosion rate data provided an additional falsification of the end-member sediment flux laws, showing support again for the nonlinear model of sediment flux. The critical gradient of this model was also estimated using the dimensionless data, yielding similar results to those presented in Chapter 3.

The final research chapter, Chapter 5, presented analysis of the influence of grid resolution on the use of topographic analysis to make geomorphic observations. Measurements of topographic curvature as resolution is decreased were made showing that in all three landscapes studied the extremes of curvature are lost rapidly beyond 4 meter grid sizes; however the inter-quartile range does not change considerably in each case as grid size is increased. The estimation of the sediment transport coefficient through measurement of hilltop curvature was shown to be possible using lower resolution topographic data, particularly where the hilltops are broad, as is the case in Gabilan Mesa. Channels were extracted at a range of resolutions between 1 and 30 meters using a process based method, which relies on the expected topographic predictions of the channel to hillslope transition based on a process model of landscape evolution, and a geometric method, which uses the geometry of the landscape alone. Using both qualitative and quantitative methods of evaluation, the geometric method was shown to be more robust as grid resolution was degraded. The resolution sensitivity of the hillslope length and relief measurement technique developed in Chapter 3 was also evaluated, demonstrating the ability to accurately constrain these parameters in low resolution data up to 30 meter gird size. This would allow the analyses developed in Chapter 4 to be performed in landscapes where high resolution topography is not available.

From these three research chapters three broad themes of conclusions can be

drawn, considering general developments in topographic analysis, the implications of these results upon theories of hillslope sediment transport and high resolution observations of landscape morphology in landscapes considered qualitatively to be morphologically uniform.

6.1 Topographic Analysis

6.1.1 Channel extraction

For many applications of topographic analysis, the ability to distinguish between hillslope and fluvial domains is crucial, particularly where geometric measurements on hillslopes or channels are being performed. Consequently, the extraction of accurate channel networks from topographic data remains an open area of research and much progress has been made in developing techniques suited to high resolution topography. In Chapter 5 I demonstrate a clear difference in performance between a geometric method of channel extraction, which I developed for this thesis based on the advances of Passalacqua *et al.* (2010) and Pelletier (2013) and DrEICH (Clubb *et al.*, 2014), a process based method. Both methods extract high order channels reasonably well, which is to be expected as the main trunk channels in a landscape will have the largest topographic signature expressed over the largest lengthscale and so are well suited to be captured in low resolution topography. The main difference between the methods comes in the identification of lower order channels: the DrEICH method often fails to identify a topographic signature of a process transition as this is a meter scale feature which is rapidly lost as grid size is increased, whereas the geometric method will identify the upper reaches of the channel network based on curvature alone, meaning that

even as channel head features are lost, the placement of the channel head in lower resolution data will not move downslope as rapidly as with the DrEICH method.

This shows that even though the DrEICH method was shown to outperform several geometric methods on 1 meter resolution data (Clubb *et al.*, 2014), the inverse is true as grid sizes are increased and therefore such evaluations of any new method's resolution sensitivity should be performed routinely, to set the constraints better for the application of a new technique beyond the original study.

6.1.2 Hillslope length and relief

Producing software which can measure hillslope length and relief accurately across a range of topographic data resolutions provides new hillslope metrics which can be applied in a diverse range of contexts. The use of slope area plots to quantify hillslope length and identify a hillslope-fluvial transition has been applied by countless workers across numerous landscapes, and is well supported by theory and qualitative field observations. However, as the analysis presented in Chapter 3 shows, the results of slope area analysis can vary by orders of magnitude across small spatial areas, giving meaningless results in many contexts. Some of these problems can be overcome through careful manual supervision of the analysis process. However this can lead to bias in the results as data are smoothed and modified until the expected trend is observed and perhaps more importantly, precludes the technique from being applied to large datasets due to the levels of manual selection of parameters required. Using drainage density inversion to estimate hillslope length does not capture the variability inherent in landscapes, providing only a single value per drainage basin, which systematically underestimates hillslope length. This method provides useful information at the landscape scale, particularly in modeling studies due to its computational

simplicity, but is not suitable in the analysis of sediment transport or other hillslope scale processes.

I demonstrated that the flow path method also provides improved accuracy and spatial resolution of relief measurements, allowing users to move beyond calculating relief in moving windows, where the topographic signal is dampened and where relief tends to scale with window size. This has the effect of under-sampling the highest relief portions of landscapes, which are important if the full range of geomorphic processes are to be captured in an analysis. The utility of these hillslope length and relief measurements was demonstrated in Chapter 4, where dimensionless relationships between curvature and relief were used to identify signals of landscape transience and such measurements are broadly insensitive to grid resolution. Although this signature of landscape transience is nuanced, its generation requires no a priori information about a landscape and so can be rapidly deployed to new study areas as a technique to direct further analysis and potential field exploration.

6.1.3 Reproducible topographic analysis

Geomorphology has undergone several theoretical and technical revolutions over the past century and as a discipline we are still adjusting to the recent influx of high resolution data and the challenges such data volumes bring. A fundamental tenet of any scientific discipline is reproducibility, and many other fields have experienced so-called reproducibility crises as researchers attempt to validate previous results (Ioannidis *et al.*, 2009; Open Science Collaboration, 2015). Reproducing some past geomorphic research is not possible due to the lack of clear methodologies, the challenges of sharing (particularly topographic) data and the lack of documented and transparent open source analysis software.

A large part of my focus during the work which has gone into this thesis has been on attempting to ensure that every piece of research I perform is transparent and can be easily reproduced. As a direct consequence of this, all of the data and software produced for this thesis is open source and has been made available online, with code for both topographic analysis and data visualization shared on GitHub and the manuscripts for each paper archived on BitBucket. This was not always a straightforward process, with the production of well documented, clean code taking considerably longer to write than rapidly prototyped code which can only be understood by the original author.

From this effort, a number of lessons can be learned:

1. The development of research software tools needs to be acknowledged better with software routinely cited through the more frequent use of DOIs.

2. Journals need stricter software standards to require well documented code and data alongside the submission of manuscripts.

3. The peer review process needs to consider the quality and usability of the code and data provided with research papers.

4. More formal credit needs to be given to software development and data management alongside data collection and analysis.

5. Data, particularly large topographic datasets, need to be easier to cite, track and share, to foster reproduction and collaboration.

By addressing these challenges in the coming years, the field of geomorphology could lead other disciplines and accelerate progress towards new discoveries as less time will be wasted searching for data and re-writing code that was not shared effectively.

6.2 Sediment Transport

6.2.1 Estimation of the sediment transport coefficient

Chapter 5 demonstrates the use of topographic data to estimate the sediment transport coefficient. Hurst *et al.* (2013c) applied this method to identify different coefficients for parts of a landscape underlain by different lithologies, using high resolution topography. I tested this technique on three further landscapes, to understand the influence of grid resolution in the estimation of a sediment transport coefficient. From this analysis it was demonstrated that the key component of this calculation was the morphology of the ridgelines, with broad diffuse ridges such as those found in Gabilan Mesa yielding the most consistent results as grid resolution was decreased. These results potentially allow geomorphic research to be applied to locations where LiDAR data are unavailable or of low quality, provided the morphology of the landscape is suitable.

6.2.2 Sediment flux

Chapters 3 and 4 test the topographic predictions of the linear and nonlinear sediment flux laws to demonstrate that topography in four locations in the USA is consistent with sediment transport which is nonlinearly proportional to hillslope gradient, and cannot be the result of a linear sediment flux law. The two tests applied in these chapters are distinct from previous tests as they can be performed using topographic data alone, meaning that such tests can be applied wherever high resolution data is available. These tests are limited in that they are applying

1-dimensional models of hillslopes to 2-dimensional reality and require simplifying assumptions to be made in order to extract quasi one-dimensional hillslope traces from the data. Some authors have attempted to solve this problem through the use of manually selected hillslope profiles, but this technique is time consuming and challenging to reproduce and so the automated approach described in Chapter 3 is preferred.

These tests are not perfect predictors of nonlinear sediment flux, as many other models with field and theoretical support cannot be tested in this manner as they require other information not available at the scales required, such as soil thicknesses. However, across the broad continuum of sediment flux laws which have been proposed, many have their basis in the nonlinear model (cf. Dietrich *et al.*, 2003; Roering, 2008) and so this work is an important step towards identifying the most suitable sediment flux law to apply when modeling the evolution of, or broad scale sediment transport within, a landscape.

6.2.3 Critical gradients

In the application of the tests of sediment flux laws in Chapters 3 and 4, I show that it is possible to constrain the critical gradient used in the nonlinear sediment flux law for each landscape. The values computed between the two methods show good agreement, suggesting that each method is capturing the same topographic signal, however the values computed are considerably lower than many other previously reported values for the same landscapes. This discrepancy arises from the differing methods used to identify a critical gradient; previous methods identified the critical gradient though the manual identification of threshold hillslopes or through the calibration of the sediment transport coefficient calculated for several basins in a landscape. When considering a landscape as a

whole, as is done in each of the methods outlined in Chapters 3 and 4, a single critical gradient is identified.

Any soil mantled landscape can be subdivided into landscape units; each landscape can be broken into drainage basins of reducing stream orders and each basin is composed of hillslopes, which can be divided into smaller units defined by individual hillslope flow paths. Each of these segments of hillslope can have variable properties (e.g, vegetation, lithology and tectonics) which can vary how this section of hillslope responds to forcing. By performing measurements of hillslope properties at this fine a scale, a distribution of critical gradients across a landscape is sampled and when a model is fit through these measurements, it will pass through the center of the distribution, resulting in a critical gradient falling between the extremes of the dataset. This accounts for the apparent underestimation in the critical gradient values from Chapters 3 and 4 and the previously reported values, and suggests that using a single value for a landscape or a basin within such a landscape may not capture the full variability within a landscape unit. Consequently, more work must be undertaken to better characterize this distribution of critical gradients and better understand how these values relate to previous critical gradients, which could be described as maximum critical gradients in some cases.

6.3 Landscape Variability

Across Chapters 3 and 4 several of the landscapes studied are in some approximation of topographic steady state, with landscapes being described by other authors as regular or uniform (e.g., Perron *et al.*, 2009). Although this can be considered to be the case when looking at a landscape like Gabilan Mesa which has very evenly spaced ridges and valleys (Perron *et al.*, 2008a, 2009), much of

the work presented here demonstrates the local scale variability inherent within small basins in these landscapes. Even where very distinctive lengthscales can be observed through spectral analysis or qualitative observations of valley spacing, the range of hillslope length and relief measurements for individual hillslopes shows considerable variation. The distribution of the E^*R^* measurements for steady state landscapes shown in Chapter 4, when contrasted to the idealized plots produced by Roering *et al.* (2007), further highlights this discrepancy between previous observations of landscape uniformity and the data presented here. This shows that the lengthscale over which landscape properties are considered is of critical importance in determining their uniformity and these conclusions lend support to the idea of dynamic reorganization of basins within equilibrium landscapes which has been observed in modeling studies (Reinhardt and Ellis, 2015).

The morphology of the ground surface has also provided interesting results, with longer hillslope traces occurring on rougher landscapes caused by the deflection of flow paths. This is particularly apparent in the results in Chapter 5, showing the loss of hillslope curvature as grid size is increased. Such hillslope scale roughness has been attributed to the signature of pit and mound topography generated by tree throw (Roering *et al.*, 2010). However, other sources of topographic roughness exist, such as landsliding (McKean and Roering, 2004) and bedrock exposure (Milodowski *et al.*, 2015b) in addition to non-topographic noise present in LiDAR datasets. The challenge of disentangling natural and synthetic noise from such datasets is non-trivial, but must be achieved if the topographic signature of small scale processes is to be quantified at the landscape scale.

6.4 Future Research Directions

The comparison of hillslope length measurement techniques presented in Chapter 3 demonstrated the value of generating hillslope length measurements for individual hillslopes rather than at the basin- or landscape-average scale. However, slope-area plots still have value, particularly in cases where they can be used to identify channel heads (e.g., Montgomery and Foufoula-Georgiou, 1993; Orlandini *et al.*, 2011; Tarolli and Dalla Fontana, 2009) and the inversion of drainage density can be applied in models as a computationally simple proxy for hillslope length (e.g., Clubb *et al.*, 2016). As the tools to measure hillslope length as a series of flow paths have now been developed and tested in a range of settings and at a range of data resolutions (Chapters 3 to 5), these measurements can now be applied to understanding the landscape units that slope-area and drainage density derived hillslope length values represent. For example, the use of a unit contour width to convert a drainage area into a length assumes a rectangular upslope contributing area extending from the channel to the ridgeline and the inversion of drainage density assumes euclidean overland flow paths between ridge and channel. Testing these assumptions using the software developed in Chapter 3 would yield better understanding of the limitations of current theoretical and conceptual models of landscape evolution and could result in new theoretical developments regarding the representation of hillslope hydrology and the transition point between hillslope and fluvial processes, characterized as the channel head (e.g., Montgomery and Dietrich, 1988).

Work to understand the topographic signature of vegetation has yielded many significant advances in recent years, with many processes, such as tree throw, acting to roughen the surface of hillslopes (e.g., Roering *et al.*, 2010). The research presented in Chapters 3 and 4 calculated topographic gradient and curvature by fitting a polynomial surface to a moving window scaled to exceed the length

over which such processes operate, with the aim of excluding these small scale topographic disturbances from hillslope scale measurements. However, such small scale signatures can also be produced by instrument noise, processing errors and misclassification of point cloud data. Consequently, it is important to understand and quantify the sources of small scale noise in LiDAR datasets, to increase confidence in measurements of the signatures of small scale processes.

This can be achieved through the calibration and comparison of point cloud and gridded topographic data collected from airborne and terrestrial platforms. By identifying planar surfaces such as roads or runways in existing datasets, the signature of non-topographic noise can be identified and contrasted with data collected on hillslopes, with the aim of disentangling synthetic and natural sources of roughness in existing point cloud and gridded datasets. This work can be enhanced through the collection of high resolution terrestrial laser scanning data of hillslopes and tree throw mounds. Such data can again be compared to the airborne data to constrain the limits of the accurate measurement of tree throw mounds and other small scale hillslope features.

In testing the linear and nonlinear sediment flux laws in Chapter 3, a depth dependent sediment flux law was also briefly introduced (e.g., Braun *et al.*, 2001; Furbish and Fagherazzi, 2001). Such a law has much theoretical and experimental support (e.g., Heimsath *et al.*, 2005; Roering, 2008) but, as stated in Chapter 3, the topographic predictions of the law cannot be tested at present. Such a flux law does make predictions regarding the $L_H - R$ structure of landscapes in a similar manner to the linear and nonlinear models tested in Chapter 3, but requires the integration of soil thickness information at a spatial scale which is not currently available. If such data could be collected, either through the use of ground penetrating radar (e.g., Roering *et al.*, 2010) or through a large field campaign manually sampling soil thicknesses, the software developed in Chapter 3 could be easily modified to test differing depth dependent sediment flux laws. Such

work could provide considerable insight into the dynamics of sediment transport on soil mantled hillslopes.

The steady state landscapes studied in Chapter 4 demonstrated considerable variability in E^*R^* values, regardless of the level of spatial averaging performed. Theory predicts that true steady state landscapes should show little variability in such values (Roering *et al.*, 2007) and although a suite of tests have been performed to show that these landscapes are in approximate steady state (e.g., Roering *et al.*, 1999, 2007; Perron *et al.*, 2008a), large scale variability in E^*R^* values was demonstrated in Chapter 4. This suggests that although the broad scale morphology of the landscape is in topographic steady state, there is much variability in landscape form at the hillslope scale, a result demonstrated using numerical models by Reinhardt and Ellis (2015). By analyzing the spatial distribution of E^*R^* values and the associated critical gradient derived from these relationships, patterns of vegetation, aspect, lithology, soil type and thickness can be identified. These relationships could yield new understanding of the geomorphic processes which drive small scale variations in landscape morphology in landscapes traditionally described as being in steady state.

References

Abrahams, A.D. and Ponczynski, J.J. (1984). Drainage density in relation to precipitation intensity in the U.S.A. *Journal of Hydrology*, **75**, 383–388.

Ahnert, F. (1970). A comparison of theoretical slope models with slopes in the field. *Zeitschrift für Geomorphologie*, **9**, 88–101.

Ahnert, F. (1987). Approaches to dynamic equilibrium in theoretical simulations of slope development. *Earth Surface Processes and Landforms*, **12**, 3–15.

Anders, A.M., Roe, G.H., Montgomery, D.R. and Hallet, B. (2008). Influence of precipitation phase on the form of mountain ranges. *Geology*, **36**, 479–482.

Anderson, E.S., Thompson, J.A., Crouse, D.A. and Austin, R.E. (2006). Horizontal resolution and data density effects on remotely sensed LIDAR-based DEM. *Geoderma*, **132**, 406–415.

Anderson, R.S. (1994). Evolution of the Santa Cruz Mountains, California, through tectonic growth and geomorphic decay. *Journal of Geophysical Research: Solid Earth*, **99**, 20161–20179.

Anderson, R.S. (2002). Modeling the tor-dotted crests, bedrock edges, and parabolic profiles of high alpine surfaces of the Wind River Range, Wyoming. *Geomorphology*, **46**, 35–58.

Anderson, S.P., Blanckenburg, F.v. and White, A.F. (2007). Physical and Chemical Controls on the Critical Zone. *Elements*, **3**, 315–319.

Andrews, D.J. and Bucknam, R.C. (1987). Fitting degradation of shoreline scarps by a nonlinear diffusion model. *Journal of Geophysical Research: Solid Earth*, **92**, 12857–12867.

Armstrong, A.C. (1980). Simulated slope development sequences in a three-dimensional context. *Earth Surface Processes*, **5**, 265–270.

Arrowsmith, J.R. and Zielke, O. (2009). Tectonic geomorphology of the San Andreas Fault zone from high resolution topography: An example from the Cholame segment. *Geomorphology*, **113**, 70–81.

Arrowsmith, J.R., Pollard, D.D. and Rhodes, D.D. (1996). Hillslope development in areas of active tectonics. *Journal of Geophysical Research: Solid Earth*, **101**, 6255–6275.

Baldwin, E.M. (1956). Geologic map of the lower Siuslaw River area, Oregon. *United States Geological Survey*, **Oil and Gas Invest. Map OM-186**.

Baldwin, J.A., Whipple, K.X. and Tucker, G.E. (2003). Implications of the shear stress river incision model for the timescale of postorogenic decay of topography. *Journal of Geophysical Research: Solid Earth*, **108(B3)**, 2158.

Band, L.E. (1986). Topographic Partition of Watersheds with Digital Elevation Models. *Water Resources Research*, **22**, 15–24.

Benda, L. and Dunne, T. (1997). Stochastic forcing of sediment supply to channel networks from landsliding and debris flow. *Water Resources Research*, **33**, 2849–2863.

Bertram, S. (1969). The UNAMACE and the automatic photomapper. *Photogrammetric Engineering*, **35**, 569–576.

Beschta, R.L. (1978). Long-term patterns of sediment production following road construction and logging in the Oregon Coast Range. *Water Resources Research*, **14**, 1011–1016.

Bierman, P. and Steig, E.J. (1996). Estimating Rates of Denudation Using Cosmogenic Isotope Abundances in Sediment. *Earth Surface Processes and Landforms*, **21**, 125–139.

Bierman, P., Clapp, E., Nichols, K., Gillespie, A. and Caffee, M.W. (2001). Using Cosmogenic Nuclide Measurements In Sediments To Understand Background Rates Of Erosion And Sediment Transport. In R.S. Harmon and W.W.D. III, eds., *Landscape Erosion and Evolution Modeling*, 89–115, Springer US.

Binnie, S.A., Phillips, W.M., Summerfield, M.A. and Fifield, L.K. (2007). Tectonic uplift, threshold hillslopes, and denudation rates in a developing mountain range. *Geology*, **35**, 743–746.

Binnie, S.A., Phillips, W.M., Summerfield, M.A., Fifield, L.K. and Spotila, J.A. (2010). Tectonic and climatic controls of denudation rates in active orogens: The San Bernardino Mountains, California. *Geomorphology*, **118**, 249–261.

Bisson, M., Behncke, B., Fornaciai, A. and Neri, M. (2009). LiDAR-based digital terrain analysis of an area exposed to the risk of lava flow invasion: the Zafferana Etnea territory, Mt. Etna (Italy). *Natural Hazards*, **50**, 321–334.

Bollschweiler, M., Stoffel, M., Ehmisch, M. and Monbaron, M. (2007). Reconstructing spatio-temporal patterns of debris-flow activity using dendrogeomorphological methods. *Geomorphology*, **87**, 337–351.

Booth, A.M., Roering, J.J. and Perron, J.T. (2009). Automated landslide mapping using spectral analysis and high-resolution topographic data: Puget Sound lowlands, Washington, and Portland Hills, Oregon. *Geomorphology*, **109**, 132–147.

Booth, A.M., Roering, J.J. and Rempel, A.W. (2013). Topographic signatures and a general transport law for deep-seated landslides in a landscape evolution model. *Journal of Geophysical Research: Earth Surface*, **118**, 603–624.

Braun, J. and Willett, S.D. (2013). A very efficient O(n), implicit and parallel method to solve the stream power equation governing fluvial incision and landscape evolution. *Geomorphology*, **180-181**, 170–179.

Braun, J., Heimsath, A.M. and Chappell, J. (2001). Sediment transport mechanisms on soil-mantled hillslopes. *Geology*, **29**, 683–686.

Brockelbank, D.C. and Tam, A.P. (1991). Stereo elevation determination techniques for SPOT imagery. *Photogrammetric Engineering and Remote Sensing*, **57**, 1065–1073.

Brodu, N. and Lague, D. (2012). 3d terrestrial lidar data classification of complex natural scenes using a multi-scale dimensionality criterion: Applications in geomorphology. *ISPRS Journal of Photogrammetry and Remote Sensing*, **68**, 121–134.

Broscoe, A.J. (1959). *Quantitative analysis of longitudinal stream profiles of small watersheds*. Report 18, Office of Naval Research, Project NR 389-042, Columbia University Department of Geology.

Brown, E.T., Stallard, R.F., Larsen, M.C., Raisbeck, G.M. and Yiou, F. (1995). Denudation rates determined from the accumulation of in situ-produced 10be in the luquillo experimental forest, Puerto Rico. *Earth and Planetary Science Letters*, **129**, 193–202.

Burbank, D.W., Leland, J., Fielding, E., Anderson, R.S., Brozovic, N., Reid, M.R. and Duncan, C. (1996). Bedrock incision, rock uplift and threshold hillslopes in the northwestern Himalayas. *Nature*, **379**, 505–510.

Burke, B.C., Heimsath, A.M. and White, A.F. (2007). Coupling chemical weathering with soil production across soil-mantled landscapes. *Earth Surface Processes and Landforms*, **32**, 853–873.

Canny, J. (1986). A computational approach to edge-detection. *IEEE Transactions on Pattern Analysis and Machine Intelligence*, **8**, 679–698.

Carranza, E.J.M. and Castro, O.T. (2006). Predicting Lahar-Inundation Zones: Case Study in West Mount Pinatubo, Philippines. *Natural Hazards*, **37**, 331–372.

Carson, M.A. and Kirkby, M.J. (1972). *Hillslope Form and Process*, vol. 475. Cambridge University Press, Cambridge.

Carter, W., Shrestha, R., Tuell, G., Bloomquist, D. and Sartori, M. (2001). Airborne laser swath mapping shines new light on Earth's topography. *Eos, Transactions of the American Geophysical Union*, **82**, 549–555.

Casas, A., Benito, G., Thorndycraft, V. and Rico, M. (2006). The topographic data source of digital terrain models as a key element in the accuracy of hydraulic flood modelling. *Earth Surface Processes and Landforms*, **31**, 444–456.

Cavalli, M., Tarolli, P., Marchi, L. and Dalla Fontana, G. (2008). The effectiveness of airborne LiDAR data in the recognition of channel-bed morphology. *Catena*, **73**, 249–260.

Champagnac, J.D., Molnar, P., Sue, C. and Herman, F. (2012). Tectonics, climate, and mountain topography. *Journal of Geophysical Research: Solid Earth*, **117**, B02403.

Chandler, J. (1999). Effective application of automated digital photogrammetry for geomorphological research. *Earth Surface Processes and Landforms*, **24**, 51–63.

Chorley, R.J. (1957). Climate and morphometry. *The Journal of Geology*, **65**, 628–638.

Chorley, R.J. and Morgan, M.A. (1962). Comparison of Morphometric Features, Unaka Mountains, Tennessee and North Carolina, and Dartmoor, England. *Geological Society of America Bulletin*, **73**, 17–34.

Claessens, L., Heuvelink, G.B.M., Schoorl, J.M. and Veldkamp, A. (2005). DEM resolution effects on shallow landslide hazard and soil redistribution modelling. *Earth Surface Processes and Landforms*, **30**, 461–477.

Clark, G.M. (1987). Debris slide and debris flow historical events in the Appalachians south of the glacial border. *Reviews in Engineering Geology*, **7**, 125–138.

Clarke, A.L., Gruen, A. and Loon, J.C. (1982). The application of contour data for generating high fidelity grid digital elevation models. In *Proceedings Auto-Carto 5*, 213–22.

Clarke, B.A. and Burbank, D.W. (2010). Bedrock fracturing, threshold hillslopes, and limits to the magnitude of bedrock landslides. *Earth and Planetary Science Letters*, **297**, 577–586.

Clarke, B.A. and Burbank, D.W. (2011). Quantifying bedrock-fracture patterns within the shallow subsurface: Implications for rock mass strength, bedrock landslides, and erodibility. *Journal of Geophysical Research: Earth Surface*, **116**, F04009.

Clubb, F.J., Mudd, S.M., Milodowski, D.T., Hurst, M.D. and Slater, L.J. (2014). Objective extraction of channel heads from high-resolution topographic data. *Water Resources Research*, **50**, 4283–4304.

Clubb, F.J., Mudd, S.M., Attal, M., Milodowski, D.T. and Grieve, S.W. (2016). The relationship between drainage density, erosion rate, and hilltop curvature: implications for sediment transport processes. *Journal of Geophysical Research: Earth Surface*, 2015JF003747.

Codilean, A.T. (2006). Calculation of the cosmogenic nuclide production topographic shielding scaling factor for large areas using DEMs. *Earth Surface Processes and Landforms*, **31**, 785–794.

Cohen, S., Willgoose, G. and Hancock, G. (2009). The mARM spatially distributed soil evolution model: A computationally efficient modeling framework and analysis of hillslope soil surface organization. *Journal of Geophysical Research: Earth Surface*, **114**, F03001.

Cohen, S., Willgoose, G. and Hancock, G. (2010). The mARM3d spatially distributed soil evolution model: Three-dimensional model framework and analysis of hillslope and landform responses. *Journal of Geophysical Research: Earth Surface*, **115**, F04013.

Costa-Cabral, M.C. and Burges, S.J. (1994). Digital Elevation Model Networks (DEMON): A model of flow over hillslopes for computation of contributing and dispersal areas. *Water Resources Research*, **30**, 1681–1692.

Culling, W.E.H. (1960). Analytical Theory of Erosion. *The Journal of Geology*, **68**, 336–344.

Cyr, A.J., Granger, D.E., Olivetti, V. and Molin, P. (2010). Quantifying rock uplift rates using channel steepness and cosmogenic nuclide-determined erosion rates: Examples from northern and southern Italy. *Lithosphere*, **2**, 188–198.

Dadson, S.J., Hovius, N., Chen, H., Dade, W.B., Lin, J.C., Hsu, M.L., Lin, C.W., Horng, M.J., Chen, T.C., Milliman, J. and Stark, C.P. (2004). Earthquake-triggered increase in sediment delivery from an active mountain belt. *Geology*, **32**, 733–736.

Davis, W.M. (1892). The convex profile of bad-land divides. *Science*, **20**, 245–245.

Day, H.W. and Bickford, M.E. (2004). Tectonic setting of the Jurassic Smartville and Slate Creek complexes, northern Sierra Nevada, California. *Geological Society of America Bulletin*, **116**, 1515–1528.

De Rose, R.C. and Basher, L.R. (2011). Measurement of river bank and cliff erosion from sequential LIDAR and historical aerial photography. *Geomorphology*, **126**, 132–147.

Deardorff, N.D. and Cashman, K.V. (2012). Emplacement conditions of the c. 1,600-year bp Collier Cone lava flow, Oregon: a LiDAR investigation. *Bulletin of Volcanology*, **74**, 2051–2066.

Densmore, A.L., Ellis, M.A. and Anderson, R.S. (1998). Landsliding and the evolution of normal-fault-bounded mountains. *Journal of Geophysical Research: Solid Earth*, **103**, 15203–15219.

Devrani, R., Singh, V., Mudd, S.M. and Sinclair, H.D. (2015). Prediction of flash flood hazard impact from Himalayan river profiles. *Geophysical Research Letters*, **42**, 2015GL063784.

DiBiase, R.A., Whipple, K.X., Heimsath, A.M. and Ouimet, W.B. (2010). Landscape form and millennial erosion rates in the San Gabriel Mountains, CA. *Earth and Planetary Science Letters*, **289**, 134–144.

DiBiase, R.A., Heimsath, A.M. and Whipple, K.X. (2012). Hillslope response to tectonic forcing in threshold landscapes. *Earth Surface Processes and Landforms*, **37**, 855–865.

Dietrich, W.E. and Dunne, T. (1978). Sediment budget for a small catchment in mountainous terrain. *Zeitschrift für Geomorphologie, Supplementbände*, **29**, 191–206.

Dietrich, W.E. and Dunne, T. (1993). The channel head. In K. Beven and M.J. Kirkby, eds., *Channel Network Hydrology*, 175–219, John Wiley, New York.

Dietrich, W.E. and Perron, J.T. (2006). The search for a topographic signature of life. *Nature*, **439**, 411–418.

Dietrich, W.E., Wilson, C.J., Montgomery, D.R., McKean, J. and Bauer, R. (1992). Erosion thresholds and land surface morphology. *Geology*, **20**, 675–679.

Dietrich, W.E., Wilson, C.J., Montgomery, D.R. and McKean, J. (1993). Analysis of Erosion Thresholds, Channel Networks, and Landscape Morphology Using a Digital Terrain Model. *The Journal of Geology*, **101**, 259–278.

Dietrich, W.E., Bellugi, D.G., Sklar, L.S., Stock, J.D., Heimsath, A.M. and Roering, J.J. (2003). Geomorphic Transport Laws for Predicting Landscape form and Dynamics. In P.R. Wilcock and R.M. Iverson, eds., *Prediction in Geomorphology*, 103–132, American Geophysical Union, Washington, D.C.

Dillencourt, M.B., Samet, H. and Tamminen, M. (1992). A General Approach to Connected-component Labeling for Arbitrary Image Representations. *Journal of the ACM*, **39**, 253–280.

Dixon, J.L., Heimsath, A.M., Kaste, J. and Amundson, R. (2009). Climate-driven processes of hillslope weathering. *Geology*, **37**, 975–978.

Dohrenwend, J.C. (1978). Systematic valley asymmetry in the central California Coast Ranges. *Geological Society of America Bulletin*, **89**, 891–900.

Dohrenwend, J.C. (1979). Morphologic Analysis of Gabilan Mesa by Iterative Contour-Generalization: An Improved Method of Geomorphic Cartographic Analysis. *SEPM Pacific Coast Paleogeography Field Guide #4, Menlo Park, California*, 83–87.

Dunne, T., Zhang, W. and Aubry, B.F. (1991). Effects of Rainfall, Vegetation, and Microtopography on Infiltration and Runoff. *Water Resources Research*, **27**, 2271–2285.

Dunne, T., Malmon, D.V. and Mudd, S.M. (2010). A rain splash transport equation assimilating field and laboratory measurements. *Journal of Geophysical Research: Earth Surface*, **115**, F01001.

Dunne, T., Malmon, D.V. and Dunne, K.B.J. (2016). Limits on the morphogenetic role of rain splash transport in hillslope evolution. *Journal of Geophysical Research: Earth Surface*, **121**, 2015JF003737.

Durham, D.L. (1974). Geology of the southern Salinas Valley area, California. *U.S. Geological Survey Professional Paper*, **819**, 1–111.

Elliott, K.J. and Swank, W.T. (2008). Long-term changes in forest composition and diversity following early logging (1919-1923) and the decline of American chestnut (Castanea dentata). *Plant Ecology*, **197**, 155–172.

Erskine, R.H., Green, T.R., Ramirez, J.A. and MacDonald, L.H. (2007). Digital Elevation Accuracy and Grid Cell Size: Effects on Estimated Terrain Attributes. *Soil Science Society of America Journal*, **71**, 1371–1380.

Evans, I.S. (1980). An integrated system of terrain analysis and slope mapping. *Zeitschrift für Geomorphologie, Supplementbände*, **36**, 274–295.

Evans, J. and Hudak, A. (2007). A Multiscale Curvature Algorithm for Classifying Discrete Return LiDAR in Forested Environments. *IEEE Transactions on Geoscience and Remote Sensing*, **45**, 1029–1038.

Faill, R.T. (1998). A geologic history of the north-central Appalachians; Part 3, The Alleghany Orogeny. *American Journal of Science*, **298**, 131–179.

Favalli, M., Fornaciai, A. and Pareschi, M.T. (2009). LIDAR strip adjustment: Application to volcanic areas. *Geomorphology*, **111**, 123–135.

Fernandes, N.F. and Dietrich, W.E. (1997). Hillslope evolution by diffusive processes: The timescale for equilibrium adjustments. *Water Resources Research*, **33**, 1307–1318.

Fisher, G.B., Bookhagen, B. and Amos, C.B. (2013). Channel planform geometry and slopes from freely available high-spatial resolution imagery and DEM fusion: Implications for channel width scalings, erosion proxies, and fluvial signatures in tectonically active landscapes. *Geomorphology*, **194**, 46–56.

Fleming, M.D. and Hoffer, R.M. (1979). Machine processing of Landsat MSS data and LARS Technical Report 062879. *Laboratory for applications of remote sensing, Purdue University, West Lafayette, IN, USA*.

Flint, J.J. (1974). Stream gradient as a function of order, magnitude, and discharge. *Water Resources Research*, **10**, 969–973.

Foufoula-Georgiou, E., Ganti, V. and Dietrich, W.E. (2010). A nonlocal theory of sediment transport on hillslopes. *Journal of Geophysical Research: Earth Surface*, **115**, F00A16.

Francioni, M., Salvini, R., Stead, D., Giovannini, R., Riccucci, S., Vanneschi, C. and Gull'i, D. (2015). An integrated remote sensing-GIS approach for the analysis of an open pit in the Carrara marble district, Italy: Slope stability assessment through kinematic and numerical methods. *Computers and Geotechnics*, **67**, 46–63.

Freeman, T.G. (1991). Calculating catchment area with divergent flow based on a regular grid. *Computers & Geosciences*, **17**, 413–422.

Furbish, D.J. (2003). Using the dynamically coupled behavior of land-surface geometry and soil thickness in developing and testing hillslope evolution models. In P.R. Wilcock and R.M. Iverson, eds., *Prediction in Geomorphology*, 169–181, American Geophysical Union.

Furbish, D.J. and Fagherazzi, S. (2001). Stability of creeping soil and implications for hillslope evolution. *Water Resources Research*, **37**, 2607–2618.

Furbish, D.J. and Roering, J.J. (2013). Sediment disentrainment and the concept of local versus nonlocal transport on hillslopes. *Journal of Geophysical Research: Earth Surface*, **118**, 937–952.

Furbish, D.J., Hamner, K.K., Schmeeckle, M., Borosund, M.N. and Mudd, S.M. (2007). Rain splash of dry sand revealed by high-speed imaging and sticky paper splash targets. *Journal of Geophysical Research: Earth Surface*, **112**, F01001.

Furbish, D.J., Haff, P.K., Dietrich, W.E. and Heimsath, A.M. (2009). Statistical description of slope-dependent soil transport and the diffusion-like coefficient. *Journal of Geophysical Research: Earth Surface*, **114**, F00A05.

Gabet, E.J. (2000). Gopher bioturbation: field evidence for non-linear hillslope diffusion. *Earth Surface Processes and Landforms*, **25**, 1419–1428.

Gabet, E.J. and Mudd, S.M. (2010). Bedrock erosion by root fracture and tree throw: A coupled biogeomorphic model to explore the humped soil production function and the persistence of hillslope soils. *Journal of Geophysical Research: Earth Surface*, **115**, F04005.

Gabet, E.J., Pratt-Sitaula, B.A. and Burbank, D.W. (2004). Climatic controls on hillslope angle and relief in the Himalayas. *Geology*, **32**, 629–632.

Gabet, E.J., Perron, J.T. and Johnson, D.L. (2014). Biotic origin for Mima mounds supported by numerical modeling. *Geomorphology*, **206**, 58–66.

Gabet, E.J., Mudd, S.M., Milodowski, D.T., Yoo, K., Hurst, M.D. and Dosseto, A. (2015). Local topography and erosion rate control regolith thickness along a ridgeline in the Sierra Nevada, California. *Earth Surface Processes and Landforms*, 1779–1790.

Gabriels, D. (1999). The effect of slope length on the amount and size distribution of eroded silt loam soils: short slope laboratory experiments on interrill erosion. *Geomorphology*, **28**, 169–172.

Galehouse, J.S. (1967). Provenance and Paleocurrents of the Paso Robles Formation, California. *Geological Society of America Bulletin*, **78**, 951–978.

Gallen, S.F., Wegmann, K.W., Frankel, K.L., Hughes, S., Lewis, R.Q., Lyons, N., Paris, P., Ross, K., Bauer, J.B. and Witt, A.C. (2011). Hillslope response to knickpoint migration in the Southern Appalachians: implications for the evolution of post-orogenic landscapes. *Earth Surface Processes and Landforms*, **36**, 1254–1267.

Gallen, S.F., Wegmann, K.W. and Bohnenstieh, D.R. (2013). Miocene rejuvenation of topographic relief in the southern Appalachians. *GSA Today*, **23**, 4–10.

Gao, J. (1997). Resolution and accuracy of terrain representation by grid DEMs at a micro-scale. *International Journal of Geographical Information Science*, **11**, 199–212.

Gilbert, G.K. (1877). *Report on the Geology of the Henry Mountains*. US Government Printing Office.

Gilbert, G.K. (1896). The origin of hypotheses, illustrated by the discussion of a topographic problem. *Science*, **3**, 1–13.

Gilbert, G.K. (1909). The convexity of hilltops. *The Journal of Geology*, **17**, 344–350.

Giles, P.T. and Franklin, S.E. (1996). Comparison of derivative topographic surfaces of a DEM generated from stereoscopic SPOT images with field measurements. *Photogrammetric Engineering and Remote Sensing*, **62**, 1165–1171.

Gosse, J.C. and Phillips, F.M. (2001). Terrestrial in situ cosmogenic nuclides: theory and application. *Quaternary Science Reviews*, **20**, 1475–1560.

Granger, D.E., Kirchner, J.W. and Finkel, R. (1996). Spatially averaged long-term erosion rates measured from in situ-produced cosmogenic nuclides in alluvial sediment. *Journal of Geology*, **104**, 249–257.

Gregory, K.J. and Walling, D.E. (1968). The Variation of Drainage Density Within a Catchment. *International Association of Scientific Hydrology Bulletin*, **13**, 61–68.

Guth, P.L. (1999). Contour line "ghosts" in USGS level 2 DEMs. *Photogrammetric Engineering and Remote Sensing*, **65**, 289–296.

Guzzetti, F., Ardizzone, F., Cardinali, M., Rossi, M. and Valigi, D. (2009). Landslide volumes and landslide mobilization rates in Umbria, central Italy. *Earth and Planetary Science Letters*, **279**, 222–229.

Hack, J.T. and Goodlett, J.C. (1960). *Geomorphology and Forest Ecology of a Mountain Region in the Central Appalachians*. US Government Printing Office Washington, DC.

Hales, T.C. and Roering, J.J. (2007). Climatic controls on frost cracking and implications for the evolution of bedrock landscapes. *Journal of Geophysical Research: Earth Surface*, **112**, F02033.

Hales, T.C., Ford, C.R., Hwang, T., Vose, J.M. and Band, L.E. (2009). Topographic and ecologic controls on root reinforcement. *Journal of Geophysical Research: Earth Surface*, **114**, F03013.

Hales, T.C., Scharer, K.M. and Wooten, R.M. (2012). Southern Appalachian hillslope erosion rates measured by soil and detrital radiocarbon in hollows. *Geomorphology*, **138**, 121–129.

Hampel, F.R., Ronchetti, E.M., Rousseeuw, P.J. and Stahel, W.A. (2011). *Robust Statistics: The Approach Based on Influence Functions*. John Wiley & Sons.

Han, S., Kim, S., Hoon Jung, J., Kim, C., Yu, K. and Heo, J. (2012). Development of a hashing-based data structure for the fast retrieval of 3d terrestrial laser scanned data. *Computers & Geosciences*, **39**, 1–10.

Hancock, G.R. and Evans, K.G. (2006). Channel head location and characteristics using digital elevation models. *Earth Surface Processes and Landforms*, **31**, 809–824.

Hancock, G.R., J.B.C., L. and Coulthard, T.J. (2015). Catchment reconstruction - erosional stability at millennial time scales using landscape evolution models. *Geomorphology*, **231**, 15–27.

Haugerud, R.A., Harding, D.J., Johnson, S.Y., Harless, J.L., Weaver, C.S. and Sherrod, B.L. (2003). High-resolution lidar topography of the Puget Lowland, Washington. *GSA Today*, **13**, 4–10.

He, L., Chao, Y. and Suzuki, K. (2008). A Run-Based Two-Scan Labeling Algorithm. *IEEE Transactions on Image Processing*, **17**, 749–756.

He, L.F., Chao, Y.Y. and Suzuki, K. (2013). An Algorithm for Connected-Component Labeling, Hole Labeling and Euler Number Computing. *Journal of Computer Science and Technology*, **28**, 468–478.

Heimsath, A.M., Chappell, J., Dietrich, W.E., Nishiizumi, K. and Finkel, R.C. (2000). Soil production on a retreating escarpment in southeastern Australia. *Geology*, **28**, 787–790.

Heimsath, A.M., Dietrich, W.E., Nishiizumi, K. and Finkel, R.C. (2001). Stochastic processes of soil production and transport: erosion rates, topographic variation and cosmogenic nuclides in the Oregon Coast Range. *Earth Surface Processes and Landforms*, **26**, 531–552.

Heimsath, A.M., Furbish, D.J. and Dietrich, W.E. (2005). The illusion of diffusion: Field evidence for depth-dependent sediment transport. *Geology*, **33**, 949–952.

Heritage, G. and Hetherington, D. (2007). Towards a protocol for laser scanning in fluvial geomorphology. *Earth Surface Processes and Landforms*, **32**, 66–74.

Herman, F. and Braun, J. (2006). A parametric study of soil transport mechanisms. *Geological Society of America Special Papers*, **398**, 191–200.

Hicks, L.E. (1892). Some elements of land sculpture. *Geological Society of America Bulletin*, **4**, 133–146.

Hicks, L.E. (1893). The convex profile of bad-land divides. *Science*, **21**, 232–3.

Hillel, D. (1980). *Fundamentals of Soil Physics*. Academic Press, San Diego.

Hilley, G.E. and Arrowsmith, J.R. (2008). Geomorphic response to uplift along the Dragon's Back pressure ridge, Carrizo Plain, California. *Geology*, **36**, 367–370.

Hobley, D.E.J., Howard, A.D. and Moore, J.M. (2014). Fresh shallow valleys in the Martian midlatitudes as features formed by meltwater flow beneath ice. *Journal of Geophysical Research-Planets*, **119**, 128–153.

Hodge, R., Brasington, J. and Richards, K. (2009). In situ characterization of grain-scale fluvial morphology using Terrestrial Laser Scanning. *Earth Surface Processes and Landforms*, **34**, 954–968.

Hodgson, M.E., Jensen, J.R., Schmidt, L., Schill, S. and Davis, B. (2003). An evaluation of LIDAR- and IFSAR-derived digital elevation models in leaf-on conditions with USGS Level 1 and Level 2 DEMs. *Remote Sensing of Environment*, **84**, 295–308.

Hooke, R.L. (2000). On the history of humans as geomorphic agents. *Geology*, **28**, 843–846.

Horn, B.K.P. (1981). Hill shading and the reflectance map. *Proceedings of the IEEE*, **69**, 14–47.

Horton, R.E. (1932). Drainage-basin characteristics. *Transactions, American Geophysical Union*, **13**, 350.

Horton, R.E. (1945). Erosional Development of Streams and Their Drainage Basins; Hydrophysical Approach to Quantitative Morphology. *Geological Society of America Bulletin*, **56**, 275–370.

Hovius, N. (1996). Regular spacing of drainage outlets from linear mountain belts. *Basin Research*, **8**, 29–44.

Hovius, N., Stark, C.P. and Allen, P.A. (1997). Sediment flux from a mountain belt derived by landslide mapping. *Geology*, **25**, 231–234.

Howard, A.D. (1994). A detachment-limited model of drainage basin evolution. *Water Resources Research*, **30**, 2261–2285.

Howard, A.D. (1997). Badland morphology and evolution: Interpretation using a simulation model. *Earth Surface Processes and Landforms*, **22**, 211–227.

Hughes, T.A., Shope, A.R. and Baxter, F.S. (1971). USGS automatic orthophoto system. *Photogrammetric Engineering*, **37**, 1055–1062.

Hursh, C.R. (1941). The geomorphic aspects of mudflows as a type of accelerated erosion in the Southern Appalachian. *American Geophysics Union Reports and Papers, General Assembly*, 253–254.

Hurst, M.D., Mudd, S.M., Walcott, R., Attal, M. and Yoo, K. (2012). Using hilltop curvature to derive the spatial distribution of erosion rates. *Journal of Geophysical Research: Earth Surface*, **117**, F02017.

Hurst, M.D., Ellis, M.A., Royse, K.R., Lee, K.A. and Freeborough, K. (2013a). Controls on the magnitude-frequency scaling of an inventory of secular landslides. *Earth Surface Dynamics*, **1**, 67–78.

Hurst, M.D., Mudd, S.M., Attal, M. and Hilley, G. (2013b). Hillslopes Record the Growth and Decay of Landscapes. *Science*, **341**, 868–871.

Hurst, M.D., Mudd, S.M., Yoo, K., Attal, M. and Walcott, R. (2013c). Influence of lithology on hillslope morphology and response to tectonic forcing in the northern Sierra Nevada of California. *Journal of Geophysical Research: Earth Surface*, **118**, 832–851.

Hutchinson, M.F. (1989). A new procedure for gridding elevation and stream line data with automatic removal of spurious pits. *Journal of Hydrology*, **106**, 211–232.

Hutchinson, M.F. and Dowling, T.I. (1991). A continental hydrological assessment of a new grid-based digital elevation model of Australia. *Hydrological Processes*, **5**, 45–58.

Ioannidis, J.P.A., Allison, D.B., Ball, C.A., Coulibaly, I., Cui, X., Culhane, A.C., Falchi, M., Furlanello, C., Game, L., Jurman, G., Mangion, J., Mehta, T., Nitzberg, M., Page, G.P., Petretto, E. and van Noort, V. (2009). Repeatability of published microarray gene expression analyses. *Nature Genetics*, **41**, 149–155.

Istanbulluoglu, E., Tarboton, D.G., Pack, R.T. and Luce, C. (2002). A probabilistic approach for channel initiation. *Water Resources Research*, **38**, 1325–1339.

Jackson, M. and Roering, J.J. (2009). Post-fire geomorphic response in steep, forested landscapes: Oregon Coast Range, USA. *Quaternary Science Reviews*, **28**, 1131–1146.

James, L.A., Watson, D.G. and Hansen, W.F. (2007). Using LiDAR data to map gullies and headwater streams under forest canopy: South Carolina, USA. *Catena*, **71**, 132–144.

Javernick, L., Brasington, J. and Caruso, B. (2014). Modeling the topography of shallow braided rivers using Structure-from-Motion photogrammetry. *Geomorphology*, **213**, 166–182.

Jefferson, A.J. and McGee, R.W. (2013). Channel network extent in the context of historical land use, flow generation processes, and landscape evolution in the North Carolina Piedmont. *Earth Surface Processes and Landforms*, **38**, 601–613.

Jenkins, G. and Watts, D. (1968). *Spectral Analysis and its Applications*. Holden-Day, San Francisco.

Jenson, S.K. (1991). Applications of hydrologic information automatically extracted from digital elevation models. *Hydrological Processes*, **5**, 31–44.

Jenson, S.K. and Domingue, J.O. (1988). Extracting topographic structure from digital elevation data for geographic information system analysis. *Photogrammetric Engineering and Remote Sensing*, **54**, 1593–1600.

Jones, A.F., Brewer, P.A., Johnstone, E. and Macklin, M.G. (2007). High-resolution interpretative geomorphological mapping of river valley environments using airborne LiDAR data. *Earth Surface Processes and Landforms*, **32**, 1574–1592.

Jones, E., Oliphant, T. and Peterson, P. (2001). *SciPy: Open source scientific tools for Python*. [Online; accessed 2015-08-03].

Julian, J.P., Elmore, A.J. and Guinn, S.M. (2012). Channel head locations in forested watersheds across the mid-Atlantic United States: A physiographic analysis. *Geomorphology*, **177-178**, 194–203.

Kelsey, H.M., Ticknor, R.L., Bockheim, J.G. and Mitchell, E. (1996). Quaternary upper plate deformation in coastal Oregon. *Geological Society of America Bulletin*, **108**, 843–860.

Kenward, T., Lettenmaier, D.P., Wood, E.F. and Fielding, E. (2000). Effects of digital elevation model accuracy on hydrologic predictions. *Remote Sensing of Environment*, **74**, 432–444.

Kim, H., Arrowsmith, J., Crosby, C.J., Jaeger-Frank, E., Nandigam, V., Memon, A., Conner, J., Baden, S.B. and Baru, C. (2006). An efficient implementation of a local binning algorithm for digital elevation model generation of LiDAR/ALSM dataset. In *AGU Fall Meeting Abstracts*, vol. 1, 0921, San Francisco.

Kinnell, P.I.A. (2009). The influence of raindrop induced saltation on particle size distributions in sediment discharged by rain-impacted flow on planar surfaces. *Catena*, **78**, 2–11.

Kirby, E. and Ouimet, W. (2011). Tectonic geomorphology along the eastern margin of Tibet: insights into the pattern and processes of active deformation adjacent to the Sichuan Basin. *Geological Society, London, Special Publications*, **353**, 165–188.

Kirby, E., Whipple, K.X., Tang, W. and Chen, Z. (2003). Distribution of active rock uplift along the eastern margin of the Tibetan Plateau: Inferences from bedrock channel longitudinal profiles. *Journal of Geophysical Research: Solid Earth*, **108(B4)**, 2217.

Kirby, E., Johnson, C., Furlong, K. and Heimsath, A. (2007). Transient channel incision along Bolinas Ridge, California: Evidence for differential rock uplift adjacent to the San Andreas fault. *Journal of Geophysical Research: Earth Surface*, **112**, F03S07.

Kirkby, M.J. (1980). The stream head as a significant geomorphic threshold. In D.R. Coates and J.D. Vitek, eds., *Thresholds in Geomorphology*, 53–73, Allen and Unwin, Winchester, Massachusetts.

Klar, A., Aharonov, E., Kalderon-Asael, B. and Katz, O. (2011). Analytical and observational relations between landslide volume and surface area. *Journal of Geophysical Research: Earth Surface*, **116**, F02001.

Koons, P.O. (1989). The topographic evolution of collisional mountain belts; a numerical look at the Southern Alps, New Zealand. *American Journal of Science*, **289**, 1041–1069.

Korup, O. (2008). Rock type leaves topographic signature in landslide-dominated mountain ranges. *Geophysical Research Letters*, **35**, L11402.

Krieger, G., Moreira, A., Fiedler, H., Hajnsek, I., Werner, M., Younis, M. and Zink, M. (2007). TanDEM-X: A Satellite Formation for High-Resolution SAR Interferometry. *IEEE Transactions on Geoscience and Remote Sensing*, **45**, 3317–3341.

Krishnan, S., Crosby, C., Nandigam, V., Phan, M., Cowart, C., Baru, C. and Arrowsmith, R. (2011). OpenTopography: A services oriented architecture for community access to LIDAR topography. In *Proceedings of the 2nd International Conference on Computing for Geospatial Research & Applications*, COM.Geo '11, 7:1–7:8, ACM, New York, NY, USA.

Lague, D. (2014). The stream power river incision model: evidence, theory and beyond. *Earth Surface Processes and Landforms*, **39**, 38–61.

Lague, D., Brodu, N. and Leroux, J. (2013). Accurate 3d comparison of complex topography with terrestrial laser scanner: Application to the Rangitikei canyon (N-Z). *ISPRS Journal of Photogrammetry and Remote Sensing*, **82**, 10–26.

Lane, S.N., James, T.D. and Crowell, M.D. (2000). Application of digital photogrammetry to complex topography for geomorphological research. *The Photogrammetric Record*, **16**, 793–821.

Larsen, I.J., Montgomery, D.R. and Greenberg, H.M. (2014). The contribution of mountains to global denudation. *Geology*, **42**, 527–530.

Lashermes, B., Foufoula-Georgiou, E. and Dietrich, W.E. (2007). Channel network extraction from high resolution topography using wavelets. *Geophysical Research Letters*, **34**, L23S04.

Lavé, J. and Avouac, J.P. (2001). Fluvial incision and tectonic uplift across the Himalayas of central Nepal. *Journal of Geophysical Research*, **106**, 26–561.

Lea, N.L. (1992). An aspect driven kinematic routing algorithm. In A.J. Parsons and A.D. Abrahams, eds., *Overland flow: hydraulics and erosion mechanics*, 393–407, University College London Press, London.

Legleiter, C.J. (2012). Remote measurement of river morphology via fusion of LiDAR topography and spectrally based bathymetry. *Earth Surface Processes and Landforms*, **37**, 499–518.

Leopold, L. and Maddock Jr., T. (1953). The hydraulic geometry of stream channels and some physiographic implications. USGS Numbered Series, Professional Paper No. 252.

Leopold, L. and Miller, J. (1956). Ephemeral streams; hydraulic factors and their relation to the drainage net. USGS Numbered Series, Professional Paper No. 282-A.

Lin, C.W., Tseng, C.M., Tseng, Y.H., Fei, L.Y., Hsieh, Y.C. and Tarolli, P. (2013). Recognition of large scale deep-seated landslides in forest areas of Taiwan using high resolution topography. *Journal of Asian Earth Sciences*, **62**, 389–400.

Lindsay, J.B. and Creed, I.F. (2005). Removal of artifact depressions from digital elevation models: towards a minimum impact approach. *Hydrological Processes*, **19**, 3113–3126.

Liu, B., Nearing, M., Shi, P. and Jia, Z. (2000). Slope Length Effects on Soil Loss for Steep Slopes. *Soil Science Society of America Journal*, **64**, 1759–1763.

Liu, X. (2008). Airborne LiDAR for DEM generation: some critical issues. *Progress in Physical Geography*, **32**, 31–49.

Liu, Z., Peng, M. and Di, K. (2014). A continuative variable resolution digital elevation model for ground-based photogrammetry. *Computers & Geosciences*, **62**, 71–79.

Lorenz, R.D., Lopes, R.M., Paganelli, F., Lunine, J.I., Kirk, R.L., Mitchell, K.L., Soderblom, L.A., Stofan, E.R., Ori, G., Myers, M., Miyamoto, H., Radebaugh, J., Stiles, B., Wall, S.D. and Wood, C.A. (2008). Fluvial channels on Titan: Initial Cassini RADAR observations. *Planetary and Space Science*, **56**, 1132–1144.

Löscher, W. (1967). Some aspects of orthophoto technology. *The Photogrammetric Record*, **5**, 419–432.

Lumia, R., Shapiro, L. and Zuniga, O. (1983). A new connected components algorithm for virtual memory computers. *Computer Vision, Graphics, and Image Processing*, **22**, 287–300.

Mangold, N. and Ansan, V. (2006). Detailed study of an hydrological system of valleys, a delta and lakes in the Southwest Thaumasia region, Mars. *Icarus*, **180**, 75–87.

Mankoff, K.D. and Russo, T.A. (2013). The Kinect: a low-cost, high-resolution, short-range 3d camera. *Earth Surface Processes and Landforms*, **38**, 926–936.

Mark, D.M. (1984). Automated Detection Of Drainage Networks From Digital Elevation Models. *Cartographica: The International Journal for Geographic Information and Geovisualization*, **21**, 168–178.

Marr, D. and Hildreth, E. (1980). Theory of Edge-Detection. *Proceedings of the Royal Society Series B-Biological Sciences*, **207**, 187–217.

Marshall, J.A. and Roering, J.J. (2014). Diagenetic variation in the Oregon Coast Range: Implications for rock strength, soil production, hillslope form, and landscape evolution. *Journal of Geophysical Research: Earth Surface*, **119**, 2013JF003004.

Martz, L.W. and Garbrecht, J. (1998). The treatment of flat areas and depressions in automated drainage analysis of raster digital elevation models. *Hydrological Processes*, **12**, 843–855.

Mathier, L., Roy, A.G. and Paré, J.P. (1989). The effect of slope gradient and length on the parameters of a sediment transport equation for sheetwash. *Catena*, **16**, 545–558.

Matmon, A., Bierman, P.R., Larsen, J., Southworth, S., Pavich, M. and Caffee, M. (2003). Temporally and spatially uniform rates of erosion in the southern Appalachian Great Smoky Mountains. *Geology*, **31**, 155–158.

McKean, J. and Roering, J. (2004). Objective landslide detection and surface morphology mapping using high-resolution airborne laser altimetry. *Geomorphology*, **57**, 331–351.

McKean, J., Nagel, D., Tonina, D., Bailey, P., Wright, C.W., Bohn, C. and Nayegandhi, A. (2009). Remote Sensing of Channels and Riparian Zones with a Narrow-Beam Aquatic-Terrestrial LIDAR. *Remote Sensing*, **1**, 1065–1096.

McKean, J.A., Dietrich, W.E., Finkel, R.C., Southon, J.R. and Caffee, M.W. (1993). Quantification of soil production and downslope creep rates from cosmogenic 10be accumulations on a hillslope profile. *Geology*, **21**, 343–346.

McKean, J.A., Isaak, D.J. and Wright, C.W. (2008). Geomorphic controls on salmon nesting patterns described by a new, narrow-beam terrestrial-aquatic lidar. *Frontiers in Ecology and the Environment*, **6**, 125–130.

Meng, X., Wang, L., Silván-Cárdenas, J.L. and Currit, N. (2009). A multi-directional ground filtering algorithm for airborne LIDAR. *ISPRS Journal of Photogrammetry and Remote Sensing*, **64**, 117–124.

Meng, X., Currit, N. and Zhao, K. (2010). Ground Filtering Algorithms for Airborne LiDAR Data: A Review of Critical Issues. *Remote Sensing*, **2**, 833–860.

Micheletti, N., Chandler, J.H. and Lane, S.N. (2015). Investigating the geomorphological potential of freely available and accessible structure-from-motion photogrammetry using a smartphone. *Earth Surface Processes and Landforms*, **40**, 473–486.

Milledge, D.G., Lane, S.N. and Warburton, J. (2009). The potential of digital filtering of generic topographic data for geomorphological research. *Earth Surface Processes and Landforms*, **34**, 63–74.

Milodowski, D.T., Mudd, S.M. and Mitchard, E.T. (2015a). Erosion rates as a potential bottom-up control of forest structural characteristics in the Sierra Nevada Mountains. *Ecology*, **96**, 31–38.

Milodowski, D.T., Mudd, S.M. and Mitchard, E.T.A. (2015b). Topographic roughness as a signature of the emergence of bedrock in eroding landscapes. *Earth Surface Dynamics*, **3**, 483–499.

Mitas, L. and Mitasova, H. (1999). Spatial interpolation. In P. Longley, M. Goodchild, D. Maguire and D. Rhind, eds., *Geographical Information Systems: Principles, Techniques, Management and Applications*, 481–492, Wiley.

Mitasova, H. and Hofierka, J. (1993). Interpolation by regularized spline with tension: II. Application to terrain modeling and surface geometry analysis. *Mathematical Geology*, **25**, 657–669.

Mitasova, H. and Mitas, L. (1993). Interpolation by regularized spline with tension: I. Theory and implementation. *Mathematical Geology*, **25**, 641–655.

Mitasova, H., Hofierka, J., Zlocha, M. and Iverson, L.R. (1996). Modelling topographic potential for erosion and deposition using GIS. *International journal of geographical information systems*, **10**, 629–641.

Moglen, G.E., Eltahir, E.A.B. and Bras, R.L. (1998). On the sensitivity of drainage density to climate change. *Water Resources Research*, **34**, 855–862.

Montgomery, D.R. (2001). Slope Distributions, Threshold Hillslopes, and Steady-state Topography. *American Journal of Science*, **301**, 432–454.

Montgomery, D.R. and Brandon, M.T. (2002). Topographic controls on erosion rates in tectonically active mountain ranges. *Earth and Planetary Science Letters*, **201**, 481–489.

Montgomery, D.R. and Dietrich, W.E. (1988). Where do channels begin? *Nature*, **336**, 232–234.

Montgomery, D.R. and Dietrich, W.E. (1989). Source areas, drainage density, and channel initiation. *Water Resources Research*, **25**, 1907–1918.

Montgomery, D.R. and Dietrich, W.E. (1992). Channel initiation and the problem of landscape scale. *Science*, **255**, 826–830.

Montgomery, D.R. and Dietrich, W.E. (1994). A physically based model for the topographic control on shallow landsliding. *Water Resources Research*, **30**, 1153–1171.

Montgomery, D.R. and Foufoula-Georgiou, E. (1993). Channel network source representation using digital elevation models. *Water Resources Research*, **29**, 3925–3934.

Montgomery, D.R., Sullivan, K. and Greenberg, H.M. (1998). Regional test of a model for shallow landsliding. *Hydrological Processes*, **12**, 943–955.

Montgomery, D.R., Schmidt, K.M., Greenberg, H.M. and Dietrich, W.E. (2000). Forest clearing and regional landsliding. *Geology*, **28**, 311–314.

Moore, I. and Grayson, R. (1991). Terrain-Based Catchment Partitioning and Runoff Prediction Using Vector Elevation Data. *Water Resources Research*, **27**, 1177–1191.

Moore, I.D., O'Loughlin, E.M. and Burch, G.J. (1988). A contour-based topographic model for hydrological and ecological applications. *Earth Surface Processes and Landforms*, **13**, 305–320.

Moore, I.D., Grayson, R.B. and Ladson, A.R. (1991). Digital terrain modelling: A review of hydrological, geomorphological, and biological applications. *Hydrological Processes*, **5**, 3–30.

Morris, D.G. and Heerdegen, R.G. (1988). Automatically derived catchment boundaries and channel networks and their hydrological applications. *Geomorphology*, **1**, 131–141.

Mudd, S.M. (2016). Detection of transience in eroding landscapes. *Earth Surface Processes and Landforms*.

Mudd, S.M. and Furbish, D.J. (2004). Influence of chemical denudation on hillslope morphology. *Journal of Geophysical Research: Earth Surface*, **109**, F02001.

Mudd, S.M. and Furbish, D.J. (2005). Lateral migration of hillcrests in response to channel incision in soil-mantled landscapes. *Journal of Geophysical Research: Earth Surface*, **110**, F04026.

Mudd, S.M. and Furbish, D.J. (2007). Responses of soil-mantled hillslopes to transient channel incision rates. *Journal of Geophysical Research: Earth Surface*, **112**, F03S18.

Mudd, S.M., Attal, M., Milodowski, D.T., Grieve, S.W.D. and Valters, D.A. (2014). A statistical framework to quantify spatial variation in channel gradients using the integral method of channel profile analysis. *Journal of Geophysical Research: Earth Surface*, **119**, 2013JF002981.

Mudd, S.M., Harel, M.A., Hurst, M.D., Grieve, S.W.D. and Marrero, S.M. (2016). The CAIRN method: Automated, reproducible calculation of catchment-averaged denudation rates from cosmogenic radionuclide concentrations. *Earth Surface Dynamics Discussions*.

Muhs, D.R., Simmons, K.R., Schumann, R.R., Groves, L.T., DeVogel, S.B., Minor, S.A. and Laurel, D. (2014). Coastal tectonics on the eastern margin of the Pacific Rim: late Quaternary sea-level history and uplift rates, Channel Islands National Park, California, USA. *Quaternary Science Reviews*, **105**, 209–238.

Murphy, P.N.C., Ogilvie, J., Meng, F.R. and Arp, P. (2008). Stream network modelling using lidar and photogrammetric digital elevation models: a comparison and field verification. *Hydrological Processes*, **22**, 1747–1754.

Nearing, M.A. (1997). A single, continuous function for slope steepness influence on soil loss. *Soil Science Society of America Journal*, **61**, 917–919.

Notebaert, B., Verstraeten, G., Govers, G. and Poesen, J. (2009). Qualitative and quantitative applications of LiDAR imagery in fluvial geomorphology. *Earth Surface Processes and Landforms*, **34**, 217–231.

O'Callaghan, J.F. and Mark, D.M. (1984). The extraction of drainage networks from digital elevation data. *Computer Vision, Graphics, and Image Processing*, **28**, 323–344.

Oguchi, T. (1997). Drainage density and relative relief in humid steep mountains with frequent slope failure. *Earth Surface Processes and Landforms*, **22**, 107–120.

O'Loughlin, E.M. (1986). Prediction of Surface Saturation Zones in Natural Catchments by Topographic Analysis. *Water Resources Research*, **22**, 794–804.

Open Science Collaboration (2015). Estimating the reproducibility of psychological science. *Science*, **349**, aac4716.

Orlandini, S., Tarolli, P., Moretti, G. and Dalla Fontana, G. (2011). On the prediction of channel heads in a complex alpine terrain using gridded elevation data. *Water Resources Research*, **47**, W02538.

Ouimet, W.B., Whipple, K.X. and Granger, D.E. (2009). Beyond threshold hillslopes: Channel adjustment to base-level fall in tectonically active mountain ranges. *Geology*, **37**, 579–582.

Oyarzun, R., Doblas, M., López-Ruiz, J. and Cebrá, J.M. (1997). Opening of the central Atlantic and asymmetric mantle upwelling phenomena: Implications for long-lived magmatism in western North Africa and Europe. *Geology*, **25**, 727–730.

Palamara, D.R., Nicholson, M., Flentje, P., Baafi, E. and Brassington, G.M. (2007). An evaluation of airborne laser scan data for coalmine subsidence mapping. *International Journal of Remote Sensing*, **28**, 3181–3203.

Passalacqua, P., Do Trung, T., Foufoula-Georgiou, E., Sapiro, G. and Dietrich, W.E. (2010). A geometric framework for channel network extraction from lidar: Nonlinear diffusion and geodesic paths. *Journal of Geophysical Research: Earth Surface*, **115**, F01002.

Passalacqua, P., Belmont, P. and Foufoula-Georgiou, E. (2012). Automatic geomorphic feature extraction from lidar in flat and engineered landscapes. *Water Resources Research*, **48**, W03528.

Passalacqua, P., Belmont, P., Staley, D.M., Simley, J.D., Arrowsmith, J.R., Bode, C.A., Crosby, C., DeLong, S.B., Glenn, N.F., Kelly, S.A., Lague, D., Sangireddy, H., Schaffrath, K., Tarboton, D.G., Wasklewicz, T. and Wheaton, J.M. (2015). Analyzing high resolution topography for advancing the understanding of mass and energy transfer through landscapes: A review. *Earth-Science Reviews*, **148**, 174–193.

Pelletier, J.D. (2010). Minimizing the grid-resolution dependence of flow-routing algorithms for geomorphic applications. *Geomorphology*, **122**, 91–98.

Pelletier, J.D. (2013). A robust, two-parameter method for the extraction of drainage networks from high-resolution digital elevation models (DEMs): Evaluation using synthetic and real-world DEMs. *Water Resources Research*, **49**, 75–89.

Pelletier, J.D. and Cline, M.L. (2007). Nonlinear slope-dependent sediment transport in cinder cone evolution. *Geology*, **35**, 1067–1070.

Pelletier, J.D., McGuire, L.A., Ash, J.L., Engelder, T.M., Hill, L.E., Leroy, K.W., Orem, C.A., Rosenthal, W.S., Trees, M.A., Rasmussen, C. and Chorover, J. (2011). Calibration and testing of upland hillslope evolution models in a dated landscape: Banco Bonito, New Mexico. *Journal of Geophysical Research: Earth Surface*, **116**, F04004.

Perona, P. and Malik, J. (1990). Scale-space and edge detection using anisotropic diffusion. *IEEE Transactions on Pattern Analysis and Machine Intelligence*, **12**, 629–639.

Perron, J.T. and Royden, L. (2013). An integral approach to bedrock river profile analysis. *Earth Surface Processes and Landforms*, **38**, 570–576.

Perron, J.T., Dietrich, W.E. and Kirchner, J.W. (2008a). Controls on the spacing of first-order valleys. *Journal of Geophysical Research: Earth Surface*, **113**, F04016.

Perron, J.T., Kirchner, J.W. and Dietrich, W.E. (2008b). Spectral signatures of characteristic spatial scales and nonfractal structure in landscapes. *Journal of Geophysical Research: Earth Surface*, **113**, F04003.

Perron, J.T., Kirchner, J.W. and Dietrich, W.E. (2009). Formation of evenly spaced ridges and valleys. *Nature*, **460**, 502–505.

Perroy, R.L., Bookhagen, B., Asner, G.P. and Chadwick, O.A. (2010). Comparison of gully erosion estimates using airborne and ground-based LiDAR on Santa Cruz Island, California. *Geomorphology*, **118**, 288–300.

Perroy, R.L., Bookhagen, B., Chadwick, O.A. and Howarth, J.T. (2012). Holocene and Anthropocene Landscape Change: Arroyo Formation on Santa Cruz Island, California. *Annals of the Association of American Geographers*, **102**, 1229–1250.

Peucker, T.K. and Douglas, D.H. (1975). Detection of Surface-Specific Points by Local Parallel Processing of Discrete Terrain Elevation Data. *Computer Graphics and Image Processing*, **4**, 375–387.

Peucker, T.K., Fowler, R.J., Little, J.J. and Mark, D.M. (1978). The triangulated irregular network. In *American Society for Photogrammetry Proceedings Digital Terrain Models Symposium*, vol. 516, 532.

Pinet, P. and Souriau, M. (1988). Continental erosion and large-scale relief. *Tectonics*, **7**, 563–582.

Pinter, N. and Vestal, W.D. (2005). El Niño-driven landsliding and postgrazing vegetative recovery, Santa Cruz Island, California. *Journal of Geophysical Research: Earth Surface*, **110**, F02003.

Pinter, N., Lueddecke, S.B., Keller, E.A. and Simmons, K.R. (1998). Late Quaternary slip on the Santa Cruz Island fault, California. *Geological Society of America Bulletin*, **110**, 711–722.

Pinter, N., Sorlien, C.C. and Scott, A.T. (2003). Fault-related fold growth and isostatic subsidence, California Channel Islands. *American Journal of Science*, **303**, 300–318.

Poggio, L. and Soille, P. (2012). Influence of pit removal methods on river network position. *Hydrological Processes*, **26**, 1984–1990.

Price, J.R., Velbel, M.A. and Patino, L.C. (2005). Allanite and epidote weathering at the Coweeta Hydrologic Laboratory, western North Carolina, U.S.A. *American Mineralogist*, **90**, 101–114.

Qin, C.Z. and Zhan, L. (2012). Parallelizing flow-accumulation calculations on graphics processing units-From iterative DEM preprocessing algorithm to recursive multiple-flow-direction algorithm. *Computers & Geosciences*, **43**, 7–16.

Quinn, P., Beven, K., Chevallier, P. and Planchon, O. (1991). The prediction of hillslope flow paths for distributed hydrological modelling using digital terrain models. *Hydrological Processes*, **5**, 59–79.

Rabus, B., Eineder, M., Roth, A. and Bamler, R. (2003). The shuttle radar topography mission-a new class of digital elevation models acquired by spaceborne radar. *ISPRS Journal of Photogrammetry and Remote Sensing*, **57**, 241–262.

Rehak, K., Bookhagen, B., Strecker, M.R. and Echtler, H.P. (2010). The topographic imprint of a transient climate episode: the western Andean flank between 15.5 degrees and 41.5 degrees S. *Earth Surface Processes and Landforms*, **35**, 1516–1534.

Reinhardt, L. and Ellis, M.A. (2015). The emergence of topographic steady state in a perpetually dynamic self-organized critical landscape. *Water Resources Research*, **51**, 4986–5003.

Reneau, S.L. and Dietrich, W.E. (1991). Erosion rates in the southern oregon coast range: Evidence for an equilibrium between hillslope erosion and sediment yield. *Earth Surface Processes and Landforms*, **16**, 307–322.

Reneau, S.L., Dietrich, W.E., Rubin, M., Donahue, D.J. and Jull, A.J.T. (1989). Analysis of hillslope erosion rates using dated colluvial deposits. *The Journal of Geology*, **97**, 45–63.

Riebe, C.S., Kirchner, J.W., Granger, D.E. and Finkel, R.C. (2000). Erosional equilibrium and disequilibrium in the Sierra Nevada, inferred from cosmogenic 26al and 10be in alluvial sediment. *Geology*, **28**, 803–806.

Riebe, C.S., Kirchner, J.W. and Finkel, R.C. (2003). Long-term rates of chemical weathering and physical erosion from cosmogenic nuclides and geochemical mass balance. *Geochimica et Cosmochimica Acta*, **67**, 4411–4427.

Riebe, C.S., Kirchner, J.W. and Finkel, R.C. (2004). Erosional and climatic effects on long-term chemical weathering rates in granitic landscapes spanning diverse climate regimes. *Earth and Planetary Science Letters*, **224**, 547–562.

Rinaldo, A., Dietrich, W.E., Rigon, R., Vogel, G.K. and Rodrlguez-lturbe, I. (1995). Geomorphological signatures of varying climate. *Nature*, **374**, 632–635.

Roering, J.J. (2008). How well can hillslope evolution models "explain" topography? Simulating soil transport and production with high-resolution topographic data. *Geological Society of America Bulletin*, **120**, 1248–1262.

Roering, J.J. and Gerber, M. (2005). Fire and the evolution of steep, soil-mantled landscapes. *Geology*, **33**, 349–352.

Roering, J.J., Kirchner, J.W. and Dietrich, W.E. (1999). Evidence for nonlinear, diffusive sediment transport on hillslopes and implications for landscape morphology. *Water Resources Research*, **35**, 853–870.

Roering, J.J., Kirchner, J.W. and Dietrich, W.E. (2001). Hillslope evolution by nonlinear, slope-dependent transport: Steady state morphology and equilibrium adjustment timescales. *Journal of Geophysical Research: Solid Earth*, **106**, 16499–16513.

Roering, J.J., Perron, J.T. and Kirchner, J.W. (2007). Functional relationships between denudation and hillslope form and relief. *Earth and Planetary Science Letters*, **264**, 245–258.

Roering, J.J., Marshall, J., Booth, A.M., Mort, M. and Jin, Q. (2010). Evidence for biotic controls on topography and soil production. *Earth and Planetary Science Letters*, **298**, 183–190.

Roering, J.J., Mackey, B.H., Marshall, J.A., Sweeney, K.E., Deligne, N.I., Booth, A.M., Handwerger, A.L. and Cerovski-Darriau, C. (2013). "You are HERE": Connecting the dots with airborne lidar for geomorphic fieldwork. *Geomorphology*, **200**, 172–183.

Rosenbloom, N.A. and Anderson, R.S. (1994). Hillslope and channel evolution in a marine terraced landscape, Santa Cruz, California. *Journal of Geophysical Research: Solid Earth*, **99**, 14013–14029.

Rosenfeld, A. and Pfaltz, J.L. (1966). Sequential operations in digital picture processing. *Journal of the ACM*, **13**, 471–494.

Rosser, N.J., Petley, D.N., Lim, M., Dunning, S.A. and Allison, R.J. (2005). Terrestrial laser scanning for monitoring the process of hard rock coastal cliff erosion. *Quarterly Journal of Engineering Geology and Hydrogeology*, **38**, 363–375.

Royden, L.H., Clark, M.K. and Whipple, K.X. (2000). Evolution of river elevation profiles by bedrock incision: Analytical solutions for transient river profiles related to changing uplift and precipitation rates. *Eos, Transactions of the American Geophysical Union*, **81**, 48.

Saha, A.K., Gupta, R.P. and Arora, M.K. (2002). GIS-based Landslide Hazard Zonation in the Bhagirathi (Ganga) Valley, Himalayas. *International Journal of Remote Sensing*, **23**, 357–369.

Salvini, R., Vanneschi, C., Riccucci, S., Francioni, M. and Gullí, D. (2015). Application of an integrated geotechnical and topographic monitoring system in the Lorano marble quarry (Apuan Alps, Italy). *Geomorphology*, **241**, 209–223.

Samet, H. (1981). Connected Component Labeling Using Quadtrees. *Journal of the ACM*, **28**, 487–501.

Samet, H. (1984). The Quadtree and Related Hierarchical Data Structures. *ACM Computing Surveys*, **16**, 187–260.

Schmidt, J., Evans, I.S. and Brinkmann, J. (2003). Comparison of polynomial models for land surface curvature calculation. *International Journal of Geographical Information Science*, **17**, 797–814.

Schmidt, K.M., Roering, J.J., Stock, J.D., Dietrich, W.E., Montgomery, D.R. and Schaub, T. (2001). The variability of root cohesion as an influence on shallow landslide susceptibility in the Oregon Coast Range. *Canadian Geotechnical Journal*, **38**, 995–1024.

Schoorl, J.M., Sonneveld, M.P.W. and Veldkamp, A. (2000). Three-dimensional landscape process modelling: The effect of DEM resolution. *Earth Surface Processes and Landforms*, **25**, 1025–1034.

Schumm, S.A. (1956). Evolution of Drainage Systems and Slopes in Badlands at Perth Amboy, New Jersey. *Geological Society of America Bulletin*, **67**, 597–646.

Schürch, P., Densmore, A.L., Rosser, N.J., Lim, M. and McArdell, B.W. (2011). Detection of surface change in complex topography using terrestrial laser scanning: application to the Illgraben debris-flow channel. *Earth Surface Processes and Landforms*, **36**, 1847–1859.

Schwanghart, W. and Scherler, D. (2014). Short Communication: TopoToolbox 2 - MATLAB-based software for topographic analysis and modeling in Earth surface sciences. *Earth Surface Dynamics*, **2**, 1–7.

Shakesby, R.A. and Doerr, S.H. (2006). Wildfire as a hydrological and geomorphological agent. *Earth-Science Reviews*, **74**, 269–307.

Shaw, J.A., Seldomridge, N.L., Dunkle, D.L., Nugent, P.W., Spangler, L.H., Bromenshenk, J.J., Henderson, C.B., Churnside, J.H. and Wilson, J.J. (2005). Polarization lidar measurements of honey bees in flight for locating land mines. *Optics Express*, **13**, 5853–5863.

Shelef, E. and Hilley, G.E. (2013). Impact of flow routing on catchment area calculations, slope estimates, and numerical simulations of landscape development. *Journal of Geophysical Research: Earth Surface*, **118**, 2105–2123.

Sherba, J., Blesius, L. and Davis, J. (2014). Object-Based Classification of Abandoned Logging Roads under Heavy Canopy Using LiDAR. *Remote Sensing*, **6**, 4043–4060.

Shreve, F. (1927). The vegetation of a coastal mountain range. *Ecology*, **8**, 27–44.

Shreve, R.L. (1966). Statistical law of stream numbers. *The Journal of Geology*, **74**, 17–37.

Shreve, R.L. (1967). Infinite topologically random channel networks. *The Journal of Geology*, **75**, 178–186.

Skidmore, A.K. (1989). A comparison of techniques for calculating gradient and aspect from a gridded digital elevation model. *International Journal of Geographical Information Systems*, **3**, 323–334.

Slatton, K.C., Carter, W.E., Shrestha, R.L. and Dietrich, W. (2007). Airborne Laser Swath Mapping: Achieving the resolution and accuracy required for geosurficial research. *Geophysical Research Letters*, **34**, L23S10.

Small, E.E., Anderson, R.S. and Hancock, G.S. (1999). Estimates of the rate of regolith production using 10be and 26al from an alpine hillslope. *Geomorphology*, **27**, 131–150.

Smart, G., Aberle, J., Duncan, M. and Walsh, J. (2004). Measurement and analysis of alluvial bed roughness. *Journal of Hydraulic Research*, **42**, 227–237.

Snavely Jr, P.D., Wagner, H.C. and MacLeod, N.S. (1964). Rhythmic-bedded eugeosynclinal deposits of the Tyee formation, Oregon Coast Range. *Kansas Geological Survey Bulletin*, **169**, 461–480.

Snyder, N.P., Whipple, K.X., Tucker, G.E. and Merritts, D.J. (2000). Landscape response to tectonic forcing: Digital elevation model analysis of stream profiles in the Mendocino triple junction region, northern California. *Geological Society of America Bulletin*, **112**, 1250–1263.

Sofia, G., Tarolli, P., Cazorzi, F. and Dalla Fontana, G. (2011). An objective approach for feature extraction: distribution analysis and statistical descriptors for scale choice and channel network identification. *Hydrology and Earth System Sciences*, **15**, 1387–1402.

Sofia, G., Pirotti, F. and Tarolli, P. (2013). Variations in multiscale curvature distribution and signatures of LiDAR DTM errors. *Earth Surface Processes and Landforms*, **38**, 1116–1134.

Sofia, G., Marinello, F. and Tarolli, P. (2014). A new landscape metric for the identification of terraced sites: The Slope Local Length of Auto-Correlation (SLLAC). *ISPRS Journal of Photogrammetry and Remote Sensing*, **96**, 123–133.

Sofia, G., Tarolli, P., Cazorzi, F. and Dalla Fontana, G. (2015). Downstream hydraulic geometry relationships: Gathering reference reach-scale width values from LiDAR. *Geomorphology*, **250**, 236–248.

Sofia, G., Marinello, F. and Tarolli, P. (2016). Metrics for quantifying anthropogenic impacts on geomorphology: road networks. *Earth Surface Processes and Landforms*, **41**, 240–255.

Soille, P. (2004a). Morphological carving. *Pattern Recognition Letters*, **25**, 543–550.

Soille, P. (2004b). Optimal removal of spurious pits in grid digital elevation models. *Water Resources Research*, **40**, W12509.

Soille, P., Vogt, J. and Colombo, R. (2003). Carving and adaptive drainage enforcement of grid digital elevation models. *Water Resources Research*, **39**, 1366–1379.

Soille, P.J. and Ansoult, M.M. (1990). Automated Basin Delineation from Digital Elevation Models Using Mathematical Morphology. *Signal Processing*, **20**, 171–182.

Sørensen, R. and Seibert, J. (2007). Effects of DEM resolution on the calculation of topographical indices: TWI and its components. *Journal of Hydrology*, **347**, 79–89.

Stock, G.M., Anderson, R.S. and Finkel, R.C. (2004). Pace of landscape evolution in the Sierra Nevada, California, revealed by cosmogenic dating of cave sediments. *Geology*, **32**, 193–196.

Stock, J. and Dietrich, W.E. (2003). Valley incision by debris flows: Evidence of a topographic signature. *Water Resources Research*, **39**, 1089–1123.

Stoffel, M. and Bollschweiler, M. (2008). Tree-ring analysis in natural hazards research - an overview. *Natural Hazards & Earth System Sciences*, **8**, 187–202.

Strahler, A.N. (1952). Hypsometric (area-Altitude) Analysis of Erosional Topography. *Geological Society of America Bulletin*, **63**, 1117–1142.

Strahler, A.N. (1957). Quantitative analysis of watershed geomorphology. *Eos, Transactions of the American Geophysical Union*, **38**, 913–920.

Suzuki, K., Horiba, I. and Sugie, N. (2003). Linear-time connected-component labeling based on sequential local operations. *Computer Vision and Image Understanding*, **89**, 1–23.

Sweeney, K.E., Roering, J.J. and Ellis, C. (2015). Experimental evidence for hillslope control of landscape scale. *Science*, **349**, 51–53.

Swift Jr., L.W., Cunningham, G.B. and Douglass, J.E. (1988). Climatology and Hydrology. In W.T. Swank and D.A.C. Jr, eds., *Forest Hydrology and Ecology at Coweeta*, no. 66 in Ecological Studies, 35–55, Springer New York.

Talling, P.J., Stewart, M.D., Stark, C.P., Gupta, S. and Vincent, S.J. (1997). Regular spacing of drainage outlets from linear fault blocks. *Basin Research*, **9**, 275–302.

Tarboton, D.G. (1997). A new method for the determination of flow directions and upslope areas in grid digital elevation models. *Water Resources Research*, **33**, 309–319.

Tarboton, D.G., Bras, R.L. and Rodriguez-Iturbe, I. (1991). On the extraction of channel networks from digital elevation data. *Hydrological Processes*, **5**, 81–100.

Tarolli, P. (2014). High-resolution topography for understanding Earth surface processes: Opportunities and challenges. *Geomorphology*, **216**, 295–312.

Tarolli, P. and Dalla Fontana, G. (2009). Hillslope-to-valley transition morphology: New opportunities from high resolution DTMs. *Geomorphology*, **113**, 47–56.

Tarolli, P. and Sofia, G. (2016). Human topographic signatures and derived geomorphic processes across landscapes. *Geomorphology*, **255**, 140–161.

Tarolli, P., Sofia, G. and Fontana, G.D. (2010). Geomorphic features extraction from high-resolution topography: landslide crowns and bank erosion. *Natural Hazards*, **61**, 65–83.

Tarolli, P., Calligaro, S., Cazorzi, F. and Dalla Fontana, G. (2013). Recognition of surface flow processes influenced by roads and trails in mountain areas using high-resolution topography. *European Journal of Remote Sensing*, **46**, 176–197.

Tarolli, P., Preti, F. and Romano, N. (2014). Terraced landscapes: From an old best practice to a potential hazard for soil degradation due to land abandonment. *Anthropocene*, **6**, 10–25.

Tarolli, P., Sofia, G., Calligaro, S., Prosdocimi, M., Preti, F. and Dalla Fontana, G. (2015). Vineyards in Terraced Landscapes: New Opportunities from Lidar Data. *Land Degradation & Development*, **26**, 92–102.

Tesfa, T.K., Tarboton, D.G., Watson, D.W., Schreuders, K.A.T., Baker, M.E. and Wallace, R.M. (2011). Extraction of hydrological proximity measures from DEMs using parallel processing. *Environmental Modelling & Software*, **26**, 1696–1709.

Thoma, D.P., Gupta, S.C., Bauer, M.E. and Kirchoff, C.E. (2005). Airborne laser scanning for riverbank erosion assessment. *Remote Sensing of Environment*, **95**, 493–501.

Thompson, J.A., Bell, J.C. and Butler, C.A. (2001). Digital elevation model resolution: effects on terrain attribute calculation and quantitative soil-landscape modeling. *Geoderma*, **100**, 67–89.

Thompson, S.E., Katul, G.G. and Porporato, A. (2010). Role of microtopography in rainfall-runoff partitioning: An analysis using idealized geometry. *Water Resources Research*, **46**, W07520.

Thornton, E.B., Sallenger, A., Sesto, J.C., Egley, L., McGee, T. and Parsons, R. (2006). Sand mining impacts on long-term dune erosion in southern Monterey Bay. *Marine Geology*, **229**, 45–58.

Trauerstein, M., Norton, K.P., Preusser, F. and Schlunegger, F. (2013). Climatic imprint on landscape morphology in the western escarpment of the Andes. *Geomorphology*, **194**, 76–83.

Travis, M.R., Elsner, G.H., Iverson, W.D. and Johnson, C.G. (1975). *VIEWIT: computation of seen areas, slope, and aspect for land-use planning*. Pacific Southwest Research Station, U.S. Forest Service, Berkeley, CA.

Trevisani, S., Cavalli, M. and Marchi, L. (2010). Reading the bed morphology of a mountain stream: a geomorphometric study on high-resolution topographic data. *Hydrology & Earth System Sciences*, **14**, 393–405.

Tribe, A. (1992). Automated recognition of valley lines and drainage networks from grid digital elevation models: a review and a new method. *Journal of Hydrology*, **139**, 263–293.

Tseng, C.M., Lin, C.W., Dalla Fontana, G. and Tarolli, P. (2015). The topographic signature of a major typhoon. *Earth Surface Processes and Landforms*, **40**, 1129–1136.

Tucker, G.E. and Bradley, D.N. (2010). Trouble with diffusion: Reassessing hillslope erosion laws with a particle-based model. *Journal of Geophysical Research: Earth Surface*, **115**, F00A10.

Tucker, G.E. and Bras, R.L. (1998). Hillslope processes, drainage density, and landscape morphology. *Water Resources Research*, **34**, 2751–2764.

Tucker, G.E. and Slingerland, R. (1997). Drainage basin responses to climate change. *Water Resources Research*, **33**, 2031–2047.

Tucker, G.E., Catani, F., Rinaldo, A. and Bras, R.L. (2001). Statistical analysis of drainage density from digital terrain data. *Geomorphology*, **36**, 187–202.

Vaze, J., Teng, J. and Spencer, G. (2010). Impact of DEM accuracy and resolution on topographic indices. *Environmental Modelling & Software*, **25**, 1086–1098.

Vertessy, R., Hatton, T., Oshaughnessy, P. and Jayasuriya, M. (1993). Predicting Water Yield from a Mountain Ash Forest Catchment Using a Terrain Analysis Based Catchment Model. *Journal of Hydrology*, **150**, 665–700.

Vianello, A., Cavalli, M. and Tarolli, P. (2009). LiDAR-derived slopes for headwater channel network analysis. *Catena*, **76**, 97–106.

Volker, H.X., Wasklewicz, T.A. and Ellis, M.A. (2007). A topographic fingerprint to distinguish alluvial fan formative processes. *Geomorphology*, **88**, 34–45.

Walker, J.P. and Willgoose, G.R. (2006). A Comparative Study of Australian Cartometric and Photogrammetric Digital Elevation Model Accuracy. *Photogrammetric Engineering & Remote Sensing*, **72**, 771–779.

Wang, L. and Liu, H. (2006). An efficient method for identifying and filling surface depressions in digital elevation models for hydrologic analysis and modelling. *International Journal of Geographical Information Science*, **20**, 193–213.

Warren, S.D., Hohmann, M.G., Auerswald, K. and Mitasova, H. (2004). An evaluation of methods to determine slope using digital elevation data. *Catena*, **58**, 215–233.

Westoby, M.J., Brasington, J., Glasser, N.F., Hambrey, M.J. and Reynolds, J.M. (2012). "Structure-from-Motion" photogrammetry: A low-cost, effective tool for geoscience applications. *Geomorphology*, **179**, 300–314.

Whipple, K.X. and Tucker, G.E. (1999). Dynamics of the stream-power river incision model: Implications for height limits of mountain ranges, landscape response timescales, and research needs. *Journal of Geophysical Research: Solid Earth*, **104**, 17661–17674.

Wieczorek, G.F., Morgan, B.A. and Campbell, R.H. (2000). Debris-flow hazards in the Blue Ridge of central Virginia. *Environmental & Engineering Geoscience*, **6**, 3–23.

Wieczorek, G.F., Mossa, G.S. and Morgan, B.A. (2004). Regional debris-flow distribution and preliminary risk assessment from severe storm events in the Appalachian Blue Ridge Province, USA. *Landslides*, **1**, 53–59.

Wiener, N. (1949). *Extrapolation, Interpolation, and Smoothing of Stationary Time Series*, vol. 2. MIT press Cambridge, MA.

Willgoose, G., Bras, R.L. and Rodriguez-Iturbe, I. (1991). A coupled channel network growth and hillslope evolution model: 2. Nondimensionalization and applications. *Water Resources Research*, **27**, 1685–1696.

Wise, S. (2000). Assessing the quality for hydrological applications of digital elevation models derived from contours. *Hydrological Processes*, **14**, 1909–1929.

Witt, A.C. (2005). A brief history of debris flow occurrence in the French Broad River Watershed, western North Carolina. *North Carolina Geographer*, **13**, 58–82.

Wobus, C., Whipple, K.X., Kirby, E., Snyder, N., Johnson, J., Spyropolou, K., Crosby, B. and Sheehan, D. (2006). Tectonics from topography: Procedures, promise, and pitfalls. *Geological Society of America Special Papers*, **398**, 55–74.

Wolock, D.M. and McCabe, G.J. (2000). Differences in topographic characteristics computed from 100- and 1000-m resolution digital elevation model data. *Hydrological Processes*, **14**, 987–1002.

Wolock, D.M. and Price, C.V. (1994). Effects of digital elevation model map scale and data resolution on a topography-based watershed model. *Water Resources Research*, **30**, 3041–3052.

Wooten, R.M., Gillon, K.A., Witt, A.C., Latham, R.S., Douglas, T.J., Bauer, J.B., Fuemmeler, S.J. and Lee, L.G. (2007). Geologic, geomorphic, and meteorological aspects of debris flows triggered by Hurricanes Frances and Ivan during September 2004 in the Southern Appalachian Mountains of Macon County, North Carolina (southeastern USA). *Landslides*, **5**, 31–44.

Wu, S., Li, J. and Huang, G.H. (2008). A study on DEM-derived primary topographic attributes for hydrologic applications: Sensitivity to elevation data resolution. *Applied Geography*, **28**, 210–223.

Wu, W. and Sidle, R. (1995). A Distributed Slope Stability Model for Steep Forested Basins. *Water Resources Research*, **31**, 2097–2110.

Yamaguchi, Y., Kahle, A., Tsu, H., Kawakami, T. and Pniel, M. (1998). Overview of Advanced Spaceborne Thermal Emission and Reflection Radiometer (ASTER). *IEEE Transactions on Geoscience and Remote Sensing*, **36**, 1062–1071.

Yokoyama, R., Shirasawa, M. and Pike, R.J. (2002). Visualizing topography by openness: a new application of image processing to digital elevation models. *Photogrammetric Engineering and Remote Sensing*, **68**, 257–266.

Yoo, K., Amundson, R., Heimsath, A.M. and Dietrich, W.E. (2005). Process-based model linking pocket gopher (Thomomys bottae) activity to sediment transport and soil thickness. *Geology*, **33**, 917–920.

Yoo, K., Amundson, R., Heimsath, A.M., Dietrich, W.E. and Brimhall, G.H. (2007). Integration of geochemical mass balance with sediment transport to calculate rates of soil chemical weathering and transport on hillslopes. *Journal of Geophysical Research: Earth Surface*, **112**, F02013.

Yoo, K., Weinman, B., Mudd, S.M., Hurst, M., Attal, M. and Maher, K. (2011). Evolution of hillslope soils: The geomorphic theater and the geochemical play. *Applied Geochemistry*, **26, Supplement**, S149–S153.

Zevenbergen, L.W. and Thorne, C.R. (1987). Quantitative analysis of land surface topography. *Earth Surface Processes and Landforms*, **12**, 47–56.

Zhang, K. and Whitman, D. (2005). Comparison of Three Algorithms for Filtering Airborne Lidar Data. *Photogrammetric Engineering & Remote Sensing*, **71**, 313–324.

Zhang, T.Y. and Suen, C.Y. (1984). A Fast Parallel Algorithm for Thinning Digital Patterns. *Communications of the ACM*, **27**, 236–239.

Zhang, W. and Montgomery, D.R. (1994). Digital elevation model grid size, landscape representation, and hydrologic simulations. *Water Resources Research*, **30**, 1019–1028.